THE DEVELOPMENT OF ULTRA-HIGH STRENGTH PEARLITIC STEEL WIRES

Tamar Judith Itay

A dissertation submitted to the Faculty of Engineering, University of the Witwatersrand, Johannesburg, in fulfilment of the requirements for the Degree of Doctor of Philosophy.

Department of Metallurgy
University of the Witwatersrand
November 1995

DECLARATION

I declare that this dissertation is my own unaided work except where due acknowledgement is made to others. It is being submitted for the Degree of Doctor of Philosophy to the University of the Witwatersrand, Johannesburg. It has not been submitted before for any degree or examination to any other University.

T I Itay

Tamar Judith Itay

29 day of November 1985.

ACKNOWLEDGEMENTS

I wish to express my deep appreciation to Dr J.V. Bee for his helpful and stimulating supervision and his encouragement throughout the period of this research. I am also very grateful to Prof. G.G. Garrett for his enthusiasm and support during the course of this work.

I would like to thank Mr E.A. Shipley for his constructive advice and Dr G.D.W. Smith for his useful suggestions for alloy compositions and for many valuable and stimulating discussions.

I wish to thank the head of the R&D department in Haggie Rand Limited, Mr P. White, for providing laboratory facilities and Messrs A. Heap and M. Reeves for their collaboration in part of this research.

Acknowledgements are also made to the Technical Staff of this laboratory, in particular Mr J. Moore for his help with machining and fabrication of specimens, Mr J. Raftopoulos for his aid and advice in furnace construction and Mr A. Nutton for his assistance in alloy fabrication.

It is a pleasure to thank the director of the Electron Microscope Unit at this university, Dr M. Witcomb, and the technical staff for their assistance during the course of this work.

I am also very grateful to my friends and colleagues in this department for many useful and stimulating discussions, and in particular Prof. R.P. King for his advice in the use of the image analyser.

I am indebted to Mrs Nicole Couvaras for her patient and accurate tying of this manuscript.

I would like to thank my husband, Michael, and my children, Amit and Shimrit for their endless support and tolerance during the production of this thesis.

Finally, I would like to thank Haggie Rand Limited, the University Senior Bursary Fund and the Council for Scientific Industrial Research (CSIR) for their financial support.

CONTENTS

CONTENTS (continued)

CONTENTS (continued)

CONTENTS (continued)

CONTENTS (continued)

CONTENTS (continued)

CONTENTS (continued)

CONTENTS (continued)

ABSTRACT

This thesis describes a systematic investigation of the influence of alloying additions on the microstructure and mechanical properties of eutectoid carbon steels. The goal of this work was to develop an alloy which would provide a tensile strength in excess of 2500 MPa in drawn wire.

Alloys were fabricated using vacuum induction melting, casting and hot-rolling. Specimens of each material were heat treated to produce pearlitic structures. Microstructures were evaluated using light, scanning electron and transmission electron microscopy. Mechanical properties were determined from hardness and tensile tests. Suitable heat treated rods were subjected to drawing trials, and the structures and properties re-determined.

In the initial part of the study, the influence of chromium and manganese addition on the properties of a high purity carbon alloy were studied. This work demonstrated the benefits of these small alloying additions on strength, while maintaining adequate ductility.

In subsequent work the additional effects of alloying with silicon were studied. Of the alloys investigated, the 2Si-1Cr composition achieved a drawn strength in excess of

2500 MPa. This material also exhibited acceptable values in standard shear and torsion tests for commercial wires.

Since the strength of steel is strongly dependent on carbon content, the further influence of this variable on properties was examined using the 2Si-1Cr base composition. Increasing the carbon content to 0.9% did provide additional strength, but increased the ageing susceptibility during drawing.

The work was extended towards commercial compositions by preparing 2Si-1Cr alloys using a commercial eutectoid carbon-manganese steel base. Again, in the as-drawn condition, the strength goal was exceeded. However, these materials exhibited inferior ductility compared with the high-purity alloys. This is thought to be due to ageing.

A brief study was also conducted on the problem of strain ageing, but no evidence for precipitation of deleterious carbides could be found even using electron microscopy.

In summary, small alloying additions are extremely effective in increasing the strength of pearlitic wire, while maintaining adequate ductility. A 2Si-1Cr alloy exhibited the best results of the materials studied. This composition has commercial potential, but may require more sophisticated production methods to provide cleaner, higher purity material. Nevertheless, this alloy is capable of providing as-drawn tensile strengths in excess of the 2500 MPa goal.

CHAPTER ONE - INTRODUCTION

Cold drawing of eutectoid carbon steels is a major production technique for the manufacture of ultra-high strength wires. Thousands of tons of such material are produced each year for applications such as high-strength wire ropes, springs and pre-stressed concrete wire.

Alloy steels are used to prepare wires when higher strengths are required than can be achieved using carbon steel. Depending on the specific alloy content, other properties such as ductility, wear, fatigue resistance and toughness can also be improved, and often maintained to higher temperatures. These properties not only depend on the type and amount of individual alloying elements but are also influenced by synergistic interactions between different elements.

In the South African mining industry, wires with tensile strengths of 2100MPa form the basis for the manufacture of ropes and cables. Significant payload advantages would occur if the tensile strength were increased by approximately 10 to 20%. The aim of this project was then to develop an understanding of the microstructural variables necessary to achieve such strength levels.

The strengths obtained by the process of wire drawing depend on the initial strength prior to drawing, and on the drawing reductions. To achieve ultra-high strength levels, the steel is usually "patented". This heat treatment consists of austenitisation followed by isothermal transformation of the steel in the pearlite nose region of the relevant TTT diagram. This produces a fine lamellar pearlitic structure. The as-patented steel is then cumulatively cold drawn to very high deformations. The strength increases progressively with increasing deformation.

Another important characteristic of the steel, therefore, is its drawability, or the extent to which the wire can be deformed without breakage. Optimum combinations of strength and drawability, both of which depend greatly on the initial microstructure, result in the attainment of the highest strength levels.

The basic philosophy of the present research was to improve strength levels using alloying additions in an attempt to:
(i) reduce the interlamellar spacing of the pearlite; and
(ii) increase the friction stress of the ferrite matrix.

It was decided therefore to concentrate this study on the elements chromium, manganese and silicon, which have been shown to influence one or both of these parameters.

Although a systematic variation of each element, alone and in combination, would have been the ideal experimental approach, the large number of required compositions from such a matrix would have been prohibitive both in cost and time. It was therefore decided to select a smaller number of alloys (generally towards a predicted maximum practical concentration) for a detailed examination of strengthening trends.

The aim of this work therefore was to study both the scientific and technical aspects of the pearlite reaction in low alloy steels. This required microstructural and mechanical property evaluation in the as-patented and drawn conditions. In particular, detailed studies were made on the following parameters:

(a) the pearlite interlamellar spacing;
(b) the nature and uniformity of the carbide phase;
(c) drawability;
(d) ageing effects during and after the drawing process;
(e) the mode of deformation; and
(f) the mode of failure in the shear and torsion tests.

This work was undertaken in collaboration with HaggieRand Limited South Africa.

CHAPTER TWO - LITERATURE REVIEW

2.1 The Austenite-Pearlite Reaction

The stability of all phases and microstructures in metals and alloys is based on the principle of minimum free energy. The driving force for any transformation is the difference in free energy between the reactants and products: ΔF_o .

In steels, the eutectoid transformation produces pearlite. This was recognised as a lamellar structure of ferrite and cementite (iron carbide) over 100 years ago by Sorby (see Honeycombe, 1981). Similar lamellar products have since been identified in a wide range of ferrous and non-ferrous eutectoids and eutectics. In solid-state transformations, these pearlitic (or discontinuous) reactions have been studied extensively. The main purpose of the present review is to summarise the existing knowledge specifically relating to eutectoid reactions in steels, with only limited reference to other alloys where the findings appear relevant.

Theoretical contributions to discontinuous precipitation reactions have been made by (for example) Brandt (1945), Zener (1946) and Hillert (1957) and were reviewed in the

symposium: "The decomposition of austenite by diffusional processes" (see Cahn and Hagel, 1962).

Many experimental studies have also been reported. These include work on plain carbon steels, (for example: Bolling and Richman (1970), Chadwick and Edmonds (1973), Cheetham and Ridley (1973), (1975), Marder and Bramfitt (1975)) on ternary eutectoids (for example : Brown and Ridley (1966), Sundquist (1969), Puls and Kirkaldy (1972), Coates (1973), Evsyukov and Pritomanova (1975), and Al-Salman et al (1979a, 1979b, 1979c)),as well as on non-ferrous eutectoid compositions,(such as Asundy and West (1966a, 1966b) and Mellor and Chadwick (1974)).

The pearlite reaction also occurs in non-eutectoid compositions. In hypo-eutectoid steels, pro-eutectoid ferrite forms prior to the transformation of austenite to pearlite while in hyper-eutectoid steels the pro-eutectoid phase is cementite. However, fully pearlitic structures can be obtained in these compositions by transformation at temperatures below the eutectoid temperature.

2.2 Nucleation of Pearlite

Pearlite forms from austenite by a nucleation and growth process. The reaction is therefore time and temperature dependent, and is controlled by diffusion.

Again, there is a wealth of data concerning both nucleation sites and the identity of the active nucleus.

Mehl and Hagel (1956) showed that pearlite nucleated almost exclusively at austenite grain boundaries. Subsequent studies however have recognised the non-equivalence of even grain boundary nucleation sites. Using a theoretical approach, Cahn and Hagel (1962) derived equations for the overall rate of pearlite formation for site-saturated transformation and distinguished grain corners, grain edges and grain surfaces in order of decreasing effectiveness. Experimental support for this hypothesis has been provided by Russev et al (1974) in a study of the effect of cooling rate on the nucleation of pearlite during continuous cooling. At low cooling rates (1.8 to 8.7 °C/min) the pearlite reaction started at grain corners, while at higher rates (14 to 16 °C/min) the pearlite nucleated on grain edges. More recently, Hawbolt et al (1983) reported that the nucleation of pearlite at prior austenite grain boundaries generally occurred preferentially at grain edges and possibly also on grain corners.

As well as grain boundaries, pearlite has also been found to nucleate on undissolved cementite (Hull et al, 1942) and pro-eutectoid cementite (Dippenaar and Honeycombe, 1973).

Repeated sectioning studies by Hillert (1962) have shown that all of the apparently separate cementite lamellae in pearlite had a common origin, while the individual lamellae form by branching during edgewise growth. Thus pearlite essentially consists of two interwoven crystals, one of ferrite and one of cementite. Further considerable attention has been given therefore to the identity of the active nucleus for pearlite formation.

In early research (D.W. Smith and Mehl, 1935; G.V. Smith and Mehl, 1942) the orientation relationship of ferrite in pearlite was found to be different from that of ferrite nucleated in austenite. It was argued that this precluded ferrite as the active nucleus. Further evidence for this hypothesis was provided by Hull et al (1942) who identified undissolved Fe_3C particles as very active nuclei for pearlite and also found that pearlitic cementite was frequently continuous with pro-eutectoid cementite.

Other studies came to different conclusions. Digges (1938) found that increasing the carbon content of hypo-eutectoid steels retarded both ferrite and pearlite reactions. He suggested that this implied they both had the same nucleus: ferrite. Aaronson (1954) also proposed that ferrite may be the initial or "informal" nucleus of pearlite.

Nicholson (1954) presented a more complex concept arguing that both ferrite and cementite could form the active nucleus, depending on temperature and composition. A similar conclusion was reached by Hillert (1962).

Dippenaar and Honeycombe (1973) carried out a detailed crystallographic study of the austenite-pearlite reaction. It was found that in pearlite colonies nucleated on "clean" austenite grain boundaries, the ferrite was related to one austenite grain by a Kurdjumov-Sachs relationship producing a low-energy semi-coherent interface. This resulted generally in a high energy incoherent interface with the adjacent grain which then provided high mobility for rapid pearlite growth.

Similarly, cementite also developed a semi-coherent interface with one austenite grain and an incoherent interface with the other. In this situation, the relationship between the ferrite and cementite was observed to be the Pitch-Petch.

$$(001)_c \;//\; (5\bar{2}\bar{1})_\alpha$$

$$(010)_c \; 2 - 3^\circ \text{ from } [11\bar{3}]_\alpha$$

$$(100)_c \; 2 - 3^\circ \text{ from } [13\bar{1}]_\alpha$$

The existence of this α - Fe_3C relationship in pearlite implies direct contact of both phases with the adjacent austenite grain.

In other pearlite colonies, a Bagaryatskii orientation relationship was found between the ferrite and cementite.

$$(100)_C \;//\; (0\bar{1}1)_\alpha$$
$$(010)_C \;//\; (1\bar{1}\bar{1})_\alpha$$
$$(001)_C \;//\; (211)_\alpha$$

Similar observations have also been made by Pitsch (1962), Morgan and Ralph (1968) and Ohmori et al (1972). In each case, these pearlites were closely associated with pro-eutectoid cementite.

It appears that either ferrite or cementite may act as the active nucleu Mehl and Hagel (1956) took the view that pearlite nodules formed by sideways nucleation and edge-ways growth. In this way, the rapid increase in the number of lamellae in a nodule which occurred during growth was explained. However,this could also result from the branching of lamellae during growth. Dippenaar and Honeycombe (1973) have shown the beginning of branching of the cementite lamellae. However, in other nodules, sideways nucleation of laths of cementite and ferrite was observed.

Cahn and Hagel (1962) have shown that once formed the pearlite nodules grow on the incoherent interface with little evidence that austenite grain boundaries can halt the advance.

2.3 The Growth of Pearlite

In a binary or ternary system, a diffusional analysis of pearlite growth is complicated by the fact that there exist two possible diffusion paths for the redistribution of the solute(s) to the two product phases. In Fe-C, for instance, carbon has the option of moving by volume diffusion through the bulk austenite, or by boundary diffusion along the austenite-ferrite and austenite-cementite interfaces.

Mathematical treatments of pearlite growth in Fe-C alloys have been attempted by Zener (1946), Hillert (1968), Bolze et al (1972) assuming volume diffusion control, and by Cahn (1959), Shapiro and Kirkaldy (1968), and Sundquist (1969) assuming boundary diffusion control.

On solving the diffusion equation applicable to pearlite growth a relationship linking V (the growth velocity), S (the interlamellar spacing) and ΔT (the amount of undercooling) may be obtained. A summary of the predictions of various eutectoid (and eutectic) growth theories has been

given by Mellor and Chadwick (1974). This is reproduced as Table 2.1. As can be seen, all the theories with the exception of those developed by Cahn (1959) and Bolze et al (1972) predict a relationship of the form $V S^n$ = constant or $V S^n \exp E/RT$ = constant.

Calculations using boundary diffusion models as the rate controlling mechanism usually gave growth rates that are higher than those observed experimentally, whereas calculations using volume diffusion yield growth rates that are too low. This would suggest that the rate-controlling process is some combination of both mechanisms, i.e. volume and boundary diffusion.

Table 2.1 Summary of the predictions of various eutectoid (and eutectic) growth theories. After Mellor and Chadwick (1974).

Author	Relationship Predicted	Growth Criterion Selected	Volume, V_α, or Boundary Diffusion, B	Assumptions Regarding ΔT's and D
Zener[11]	$V\lambda^2 \exp. E/RT$ = constant $\Delta T\lambda$ = constant	Grows at maximum velocity possible	V_α	$\Delta T_K = 0$ $D \propto \exp.-E/RT$
Jackson and Hunt[12]	$V\lambda^2$ = constant $\Delta T\lambda$ = constant	Grows at minimum ΔT for rod growth	V_α	$\Delta T_K = 0$ D = constant
Hillert[13]	$V\lambda^2$ = constant $\Delta T\lambda$ = constant	Grows at maximum velocity possible	V_α	$\Delta T_K = 0$ D = constant
Tiller[14]	$V\lambda^n$ = constant $n > 2$ $\Delta T\lambda^m$ = constant $m > 1$	Grows at maximum velocity possible	V_α	$\Delta T_K \simeq \Delta T^3$ D = constant
Bolze *et al.*[15]	$V \propto \frac{1}{\lambda}\left(1-\frac{\lambda_0}{\lambda}\right) \Big/ 1+\varphi/\lambda$	Stable state) not specified, either that which gives maximum velocity or maximum entropy production	V_α	$\Delta T_K = 0$ D = constant
Cahn[16]	Various parameters are plotted as a function of interface mobility	Grows at a velocity $\propto \Delta G \propto \Delta T$	B	D = constant Kinetic factors determine V
Hillert[13]	$V\lambda^3$ = constant $\Delta T\lambda$ = constant	Grows at maximum velocity possible	B	$\Delta T_K = 0$ D = constant
Sundquist[17]	$V\lambda^3 \exp. E/RT$ = constant $\Delta T\lambda$ = constant	Grows at a velocity so that λ on verge of instability	B	$D \propto \exp.-E/RT$
Shapiro and Kirkaldy[18]	$V\lambda^3 \exp. E/RT$ = constant $\Delta T\lambda$ = constant	Grows at a velocity corresponding to a spacing of $F\lambda_0$ where $F > 1$	B	$D \propto \exp.-E/RT$
Carpay and Van den Boomgard[19]	$V\lambda^4$ = constant $\Delta T\lambda^2$ = constant	Grows at a velocity $\propto \Delta T^2$	B	D = constant kinetic factors determine V

ΔT = Total undercooling at the interface.
ΔT_K = Kinetic undercooling due to the chemical potential difference necessary to drive the molecular attachment mechanism at the interface.
D = Diffusion coefficient.
ΔG_v = Net decrease in free energy.
λ_0 = Minimum spacing thermodynamically possible.
φ = A constant related to the stored free energy associated with solute segregation.
F = A constant.

2.4 The Interlamellar Spacing of Pearlite

The interlamellar spacing of pearlite is a parameter of major importance, technologically because of its profound influence on mechanical properties and fundamentally in terms of the kinetics of pearlite formation.

Interlamellar spacings have been the subject therefore of numerous investigations. A comprehensive review of the data on the interlamellar spacing of pearlite was presented recently by Ridley (1984).

2.4.1 Definition

It has been found that there is significant variations in the observed spacing between cementite lamellae in different areas of the same specimen. This may be due partially to the transformation of austenite to pearlite over a range of temperatures, but the main reason is the difference in the angle at which lamellae intersect the plane of the polished section. A relationship is required therefore between observed and true spacings (Figure 2.1).

The apparent spacing, S, is the perpendicular distance between lamellae measured on the random plane of polish. Assuming that all the pearlite formed at the same temperature, only those colonies with lamellae

perpendicular to the polished surface would show the true spacing S_o. However, there is experimental evidence (Pellisier et al, 1942) that even this true spacing is not a unique value, but there exists a distribution of spacings about a mean true value, $\bar{S}_o$.

A third spacing that may be considered is the intercept spacing, l, (see Figure 2.1). This is the distance between two successive lamellae taken from a test line applied randomly to the plane of polish, and will vary with the orientation of the line in that plane.

An expression for the volume fraction distribution $V_v(l)$ of the true spacing S_o, in terms of the intercept spacing distribution in number of chords per unit length, was given by Cahn and Fullman (1956) as:

$$V_v(l) = 3\, l\, N_L(l) + l^2 \frac{d\, N_L(l)}{d(l)}$$

where $N_L(l)$ is the number of chords of length l per unit length of a random secant.

The true average spacing, $\bar{S}_o$, was obtained by integrating over the whole range of intercepts: $\int_0^\infty l V_v(l)$.
This is clearly inaccurate since $\bar{S}_o$ will be infinite in the case of lamellae parallel to the secant.

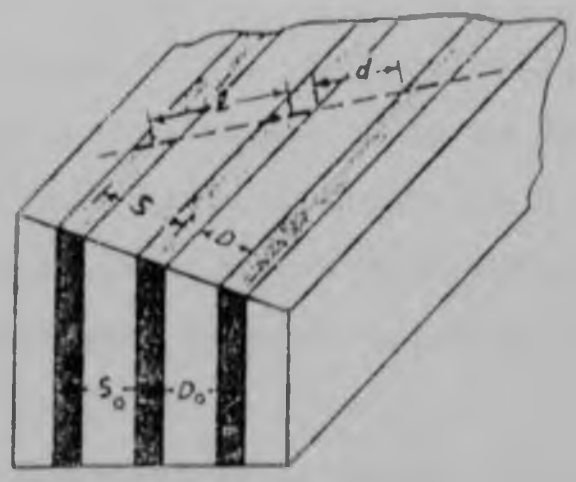

Centre - to - centre spacings
So = true spacing
S = apparent spacing
l = intercept spacing

Edge - to - edge distances
Do = true free distance
D = apparent free distance
d = intercept free distance

Figure 2.1 Classification of spacings and distances in a geometrically ideal lamellar structure. After De-Hoff and Rhines (1968).

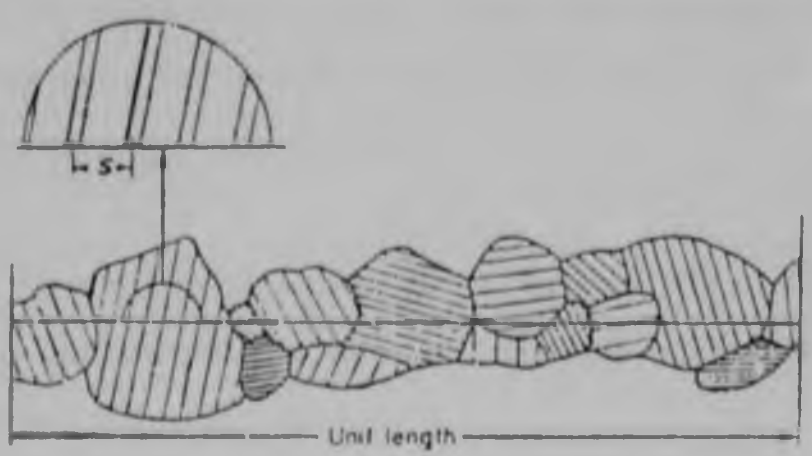

Figure 2.2 Determination of mean intercept spacing. After De-Hoff and Rhines (1968).

An alternative method for the determination of the true interlamellar spacing was developed by De Hoff and Rhines (1968) based on the original work of Gensamer et al (1942). This used lines drawn randomly on the sample surface to intersect many pearlite colonies (Figure 2.2).

These lines were oriented to intersect a large number of lamellae at all possible angles. The total length of the test secants divided by the total number of cementite platelets was defined as the mean intercept spacing, $\bar{I}$.

2.4.2 Experimental measurements

The determination of the true pearlite spacing from metallographic specimens, where the lamellae intersect the specimen surface with a range of angles, requires the application of special quantitative analytical techniques.

The results obtained using light microscopy have been analysed mainly by two methods: the total resolution and partial resolution techniques.

The more recent application of electron microscopy to the study of interlamellar spacings has led to the development of more sophisticated analyses.

2.4.2.1 The total resolution technique

Light microscopy was applied to the study of pearlite spacings in isothermally transformed steels as early as 1922 by Belaiew. The relationship between the apparent spacing (S) on the sectioning plane and the true spacing (S_o) was defined in terms of the angle (ω) between the normal to the lamellae and the plane. This gave the relationship:

$$\omega = \sec^{-1} \frac{S}{S_o}$$

In this case, the smallest apparent spacing encountered on viewing a sufficiently large area of the specimen was assumed to be equal to the true spacing. This method of determining the spacing involves two basic assumptions: (a) that the true spacing is constant, and (b) that the orientation of pearlite colonies with respect to the plane of polish is random.

Pellisier et al (1942) used a statistical analysis to calculate the distribution of apparent spacings, assuming a constant true spacing. This was compared with experimental data obtained by measuring the relative amounts of surface area occupied by various small ranges of apparent spacing. It was concluded that the interlamellar spacing of pearlite formed isothermally is not constant, but rather consists of a statistical distribution of spacings about a mean value.

Thus it was suggested that the minimum apparent spacing is not representative of the true spacing. Instead, the true spacing could be obtained from the fraction, f_s, of the area of the reference plane occupied by spacings up to a certain value of S:

$$f_s = \cos\left(\operatorname{cosec}^{-1}\frac{S}{S_o}\right)$$

In this derivation it has been assumed that the lamellae are plane. However, the curvature observed in the pearlite lamellae was not believed to affect the applicability of the derivation.

A similar method has been applied by Asundi and West (1966a) in their study of a non-ferrous eutectoid composition. A severe limitation of this technique is that it can only be applied to coarse pearlite which is fully resolvable in the light microscope.

2.4.2.2 The partial resolution technique

This "Limit Method" was devised by Gensamer et al (1940). The true spacing was estimated from measurements of the fraction (f_s) of the specimen which is unresolved by an objective lens of known resolving power, using the relationship:

$$\frac{S}{S_o} = \sqrt{1 - f_s^2}$$

where S is the spacing just resolved by the objective.

Although this method was subject to errors, Pellisier et al (1942) suggested that it is probably no more inaccurate than the direct method of measuring the average distance between lamellae on a highly magnified image. Pellisier et al (1942) and Gregory et al (1961) found experimentally that the most reliable values were obtained when $f_s \approx 0.5$. However, the errors involved are very large, and have been reported as 20% by Pellisier et al (1942) and 100% by Gregory et al (1961).

2.4.2.3 Electron microscopy techniques

Very fine interlamellar spacing may be measured using scanning and transmission, electron microscopy.

One method of obtaining S_o, was developed by Brown and Ridley (1966). Replicas were examined in a transmission electron microscope, in which the fluorescent viewing screen was inscribed with a circle of known diameter. The magnification was increased sufficiently to resolve the closest spaced lamellae, and the specimens searched to obtain images of the area with the finest spacing. The

value corresponding to the maximum number of intersections was then converted to the minimum interlamellar spacing, S', using the relation:

$$S' = \frac{1}{n} \cdot \frac{d_c}{M}$$

where n is the number of lamellae crossed at right angles to the diameter d_c at magnification M.

Another approach has been the determination of a minimum spacing in terms of the average smallest spacing which recurs throughout a given section. This method has provided reliable and consistent results. It has been employed extensively therefore, for example by Asundi and West (1966a), Bolling and Richman (1970), Puls and Kirkaldy (1972) and Sharma et al (1979).

Baán et al (1977) and Roósz et al (1980), have also reported measurements of spacings made using carbon replicas. These authors employed the method described by Pellisier et al (1942) for the determination of an average interlamellar spacing. This was achieved using the following cumulative function:

$$A_s(S_{o,1}) = A_1 \sqrt{1 - \left(\frac{S_{o,1}}{S_{o,1}}\right)^2} + A_2 \sqrt{1 - \left(\frac{S_{o,2}}{S_{o,1}}\right)^2} + \ldots\ldots + A_{i-1} \sqrt{1 - \left(\frac{S_{o,i-1}}{S_{o,1}}\right)^2}$$

where $S_{o,i}$ are the different true interlamellar spacings; and

A_i is the proportion of area occupied by each value.

Similar methods can also be applied to measurements obtained from colonies with the smallest spacings observed in the scanning electron microscope. This technique permits the study of large areas of specimens but cannot resolve very fine pearlite.

However, a significant advantage of SEM is the ability to study the arrangement of cementite lamellae in three dimensions. A special tilting device has been designed by Hillnhagen and Schauf (1980). This enables two mutually perpendicular polished surfaces to be scanned along their common edge, with precise positional control. The apparatus and the direct measurement of the true spacing (position II on surface B) are illustrated in Figure 2.3.

The examination of pearlite structures in the transmission electron microscope can also be carried out directly using thin foil specimens. Although the extremely small extent of electron-transparent material generally precludes detailed statistical analysis, it is possible to obtain values of the true spacing. This is achieved by tilting the specimen until the cementite lamellae are perpendicular to the electron beam. Results obtained using this technique have been reported recently by Mottishaw (1984).

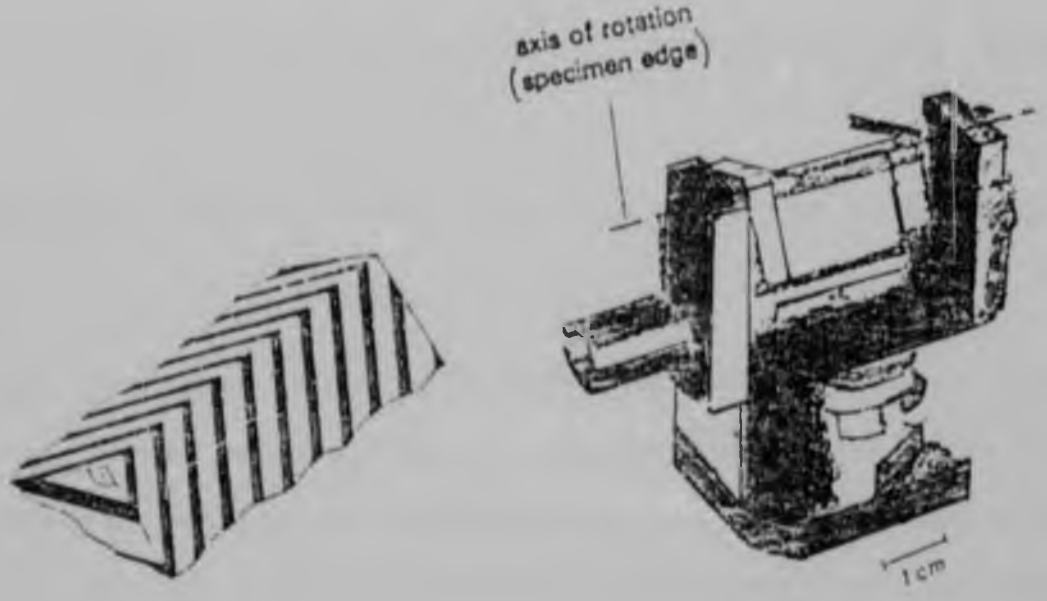

(a) (b)

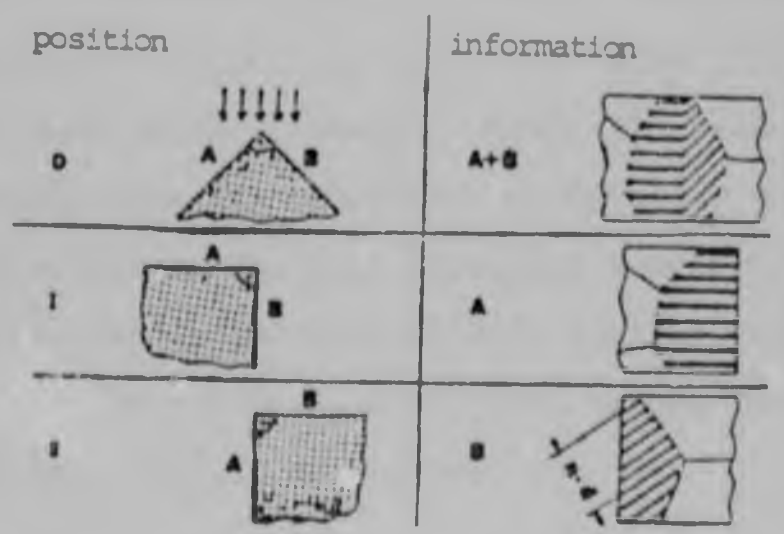

(c)

Figure 2.3 Method of interlamellar spacing measurement.
(a) Problem example
(b) Tilting device
(c) Two surface evaluation
After Hillnhagen (1980).

2.4.2.4 Relationships between the minimum spacings, mean intercept spacing and the mean true spacing

De Hoff and Rhines (1968) have obtained the relationship

$$\bar{I} = 2\bar{S}_o$$

between the mean intercept spacing and the mean true spacing. This relationship can be compared with the experimental results of Gensamer et al (1942) who found that $\bar{1}$ and $\bar{S}_o$ were related by a constant, whose value varied between 1.9 and 2.0.

Many studies have been carried out on the relationship between the minimum observed spacing and the mean true spacing. Pellisier et al (1942) reported that these values could differ by more than 50%. More recently, Asundi and West (1966a) used the same method to investigate the distribution of spacings in a eutectoid aluminium-bronze.No good agreement was obtained between theoretical and experimental distribution curves, although a mean true value 2 to 2.5 times larger than the minimum spacing was found to be the best fitting.

Pellisier et al (1942) suggested that the interlamellar spacing of pearlite actually consists of a range of S_o values statistically distributed about some mean value, which appeared to be approximately $1.65S_o$. Brown and Ridley (1969), however, have suggested that this value is

not a universal constant, but varies with time, temperature and composition. In isothermally transformed steels the factor is frequently less than 1.65.

Recent studies (Ridley, 1984) on a plain carbon eutectoid steel, isothermally transformed in the temperature range 645 to 695°C have shown that the ratio $\bar{S}_o/S$ ranged from 1.18 to 1.32 with an average value of 1.24, and tended to increase with increasing temperature. Values of $\bar{S}_o$ were obtained from $\bar{I}$ assuming $\bar{I} = 2\,\bar{S}_o$. (De Hoff and Rhines, 1968).

The distribution of spacings in cobalt eutectoid steels, transformed under forced velocity conditions, has been examined by Mellor and Edmonds (1977). The mean true spacing was found to be 1.25 times the minimum spacing. It can be seen from the reported data that there is great uncertainty on the relationship between the minimum and mean true spacing.

2.4.3 The effect of temperature

The interlamellar spacing was found to vary approximately exponentially with the temperature of reaction by Mehl (1939), who proposed the following relationship:

$$S_o = K \exp\left(-\frac{b}{T}\right)$$

where k and b are constants, and

T is the absolute temperature.

In studies of the influence of transformation temperature on the interlamellar spacing, results have been plotted therefore as the logarithm of mean true spacing against temperature or the reciprocal of absolute temperature. An example is presented in Figure 2.4.

Another expression for the calculation of interlamellar spacing, S, was derived by Zener (1946) in terms of the free energy available at temperature T for the formation of new interfaces:

$$S = \frac{2\,T_E\,\sigma_A}{\rho\,Q(T_E - T_A)} \qquad 2.1$$

where σ_A is the surface energy per unit area;

Q is the heat of transformation per unit mass;

T_E is the eutectoid temperature; and

ρ is the density

According to equation 2.1, the interlamellar spacing is inversely proportional to the amount of undercooling. A similar relationship was obtained by Hugo and Woodhead (1957), and Cheetham and Ridley (1975).

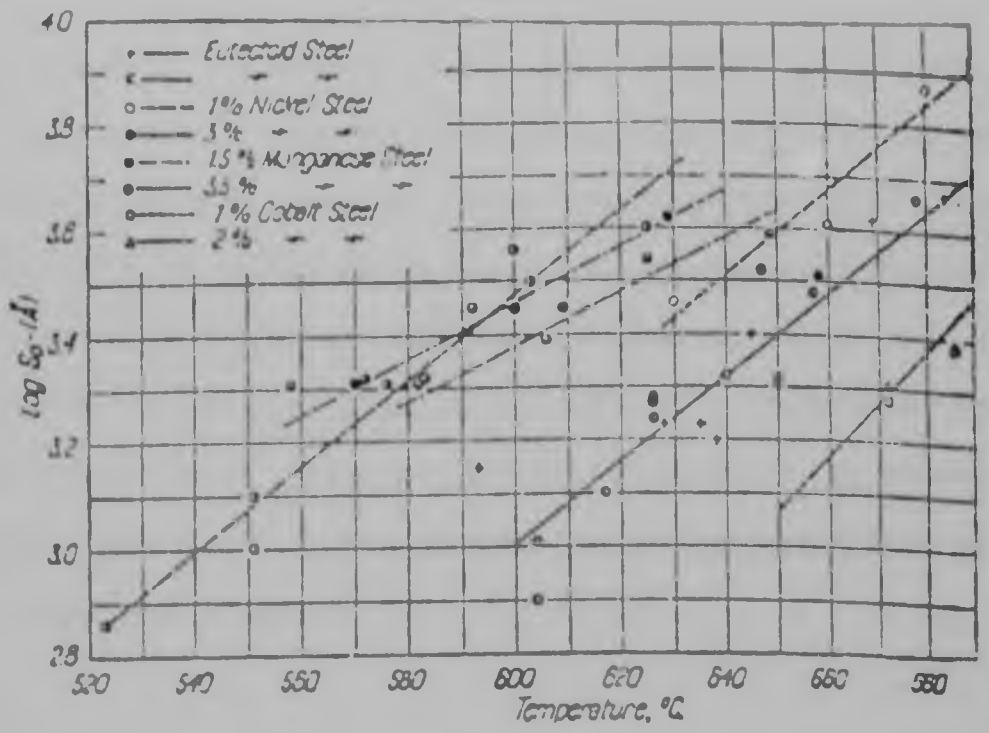

Figure 2.4 Plot of the logarithm of the mean true spacing, So, against temperature for several eutectoid medium alloy steels. After Pellisier et al (1942).

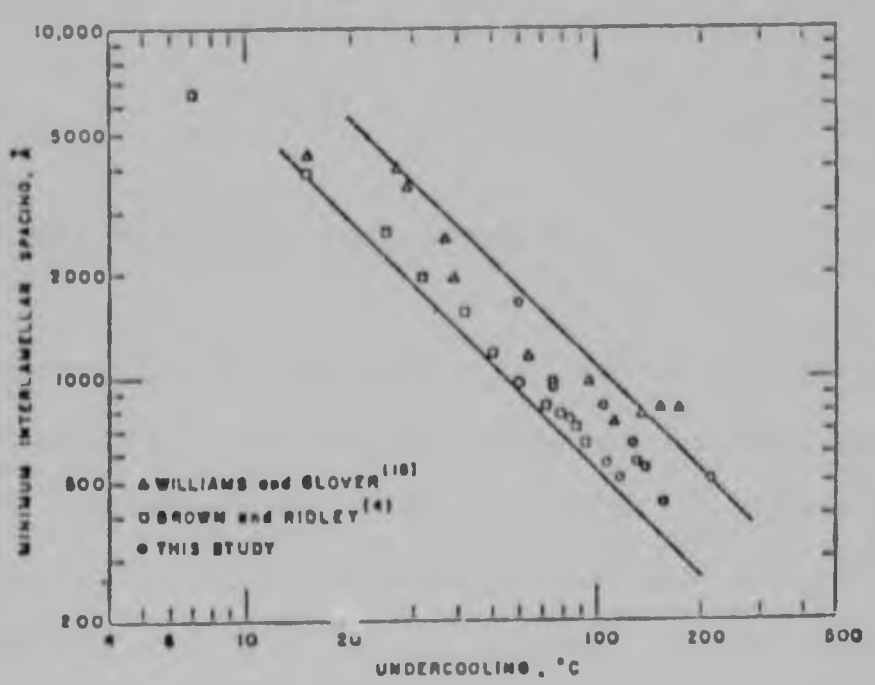

Figure 2.5 Effect of degree of undercooling on the interlamellar spacing. After Marder and Bramfitt (1975).

Based on Zener's approach, Hillert (1957) proposed a modified relationship between the interlamellar spacing and the reciprocal of undercooling, and this has been confirmed experimentally in a wide range of plain carbon and alloyed eutectoid steels by Brown and Ridley (1969), Bolling and Richman (1970), Ridley et al (1973), Cheetham and Ridley (1975), and Razik et al (1976). However, McIvor (1973) obtained a non-linear relationship from the study of some C-Mn steels.

Marder and Bramfitt investigated the effect of undercooling on the interlamellar spacings produced using continuous cooling. These results were compared with published data from isothermal transformation studies (Figure 2.5). Again, a linear relationship was observed. The average of the experimental data gave an equation of the form:

$$S\,\Delta T = 8.02 \times 10^{4}\ \text{Å K}$$

2.4.4 The effect of recalescence

The transformation of austenite to pearlite is exothermic. The quantity of heat evolved depends on the amount of austenite transforming. During cooling this heat is sufficient to cause a thermal arrest and in isothermal transformation can lead to an increase in the temperature of a sample. The latter phenomenon is termed recalescence.

Recalescence is a serious problem. In attempting to isothermally transform large samples in a liquid bath, much of the pearlite will form at temperatures above the desired optimum. This will result in both an appreciable range of spacings and a generally coarser structure (Gensamer et al, 1942). This effect is more pronounced in plain-carbon steels which transform rapidly after very short incubation times, and can only be avoided by using very small samples. In most alloyed eutectoid compositions, the transformation kinetics will be reduced and more time will be available for the dissipation of the evolved heat and the attainment of the desired transformation temperature. This should result in more uniform, finer pearlitic structures.

2.4.5 The effect of carbon content

Pellisier et al (1942) were able to show that an increase in carbon content above the eutectoid composition resulted in a decrease in the interlamellar spacing. Similar results were reported by Payne and Smith (1968). However, it should be noted that this may not necessarily be due to the effect of carbon content on the actual structure, but may result from the lowering of the transformation temperature due to the increased incubation time.

The effect of carbon content on the spacing and tensile strength of pearlite has been studied by Smith (1977) and the results are reproduced in Figure 2.6.

Chadwick and Edmonds (1973) investigated the effect of carbon content on interlamellar spacing in specimens transformed under a constant imposed velocity. They found that there was a minimum value of spacing corresponding approximately to the eutectoid carbon content. However the authors suggested that further work is needed in order to confirm the results. Cheetham and Ridley (1975) made a similar study, using isothermal transformation conditions. Again, the interlamellar spacing increased with decreasing carbon content. A further important observation from this work was the increase in degeneracy of pearlite with decreasing carbon content.

2.4.6 The effect of prior austenite grain size

It has been reported by Pellisier et al (1942), that the austenitising temperature, and therefore, the prior austenite grain size had no detectable influence on the interlamellar spacing.

Increasing the austenite grain size of a steel increases hardenability. Thus, in plain-carbon steels, coarse-grained material would be expected to transform during cooling at a lower temperature than fine-grained. Such a

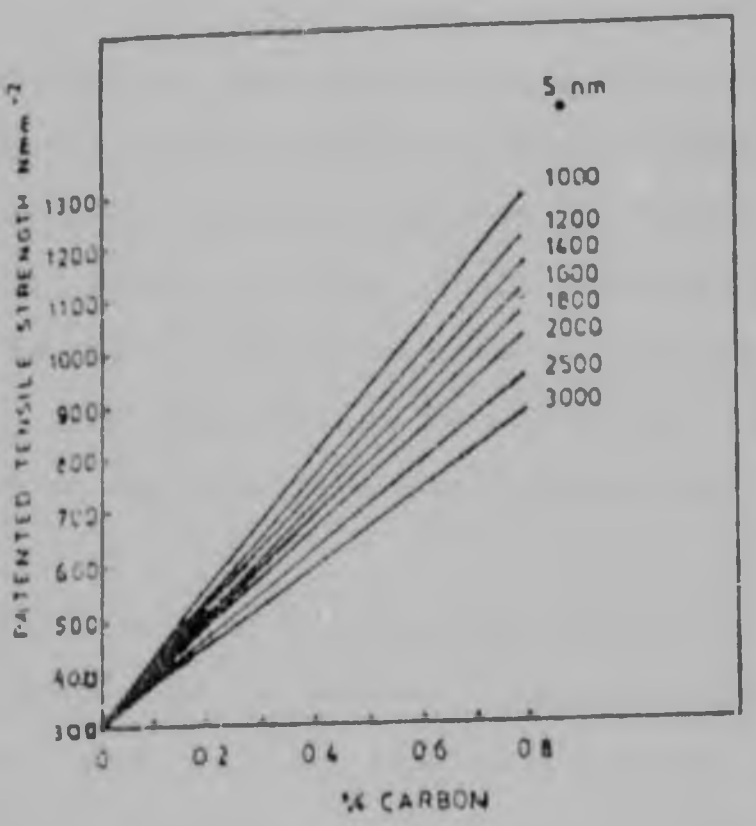

Figure 2.6 Patented tensile strength as a function of carbon content at various interlamellar spacings. After Smith (1977).

steel would exhibit a smaller pearlite spacing, producing an apparent, but not a real variation of spacing with austenite grain size.

However, Mehl and Hagel (1956) confirmed Pellisier's findings, stating that the interlamellar spacing does not vary with austenite grain size. McIvor (1973) also found that variations in the austenitising temperatures did not significantly affect the interlamellar spacing of a C-Mn steel. Agreement was also obtained by Marder and Bramfitt (1976) and Rõosz and Gáczi (1981), although Gladman et al (1972) did find that a coarse austenite grain size frequently produces a finer interlamellar spacing due to its effect on the transformation temperature.

The transformation of fine-grained austenite does lead to improved mechanical properties. Nakamura (1974) suggested that this was due to the development of a finer interlamellar spacing. This is most unlikely in view of most of the evidence presented above.

Mehl and Hagel (1956) also proposed that the interlamellar spacing does not depend on the austenite heterogenity. However, Payne and Smith (1968), found that if the austenite is not completely homogenised, the pearlite which forms during isothermal transformation tends to be coarser and less uniform, compared with that which is produced from homogenised austenite.

2.5 The Patenting Process

The patenting of steel wire is a technique introduced as early as the 1870's in Great Britain. The basic aim of the patenting process is to produce, in a steel rod or wire, a uniform microstructure with optimum properties for wire drawing.

Payne and Smith (1968) described the patenting process as consisting of three different stages:

(i) heating to the austenitising temperature;

(ii) scaking at temperature; and

(iii) cooling to the transformation temperature.

The purpose of the soaking period is to allow for some degree of austenite homogenisation. If insufficient time is allowed at the solution treatment temperature, all the carbides may not dissolve or austenite containing severe carbon concentration gradients is produced. This affects the subsequent transformation reaction and results in an inferior final microstructure. Nucleation occurs on undissolved carbides or in carbon-rich areas with a reduced incubation time, and the adjacent area of lower carbon content also transform more rapidly to give larger quantities of pro-eutectoid ferrite (containing dispersed carbides). The result is a coarser, less homogeneous structure.

Homogeneous austenite decomposes more slowly and promotes a lower transformation temperature (Cahill and James, 1968a, 1968b).

The optimum austenitising time is considered to be that which is just sufficient to promote homogeneity of the austenite. Roberts and Mehl (1943) suggested that in order to produce austenite which is completely homogeneous with respect to carbon in eutectoid steels, a soaking period of up to ten times that required to achieve initial carbide solution is required, (Figure 2.7).

The austenitising temperature also influences homogeneity. Cahill and James (1968a, 1968b) showed that higher austenitising temperatures may improve homogeneity, but results in grain coarsening. Zubov (1972) suggested that austenitising temperatures of 150-200 °C above the critical temperature were necessary to ensure uniformity of the austenite.

The isothermal transformation can be carried out in a molten (salt or lead) bath;or by continuous cooling (the "Stelmor" process). The metallurgical reactions which occur in this stage of the process have the greatest influence on the properties of the final drawn wire.

Payne and Smith (1968) suggested that owing to the temperature difference between the rod and lead bath,

Homogeneous austenite decomposes more slowly and promotes a lower transformation temperature (Cahill and James, 1968a, 1968b).

The optimum austenitising time is considered to be that which is just sufficient to promote homogeneity of the austenite. Roberts and Mehl (1943) suggested that in order to produce austenite which is completely homogeneous with respect to carbon in eutectoid steels, a soaking period of up to ten times that required to achieve initial carbide solution is required, (Figure 2.7).

The austenitising temperature also influences homogeneity. Cahill and James (1968a, 1968b) showed that higher austenitising temperatures may improve homogeneity, but results in grain coarsening. Zubov (1972) suggested that austenitising temperatures of 150-200 °C above the critical temperature were necessary to ensure uniformity of the austenite.

The isothermal transformation can be carried out in a molten (salt or lead) bath;or by continuous cooling (the "Stelmor" process). The metallurgical reactions which occur in this stage of the process have the greatest influence on the properties of the final drawn wire.

Payne and Smith (1968) suggested that owing to the temperature difference between the rod and lead bath,

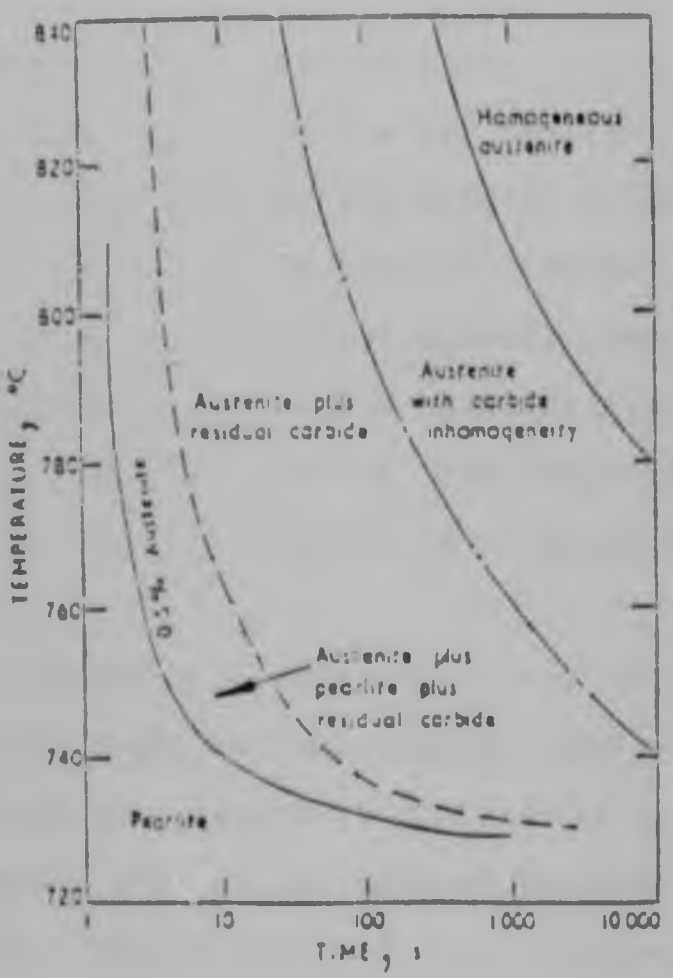

Figure 2.7 Rate of formation of austenite in eutectoid plain carbon steel. After Roberts and Mehl (1943).

cooling will occur at a mean rate according to the following formula:

$$t = \frac{rps}{2k} \log_e \frac{\theta_1 - \theta_2}{\theta_3 - \theta_2} \qquad 2.2$$

where t is the time,

r is the rod radius,

ρ is the density of material (rod),

k is the heat transfer coefficient,

s is the specific heat of material,

θ_1 is the austenitising temperature,

θ_2 is the lead temperature, and

θ_3 is the temperature at time t.

Thus assuming a constant value of k (although certain factors such as rod surface and relative velocity of coolant are known to influence this, (Armstrong and Sturgeon, 1965)); the rate of cooling depends mainly on the quench temperature and rod diameter. Cahill and James (1968b) showed that the transformation may be completed 60 °C higher than the lead bath temperature in the case of the largest rod tested (12 mm diameter), and even the smallest rod (9.6 mm diameter) completed transformation 25 °C higher.

Agarwal and Brimacombe (1981) have developed a mathematical model to predict the coupled heat flow and austenite-pearlite transformation during the cooling of eutectoid

steel rods. The model has been used to study the influence of important process variables on the transformation behaviour, under conditions of water quenching, air and lead cooling. The effect of lead bath temperature on the local temperature and fraction austenite transformed at the surface and center of a 5.5 millimeter diameter rod are shown in Figure 2.8. For a lead bath temperature of 550 °C, there will be a difference of approximately 20 °C between the centre and the surface of the rod. The model can be employed to predict the cooling requirements of a given rod size and eutectoid steel composition to achieve a desired structure (which is a function of the transformation temperature). However, the accuracy of the predictions depends critically on the availability of reliable TTT diagrams.

2.6 The Effect of Alloying Additions on the Pearlite Reaction

The effect of alloying elements on the structure, properties and transformation kinetics of steels, is well documented and a comprehensive review has been presented by Franklin, Preston and Allen (1980).

Alloying elements may influence the pearlite reaction in one or more of the following ways:

a) Partitioning - Different alloying elements may react as follows:

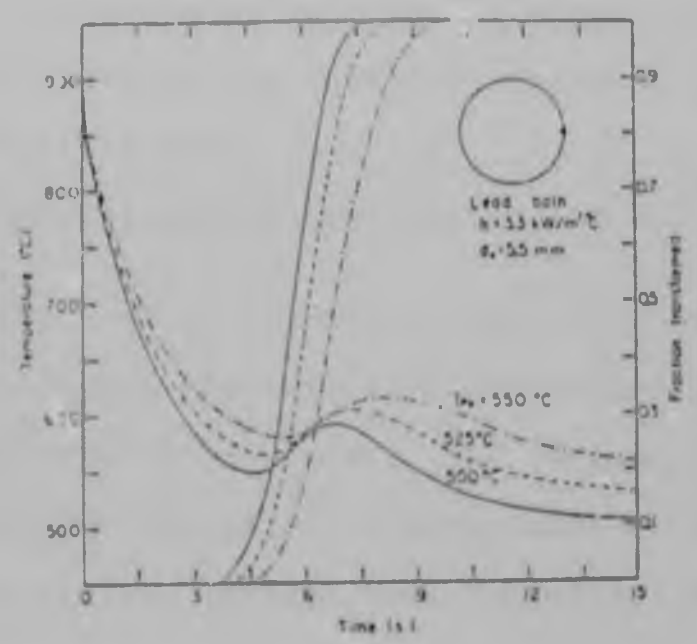

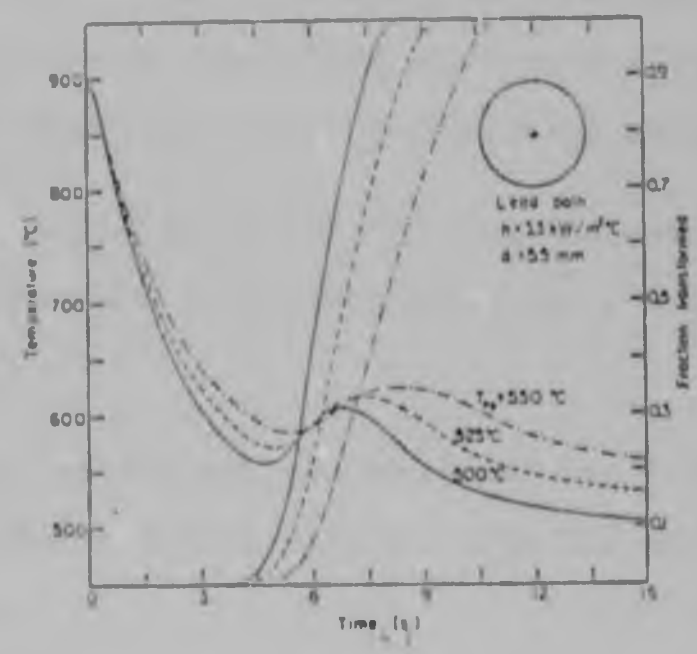

Figure 2.8 Effect of lead bath temperature on the local temperature and fraction austenite transformed at the surface and centre of a 5.5 mm diameter rod. After Agarwal and Birmacombe (1981).

(i) by partitioning to the ferrite phase;

(ii) by partitioning the cementite phase;

(iii) by non-partition.

For a detailed discussion see Section 2.6.4.

b) Precipitation - After exceeding the solid solubility limit, the alloying elements tend to precipitate in the form of hard carbide particles. The tendency of alloys to form carbides decreases in magnitude in the order: titanium, vanadium, molybdenum, tungsten, chromium, manganese.

c) Prior austenite grain size - Alloying element additions may refine or coarsen the austenite grain size. Nickel tends to refine the grain size, while silicon and chromium are grain-coarsening elements.

d) Eutectoid composition may be affected, allowing a fully pearlitic structure to be obtained with a lower carbon content.

e) The critical eutectoid temperature may increase or decrease, thereby stabilising the ferrite or austenite respectively.

f) Transformation kinetics may be affected. Manganese, chromium, molybdenum and silicon are all effective in slowing down the kinetics of the reaction, while cobalt increases it.

2.6.1 The effect on the nucleation and growth of pearlite

Since alloying elements have different tendencies to exist in the ferrite and carbide phases, it might be expected that the rate at which the decomposition of austenite occurs below T_E, would be sensitive to the concentration of alloying elements in a steel. In most cases alloying additions increase the length of the incubation period by hindering the diffusion process of redistribution of carbon and volatile elements, and also the self-diffusion of iron (Alekseyev et al 1979).

Mehl and Hagel (1956) showed that in a molybdenum steel, the nucleation rate of pearlite was reduced. A similar effect was found for manganese and nickel steels, while cobalt accelerated the transformation. Subsequent work by Bramfitt and Marder (1973) and Ridley et al (1973) confirmed that molybdenum was the most effective element in retarding the pearlite reaction. However, Brown and Ridley (1969) suggested that the pearlite nucleation rate was independent of nickel content, although the overall reaction rate was decreased due to the lowering of the eutectoid temperature.

There is a controversy over the influence of silicon. Bramfitt and Marder (1973) showed that silicon suppressed the pearlite reaction (though less effectively than

molybdenum), while Al-Salman et al (1979b) reported an increased overall reaction rate in a 2%Si eutectoid steel.*

In the case of chromium, Chance and Ridley (1978) found that the addition of 1.4% to a eutectoid steel led to a substantial displacement of the pearlite region of the TTT curve to longer times and raised the pearlite nose to higher temperatures.

A large volume of data is available on the effect of alloying elements additions on the growth rate of pearlite.

Sundquist (1969) developed a interface diffusion, local equilibrium model for the growth of pearlite, and his experimental results indicated that alloying elements affect pearlite growth purely through their effect on the thermodynamics of the system. An expression to relate the growth rate of alloy pearlite to the growth rate of plain carbon steels was given. Assuming that the alloying element did not affect the interface diffusivity of carbon, the equation for the ratio of the growth rate was given as:

$$\frac{G_a}{G} = \frac{S^2}{S_a^2} \cdot \frac{C^\gamma}{C_a^\alpha} \cdot \frac{C_a^{\gamma/\alpha} - C_a^{\gamma/cem}}{C^{\gamma/\alpha} - C^{\gamma/cem}}$$

---

* All % in this thesis are given as wt%.

where S is the interlamellar spacing (the subscript "a" refers to the alloy steel);

C^{γ} is the concentration of carbon in the austenite; and

$C^{\gamma/\alpha}$ and

$C^{\gamma/cem}$ are the carbon concentrations in austenite in the austenite-ferrite and austenite-cementite interfaces, respectively.

However, the values calculated by Razik et al (1974) using the above expression, were found to be up to four times greater than those measured.

Cahn and Hagel (1962) found that additions of molybdenum, manganese and nickel decreased the growth rate of pearlite, with molybdenum again having the most significant effect, (Figure 2.9). A similar effect of molybdenum was reported by Ridley (1976), who also showed that the pearlite growth rate in eutectoid steels was decreased by the addition of chromium, manganese, silicon and nickel. The effectiveness of manganese was found to increase sharply with increasing concentration and appeared to be comparable with that of chromium, while silicon and nickel were much less effective in reducing the growth rate.

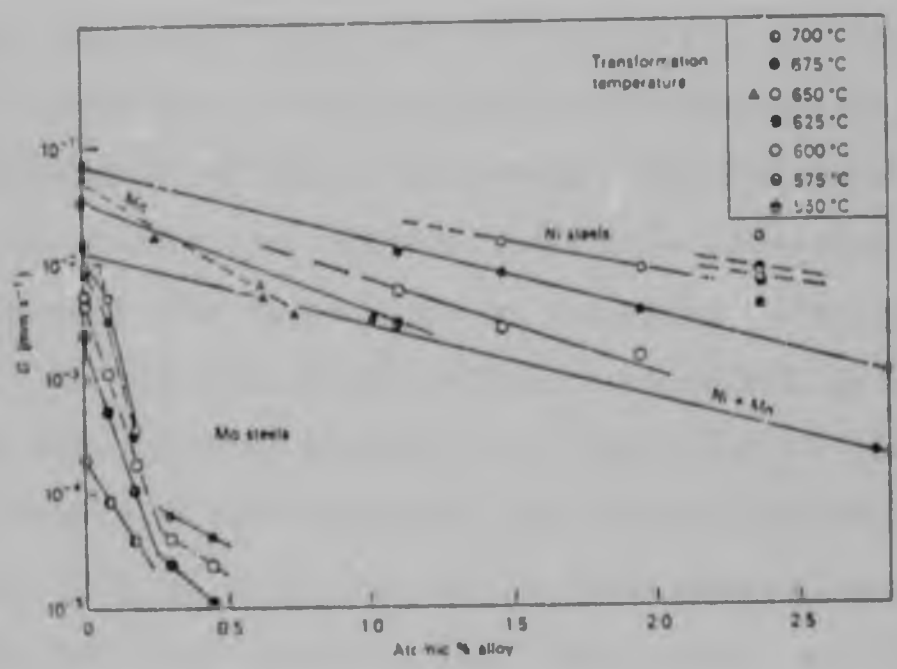

Figure 2.9 Effect of alloying elements on the rate of growth of pearlite in the temperature range 550 - 700°C. After Mehl and Hagel(1956).

In the case of manganese, Picklesimer et al (1960) found that the pearlite growth rate did not depend on the diffusion of manganese. They postulated that the decrease in growth rate was due to its influence in increasing the activation energy for those atomic movements at the moving interface which are necessitated by differences in the crystal structures between austenite and pearlite.

More recent work by Chance and Ridley (1981), on chromium eutectoid steels has shown that chromium additions produced marked retardation of pearlite growth. They proposed that at high transformation temperatures (low undercoolings) pearlite growth was controlled by boundary diffusion of chromium. However, at temperatures corresponding to the austenite bay regions produced by chromium in the TTT diagram, growth is retarded by a solute drag effect. The theory of solute drag in grain boundaries, due to impurities, has been presented by Cahn (1962) and Lücke and Stüwe (1971), and for the phase interfaces in binary alloys by Hillert and Sundman (1976).

2.6.2 The effect on the morphology of pearlite

Alloying additions can also influence pearlite morphology. Allan et al (1953) and Hahn et al (1962) reported that manganese promoted the formation of imperfect structures, consisting usually of partially globular carbides in a

ferrite matrix (rather than a well-developed lamellar structure).

Davy and Glover (1968) observed that in hypo-eutectoid steels containing 0.25 and 0.5% manganese, the pearlite tends to degenerate. However, increasing the manganese content to 1 to 2% diminished the tendency of carbides to form as boundary films and refined the pearlitic structure. At higher (5.2%) manganese contents, Cahn and Hagel (1962) reported divergent pearlite: the newly formed pearlite, starting as unresolvably fine, becoming progressively coarser as the reaction proceeds isothermally.

Pearlite degeneracy for molybdenum contents less than 0.5% was observed by Parcel and Mehl (1952), and a disordered lamellar structure was reported by Smith and Fletcher (1978) for steels containing 0.28 and 0.74% molybdenum.

2.6.3 The effect on the interlamellar spacing

A consideration of the mechanism of pearlite formation suggests that the degree of undercooling below the T_E temperature (A_1) may govern the absolute value of the interlamellar spacing (Zener, 1946). If this assumption is correct, it is of doubtful significance to compare the effect of different alloying elements simply on the basis of the absolute temperature, since the T_E temperature is affected differently by various alloying elements.

Even so, many of the studies on the effect of alloying additions on pearlite spacing are contradictory. Pellissier et al (1942) reported little direct influence of nickel and manganese additions on the spacing, while according to Mehl and Hagel (1956), nickel, manganese and molybdenum additions increase the spacing. Cobalt additions were found to decrease the spacing in both these studies.

More recently, Gladman et al (1972) also found that additions of manganese decreased the interlamellar spacing as shown in Figure 2.10.

Malik (1979) found that silicon, chromium, molybdenum and cobalt additions increased the spacing at any given undercooling. On the other hand chromium was shown to decrease the interlamellar spacing by Razik et al (1974), Zikeev and Gusienov (1979) and Cordon et al (1983).

In more complex systems, Cordon et al (1983), Mottishaw and Smith (1983) and Parsons et al (1933) reported that chromium-vanadium steels transformed to pearlite with very fine spacings. These results contradict the findings of Smith and Fletcher (1978), which suggested that these steels produced fine pearlite only in the presence of molybdenum.

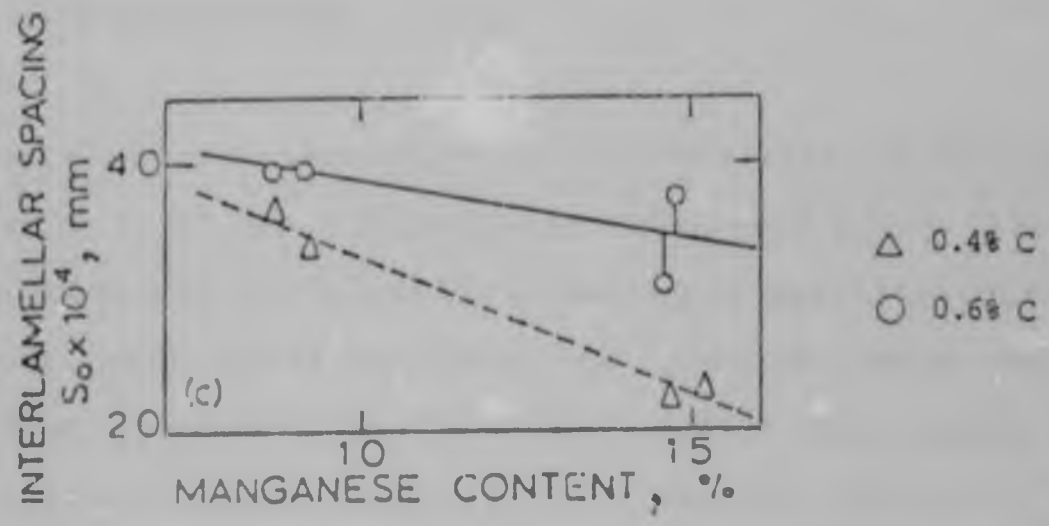

Figure 2.10 The effect of manganese content on the interlamellar spacing. After Gladman et al (1972).

The results obtained in determinations of the interlamellar spacing may also be dependent on the purity of the alloys studied. For example, the values measured by Brown and Ridley (1969) in high purity nickel steels tended to be appreciably lower than the mean true measurements reported by Pellisier et al (1942), for commercial purity steels of similar composition.

The nature of the transformation of austenite to pearlite will also be of great importance. Cahn and Hagel (1962) showed that the interlamellar spacing of pearlite formed with at partitioning would be greater than when partitioning occurs (see Section 2.6.4). This suggests that spacing versus temperature curves for alloy steels should show a distinct change in slope in the region where partitioning ceases. Support for this hypothesis has been provided by Brown and Ridley (1969), McIvor (1973) and Ridley et al (1973), although no change in slope was reported by Razik et al (1974, 1976) and Al-Salman et al (1979a, 1979b).

2.6.4 The partitioning of alloying elements

In studying the mechanism of pearlite formation, much consideration has been given to the way in which carbon and other alloying elements distribute or partition themselves between the ferrite and cementite lamellae. Partitioning

is defined as a selective diffusion or segregation of an alloy element into either ferrite or carbide. Partitioning will depend on both alloy concentration and transformation conditions.

Two different modes of growth have been observed in Fe - C - X alloys. These are:

i) growth with partition of the alloying element, X, between the parent phase (austenite), and the product phase (or phases); and

ii) growth with no partition of X between the parent and product phases.

In the cases of partitioning, the reaction is retarded considerably because of the relatively slow diffusion of the substitutional alloying elements involved.

In the case of no-partition, the alloying elements undergo no long range diffusion, although a narrow zone may be enriched or depleted, depending on whether X is an α or γ stabiliser. The reaction is controlled by the diffusion of carbon, while the alloying element affects the reaction kinetics only through its thermodynamic influence on the driving force of the reaction.

A state of para-equilibrium at the γ / α boundary, was proposed by Hultgren (1951). In this case the two adjoining phases are in equilibrium with respect to carbon only, the iron and the diffusivity of the alloying elements being too slow for redistribution.

Cahn and Hagel (1962) determined that the partitioning of subsitutional elements is a thermodynamic necessity at higher reaction temperatures, if the transformation is to proceed. At lower temperatures, there is sufficient difference in free energy to drive the reaction without partitioning.

The concept of a "no-partition temperature" was introduced by Aaronson et al (1966) and again reported by Harris and McCann (1968). For the ferrite reaction this was represented as a modified A_3 temperature below which alloying element partition does not occur. The actual temperature of the partition/no-partition transition depends on the alloy system and composition. The no-partition temperature concept is similar to the para-equilibrium concept introduced by Hultgren.

Hillert (1968) suggested that the main part of the effect of alloying elements on the transformation of austenite to ferrite, cementite, pearlite and bainite was due to the change in carbon activity. This affects the carbon

activity difference available to drive the diffusion of carbon. For low alloy contents, it was possible to calculate the change in carbon activity at the two-phase boundary from the equilibrium partition coefficient $K^{\gamma/\alpha}$ of the element between the two phases. This was defined as the ratio of the concentration of an alloying element in cementite to that in ferrite. The resultant expression obtained was of the form:

$$\ln a_c' / a_c^\circ = - \frac{K^{\gamma/\alpha} \cdot X_{Fe}^{\alpha} - X_{Fe}^{\gamma}}{X_c^{\gamma} - X_c^{\alpha}} \cdot X_M^{\alpha}$$

where a_c° and a_c' are the carbon activity values without and with the alloy content,

X_{Fe}^{α} and X_{Fe}^{γ} are the concentracion of iron in the ferrite and austenite respectively,

X_c^{α} and X_c^{γ} are the concentration of carbon in the ferrite and austenite respectively; and

X_M^{α} is the concentration of the alloying element in the ferrite.

A detailed review on the theoretical development of the partitioning problem of alloying elements to ferrite or cementite has been presented by Sharma et al (1979).

Considerable research has been carried out in order to determine partitioning in alloy steels as a function of composition and temperature. To obtain accurate data, high resolution analytical techniques are necessary and recently most emphasis has been placed on the use of field-ion microscopy/atom probe and transmission electron microscopy/energy-dispersive x-ray analysis.

According to Miller and Smith (1977) and Miller et al (1978), the atom probe is able to measure the partitioning of alloying elements and residual elements in steels with a spatial resolution of better than 1nm.

Partitioning studies using an analytical electron microscope equipped with an energy dispersive x-ray detector have been carried out by Razik et al (1974, 1976) and Al-Salman et al (1979a, 1979b).

A comparison between atom probe and scanning-transmission electron microscopy microanalysis, as techniques for studying the partitioning of alloying elements in a pearlitic steel, has been presented by Smith et al (1981).

2.6.4.1 Chromium

Chromium has been found to partition preferentially to cementite (Puls and Kirkaldy (1972), Ridley (1976), Razik et al (1976), and Mottishaw and Smith (1983)). Sharma et al (1979) observed that at high supersaturations the local equilibrium no-partition mechanism was operative and the kinetics were controlled by diffusion of carbon alone. At low supersaturations, the pearlite reaction was controlled by the boundary diffusion of chromium under local equilibrium boundary conditions. At low chromium concentrations (~ 0.1%) Miller and Smith (1977) found complete partitioning to the cementite and interface regions at reaction temperatures as low as 550 °C. Chance and Ridley (1981) also observed that chromium segregated preferentially to cementite at the pearlite reaction front for temperatures in the range 730 to 550 °C. Al-Salman et al (1979a) observed segregation of chromium to cementite at the pearlite reaction front for temperatures down to 600 °C and suggested a mechanism involving both bulk and interface diffusion.

A detailed atom probe investigation by Williams (1980) has shown evidence of extensive redistribution of chromium to cementite, at a reaction temperature of 597 °C. This was achieved via a short circuit diffusion path in the transformation interface. The partitioning of chromium did

not appear to be the rate-controlling mechanism for the reaction. The most likely explanation appeared to be rate control by a solute drag mechanism, with the partitioning of alloy elements having only a small effect.

2.6.4.2 Manganese

Puls and Kirkaldy (1972) did not detect any partitioning regime for manganese in an Fe-C-Mn steel. However, Picklesimer et al (1960) observed that manganese did partition between the ferrite and cementite during the pearlite reaction at low supersaturations.

In a study of the pro-eutectoid ferrite reaction in a number of Fe-C-Mn alloys, Purdy et al (1964) also found zero partitioning of manganese at high supersaturations, while there was definite evidence of partitioning at low supersaturations.

Miller and Smith (1977) and Miller et al (1978) observed that manganese was enriched near the interface in the cementite phase but was at approximately the same level in the centre of large cementite platelets as in the matrix (Figure 2.11).

The influence of reaction temperature was investigated by Razik et al (1974). They found that at high reaction

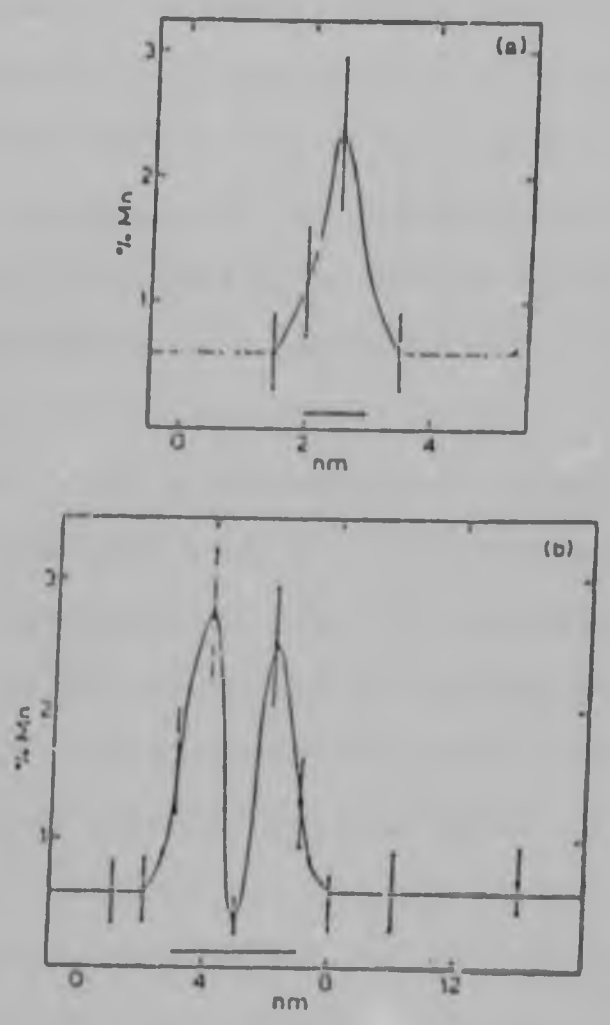

Horizontal bar represents width of carbide platelet
Vertical error bars represent $\pm\sigma$ (one standard deviation)

Figure 2.11 Manganese distribution between cementite, ferrite, and interface regions :
(a) thin (~1 nm) carbide;
(b) thicker (~4 nm) carbide platelet.
After Miller et al (1977).

temperatures the manganese partitioned preferentially to the cementite at the pearlite-austenite interface, while at lower temperatures there was no partitioning of the manganese in the freshly formed pearlite. However, manganese segregation to cementite did occur at all temperatures after pearlite had formed and continued until equilibrium values were reached.

The mechanism of manganese partitioning was studied by Mottishaw and Smith (1983). It was found that manganese partitions preferentially to the cementite by short circuit diffusion paths along the austenite-pearlite interface. Under rapid transformation conditions, however, this redistribution prccess is incomplete.

In steels containing both chromium and manganese, Al-Salman (1979a) observed simultaneous segregation of both elements. Under all circumstances the extent of manganese partitioning was less than that of chromium.

2.6.4.3 Silicon

The partitioning of silicon to pearlitic ferrite has been observed to occur extremely rapidly in the temperature range 600 to 750°C (Al-Salman et al 1979b). In a 0.7% Mn - 0.3%Si steel, Miller and Smith (1977) and Miller et al (1978) found that the silicon content of the matrix

was twice that of the cementite phase. It also appeared that the silicon level may be enriched further (and the manganese level depleted) in the ferrite phase close to the ferrite/cementite interface.

The partitioning of silicon to ferrite has been confirmed more recently by Mottishaw and Smith (1983) and Garratt-Reed and Mottishaw (1983).

2.6.4.4 Others

The partitioning of other elements is not of direct relevance to the present study. However, it may be useful to list here some references to previous work on elements which may be beneficial in future investigations.

Nickel has been found to transform in a no-partition regime in a Fe-C-Ni steel (Puls and Kirkaldy, 1972). However, in a Si-Mn steel, residual nickel and copper segregated to the ferrite-cementite interface (Miller and Smith (1977) and Miller et al (1978)).

In cobalt eutectoid steels, it has been observed that there was preferential partitioning to the ferrite at the transformation front for temperatures down to 580 °C (Ridley and Burgers, 1984).

For molybdenum, a strong carbide-former, Puls and Kirkaldy (1972) and Chance and Ridley (1978) reported partitioning into the cementite, as expected.

Similarly, Mottishaw and Smith (1983), Garratt-Reed and Mottishaw (1983) and Parsons et al (1983) found that vanadium also partitioned to the cementite.

2.6.4.5 No-partition

Picklesimer et al (1960) proposed that a no-partition temperature was detectable in a Fe-C-Mn steel, but could not determine it accurately.

Much of the subsequent work has concentrated on partitioning between austenite and pro-eutectoid ferrite. Aaronson et al (1966) studied the initial stages of transformation over a range of temperatures. No partitioning was observed for silicon, molybdenum, aluminium, chromium and copper. However, partitioning of manganese, nickel and platinum did occur above an individually characteristic critical temperature.

Razik et al (1974) examined 1.08 and 1.80% Mn alloys and observed no-partition temperatures of 683 and 649°C respectively. In a 1.29% Cr steel, a no-partition temperature was measured at 703°C (Razik et al 1976). However,

Chance and Ridley (1981) were not able to identify a no-partition temperature, although the extent of partitioning did decrease with decreasing reaction temperature.

2.3.4.6 Summary

Much research has been carried out on the effect of alloying elements in retarding the kinetics of phase transformations in steels. Nevertheless little is known about the fundamental mechanisms involved. Only very recently has experimental confirmation of partitioning between the cementite and ferrite been obtained by Smith et al (1981).

In particular, the enrichment of carbide-forming elements close to the ferrite/cementite interface has been revealed, indicating the long postulated short circuit diffusion effects. Evidence has also been found for enrichment of alloying elements near the pearlite/austenite transformation interface (Williams, 1980), indicating a solute drag effect retarding the transformation.

Fine scale chemical microanalysis in the region of the growth front using field-emission scanning transmission electron microscopy and energy-dispersive x-ray microanalysis was carried out by Garratt-Reed et al (1983) and the local redistribution of alloy elements at

the pearlite transformation front has been observed. A profile across the austenite cementite interface in a Cr-Mn-V steel is shown in Figure 2.12(a). An abrupt change occurred in the concentrations of the alloying elements, indicating that all three partition at the growth front (although not necessarily in equilibrium amounts). It was observed that those steels tested which formed "regular" pearlite colonies revealed a very complex pattern of behaviour:

i) interfaces which were concave to the growth direction showed evidence of some solute enrichment on the austenite side of the interface;

ii) interfaces convex to the growth direction showed evidence of solute depletion;

iii) planar interfaces showed no detectable solute segregation; and

iv) at deeply concave interfaces, exaggerated solute concentration peaks were sometimes found.

In a 1.6%Cr steel, in which pearlite grew with a spiky morphology, the austenite-ferrite interface was very extended in area, and relatively immobile in a direction normal to the axis of the cementite. In this case, a distinct peak was observed in the chromium distribution on the austenite side of the interface, Figure 2.12(b).

(a)

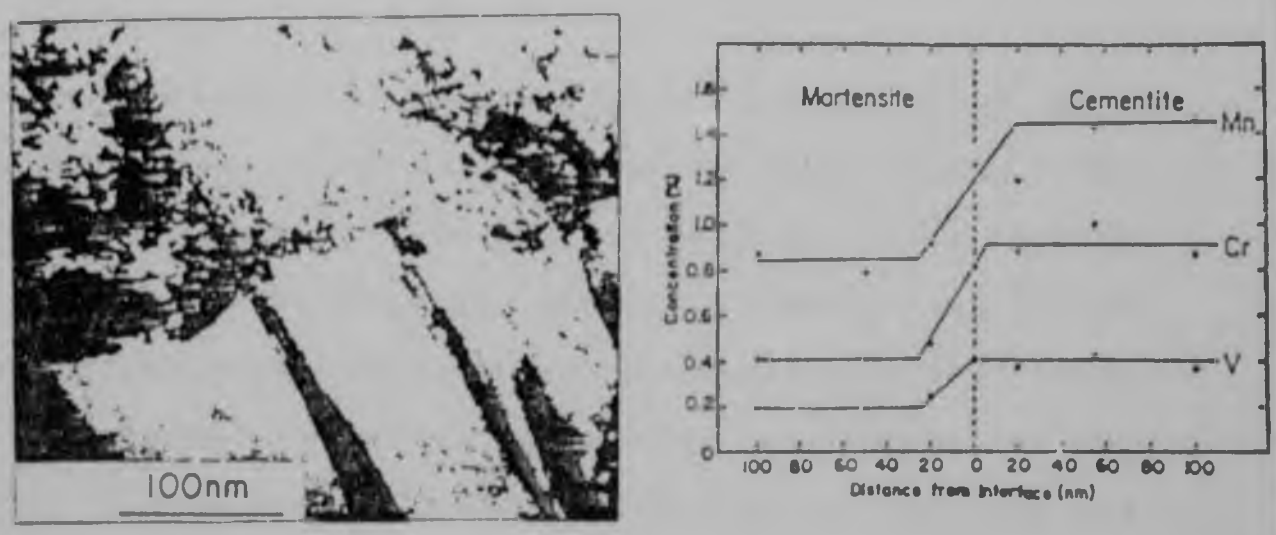

(b)

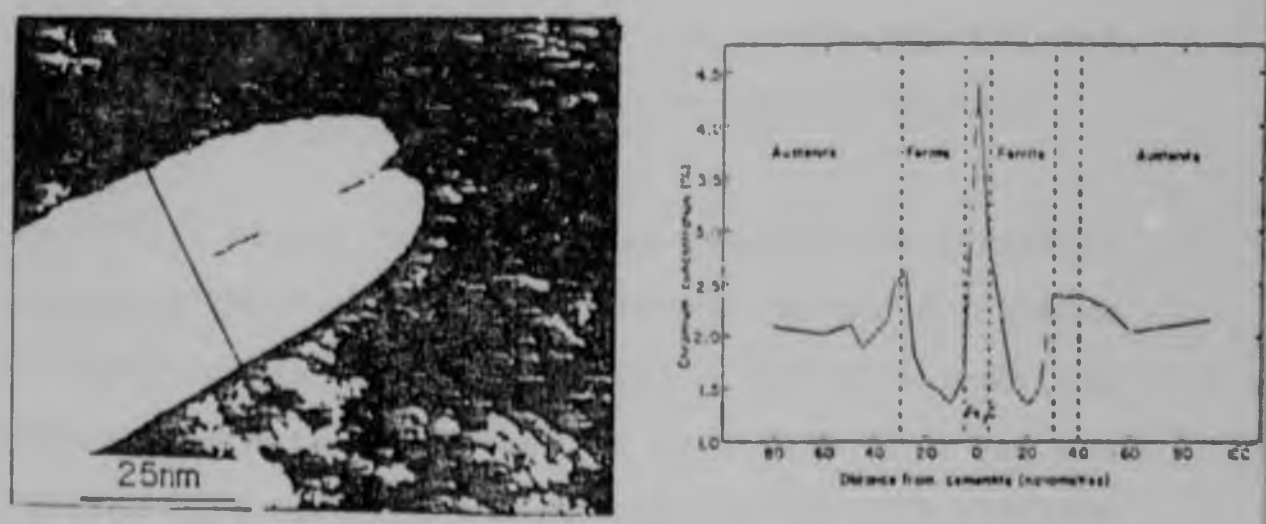

Figure 2.12 Images (left) and composition profiles (right) from indicated positions in a Cr-Mn-V steel:
(a) Growth front, with composition profile across martensite-cementite interface.
(b) Pearlite spike, with corresponding chromium profile.
After Garratt-Reed et al (1983)

2.7 The Strength and Deformation of Pearlite

The most widely used method of producing ultra high strength wires is by cold-drawing eutectoid steels. The strength obtained by this process depends on the initial strength prior to drawing (Shipley, 1962), and on the drawing reduction. The drawing speed has also been found to affect the mechanical properties (Nishimura et al, 1980): higher drawing speeds increasing the strength and decreasing the ductility of the final product as shown in Figure 2.13.

The initial microstructure must be capable of being drawn readily without fracture. Shipley (1962) and Pesche et al, (1982) have stated that the most suitable initial structure is pearlite with a fine interlamellar spacing.

Puttick (1957) found that cementite lamellae were capable of undergoing large plastic deformations and did not behave as an elastic-brittle constituent. In fine pearlite therefore, the carbide plates are also very thin and can bend during wire-drawing, rather than breaking to initiate failure (Embury et al, 1966).

According to Butcher and Pettit (1966), the main reason for the ductility of the pearlite is the discontinuous nature of the cementite lamellae. They also reported that the

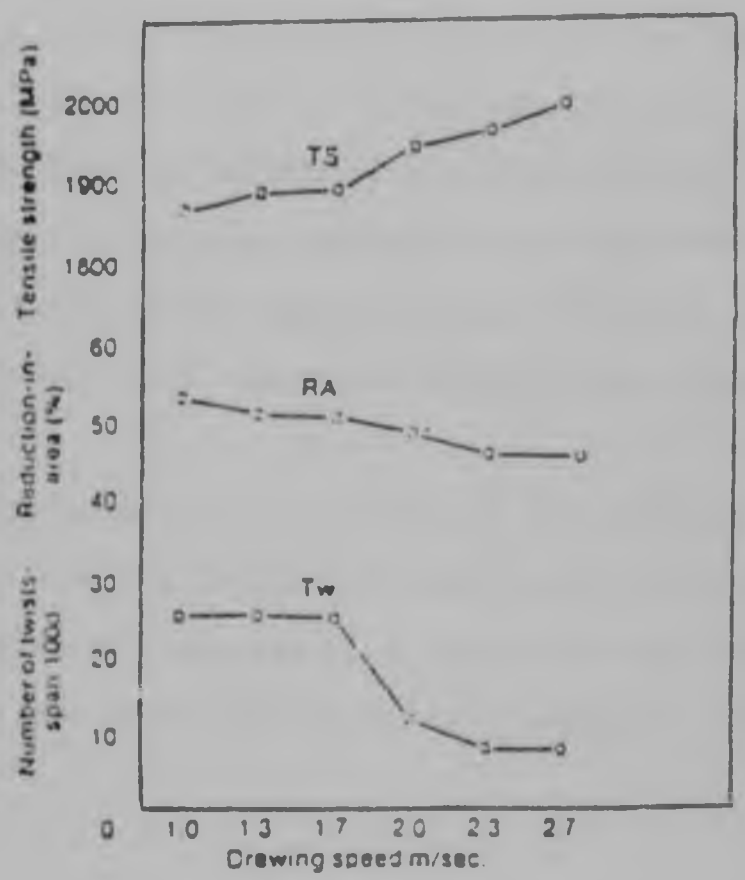

Figure 2.13 Effect of drawing speed on the mechanical properties of a 0.8%C steel. After Nishimura et al (1980).

main slip mechanisms in pearlite were slip parallel to the lamellae (as also proposed by Puttick, 1957) and slip traversing the lamellae.

Smith et al (1973) have also shown that the behaviour of the cementite phase appears to be the dominant factor in producing the high strength of drawn material. The large ductile elongation of the lamellae is responsible for the production of the fine substructure. However, they found good evidence that the cementite lamellae had fragmented.

A further advantage in the use of the finest pearlite interlamellar spacing is that the strength prior to drawing is high, and thus less drawing reduction is required to achieve a given level of tensile strength (Pickering, 1978).

In an early paper, Pickering (1965) showed that during the wire drawing process the pearlite carbide lamellae initially align themselves parallel to the drawing direction and often show kinking where they are intersected by slip bands. Following further drawing, the pearlite carbide lamellae may deform and become closer together as the ferrite slips out from between them.

The strength of drawn pearlite has typically been determined using a Hall-Petch type equation to describe the flow stress (for example by Embury and Fisher (1966), Hyzak and Bernstein (1976), and Marder and Bramfitt (1976)). The flow stress, σ_f is given by:

$$\sigma_f = \sigma_0 + k_y S^{-\frac{1}{2}} \qquad 2.3$$

where σ_0 is the apparent lattice friction stress;

k_y (the Hall-Petch proportionality constant) is a parameter representing the efficiency with which barriers block dislocations; and

S is the effective interlamellar spacing.

It can be seen from the above equation that the flow stress or yield stress may be increased by decreasing the interlamellar spacing, S, or by increasing the friction stress of the ferrite matrix, σ_0 .

Embury and Fisher (1966) performed the first systematic thin foil investigation of drawn pearlite. They found that the drawn material consisted of cells elongated in the drawing direction. The cell dimension perpendicular to the drawing direction was observed to decrease with increasing drawing strain. A log-log plot of the flow stress and the measured separation of the substructural barriers (the cell

dimensions) gave a linear relationship. The slope of this plot indicated that the stress was related to (cell size)$^{-\frac{1}{2}}$. Thus the cell walls are the barriers responsible for strengthening.

These authors then proposed an equation which accounted simply for the observed relationship between strength and prior strain of these wires:

$$\sigma_f = \sigma_o + \frac{k_y}{\sqrt{2S_o}} \exp(\varepsilon/4) \qquad 2.4$$

where σ_o is the lattice friction stress;

S_o is the original substructural spacing;

k_y is the Hall-Petch proportionality constant;

ε is the true wire drawing strain *; and

σ_f is the resultant flow stress of the material.

In a later study, Embury (1971), related the increase in flow stress, $\Delta\sigma_f$, to the dislocation densities in the cell walls, p_f , through the expression:

---

* True strains are used throughout this thesis. They are given by the equation $\varepsilon = 2\ln(D_o/D)$, where D_o and D are the rod and wire diameter, respectively.

$$\Delta\sigma_f = 0.17\, G\, b\, (p_f)^{\frac{1}{2}}$$

where G is the shear modulus; and

b is the Burger's vector.

Langford (1970) attempted to modify these findings in order to adapt the work hardening model to predict more closely the actual strength attained during wire drawing of pearlitic steels. He incorporated plane strain preferred orientation effects into the original relationship, obtaining the following equation:

$$\sigma = \sigma_o + \frac{k_y}{\sqrt{\beta S_o}} \cdot \exp\left(\frac{\varepsilon_{cm}}{2}\right) \qquad 2.5$$

where β is between 1 and 2;

σ_o, S_o, and k_y are as defined previously;

ε_{cm} is the strain in the cementite; and

σ is the strain-hardening rate.

This equation assumes a Hall-Petch type relationship between flow strength and substructural features (interlamellar spacing or cell size) and locally homogeneous plane strain elongation within the wire. Equation 2.5 produces the same numerical results as the Embury and Fisher equation (2.4), but corrects their

assumption of homogeneous axially symmetric elongation and the absence of dynamic recovery.

In a subsequent paper, Langford (1977) stated that his previous conclusions were erroneous, and proposed that the exponential strain hardening of axisymmetrically elongated pearlite is unaffected by the local plane strain elongation of individual colonies caused by the <110> wire texture.

Lenasson and Bergström (1976) developed a dislocation model for the true stress (σ) and the true strain (ε) during plastic deformation of pearlitic steels, taking into account that large strain gradients are generated in the pearlite and in the free ferrite. They proposed a relationship of the form:

$$\sigma = \sigma_{io} + \alpha G b \left\{ \frac{U_o}{\frac{0.5}{k} + \Omega_e} \left(e^{\frac{\varepsilon_m}{2}} - e^{-k\Omega_e \varepsilon_m} \right) + \rho_o e^{-k\Omega_e \varepsilon_m} \right\}^{\frac{1}{2}} \qquad 2.6$$

where

σ is the true stress ;

σ_{io} is a strain independent friction stress;

α is a constant;

G is the shear modulus;

b is the Burger's vector;

ρ_o is the dislocation density when $\varepsilon = 0$;

ε_e is the effective true average strain in the ferrite lamellae and in the free ferrite;

ε_m is the true macroscopical strain;

Ω_e is the effective probability of dislocation re-mobilisation in the ferrite;

Ω is the macroscopical Ω_e - value;

$k = \frac{\varepsilon_e}{\varepsilon_m}$ is a measure of the strain gradients (in this case k is assumed to be strain independent); and

U_o is the rate of immobilisation of mobile dislocations.

This factor, U_o , is related to the initial interlamellar spacing, S_o , by the equation

$$U_o = \frac{1}{\phi\, b\, 2S_o}$$

where $\phi = 0.5$ in bcc metals.

The authors obtained excellent agreement between equation 2.6 and the experimental results.

In situ studies of the deformation and fracture of pearlite were carried out by Porter et al (1978a, 1979). It was found that there were considerable differences in behaviour between fine and coarse pearlite. The greatest differences

appeared when the lamellae were aligned parallel to the tensile axis. Coarse pearlite deformed inhomogeneously with strain localised in narrow slip bands, whereas fine pearlite exhibited a much more uniform distribution of strain. The cementite in coarse pearlite showed only limited ductility and fractured without thinning, whereas in fine pearlite, cementite appeared ductile and was able to neck down into fragments. Figure 2.14 shows a dislocation model to account for the fundamentally different behaviour of coarse and fine pearlite with axially aligned cementite.

The stress at the tip of the pile-ups, τ_p , is approximately given by:

$$\tau_p = \frac{k\,D}{b\sqrt{2S_o}}\,\varepsilon_p$$

Where D is the distance between active slip planes;

S_o is the interlamellar spacing; and

ε_p is the plastic strain

In the case of fine pearlite with very small D, significant pile-up stresses will not develop, and fibre stresses tend to dominate tensile deformation. In coarse pearlite the pile-up stresses are dominant.

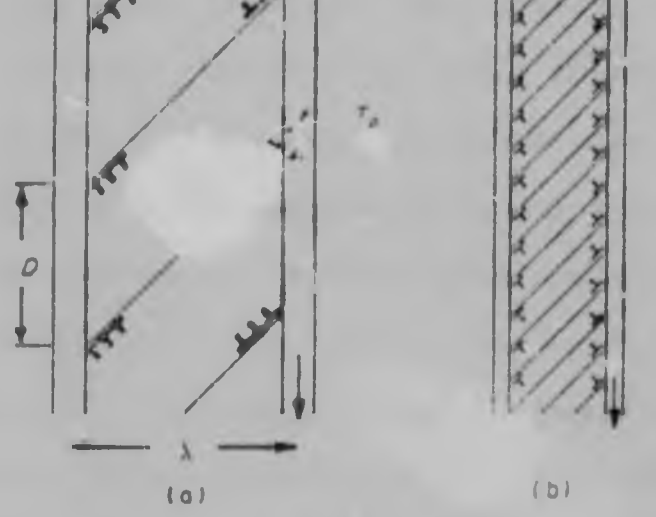

Figure 2.14 A dislocation model for the deformation of pearlite aligned parallel to the tensile axis, illustrating, (a) coarse slip and (b) fine slip in the ferrite.
After Porter et al (1978a).

2.7.1 The effect of the interlamellar spacing

According to Gensamer et al (1942), the resistance to deformation of a metallic aggregate consisting of a hard phase dispersed in a softer one is proportional to the logarithm of the mean straight path through the continuous phase. In lamellar structures this means the average distance from one plate to the adjacent one, averaged for all directions from perpendicular to parallel to the plates. If the pearlite colonies were infinite in size and the plates were perfectly plane, this average would be infinite, however, in reality the plates are always wavy and the pearlite colony size is always limited.

While it is universally agreed that the strength of pearlite is determined by the interlamellar spacing, there are differences regarding the precise form of the relationship. Hugo and Woodhead (1957) suggested that the yield stress, ultimate tensile strength and the hardness could be related by linear equations to the interlamellar spacing, to the logarithm of the interlamellar spacing, or to the reciprocal of the square root of the spacing; the last two relationships being the most satisfactory. The work of Shipley (1962) supported this hypothesis (Figure 2.15).

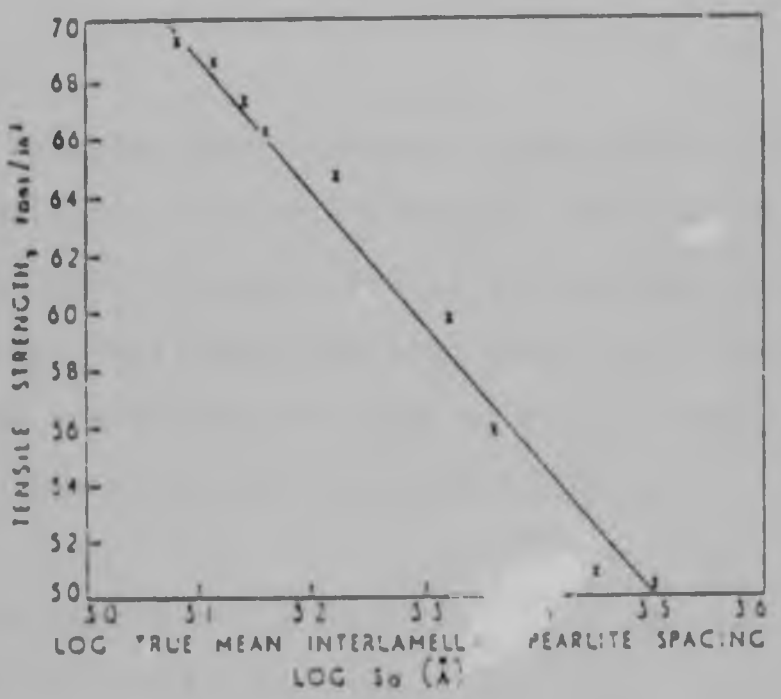

Figure 2.15 Relationship between interlamellar spacing and tensile strength of a 0.65%C steel. After Shipley (1962).

The yield strength of pearlite was observed to be solely dependent on the interlamellar spacing (Marder and Bramfitt, 1976). The relationship was given as:

$$\sigma_f = 139 + 46.4\ S^{-1}$$

It has also been suggested (Takahashi et al, 1980) that the ductility of wires is uniquely defined by the interlamellar spacing. Irrespective of the amount of drawing and steel grade; they concluded that ductility could be improved when a wire was designed to give a final cementite spacing of 28nm in the as-drawn condition.

A different point of view was given earlier by Dewey and Briers (1966) who considered that the high strength was directly related to the fine ferrite grain size, while the role of the cementite lamellae was to stabilise this grain structure during the deformation process.

For vanadium - containing steels, Chance and Ridley (1981) observed that maximum strengthening at a given vanadium level will be obtained at the highest cooling rate at which fine lamellar spacing can form.

2.7.2 The effect of prior austenite grain size

In most studies, it has been assumed that the size of the pearlite colonies is not a significant variable affecting the mechanical properties of steels (e.g. Gladman et al (1972)). It is customary, therefore, to express the grain size of eutectoid steels as the grain size of the prior austenite.

The prior austenite grain size (d) can be related to the yield strength through the Hall-Petch equation:

$$\sigma_f = \sigma_o + k\, d^{-\frac{1}{2}} \qquad 2.7$$

Where σ_f is the flow or yield stress;

σ_o is a constant which represents the resistance of the lattice to the movement of dislocations during yielding;

k is a constant called the dislocation unlocking parameter or Hall-Petch proportionality constant; and

d is the prior austenite grain size.

Hyzak and Bernstein (1976) found that equation 2.7 worked well for undeformed eutectoid steels. However, they did suggest that a structural sub-unit of constant ferrite orientation controls the yield strength and that this sub-

unit is controlled by, but is not identical to, the prior austenite grain size. A value of 0.26 MPa.m for k was reported by Karlsson and Linden (1975).

A different linear relationship was found to fit the data from the thermomechanical treatment of eutectoid steels obtained by out by Querales and Bryne (1980):

$$\sigma_f = 202 + 1.3\, d^{-\frac{1}{2}}$$

Where σ_f is the MPa; and
d is in meters

They explained that the differences in reported values of k may arise because the Hall-Petch equation was originally intended for application to more isotropic materials.

Querales and Bryne also considered that the prior austenite grain size and the interlamellar spacing affect the yield strength simultaneously. Multiple linear regression analysis, produced an equation of the form:

$$\sigma_f = 71.77 + 0.96\, d^{\frac{1}{2}} + 0.14\, 10^{-1}\, S_o^{-1}$$

Where the stress terms are in MPa: and
d and S_o are in meters.

However, it should be emphasised that the general consensus is that the yield strength is independent of the prior austenite grain size, as shown by Marder and Bramfitt (1976) and reproduced in Figure 2.16. It is seen that at a given prior austenite grain size there is a factor other than grain size that affects yield strength. This factor may be either nodule diameter and/or interlamellar spacing.

2.7.3. The effect of alloying elements

The effect of alloying elements on the strength of pearlitic steels has been studied extensively. Since different research groups studied the combined effect of different alloying elements, it is difficult to give a review of the effect of each alloying addition separately.

Silicon is a well known solid solution strengthener of ferrite. Bouse et al (1978) found that silicon additions in the region of 0.20% increased the yield strength by approximately 10%. Takahashi et al (1980) have also shown that the highest as-patented and as-drawn strengths were obtained for the steel with the highest silicon content tested (0.99%). Conversely, Franklin et al (1980) reported that increasing additions of silicon from 0.32% to 0.85% did not appear to enhance the strength levels following patenting.

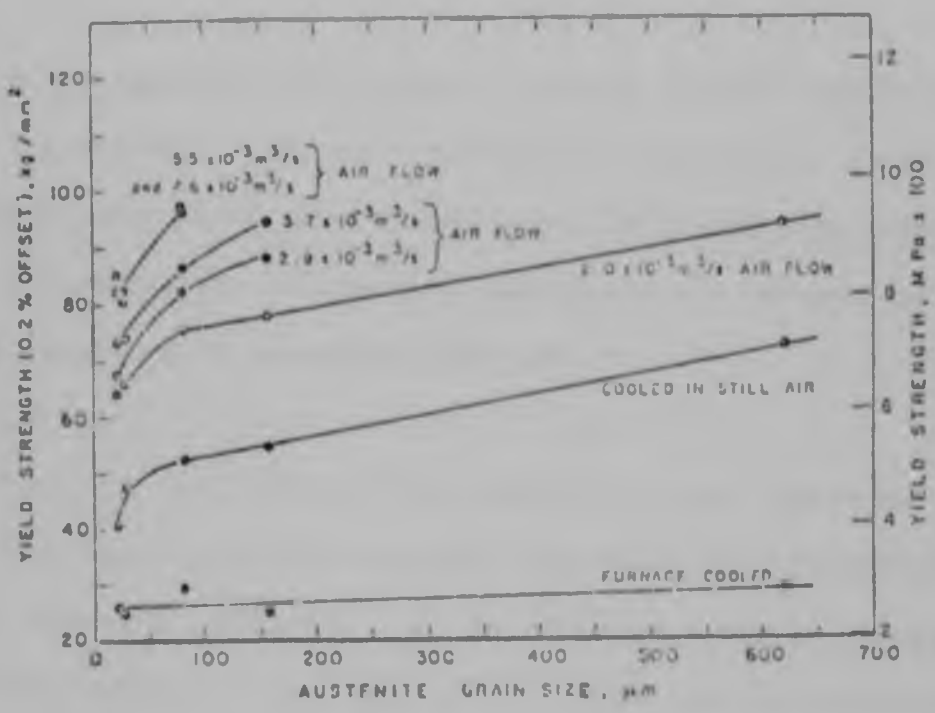

Figure 2.16 Effect of prior austenite grain size on the yield strength of a Fe-0.81%C binary alloy. After Marder and Bramfitt (1976)

Manganese is also known to be a solid solution strengthener. Additionally, it can also reduce the interlamellar spacing of pearlite (Gladman et al, 1972). Bouse et al (1978) found that manganese additions of about 0.35% increased strength by approximately 11%.

The investigation of Franklin et al (1980) confirmed the view given by Cahill and James (1968a), that lower manganese contents were beneficial in promoting higher as-patented strength. However, additions in excess of 1% led to the problem of microsegregation.

Chromium is effective in reducing the spacing of the pearlite structure through an increase of transformation energy (Patent 1404796). It is claimed that an as-patented tensile strength in excess of 1470 MPa can be achieved in a 1% chromium/niobium steel. However, Franklin et al (1980) reported low as-patented strength levels (1100 MPa) in a steel containing 0.5 per cent chromium and 0.027 per cent niobium.

Marich and Curcio (1978) reported that additions of manganese and chromium to a eutectoid led to an increase in strength. This was attributed to the decrease in transformation temperature which in turn promoted finer interlamellar spacings.

It has been shown that small concentrations of molybdenum have a marked effect on the hardenability of steel. However, Franklin et al (1980) reported no significant increase in strength on increasing the molybdenum content from 0.13 to 0.26%; contradicting reports by Smith and Fletcher (1978) in which increasing the molybdenum content to 0.30% raised the yield strength by developing a highly refined transitional pearlitic microstructure. Additional molybdenum did result, however, in bainite formation and a decrease in strength.

Vanadium forms a carbide stable up to 980°C. Alloying with vanadium may influence mechanical properties in one of the following ways:

(i) by refining the prior austenite grain size(although this does not effect the yield strength ; see Section 2.7.2);

(ii) by influencing the interlamellar spacing; or

(iii) it may provide precipitation hardening of ferrite.

Lewis and Ward (1978) reported that 0.29% vanadium additions to a pearlitic steel did indeed increase strength. Smith and Fletcher (1978) found that an addition of 0.06% vanadium to a chromium-molybdenum steel resulted in notably higher hardness and strength with no significant loss of ductility. However, they have shown that vanadium without molybdenum was not very effective in developing a

fine pearlite microstructure. Conversely, Mottishaw and Smith (1983) reported that under continuous cooling transformation conditions, combined additions of chromium and vanadium to plain carbon eutectoid steels produced strength increments of up to 200 MPa. Again this was due to the refinement of pearlite interlamellar spacing, and secondary precipitation strengthening of the ferrite phase.

Ridley et al (1981) reported that the strength of eutectoid steels containing up to 0.22% vanadium increased as the cooling rate was increased; and for a given cooling rate, as the vanadium content was increased.

2.7.4 The work hardening rate of pearlite

Honeycombe (1981) describes work (or strain) hardening as the ability of a metal to become stronger as it deforms, and perhaps as the most impressive of the plastic properties. Work hardening is governed by the generation and interaction of dislocations. Embury et al (1966) have proposed that for large plastic strains, strain hardening arises from the process of reducing the substructural barrier spacing during the working process rather than by an increase in the overall forest dislocation density.

During the wire drawing process the ferrite work hardens, and forms a dislocation substructure, and the carbide tends to develop a fibrous arrangement. This was shown by Embury and Fisher (1966), Embury et al (1966) and Chandhok et al (1966).

Karlsson and Linden (1975) attributed the high work hardening rate of pearlite to the load transfer from ferrite to cementite, with an important contribution from constraint effects of the hard phase on ferrite. The work-hardening rate was found to be independent of the initial hardness or yield stress and the interparticle distance, but was determined by the cementite morphology. Conversely, Pickering (1978) proposed that the higher the initial strength, the greater is the work-hardening rate, due to the smaller interlamellar spacing.

Shipley (1962) has shown that the rate of work hardening of pearlite increases with carbon content. However, in torsion tests Aernoudt and Sevillano (1973) found little variation in work hardening rate with carbon content (Figure 2.17).

Schmidt and Miller (1982) have shown that precipitation during deformation may enhance strain hardening by the formation of a fine dispersion of precipitates which inhibit dislocation motion. Precipitation may also cause strain softening due to depletion of solutes in the matrix.

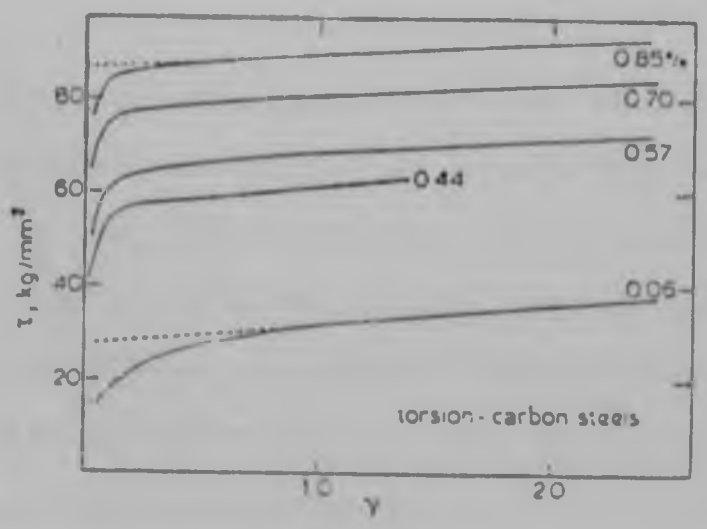

Figure 2.17 ress-strain curves of steels with different rbon contents (in torsion).
After Aernoudt and Sevillano (1973)

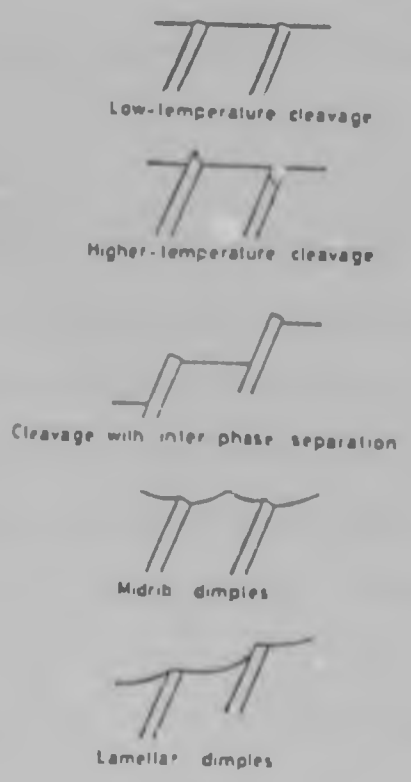

Figure 2.18 Suggested interpretations of the observed types of fracture in pearlite.
After Lindborg (1968)

2.7.5 The fracture of pearlite

The effect of plastic deformation on the flow and fracture characteristics of pearlitic steels has been extensively reported in the literature (e.g. Puttick (1957), Barnby and Johnson (1969), and Rosenfield et al (1972)). Plastic deformation preceding tensile fracture and the effect of such plastic deformation on crack nucleation and propagation have been studied.

Lindborg (1968) reported a distinct lamellar pattern on the fracture surface of a pearlitic steel and suggested that the ferrite phase governed cleavage while cementite controlled dimple formation. The interpretation of the types of fractures observed by this author are reproduced in Figure 2.18.

Miller and Smith (1970) reported microcracks found in lamellar pearlite colonies during tensile fracture, the angle between the cracks and the tensile axis showing a maximum frequency of just over 50°. The pearlite cracks were most readily observed when the cementite lamellae were oriented parallel to the tensile axis.

Pepe (1973) found that the most obvious microstructural alteration resulting from cold working a plain carbon eutectoid steel to different reduction ratios was the

fracture mode transition from cleavege to shear as the reduction ratio and strength increased.

Henry (1970) determined quantitatively the relationship between microcracking and strain rate for pearlitic microstructures. This author, as well as Rosenfield et al (1972) showed that the yield and tensile strength for a 0.69%C. - 0.7%Mn steel increased with increasing strain rate; and kinking and microcracking were observed in the deformed pearlite lamellae.

Gladman et al (1972) found the pearlite colony size to be an important parameter in controlling the fracture toughness of pearlitic steels; while Hyzak and Bernstein (1976) as well as Bouse et al (1978) came to the conclusion that the effect of colony size on the fracture process was small.

A more direct way to demonstrate which microstructural parameter controls toughness is to measure the fracture facet size and relate it to the microstructure. This type of quantitative metallography was reported by Bernstein et al (1976). They identified the facet unit as a region of constant ferrite orientation, whose size changed with the austenite grain size and, to a much smaller extent, with the pearlite colony size. In a high carbon steel it was observed by Park and Bernstein (1977), that while the

fracture path often changed direction at a colony boundary, the crack more often continued as a single cleavage facet across a number of pearlite colonies. In a later publication by the same authors (1979) the critical fracture unit was shown to be a region where the ferrite and the cementite of contiguous colonies share a common [100] orientation. The size of the orientation unit was controlled by the prior austenite grain size.

According to Marder and Bramfitt (1976), fracture stress is directly related to interlamellar spacing, S_o . The fracture stress, σ_f, is described by the following equation:

$$\sigma_f = 436.4 + 98.1\ S_o^{-1}$$

2.8 The Strain Ageing of Pearlite

Strain ageing is a process that involves the segregation of interstitial atoms to dislocations. If after stressing through the yield point a crystal is unloaded and then restrained immediately, the yield point does not return (Figure 2.19). On the other hand, if the crystal is rested for a long time at room temperature (in the case of iron) or a shorter time at an elevated temperature (50 to 150°C), the yield point returns after subsequent restraining. This

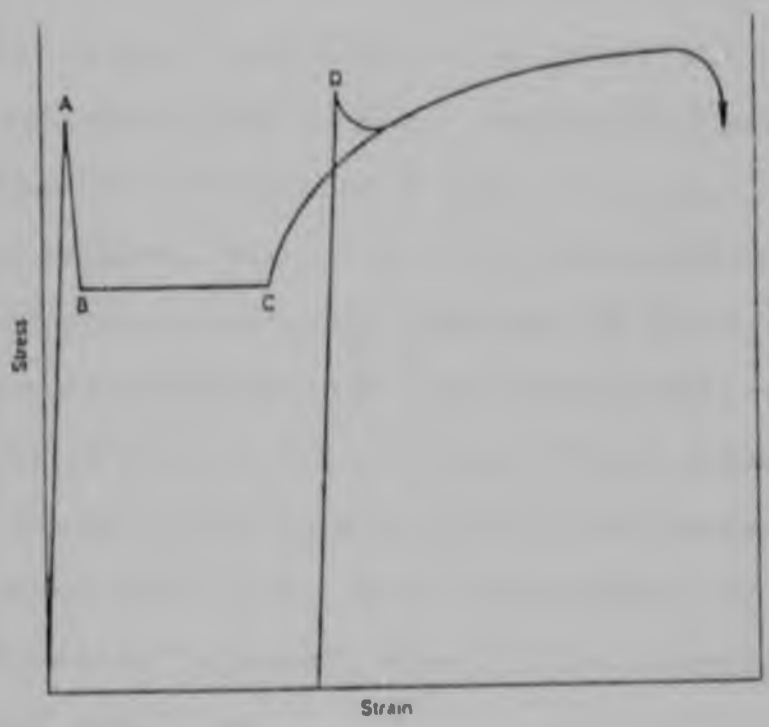

Figure 2.19 Schematic diagram of yield phenomena as shown in a tensile test. After Honeycombe, (1981)

phenomenon is known as strain ageing and involves the diffusion of solute atoms to new dislocations generated during the prior deformation, which are thus rendered immobile.

Each dislocation gathers round itself an "atmosphere" of solute atoms . The atmospheres are immobile and the dislocations are anchored along their entire length to fixed positions in the crystal. To produce plastic flow in such cases the dislocations have to be pulled away from their atmosphere, and to do this, the applied force must exceed the anchoring force. Because of the strong affinity between a dislocation and its atmosphere, this applied force will in many cases be larger than the force needed to keep the dislocations in motion once they have escaped from their atmospheres. When the dislocations are anchored and the deformation is purely elastic the material is in this strain aged condition.

According to Nabarro, the activation energy for strain ageing is the same as that for the diffusion of carbon and nitrogen in ferrite, while the time for strain ageing is of the same order as expected for the formation of atmospheres (see Cottrell, 1953).

Strong yield points are observed in b.c.c. single crystals because dislocations are firmly locked by interstitial

atoms such as carbon, oxygen and nitrogen. In polycrystalline metals, phenomena associated with the yield point are intensified, and while a sharp yield can be eliminated by the use of zone purified metal, metals of normal purity levels usually exhibit yield phenomena under appropriate testing conditions.

Polycrystalline iron exhibits strain ageing in the same way as single crystals. According to Honeycombe (1981), substantial strain ageing can occur at carbon levels around 0.002%, and as little as 0.001-0.002% nitrogen. Nitrogen is more effective because its residual solubility in α-iron (10^{-4} wt% at 20 °C) is substantially greater than that of carbon (5.10^{-5} wt%). The easiest solution to minimise the effects of nitrogen is to add small concentrations of strong nitride formers such as aluminium, titanium or vanadium, which reduce the nitrogen in solution to very low levels. Guerrieri et al (1983) reported that additions of around 0.04% aluminium have been found to be sufficient to combine almost all nitrogen (0.004%) as aluminium nitride.

The formation of interstitial atmospheres at dislocations requires diffusion of the solute. As both carbon and nitrogen diffuse very much more rapidly in iron than substitutional solutes, it is not surprising that strain ageing can take place readily in the temperature range 20 to 150 °C.

Phosphorus has also been mentioned as a strong substitutional hardening element which has a deleterious effect upon extreme drawability. This has been attributed to a change in the ageing embrittlement caused by nitrogen (Franklin and Allen, 1980). In respect of the nitrogen ageing behaviour it has been observed that there is an interaction with the elements phosphorus, carbon, oxygen and manganese, with the grain size and the cooling rate.

Yamada et al (1983) examined the strain ageing of high carbon steel wires and described methods of preventing ageing embrittlement during wire drawing and during storage at room temperature after drawing. A schematic illustration of the effect of ageing temperature on the properties of high carbon steel wire is reproduced in Figure 2.20. They proposed that the process of ageing is divided into three stages. The first stage occurs below approximately 150 °C. In this stage carbon and nitrogen dissolved in ferrite lock dislocations. In fine pearlitic steels, the amount of dissolved carbon in ferrite is small and no noticeable change in tensile properties takes place when the free nitrogen content is small. The second stage appears at a temperature above about 150 °C. Tensile strength and 0.2% proof stress increase but ductility decreases drastically with ageing, and the internal friction associated with the motion of dislocations decreases. The dissolution of some portion of lamellar

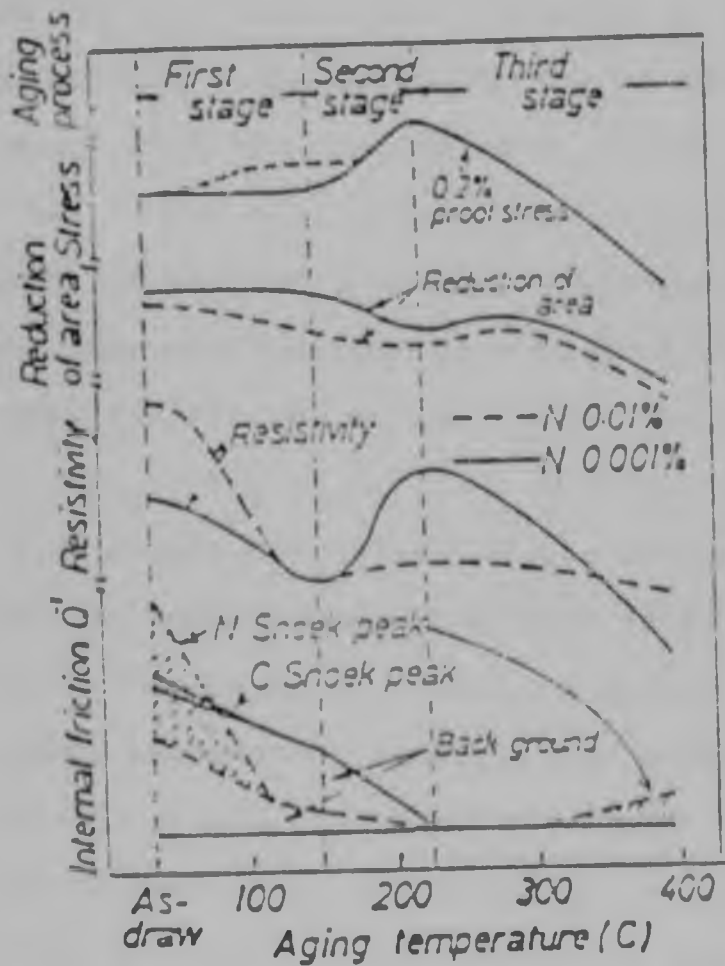

Figure 2.20 Schematic illustration of the effect of ageing temperature on the properties of high carbon steel wires. After Yamada et al (1983)

cementite is thought to take place, and the carbon atoms produced again led to dislocation locking. The third stage corresponds to overageing and leads to a decrease in the tensile strength.

2.8.1 The effect of drawing conditions

The high level of deformation present in a heavily drawn wire presumably aids the migration of carbon atoms. The presence of point and line defects in both the ferrite and cementite phases will enhance carbon migration and the refinement of the interlamellar spacing will reduce the distance over which carbon atoms have to move in order to effectively pin all the mobile dislocations.

Figure 2.21 shows the effect of the variation in drawing speed on the ageing characteristic of finished wires as obtained by Yamada et al (1983). A drastic change in 0.2% proof stress and tensile strength was observed in the wire drawn at 0.05 m/min by ageing at around 200°C. However, there was no such significant change in properties in the wire drawn at 300 m/min, indicating that second stage ageing had progressed during drawing in the latter wire, but not in the former.

Stephenson et al (1983) developed a shear test in order to study the effects of cold work and artificial ageing.

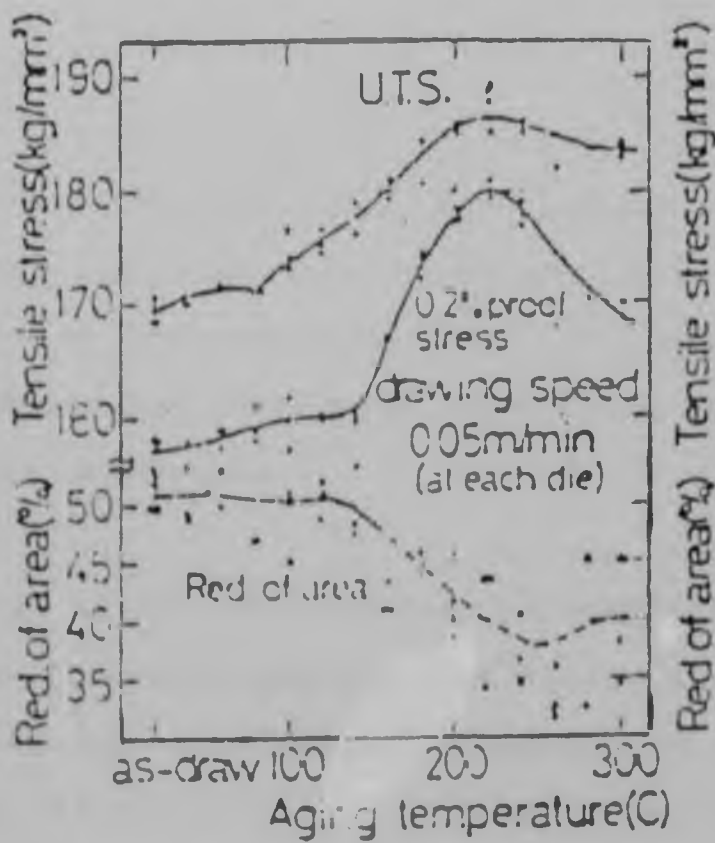

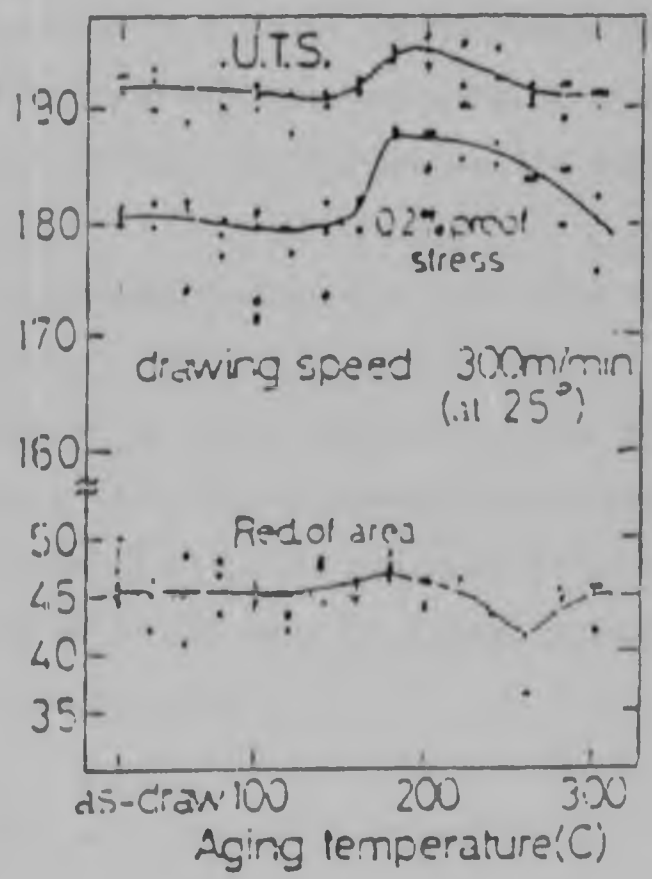

Figure 2.21 Effect of variation in drawing speed on the change in room temperature tensile properties due to ageing for 5 minutes.
After Yamada et al (1983)

According to their findings, wires manufactured by drawing to high overall strains have been shown to be more susceptible to the embrittlement effect of strain ageing, to such an extent that the ageing mechanism appears to operate at room temperature.

Nishimura et al (1980) carried out intermediate ageing treatments at different temperatures during the drawing process. The change in mechanical properties in the drawn wire resulting from the ageing treatment are shown in Figure 2.22. It can be seen that when the ageing temperature approaches the "blue brittleness region", the yield and tensile strength increase while the number of twists, reduction in area and elongation are reduced.

The effect of intermediate ageing was also reported by Yamada et al (1983). They suggested that if a wire is heated extensively at an intermediate die and goes through second stage ageing but is not heated above approximately 100 °C at the finishing die, the mechanical properties of the wire so produced still tend to change markedly during storage at room temperature.

Great emphasis has been placed on the need for direct water cooling of the wires at the die exit in order to control excessive rises in temperature, thus preventing or minimising strain ageing and improving wire ductility. This has

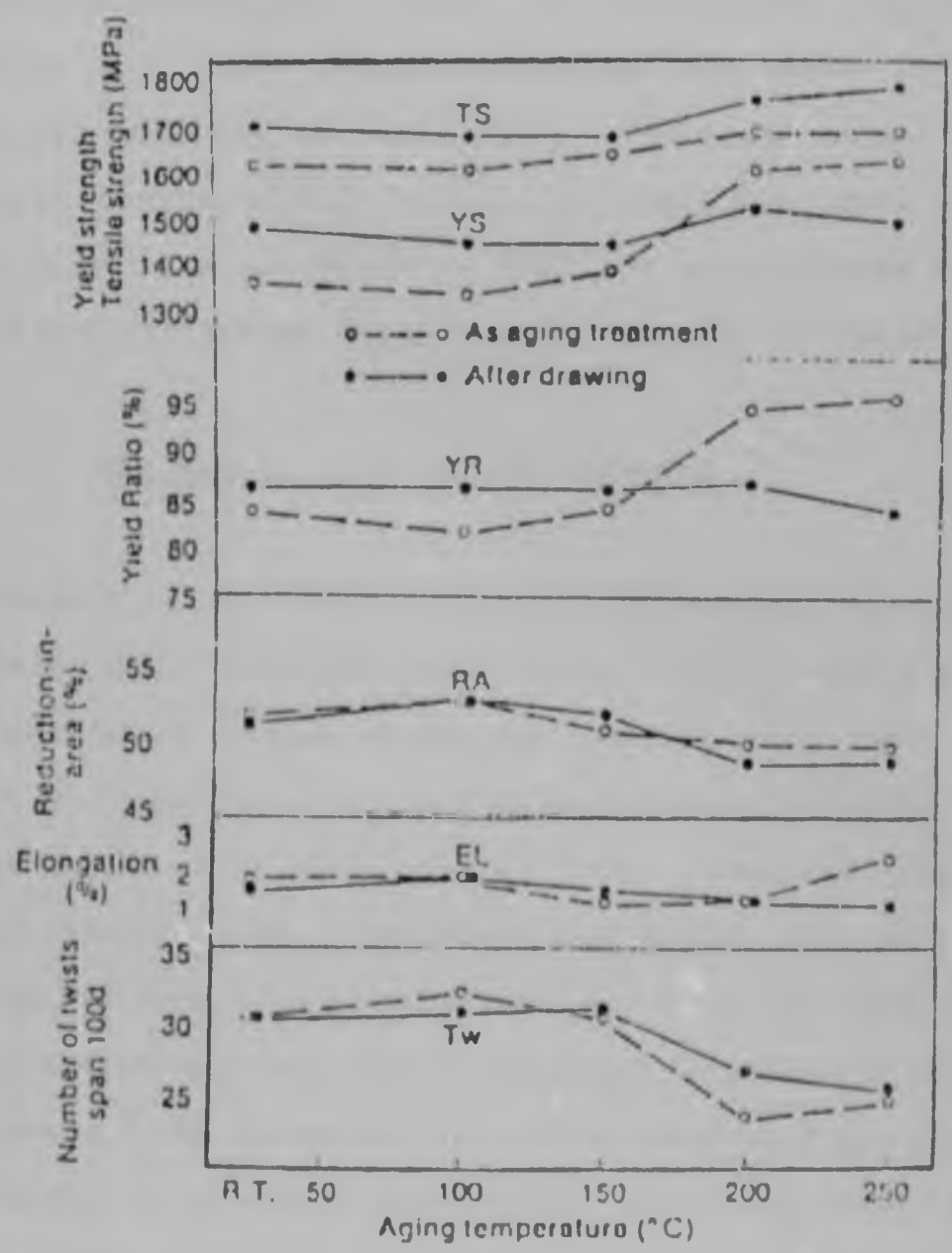

Figure 2.22 Change in mechanical properties resulting from an ageing treatment.
After Nishimura et al (1980)

been studied by (among others), Liska (1980), Nishimura et al (1980), Guerrieri et al (1983), Yamada et al (1983), and Pawelski and Keuper (1984). In Figure 2.23 the ratio of outlet and inlet temperatures of the wire is plotted against the rate of water flow. The graph shows that the drop in temperature is greater at small diameters of wires. The graph also demonstrates that the cooling rate for lower wire drawing speeds depends upon the rate of water flow.

2.8.2 The effect of alloying elements

Mazzucato et al (1981) compared the ageing susceptibility of wire rods from chromium steel (0.5%) and a steel of conventional composition by prestraining the samples (ε = 3%), ageing at temperatures between 100 and 250°C and restraining to rupture at room temperature. The difference, $\Delta\sigma$ between the yield strength of the material and the stress achieved at the end of pre-deformation was used as a parameter to evaluate the ageing tendency. The trends of this parameter and the ductility variation with ageing temperature are illustrated in Figure 2.24. The increase in strength of the two steels was very similar, while the decrease in ductility of the chromium steel after ageing was less sensitive than that of the conventional steel, since the fracture remained completely ductile even at maximum ageing.

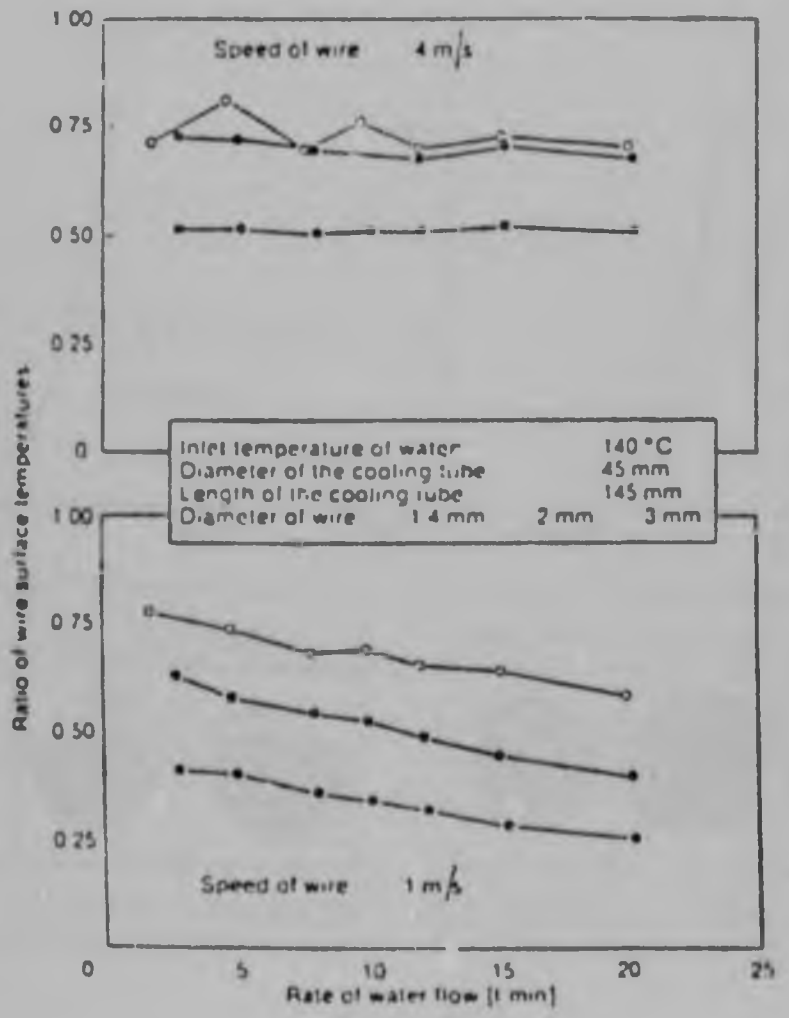

Figure 2.23 Surface temperature as a function of the rate of water flow and the diameter of the wire. After Pawelski and Keuper (1984)

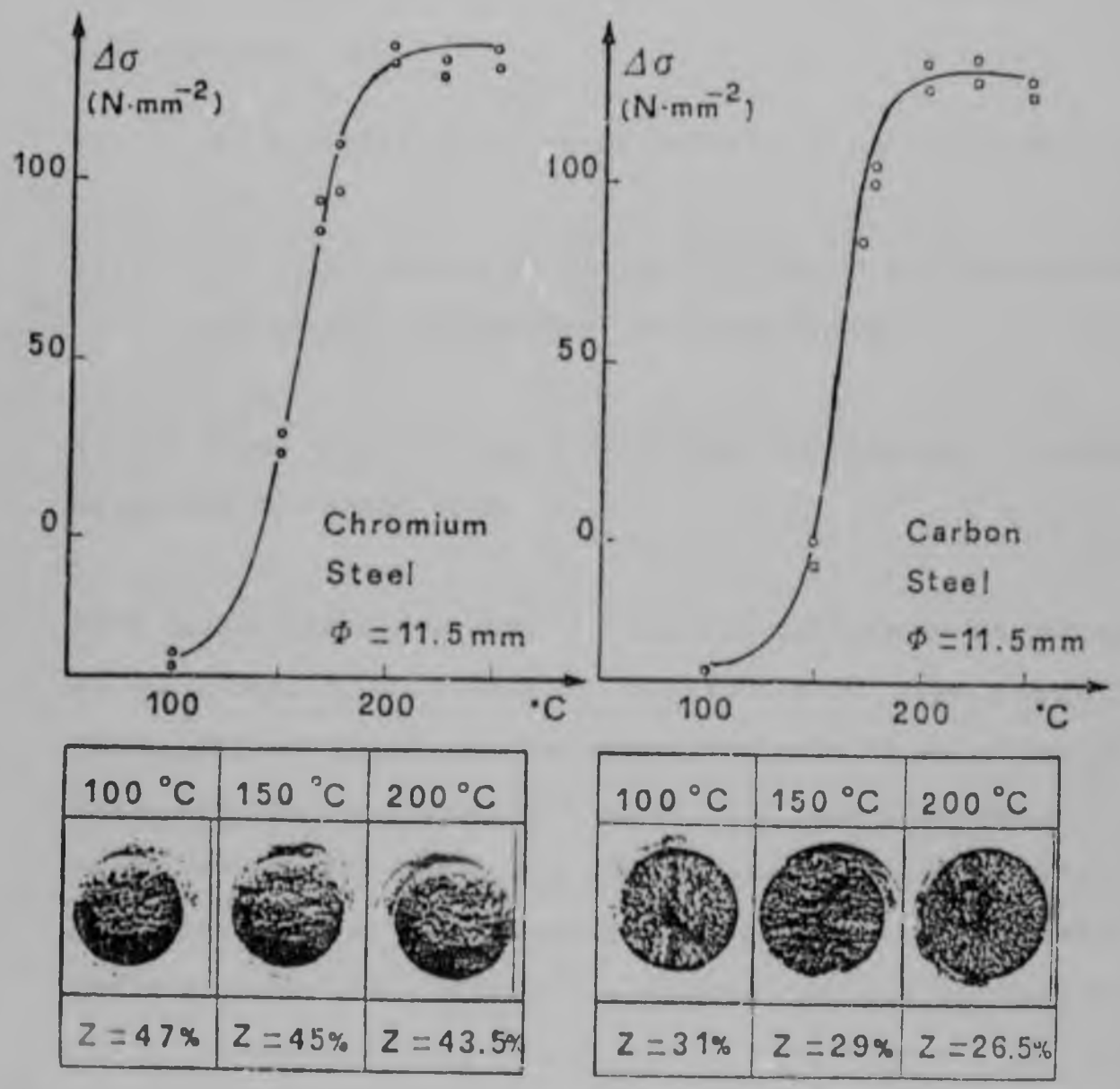

Figure 2.24 Strain ageing behaviour of the wire rods of different compositions.
After Mazzucato et al (1981)

The effect of manganese and silicon on the ageing behaviour of ferrite has been investigated by Leslie (1961) by the determination of:

(i) the temperature at which metastable carbides appear; and

(ii) the temperature at which nucleation begins within the matrix, independent of dislocations.

It was found that silicon raised both temperatures whereas manganese decreased them.

Wert (1952) has shown that the rate of diffussion of carbon at 40 °C was unaffected by additions of 0.5% nickel, chromium, manganese or vanadium, or by 0.9% molybdenum. Also, the rate of precipitation at 150°C was the same as in Fe-C, except for the alloy containing vanadium in which precipitation was considerably faster. The alloys tested contained markedly different concentrations of carbon, which tended to complicate the interpretation of the results.

Korzekwa et al (1982) observed that room temperature ageing does occur in dual phase steels. The precipitation process by which ageing occurred was found to be dependent on the degree of segregation of alloying elements during processing.

Ochioni et al (1983) tested high silicon eutectoid steels. It was observed that increasing the silicon content affected the characteristics of strain ageing and recovery of high carbon steel wire with a fine lamellar structure and a high dislocation density. In the case of a 1.22% silicon steel an increase of 60-80 MPa was observed after stress relieving at temperatures between 350 and 400 °C. Diffusion data for carbon in ferrite (Kristhal, 1970) showed that silicon additions reduce carbon mobility by a substantial amount, especially at low temperatures.

2.9 Choice of Alloys for Investigation

From the discussion on the effect of alloying elements on the pearlite reaction (Section 2.6), it appears that manganese, chromium, silicon, molybdenum, vanadium and perhaps cobalt are the most suitable alloying additions in order to achieve the goal of this project.

It was decided to investigate the potential benefits of chromium, manganese, and silicon because of their influence on the following parameters:

i) Reaction kinetics. All three elements retard the reaction kinetics.

ii) Solid solution strengthening. Silicon gives significant solid solution hardening of the ferrite, while the manganese effect is not so remarked. Chromium provides solid solution hardening of the cementite.

iii) Interlamellar spacing. Chromium was shown to decrease the interlamellar spacing, however, manganese showed an opposite trend. Because of its influence on the reaction kinetics, silicon is expected to provide regular pearlitic structures.

In deciding on the series of alloys which should be prepared in carrying out this investigation, two factors which could represent conflicting interests had to be considered. The first factor is related to the precise determination of the individual effects of alloying additions on the microstructural development of pearlitic structures and the mechanical properties produced. For this purpose and in order to obtain adequate scientific understanding, high purity materials are necessary. The second factor requires the selection of compositions which are easily attainable by steel suppliers and thus represent commercial grade quality, containing various impurity concentrations.

The nominal compositions of the alloys for a preliminary study are listed below:

Plain carbon eutectoid;

1Cr-1/4Mn-0.8C; and

1Cr-1Mn-0.8C.

In the series of alloys for detailed evaluation the additional effect of silicon was investigated, using nominal compositions of:

2Si-1Cr-0.8C

2Si-1Mn-0.8C

1Si-1Cr-1Mn-0.8C

2Si-1Cr-1Mn-0.8C.

A carbon content of 0.8% would result in some of the alloys having nominally hyper-eutectoid composition. However, since carbon is the stronger hardening element, significant reductions in carbon content in order to achieve eutectoid compositions, would adversely affect the maximum strength levels achievable.

CHAPTER THREE - EXPERIMENTAL TECHNIQUES

3.1 Alloys for a Preliminary Study

These alloys were prepared from high-purity base materials by vacuum induction melting at Sheffield University. The material was supplied in the cast and extruded condition as rod with nominal diameters of 9.5 and 12mm. The latter was subsequently drawn to 9.5mm prior to patenting and further working. The compositions of the alloys are listed in Table 3.1. The alloys were analysed at Sheffield University using quantometry and wet chemical techniques.

3.2 Alloys for Detailed Evaluation

These alloys were prepared using the new production facilities commissioned in the University of the Witwatersrand, and by vacuum induction melting at Sheffield University.

3.2.1 Materials

In this section of the study two types of alloys were fabricated: high purity and commercial grade. In the former, specific compositions were achieved by the addition of high purity alloying elements to electrolytic iron, while in the other series similar alloying additions were made to a commercial eutectoid C-Mn steel.

Table 3.1 Chemical compositions of the alloys for a preliminary study.

Alloy	C ± 0.01	Cr ± 0.02	Mn ± 0.02	Al ± 0.003	Others
Fe-C	0.84	*	*	0.021	*
1Cr-1/4Mn	0.84	0.97	0.25	0.018	*
1Cr-1Mn	0.85	1.00	1.04	0.019	*

* less than 0.02

All these alloys were analysed by Haggie Rand Limited, Standard Brass and S.I.B., using spectrographic and wet chemical methods. The compositions were determined for sections from the top and bottom of each cast ingot and the values were found to be within acceptable limits. The compositions studied are reproduced in Tables 3.2(a and b).

3.2.2 Melting and casting

Each alloy was produced as a 6Kg ingot with a 60mm square cross section. Melting was carried out in a Leybold-Heraeus vacuum induction unit, equipped with a vacuum lock system which permits the charging of alloying elements during the melting cycle. All the alloys were melted and cast under a partial pressure of argon. The only difference in procedure was that the high purity alloys

Table 3.2(a) Chemical compositions of the Sheffield alloys for detailed evaluation (in weight %).

Alloy	C ± 0.01	Cr ± 0.02	Mn ± 0.02	Si ± 0.02	Others
2Si-1Mn	0.81	-	1.01	1.89	*
2Si-1Cr	0.82	0.98	-	1.88	*
1Si-1Cr-1Mn	0.83	1.00	0.97	0.98	*
2Si-1Cr-1Mn	0.86	0.97	0.96	1.95	*

* less than 0.02%

Table 3.2(b) Chemical compositions of the Wits alloys for detailed evaluation (in weight %).

Alloy	C	Cr	Mn	Si	S	P	N	Oth-ers
2Si-1Cr	0.80	0.99		1.88	0.0020	0.0012	0.0029	*
2Si-1Cr-0.5C	0.46	1.06		1.86				*
2Si-1Cr-0.6C	0.61	1.03		1.87				*
2Si-1Cr-0.7C	0.67	1.02		1.72				*
2Si-1Cr-0.9C	0.92	1.02		1.85			0.0046	*
1.7Si-1Cr	0.80	1.00		1.65			0.0024	*
2Si-1C. Commercial grade	0.80	1.01	0.70	1.85	0.035	0.011	0.008	*
1.7Si-1Cr Commercial grade	0.79	1.02	0.72	1.70	0.033	0.010	0.008	*

* Less than 0.02%

were vacuum degassed, while the commercial compositions were not (in order to maintain typical residual impurity contents).

These compositions which are relatively high in carbon and silicon, have a wide freezing range and are therefore susceptible to solidification shrinkage. Considerable care was taken therefore during casting to minimise primary and secondary pipe formation in the ingots. Nevertheless, some yield loss was encountered in the laboratory "pilot" scale production route due to primary pipe formation.

3.2.3 Rolling

The as-cast ingots were mechanically worked using an experimental rolling mill with a 30 tonnes load capacity. After pre-heating at 1100°C for 2 hours in an air furnace, the ingots were first cogged to produce a 30mm square cross-section. This material was subsequently worked using shaped (section) rolls to provide the experimental 14mm diameter rod. During rolling, four to five re-heats were necessary, the time at temperature being determined by the thickness of the material.

After processing, it was found that a layer approximately 1mm in depth had been subject to decarburisation. This was removed by machining to produce a final rod diameter of 12mm.

3.3 Heat Treatment

3.3.1 Homogenisation

In this study, it was not possible to homogenise the as-rolled material, due to a lack of high temperature (1200°C) inert gas heat treatment facilities. However, sections of each alloy were partially transformed (20%) and water-quenched to estimate the uniformity of pearlite nucleation (using light microscopy) and hence determine the approximate homogeneity of the as-rolled structures.

3.3.2 Determination of TTT diagrams

A detailed knowledge of the isothermal transformation characteristics of each alloy is vital to the interpretation of the observed microstructures and the selection of suitable patenting conditions. Two techniques were employed in the determination of TTT diagrams: light metallography and dilatometry.

i) Light Metallography:

This technique was used to obtain the general form of the TTT curves. Since reactions in pearlitic steels are usually very rapid, TTT diagrams were determined using small specimens (10mm diameter by 3mm thick) in order to approximate to genuine isothermal conditions. These samples were heat treated at 50°C intervals in

the temperature range 500 - 650 °C, and the percentage transformation assessed from polished and etched specimens using light microscopy. Since it is very difficult to distinguish pearlite from bainite and martensite (produced by quenching untransformed austenite) in samples more than 70% transformed, the metallographic method provided only an approximate guide to the transformation kinetics.

ii) Dilatometry:

A more accurate determination of the TTT diagrams for some of the alloys was obtained using the high speed dilatometer facility of the Department of Metallurgy and Materials Science, University of Cambridge (by Dr. R.A. Ricks). In these experiments, thin walled (0.6mm) cylindrical specimens were induction-heated, then quenched to the transformation temperature using helium gas. The extent of transformation was obtained from the length change of the specimen, as measured by an electronic transducer.

3.3.3 The effect of austenitising treatment on the transformation products

Austenitising temperatures must be carefully chosen in order to ensure the complete dissolution of any pearlitic carbides present, and sufficient time must be allowed for the homogenisation of the austenite.

In order to explore the effect of austenitising time and temperature on the transformation characteristics, specimens were heat treated in the temperature range 920 to 1050 °C for 5 to 30 minutes. The temperatures were maintained within ± 2 °C using a thyristor controller. These samples were subsequently isothermally transformed as described in Section 3.3.4.

The effects of austenitising heat treatment were evaluated from metallographic examination and mechanical testing of these patented samples. The prior austenite grain size in each alloy and condition was again determined using partially transformed specimens.

For the alloys studied in this part of the programme, the optimum structures and properties were obtained after austenitising for 30 minutes at 1000 °C. This treatment was therefore selected as standard in all subsequent studies.

In order to maximise heat transfer during the whole patenting process, all samples were de-scaled mechanically prior to austenitisation. In addition, this heat treatment was carried out in a dry argon atmosphere to reduce further scaling and decarburisation.

3.3.4 Molten bath isothermal heat treatment

Since the transformation of austenite to pearlite occurs after very short incubation times, to obtain isothermal conditions (and hence uniform microstructures) it is necessary to carry out the required heat treatment in a medium with good hear transfer properties.

In the preliminary study (Chapter 4), both molten salt and lead baths were used to fully transform rods prior to detailed examination. It was found that samples transformed in lead exhibited superior properties, and this medium was used therefore in all subsequent studies. The conditions in the molten bath are also of great importance, since in a static medium a temperature build-up can occur around the workpiece. All these heat treatments were carried out therefore with liquid circulation (generated by mechanical stirring). This further improves heat transfer.

After austenitisation, specimens for isothermal transformation were removed from the high temperature furnace, plunged directly into the molten bath, and vigoriously agitated (to ensure optimum heat transfer). The samples were transformed for various times in the temperature range 520 - 680 °C, at 10 °C intervals, then water quenched. The temperature of the lead was maintained within $\pm$ 1 °C again using a thyristor controller. The

actual reaction temperature was measured using a chromel-alumel thermocouple (shielded by stainless steel) inserted in a small hole drilled along the axis of the rod. This temperature was recorded as a function of time (e.g. Figure 3.1). It can be seen that the temperature remains constant after an initial small perturbation. The initial, transient temperature rise (5°C) is due to recalescence, and was only observed in the heat treatment of large samples. This was unavoidable given the relatively small lead baths available.

3.4 Mechanical Testing

3.4.1 Hardness tests

Hardness values were obtained using a Vickers Diamond Hardness machine with a load of 20Kg. Micro-hardness tests were carried out using a Durimet Leitz microhardness tester with loads of 100g and 200g. The tests were performed on polished specimens. The hardness values were taken as the mean of at least ten impressions. In cases where the specimens dimension were too small for meaningful hardness measurements (Hounsfield specimens) to be carried out, the values were obtained from strength-hardness conversion tables.

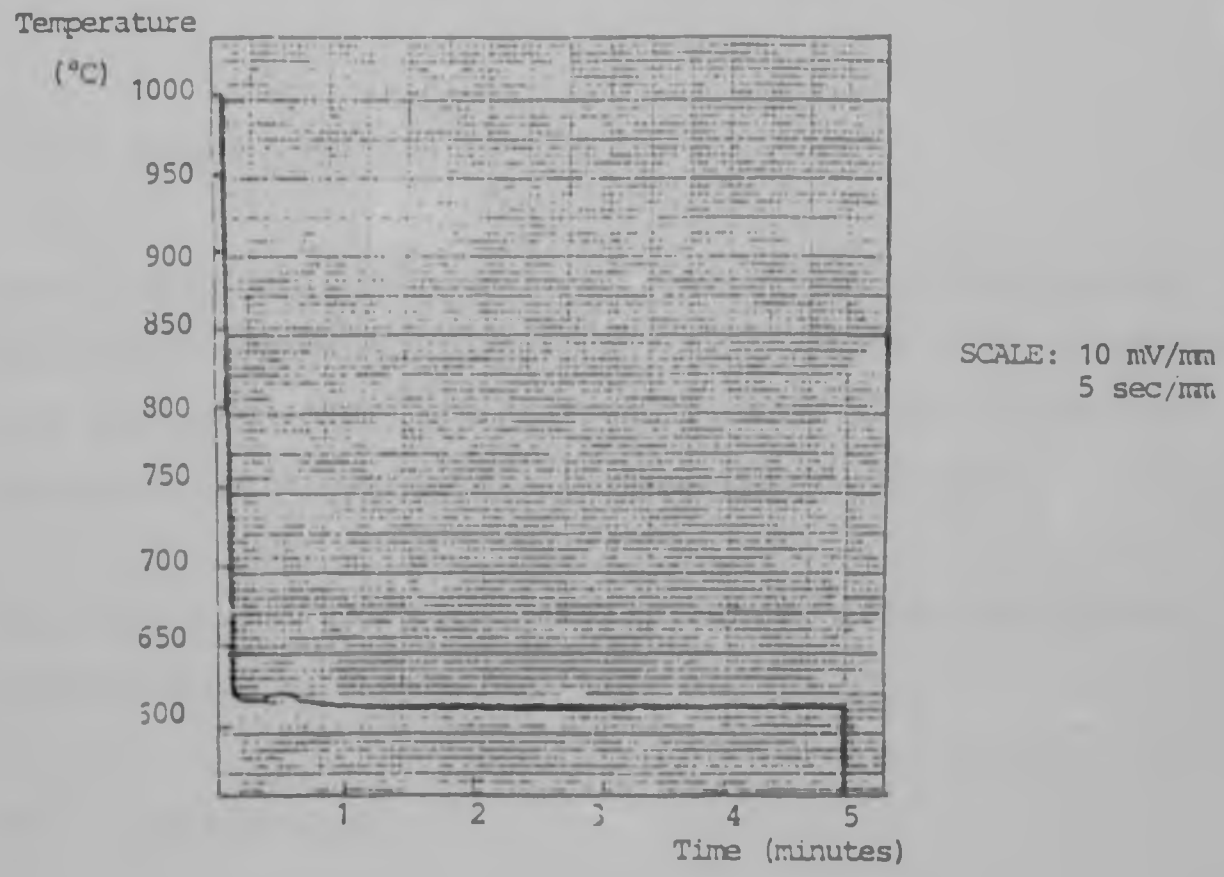

Figure 3.1 Cooling curve during isothermal transformation exhibiting recalescence.

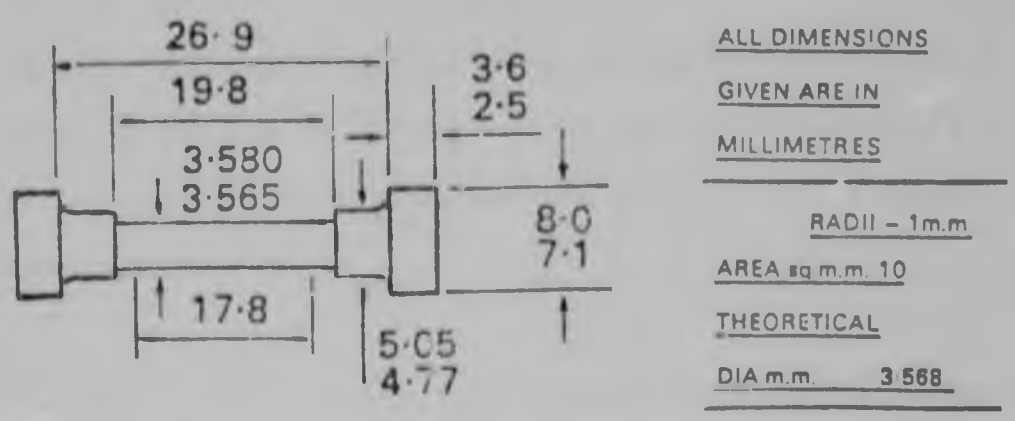

Figure 3.2 Standard metric round tensile test piece. Gauge length equals five times diameter.

3.4.2 Tensile tests

Rods were fully annealed to facilitate machining of Hounsfield double shouldered specimens (Figure 3.2). These specimens were then patented and cleaned prior to tensile testing using an ESH 50kN universal testing machine.

Patented rods were also tensile tested using an Instron 250kN machine at Haggie Rand Limited.

3.5 Metallography

3.5.1 Light microscopy

Samples were mounted in epoxy resin and wet ground with silicon carbide papers (220 to 1000 grit), followed by diamond lapping to a final 1/4 µm polish.

The pearlitic structures were etched in a 2% Nital solution for 5 seconds. Photomicrographs were obtained using a Nikon Optiphot (light) microscope with magnifications up to 1000 times. Little pearlite was resolvable in this range of magnifications.

The prior austenite grain size was measured using the mean linear intercept (MLI) method on partially transformed specimens in which the prior austenite boundaries were "decorated" with pearlite.

3.5.2 Scanning electron microscopy (SEM)

Since the pearlite spacings of interest in this study are below the resolution limit of the light microscope, SEM was used to obtain detailed microstructural information. Two instruments were employed; a JEOL T20 and a Cambridge S-IV stereoscan. These were operated in the normal scanning mode to provide secondary electron images.

Specimen preparation techniques were the same as for light microscopy, except that the etching time in Nital was reduced to 2 seconds.

Some problems were encountered initially due to contamination of the surface during examination. It was necessary therefore to ultrasonically clean the specimens in alcohol between each polishing and etching stage.

The samples were subsequently coated by sputtering a 20nm gold or gold-palladium layer using a Polaron SEM coating unit E 5100. The film thickness was measured with a Polaron film thickness monitor E 5500.

Magnifications up to 60,000 times were obtained by using the optimum conditions of the microscope. Photographs were taken of at least 20 different areas of each sample.

3.5.3 Conventional transmission electron microscopy (CTEM)

3.5.3.1 Replicas

Replicas of the pearlitic structures were obtained using a standard 2-stage technique. A cellulose-acetate tape, partially dissolved in acetone, was applied to the etched surface. After removal from the surface, the replicas were shadowed with gold-palladium using an Edwards evaporation unit under the following conditions:

a) 10mm gold-palladium wire, 1.2mm thickness;

b) shadowing angle 40°; and

c) distance between source and substrate, 100mm.

This was followed by the further deposition of a carbon film (10nm in thickness). The plastic replicas were then cut into 3mm squares, placed on 3mm diameter grids and the cellulose-acetate dissolved in acetone.

3.5.3.2 Thin foils

To prepare thin foils, 3mm diameter discs (0.9mm in thickness) were obtained from rods and wires using an Isocut low speed diamond saw. These discs were then ground on 600 grade silicon carbide paper to a thickness of 0.1mm. Electro-polishing and thinning were then carried out in a commercial Fischione twin jet polisher.

Pearlitic microstructures are difficult to thin electrolytically, due to the markedly different polishing characteristics of the ferrite and cementite phases. However, some success was achieved using a solution of 5% perchloric acid in methanol, an applied voltage of 30-40V and a solution temperature of -30 °C.

These thin foils were cleaned (and thinned further where necessary) by ion bombardment in a Gatan dual ion mill model 600.

Both thin foils and replicas were examined in a JEOL 100C TEM/STEM.

3.6 Interlamellar Spacing Measurement

In this study, it was decided to determine the interlamellar spacing of pearlite by the measurement of the average smallest spacing observed in a specimen. This value was obtained using the mean linear intercept method on secants drawn perpendicular to the finest lamellae observed in each of the SEM micrographs. Twenty micrographs of each specimen were analysed.

Measurements were made initially using a graticular magnifying glass, and subsequently with the aid of a Kontron image analyser. This interactive, image analysis

system (IBAS) was attached to a Zeiss light microscope and SEM negatives were observed using transmitted light (Figure 3.3). The image can be processed and transformed to eliminate all but the essential structure, as determined by the user. Stereological data can then be obtained and printed directly or stored on disc for further processing. The programme used to determine interlamellar spacings is given in Appendix A.

A Nikon V-12 profile projector attached to a Nikon data processor DP-200 for two dimensional measurements was utilised in order to carry out interlamellar spacing measurements. Reflected and transmitted light facilities enabled the analysis of SEM negatives and positives.

3.7 Drawing Trials

Drawing trials were carried out on 10 and 12mm diameter rods at the R & D department, Haggie Rand Limited, using a single hole wire drawing machine (Figure 3.4).

Prior to drawing, the patented rods were pickled in 10% inhibited hydrochloric acid at 60 °C for 15 to 20 minutes and subsequently rinsed in three different water tanks. A phosphate coating was then applied at 70 °C for 7 minutes before rinsing in boiling borax at 95 °C for one minute. The drawing soap used in the trials was Durpon 624N which had been dried at 100 °C for 24 hours prior to use.

Figure 3.3 Image analyser; the lamellar structure is shown on the screen.

(a)

(b)

Figure 3.4 Wire drawing machine.
(a) drum
(b) die box

The design of a typical wire drawing die is shown in Figure 3.5. The complete die set used in all the trials is given in Table 3.3, together with the cumulative total true strain, the reduction in area between passes and the total reduction in area.

The true strain was calculated from the equation:

$$\varepsilon = 2\ln \frac{D_o}{D_i}$$

Where D_o is the initial rod diameter (12mm); and

D_i is the die diameter

Prior to drawing through each die, one end of the material was reduced to the next die diameter using pointing rolls (Figure 3.6).

Wires were drawn at a standard speed of $0.4 m.s^{-1}$.

To reduce overheating of the wire, a water cooling unit (Figure 3.7) was placed immediately after the die in order to achieve a wire temperature less than 40 °C within 100mm of the exit of the die. Because of length limitations, this unit could only be used with the dies of 6.4mm diameter and less.

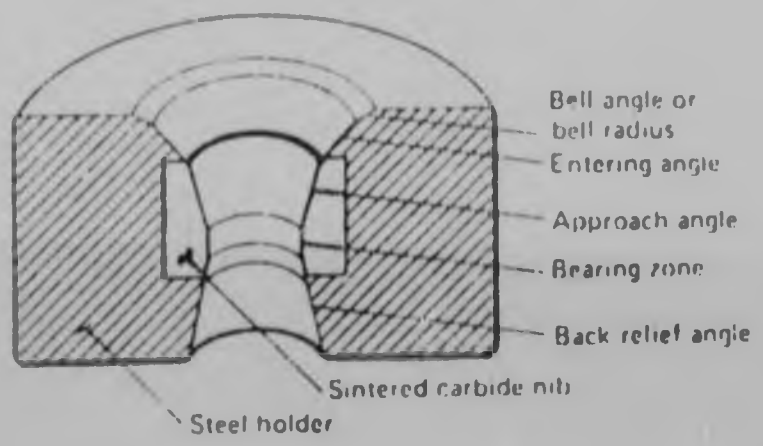

Figure 3.5 Schematic cross section (not to scale) of a single-hole die employing a nib of sintered carbide mounted in a circular steel holder.

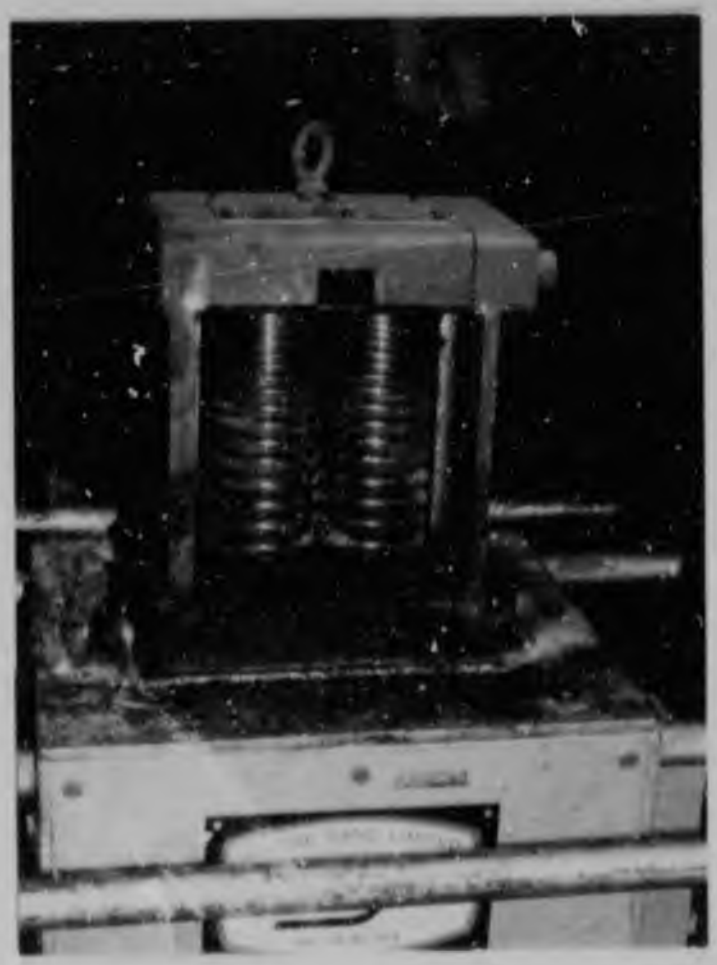

Figure 3.6 Pointing rolls

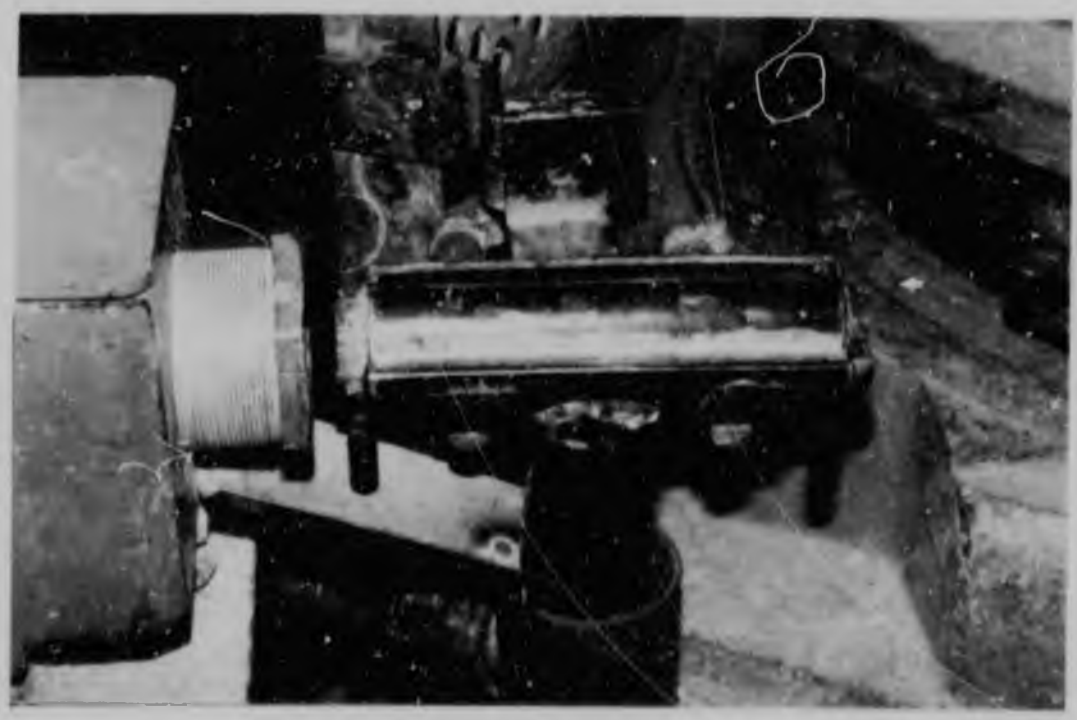

Figure 3.7 Water cooling unit

Table 3.3 Die set for wire drawing

Die diameter (mm)	True strain (ε)	Reduction in Area (%)	Total Reduction in Area (%)
12.00	0	-	-
10.76	0.22	19.60	19.60
9.67	0.43	19.20	35.06
8.69	0.65	24.48	47.56
7.56	0.92	24.31	60.31
6.42	1.25	27.89	71.37
5.53	1.55	25.79	78.76
4.82	1.82	24.02	83.87
4.25	2.07	22.24	87.45
3.79	2.30	20.50	90.02
3.40	2.52	19.50	92.00
3.15	2.68	14.21	93.11
2.94	2.81	12.88	94.00

3.8 Wire Testing

3.8.1 Tensile tests

In order to obtain work hardening curves for each alloy, tensile specimens of about 200mm length were cut after each drawing pass and tested using the Instron universal testing machine.

3.8.2 Torsion tests

Torsion and shear tests were performed after the last two passes of drawing, to assess the ductility and mode of fracture of the wires. In the torsion test, the number of twists to failure, on a gauge length equal to 100 times the wire diameter, was determined using a Denison T17M machine. The fracture shape and appearance of the wire is graded into different categories as listed in Table 3.4.

Torsion test results of a minimum of 20 turns to failure, and a B type break are considered to be acceptable.

3.8.3 Shear tests

The shear test was designed by Bridon Wires Limited for testing individual wires in order to simulate the high stress concentration at contact points in a rope.

The tests were carried out in a standard Instron tensile testing machine. The wire test sample is loaded in the usual way and a small preload applied. A special hydraulic compression jig is then clipped onto the wire specimen. A specific pressure (determined by the wire diameter) is applied to the compression device and the sample then tested to failure in tension. The amount of cross head movement between peak load and the point of fracture

Table 3.4 Torsion test piece quality rating

Rating	Appearance
A_1	i) Even twisting throughout the test length. ii) No splitting or waviness. iii) Fracture clean and square ended. iv) No secondary (recoil) breaks.
A_2	i) Even twisting throughout the test length. ii) No splitting or waviness. iii) Fracture clean and square ended. iv) A secondary fracture with a helical or stepped face is permitted.
B	i) Even twisting throughout the test length. ii) Slight waviness permitted. iii) Primary fracture preferably square ended but a slightly stepped or helical face is permitted. iv) A secondary fracture with a helical or stepped face is permitted.
C	i) May be uneven twisting and only local twisting in the worst cases. ii) Splitting and waviness will be present. iii) Primary and any secondary fractures will usually show a pronounced stepped or helical form.

provides a good indication of local elongation. (This is a good approximation providing that the specimen length is kept reasonably short, e.g. 500-100 times the wire diameter). The shear test jig and the fracture types are shown in Figure 3.8.

3.8.4 Ageing trials

These tests were carried out to determine whether the heavily drawn ultra-high strength wires are subject to degradation of their properties by strain ageing. Wires drawn to high true strain values were heat treated at 50 °C for 1, 10, 50 and 100 hours. Shear tests were then used in order to study the combined effect of prior cold work and the ageing time and temperature on the ductility of the wires.

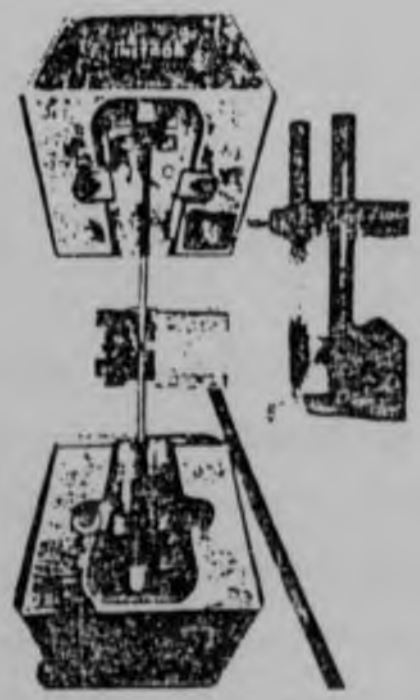

(a)

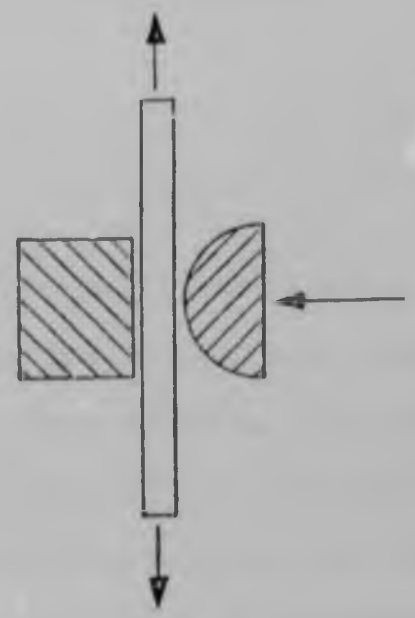

(b)

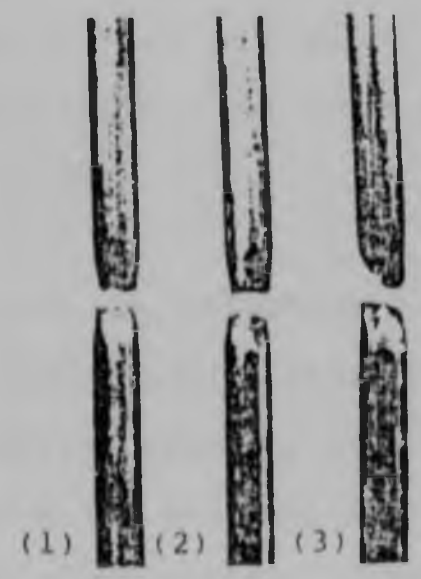

(c)

Figure 3.8 Shear test
(a) Instron and shear test jig
(b) Diagrammatic sketch of shear test arrangement
(c) Shear test fracture types:
(1) normal tensile test fracture
(2) ductile shear test fracture
(3) brittle shear test fracture
After Stephenson et al (1983)

CHAPTER FOUR - PRELIMINARY INVESTIGATION

4.1 Alloys Compositions

In the selection of alloys for an initial investigation of the potential benefits of chromium additions, the chosen alloys represent a compromise to some extent. The base alloy is an ultra high purity Fe-C composition, while the chromium steels, although prepared from high purity base materials, also contain controlled additions of manganese. Since these alloys do not contain significant sulphur concentrations, the manganese contents are intended to represent levels over and above those necessary for complete desulphurisation and which might therefore pertain to commercial steels.

For these alloys the objectives of the study were to determine the transformation characteristics, to determine the interlamellar spacing variations, to test the drawability and to measure the patented and drawn strengths. The compositions of the alloys used in this preliminary investigation are listed in Table 4.1.

Table 4.1 Chemical compositions of the first series of alloys (in weight %).

Alloy	C + 0.01	Cr + 0.02	Mn + 0.02	Al + 0.003	Others
Fe-C	0.84	*	*	0.021	*
1Cr-1/4Mn	0.84	0.97	0.25	0.018	*
1Cr-1Mn	0.85	1.00	1.04	0.019	*

* less than 0.02

4.2 Results and Discussion

4.2.1 TTT diagram

4.2.1.. Metallographic determination

The general form of the TTT diagram was determined using light microscopy to estimate the percentage transformation of the samples transformed at different temperatures and times. The approximate curves for the three alloys examined are reproduced in Figures 4.1 to 4.3.

The prior austenite grain size was of the order of 50 un in each alloy.

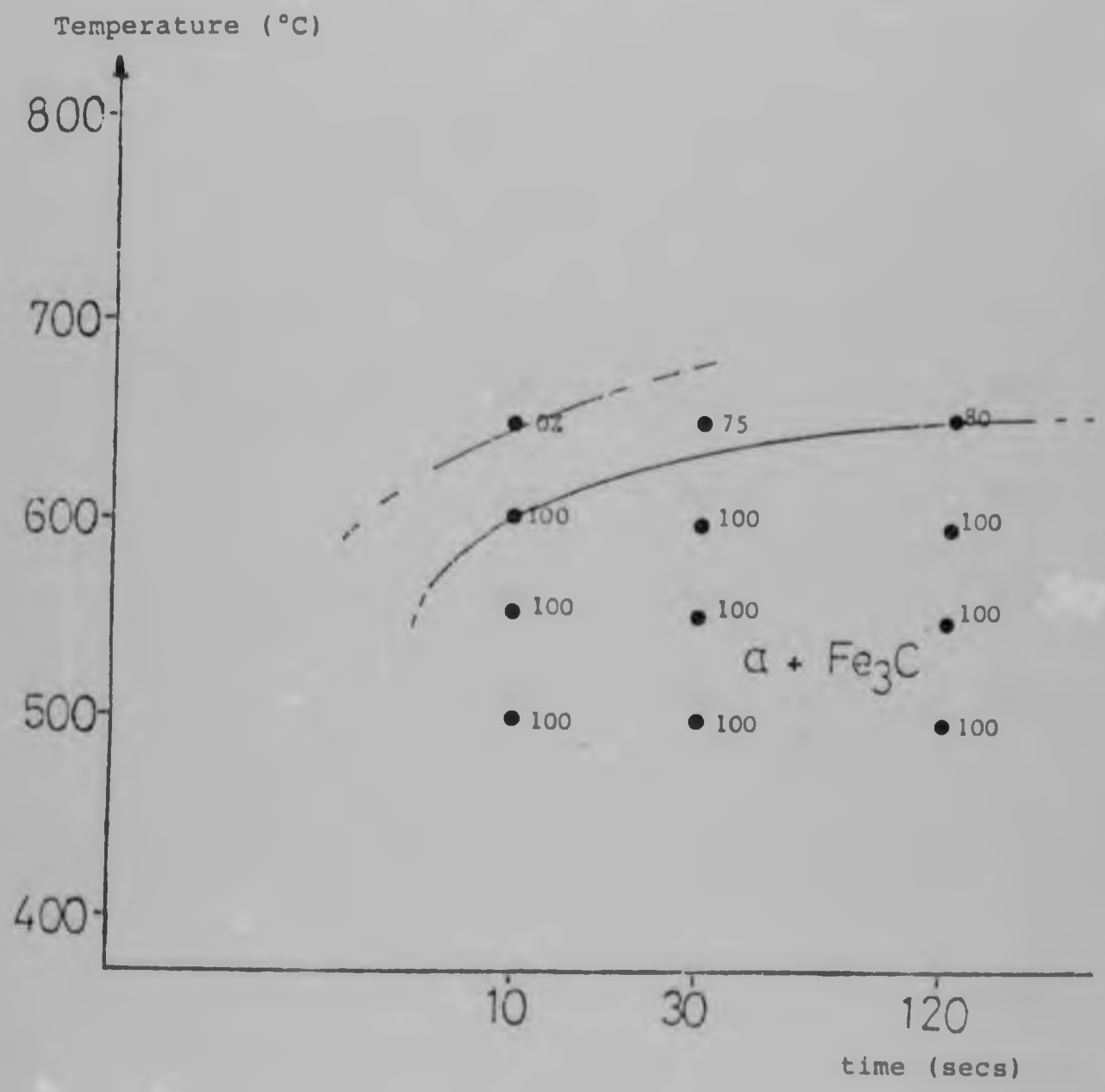

Figure 4.1 TTT diagram of the Fe-C alloy determined by metallography.

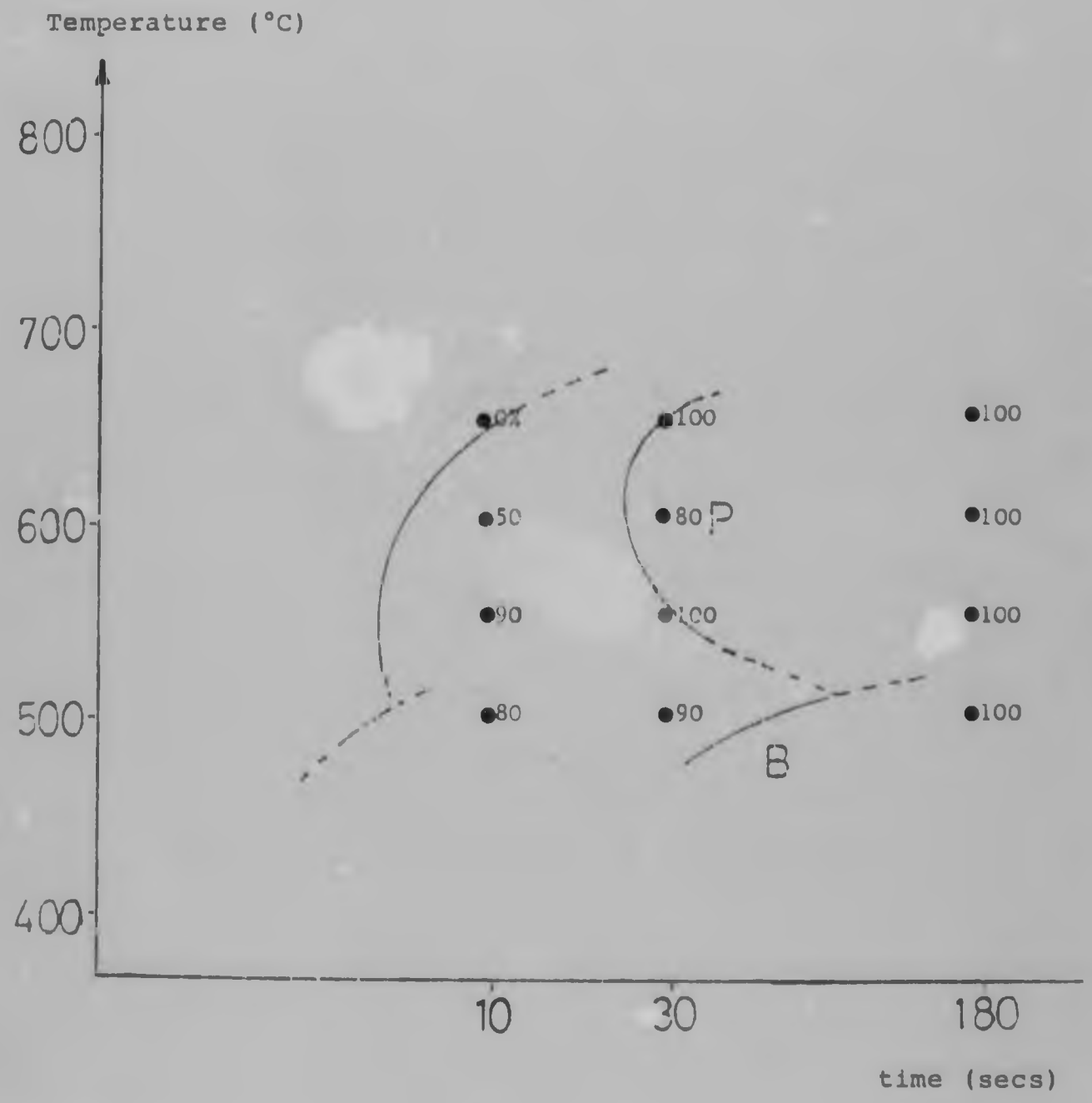

Figure 4.2 TTT diagram of the 1Cr-1/4Mn alloy determined by metallography

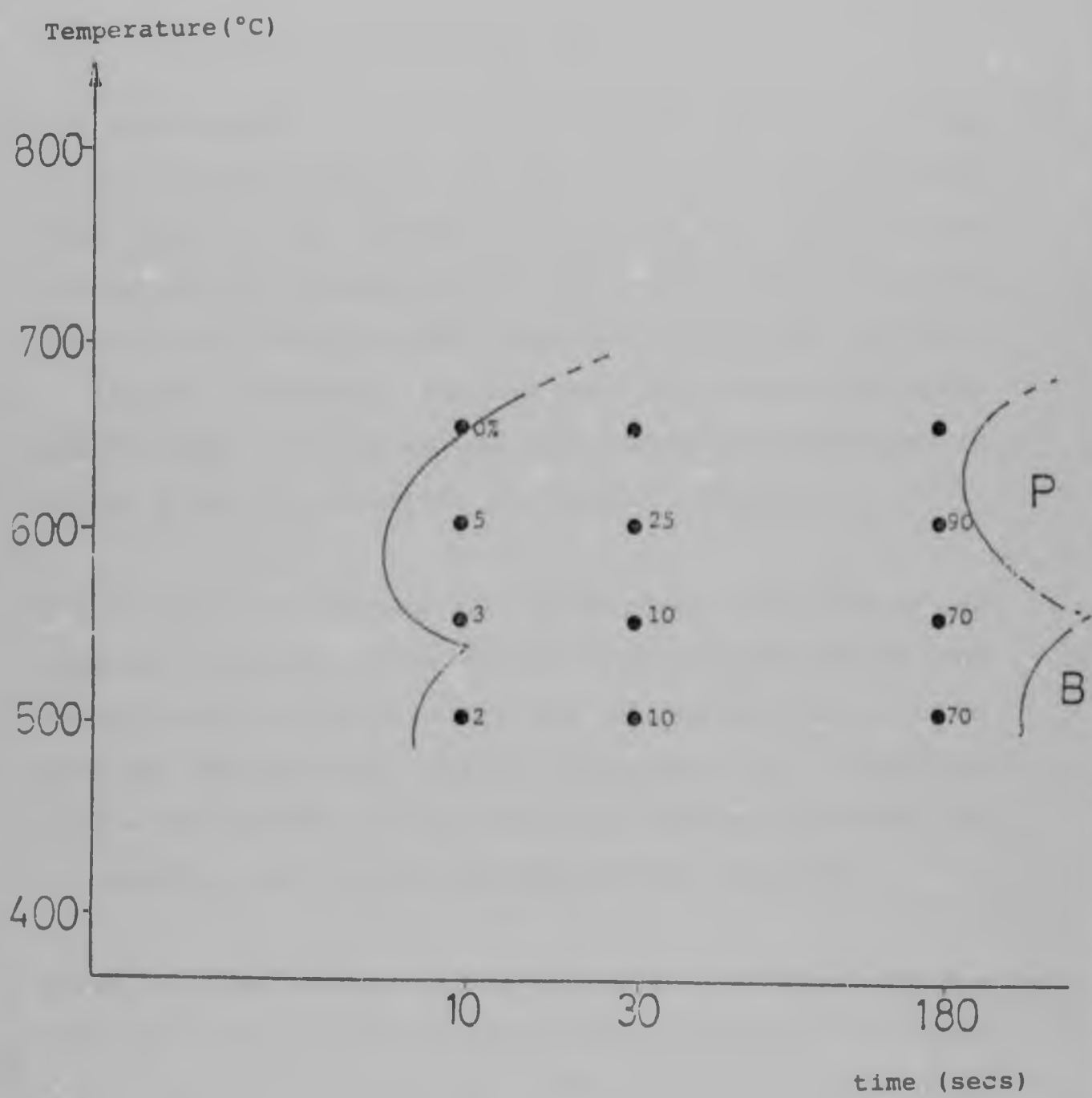

Figure 4.3 TTT diagram of the 1Cr-1Mn alloy as determined by metallography.

4.2.1.2 Dilatometric determination

The experimental curves for the three alloys analysed are given in Figures 4.4 to 4.6. The average grain size here was 175 μm. It can be seen that for the iron-carbon alloy the incubation time at the nose of the C-curve is too short for accurate determination. However, the form of the curve is clearly delineated. For the two alloy steels (1Cr-1/4Mn and 1Cr-1Mn), the curves are well defined and separated in terms of both the pearlite and bainite reactions.

The diagram in Figure 4.7 illustrates the effects of combined chromium and manganese alloying additions on the transformation characte .ics. The temperature of the nose of the pearlite .gion is raised, the incubation period for transformation is significantly increased and the pearlite and bainite regions are well separated.

Based on these results, temperatures were selected for the lead bath heat treatment which should provide the finest pearlitic microstructures. The heat treatments were carried out in the temperature range 520 to 660°C, at 10°C intervals.

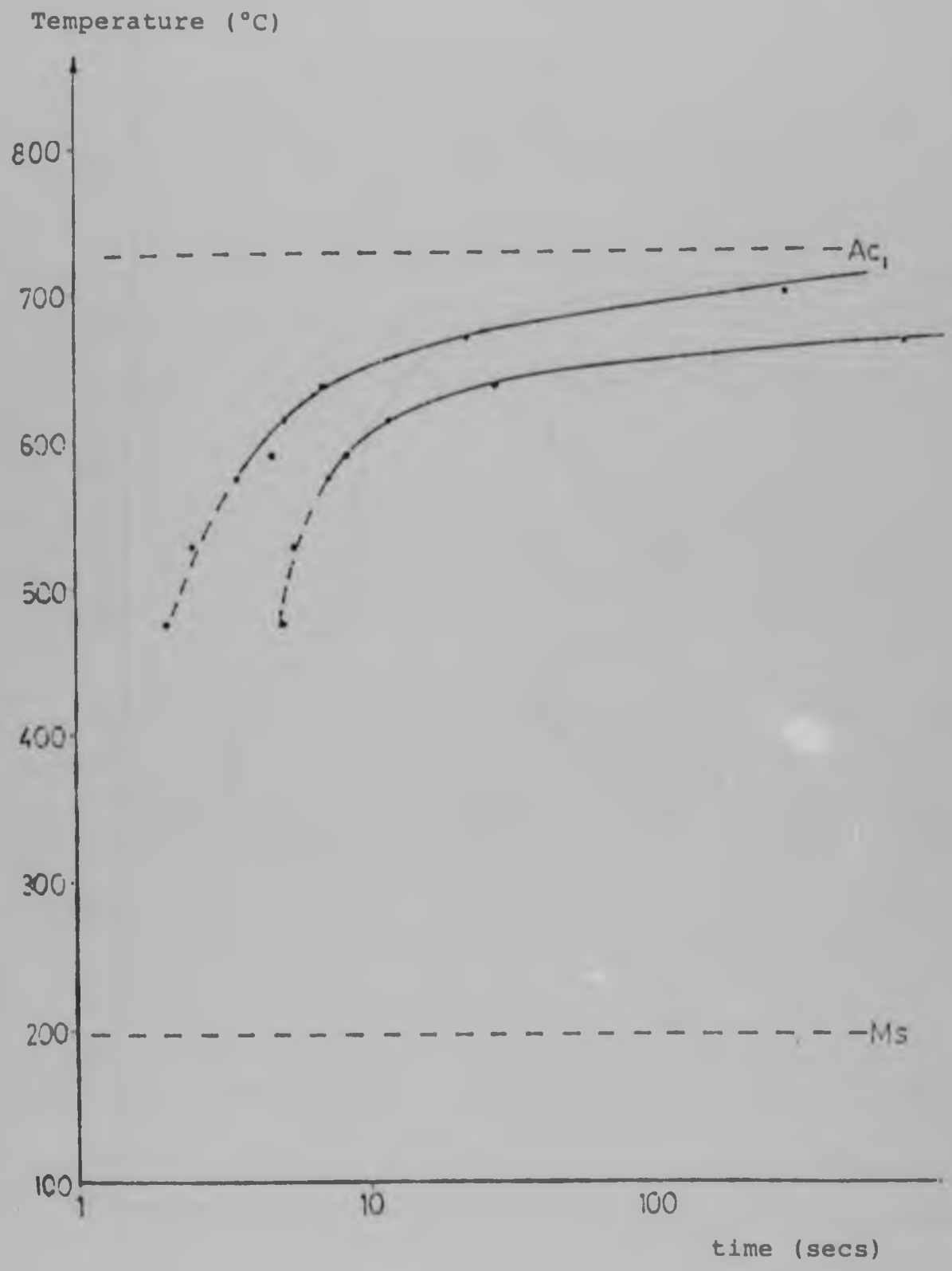

Figure 4.4 TTT diagram of the Fe-C alloy determined by dilatometry.

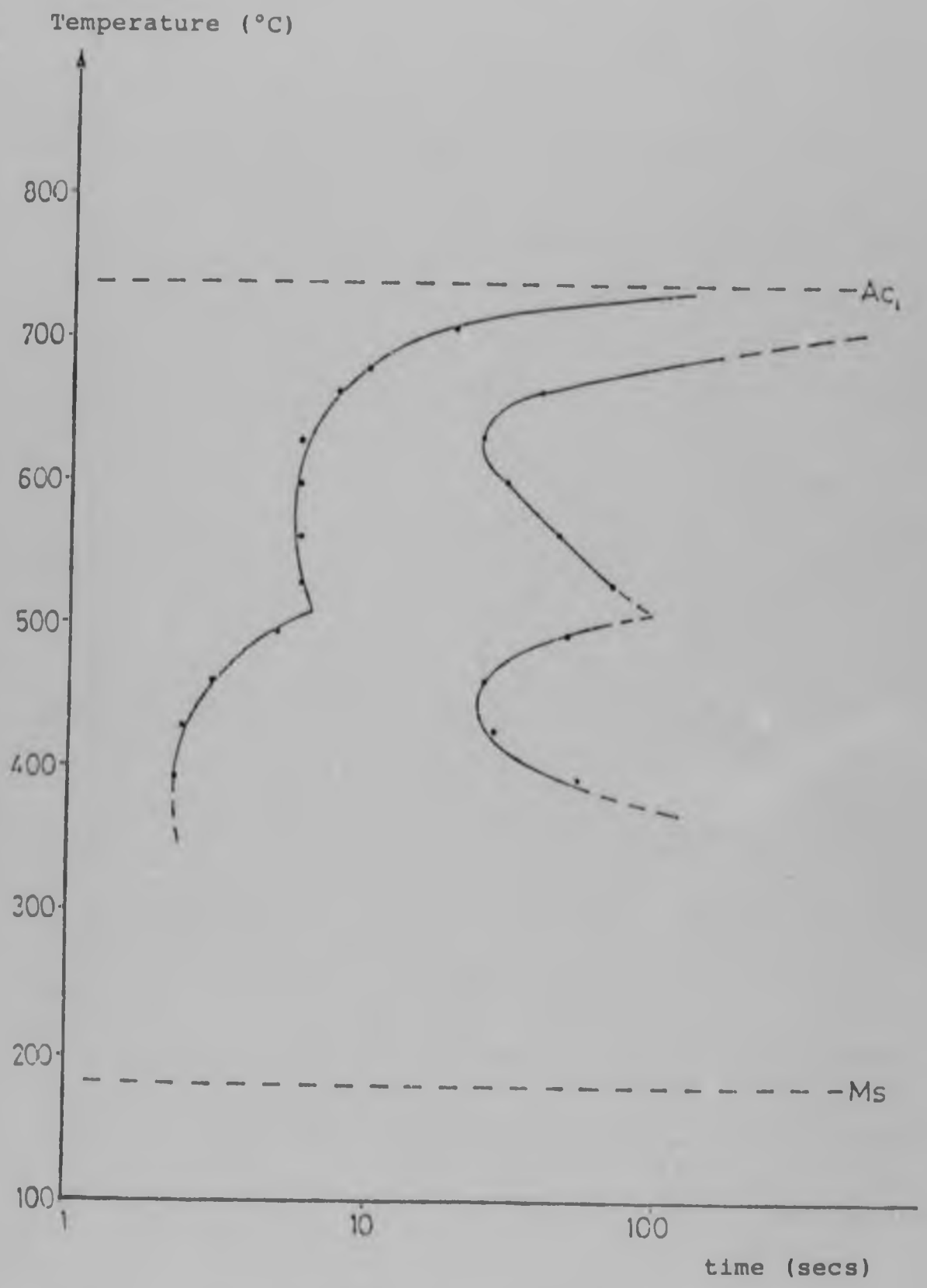

Figure 4.5 TTT diagram cf the 1Cr-1/4Mn alloy determined by dilatometry.

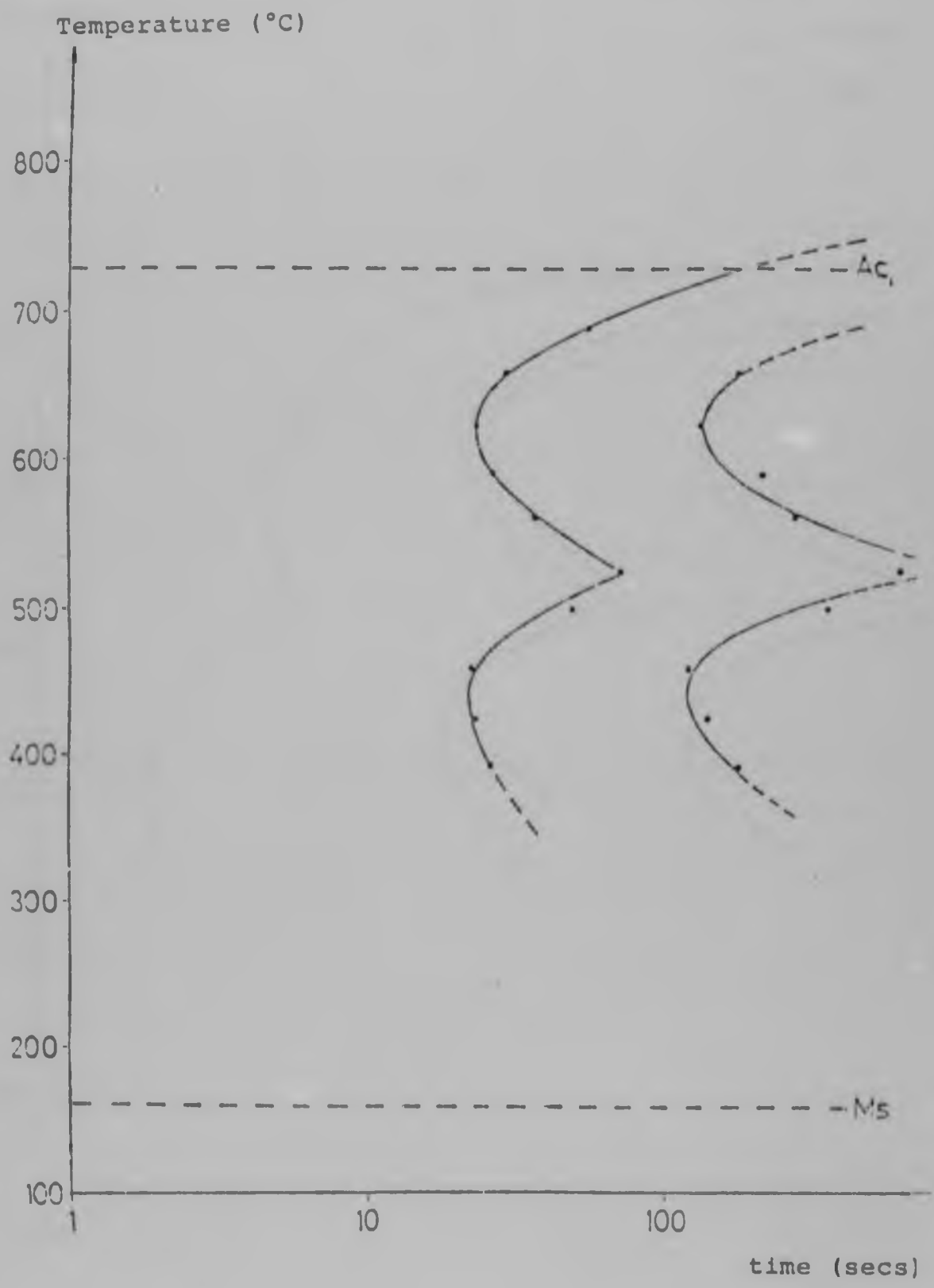

Figure 4.6 TTT diagram of the 1Cr-1Mn alloy determined by dilatometry.

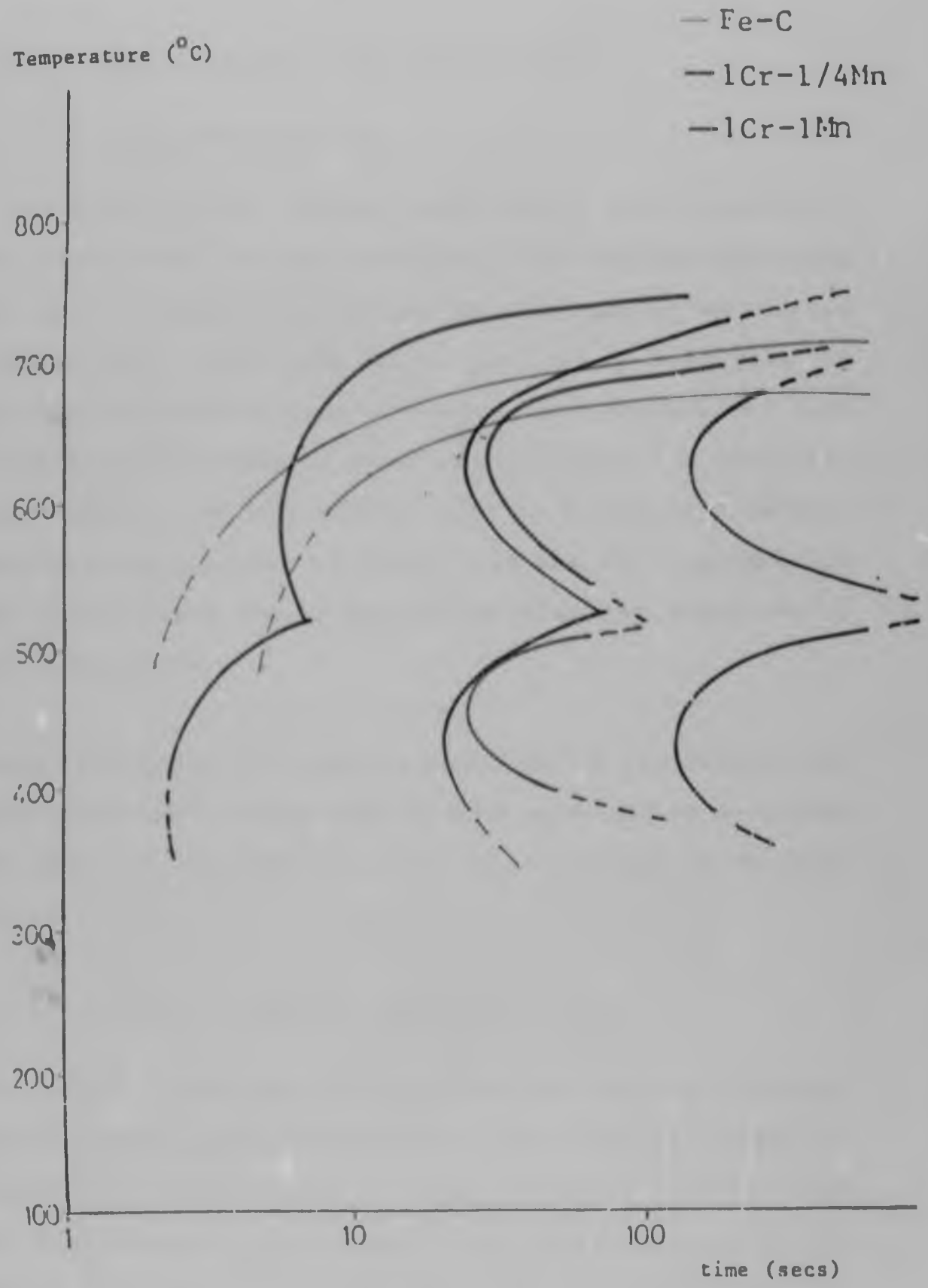

Figure 4.7 TTT diagrams of the Fe-C, 1Cr-1/4Mn and 1Cr-1Mn alloys.

4.2.2 Metallography of as-patented rods

4.2.2.1 Light metallography

At the higher transformation temperatures, the formation of pearlite nodules in these relatively fine grained materials was readily detectable, Figure 4.8. In samples which were almost fully transformed, it was often difficult to distinguish untransformed austenite (now martensite) from certain orientations of pearlite colonies. It was also impossible in the iron-carbon alloy to distinguish between pearlite and bainite, although this was not a problem in the alloy steels due to the marked acicular character of the latter phase.

Since the lamellar structure could not be resolved in the light microscope, these results were used only to determine the form of the TTT diagrams as described in Section 4.2.1.1.

4.2.2.2 Scanning electron microscopy (SEM)

For determination of the interlamellar spacing, scanning electron microscopy techniques were used in order to resolve the fine microstructures. In order to check that the samples were fully transformed, a rapid survey of the whole surface was carried out at relative low magnifications of about 3,000 times (Figure 4.9).

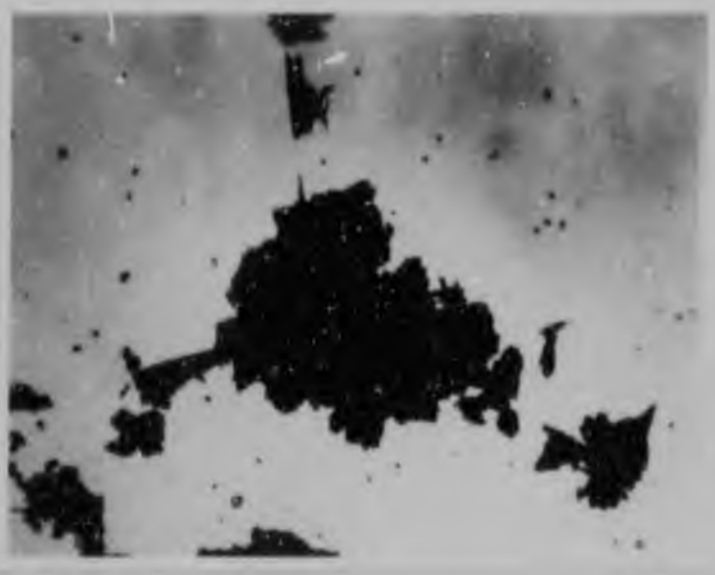

Figure 4.8 Pearlite nodule nucleated at a triple point. (Light micrograph)

Figure 4.9 SEM micrograph of a sample transformed at a low temperature.

At transformation temperatures below the nose of the TTT curve, another eutectoid product, upper bainite, was observed (Figure 4.10). There was a tendency for this to form as a ribbon along prior austenite grain boundaries (Figure 4.11). In a number of cases the detailed morphology was such that a carbide film was formed at the boundary, with a ribbon of free ferrite beside it. The bainite morphology was variable, but was always very coarse compared with the pearlitic regions of the same specimen.

Due to the different angles of intersection of various pearlite colonies with the specimen surface, a very large apparent spread in the interlamellar spacing was observed (Figure 4.12).

The microstructures of the different steels transformed at 600 °C are shown in Figure 4.13. A regular lamellar structure was observed in all three steels. At higher temperatures in the iron-carbon alloy the cementite lamellae increasingly tended to spheroidise.

The variation in the average minimum interlamellar spacing with temperature for both alloy steels is shown in Figure 4.14. The behaviour of a commercial plain carbon steel is also included since this represents a more valid comparison than the ultra-high purite iron-carbon alloy.

1.5um

Figure 4.10 Coarse bainite in a fine pearlite matrix. (SEM micrograph)

4 um

Figure 4.11 Upper bainite along prior austenite grain boundaries in fine pearlite matrix. (SEM micrograph)

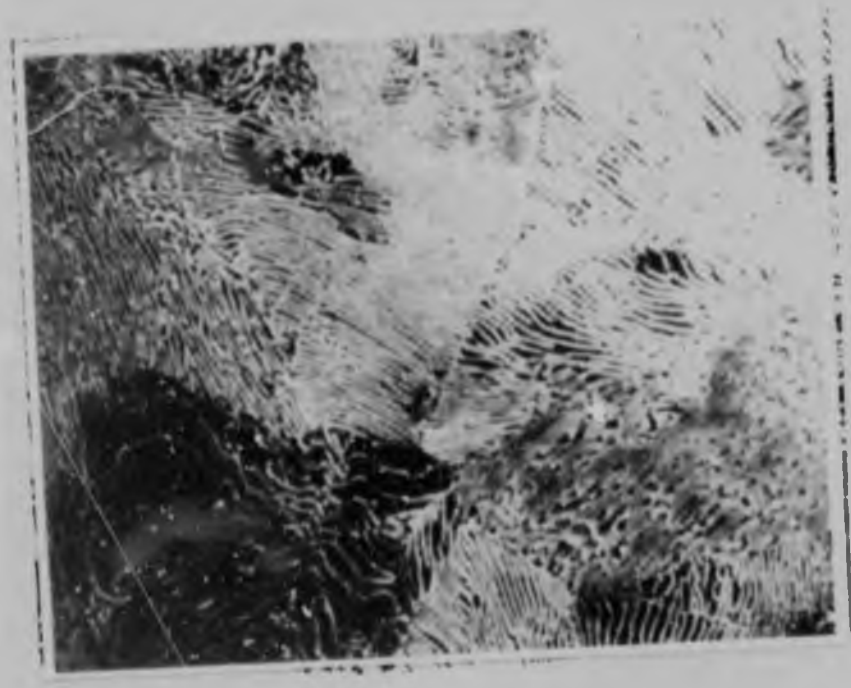

Figure 4.12 Apparent spread of interlamellar spacings (SEM micrograph)

(a)

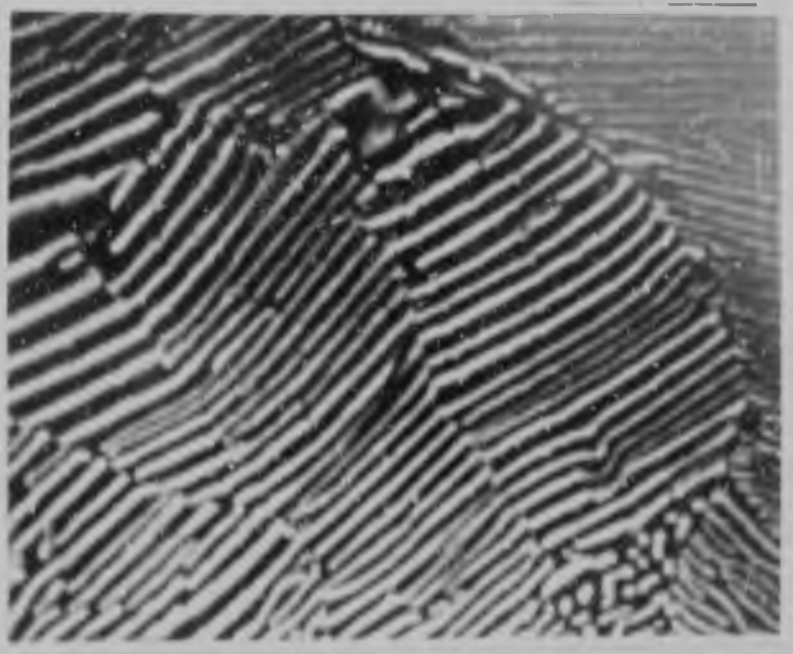

1.0μm

(b)

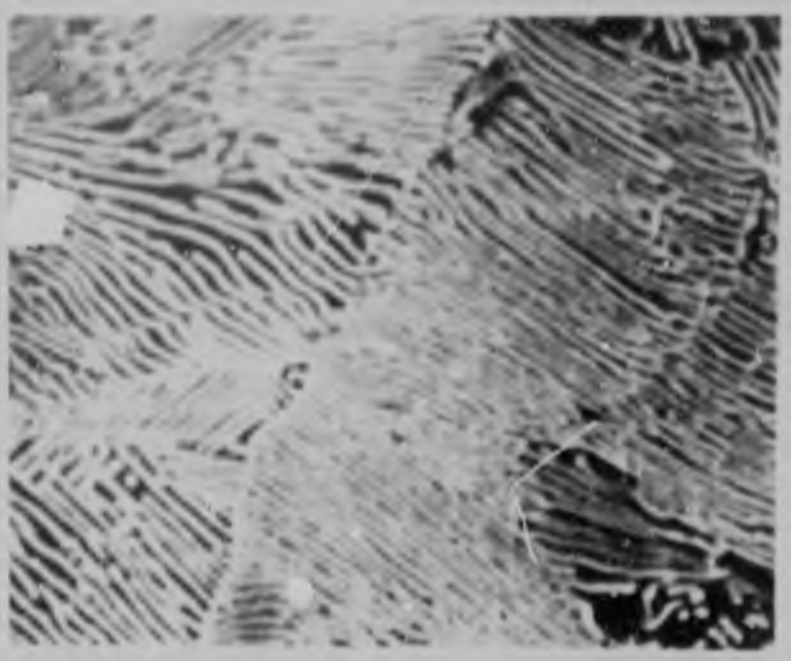

1.0μm

(c)

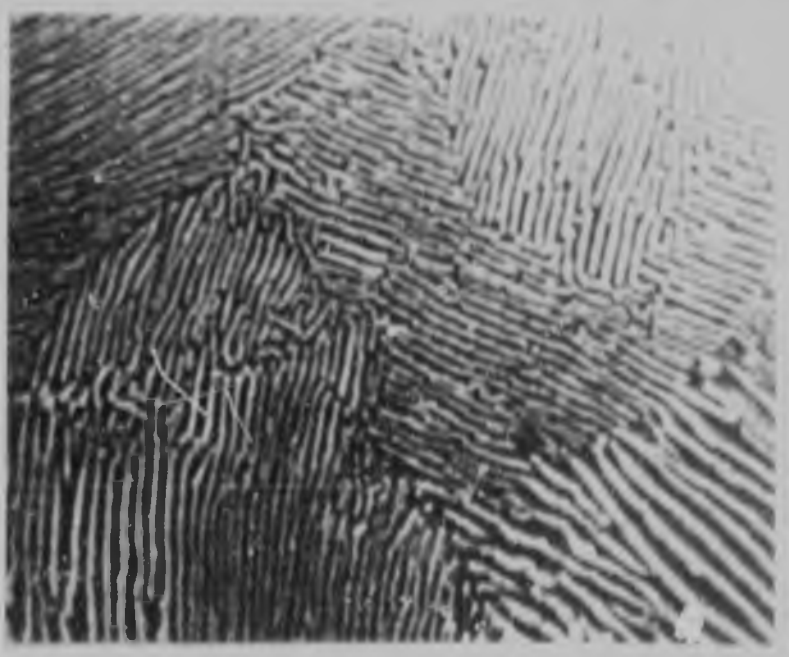

1.0μm

Figure 4.13 Microstructures of samples transformed at 600 °C (a) Fe-C, (b) 1Cr-1/4Mn, (c) 1Cr-1Mn. (SEM micrographs)

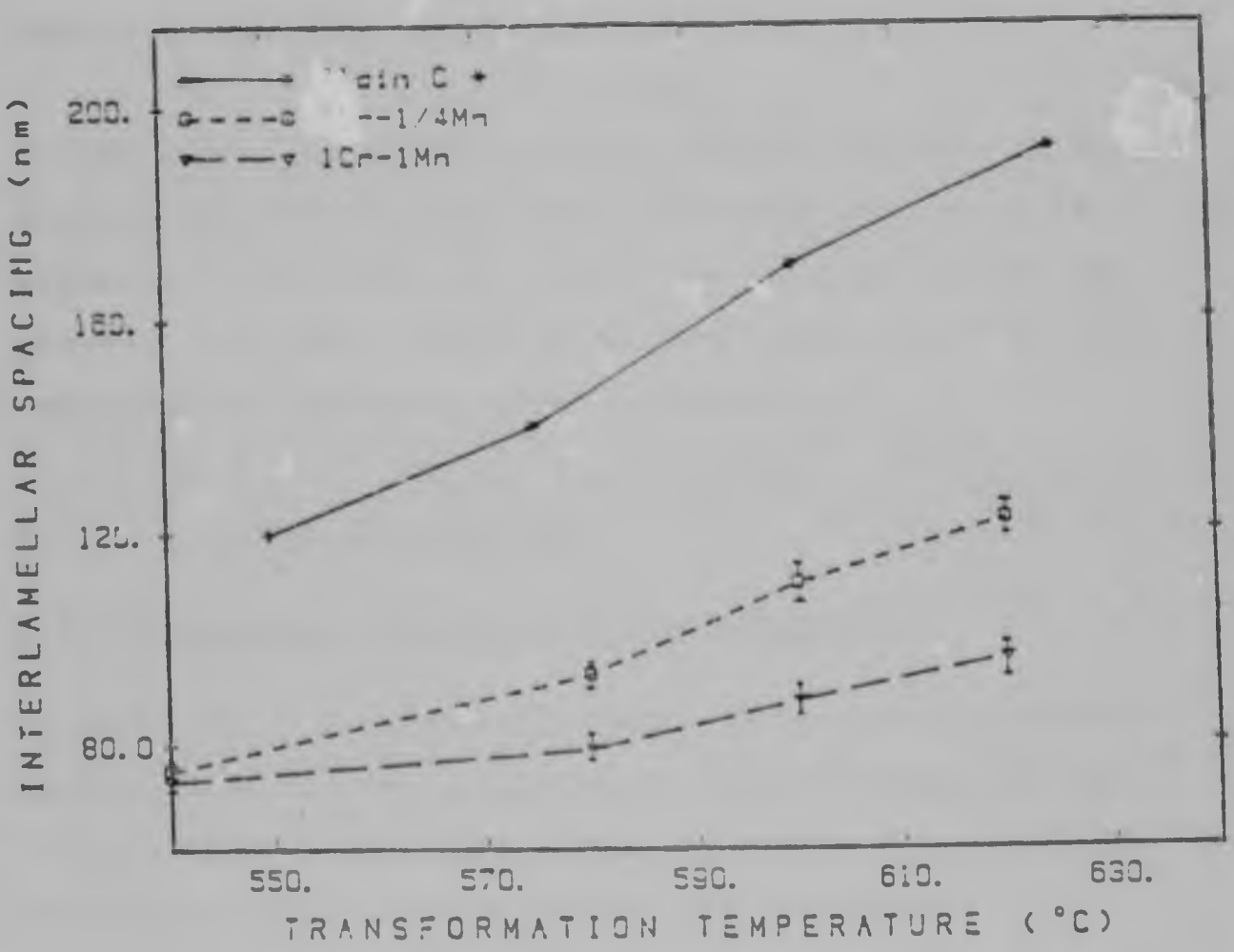

Figure 4.14 Interlamellar spacing as a function of the transformation temperature in the Cr-Mn alloys compared with a plain carbon steel.
* After Smith and Speirs.

4.2.2.3 Conventional transmission electron microscopy (CTEM)

Thin foil specimens were used to evaluate substructural characteristics of the steels in the as-patented condition.

In the iron-carbon alloy, most of the pearlite colonies appeared extremely regular (Figure 4.15) with both uniform spacing and distribution of the lamellae.

In the 1Cr-$^{1}/_{4}$Mn steels, a more complex pattern of the cementite distribution was observed (Figure 4.16). However, in the 1Cr-1Mn steel the microstructure was greatly refined, with a marked reduction in the interlamellar spacing as shown in Figure 4.17.

4.2.3 Mechanical properties

4.2.3.1 Effect of the austenitising treatment

In this initial investigation, the effect of both austenitising time and temperature were determined for the 1Cr-1Mn alloy. This alloy was subjected to six different austenitisation treatments as given in Table 4.2.

The hardness values obtained as a function of the austenitising time and temperature are given in Table 4.3 and plotted in Figure 4.18. It is clear that both time and temperature of austenitisation have a marked effect on hardness.

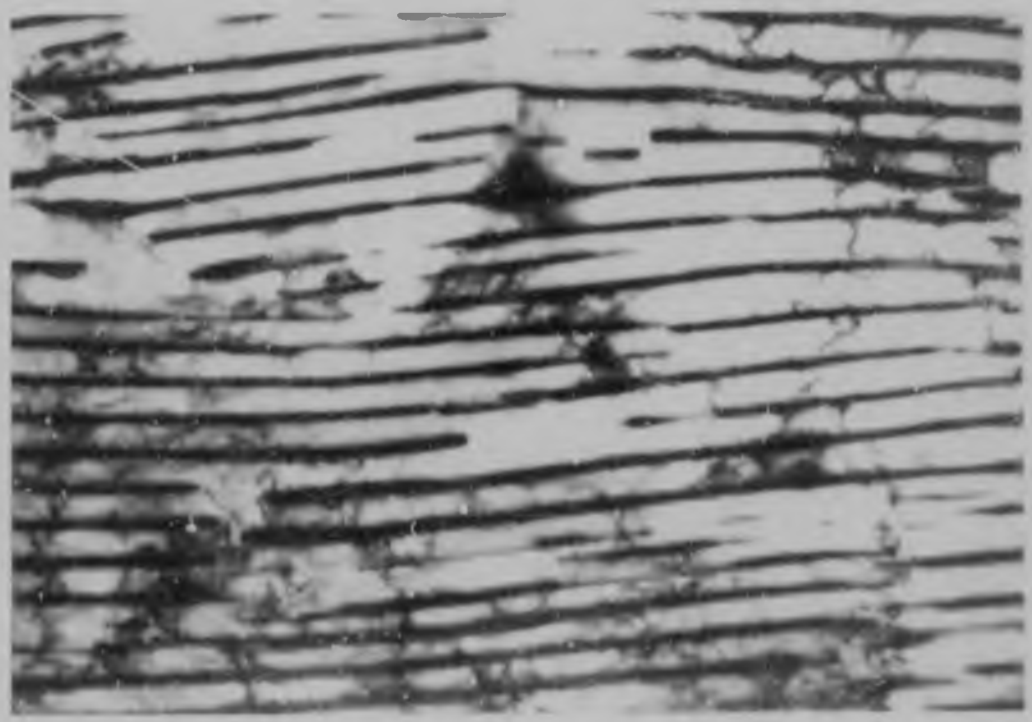

0.15μm

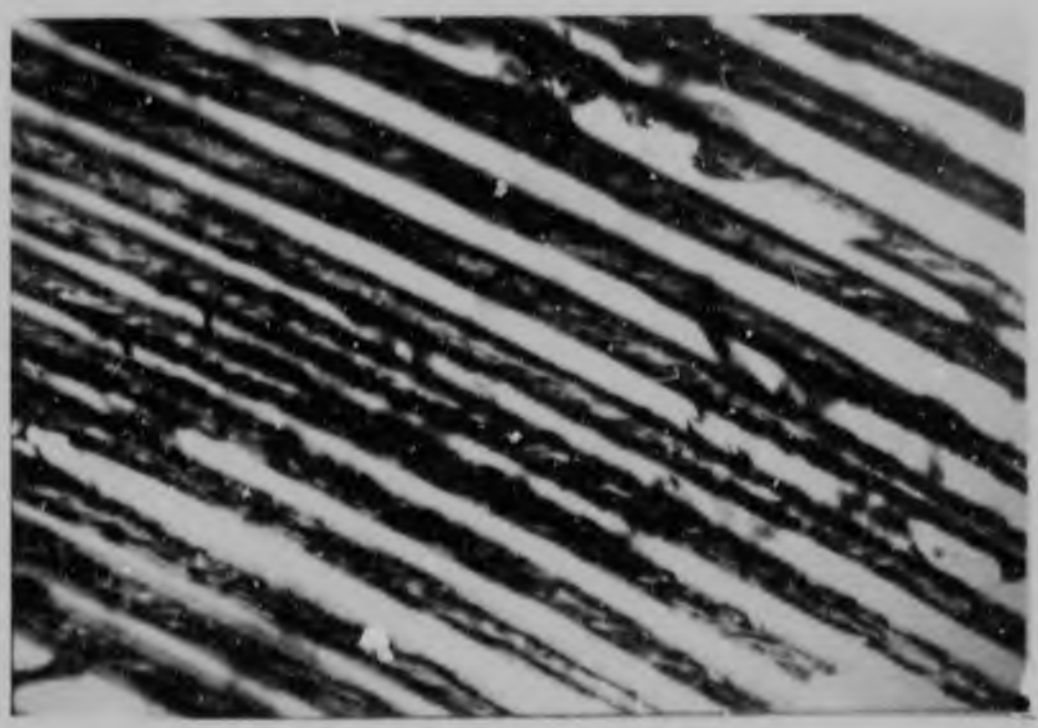

0.2μm

Figure 4.15 Regular pearlite colonies in a high purity Fe-C alloy. (TEM micrographs)

Figure 4.16 Complex pattern of the cementite distribution in the 1Cr-1/4Mn alloy (TEM micrographs)

(a)

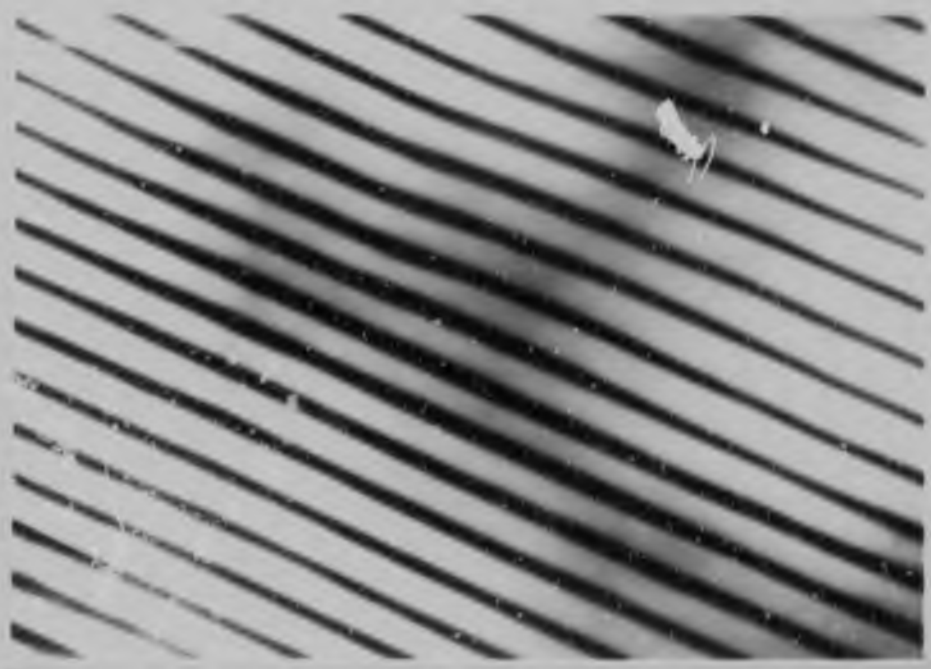

0.1μm

(b)

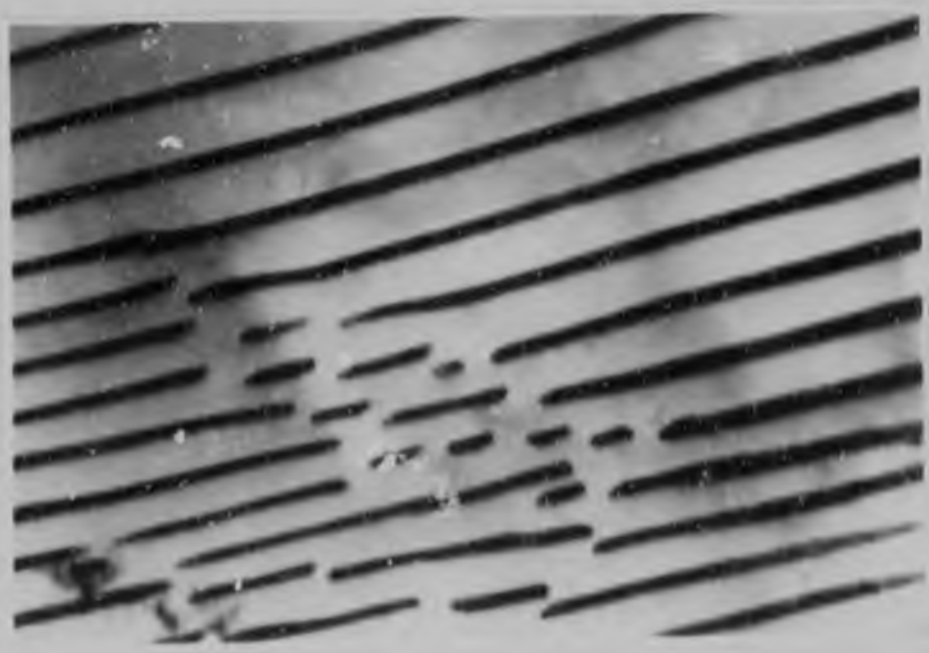

0.2μm

Figure 4.17 TEM micrographs of the 1Cr-1Mn alloy, showing:
(a) very fine and uniform pearlite,
(b) fragmentation of the cementite lamellae.

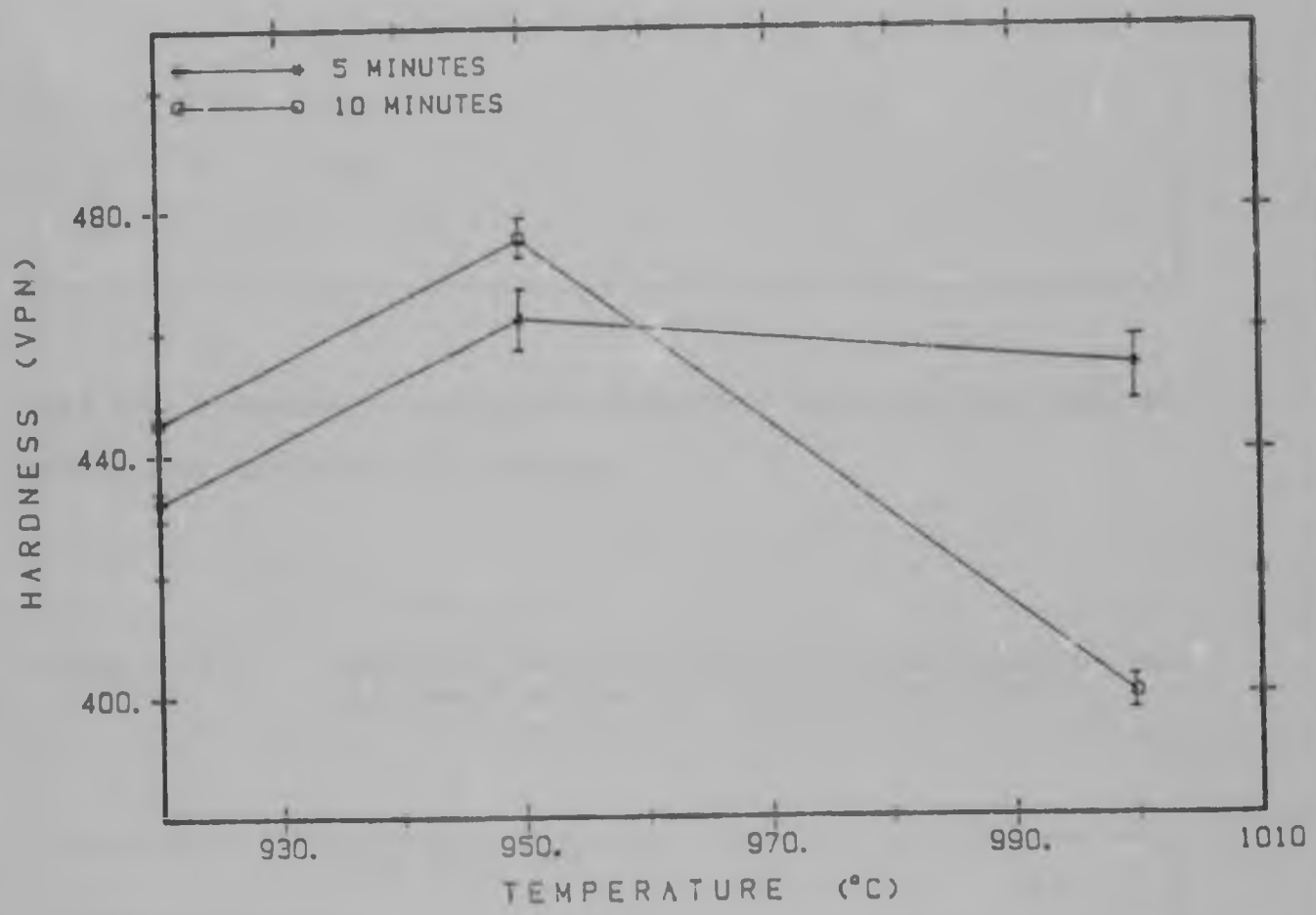

Figure 4.18 The effect of the austenitising time and temperature on the hardness of the alloy 1Cr-1Mn.

Table 4.2 Austenitising treatments for the 1Cr-1Mn alloy

Temperature (°C)	Time (minutes)
1000	5, 10
950	5, 10
920	5, 10

All the specimens were then quenched into molten lead at 540°C and held for 15 minutes.

Table 4.3 Hardness as a function of austenitising time and temperature for the 1Cr-1Mn alloy.

Temperature (°C) \ Time (minutes)	5	10
920	432	445
950	462	475
1000	454	400

Austenitisation at 920°C may not ensure full homogeneity. Areas of relatively clean ferrite were observed which would account for the lower hardness values. A temperature of 950 °C gave the highest values. At 1000 °C, austenite growth resulted in a reduction in hardness.

Examination using SEM showed some degree of bainite formation in all the specimens. This was more extensive in specimens austenitised for the shorter period at the lower temperature (920 °C) as shown in Figure 4.19.

4.2.3.2 Mechanical properties of the as-patented rods

Tensile strength, ductility and hardness were measured in samples austenitised at 950 °C for 20 minutes and transformed in the temperature range 540 to 660 °C. The results are listed in Table 4.4 and plotted in Figures 4.20 to 4.22.

In Figure 4.23, the as-patented strength values are compared with a commercial plain carbon steel.

The highest strength and hardness values were measured for a structure that was found to contain some bainite. The

(a)

2um

(b)

5um

(c)

5um

Figure 4.19 SEM micrographs of the alloy 1Cr-1Mn austenitised at different temperatures for 5 minutes. (a) 920 °C, (b) 950 °C, (c) 1000 °C.

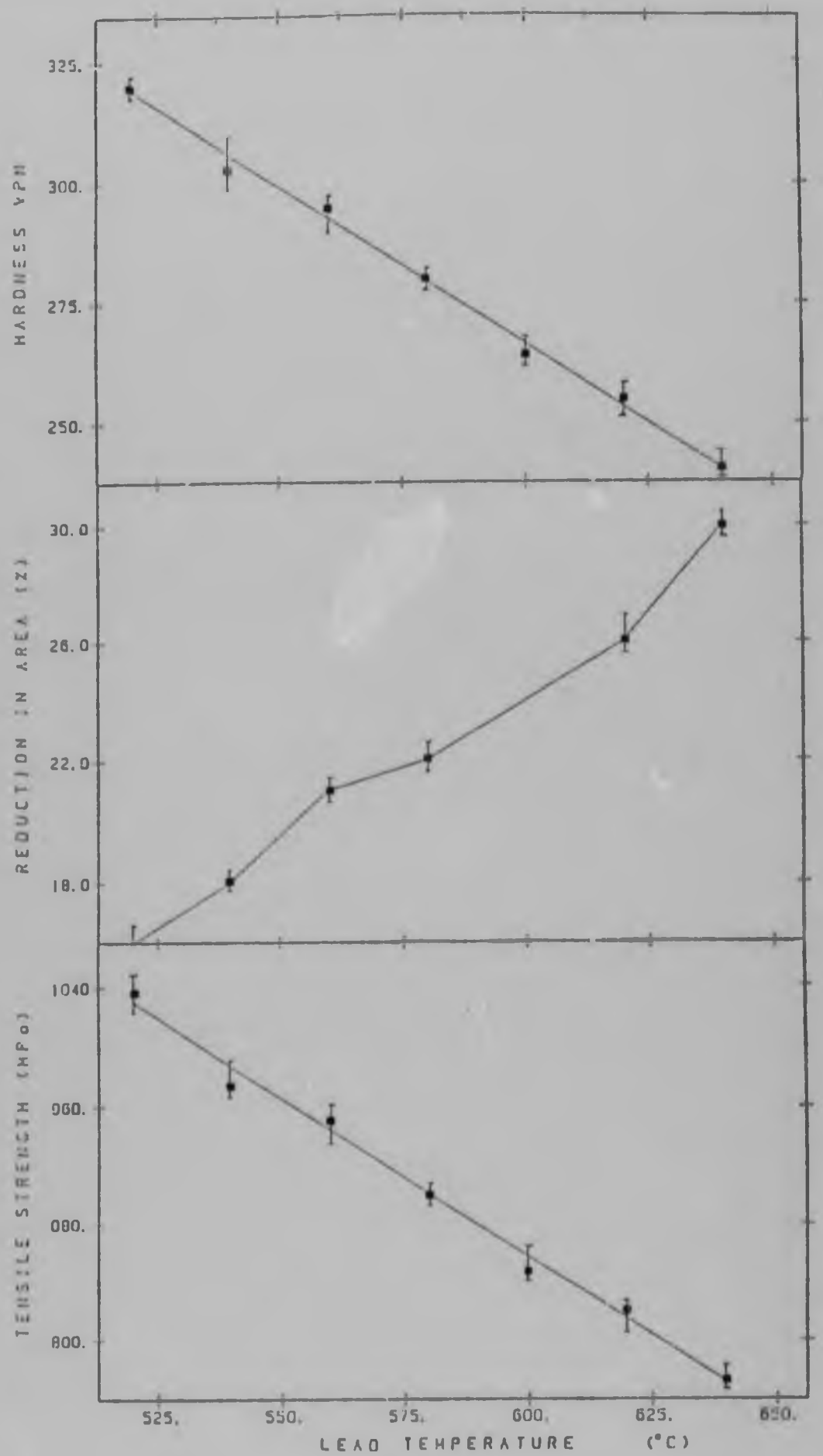

Figure 4.20 Mechanical properties of the Fe-C alloy.

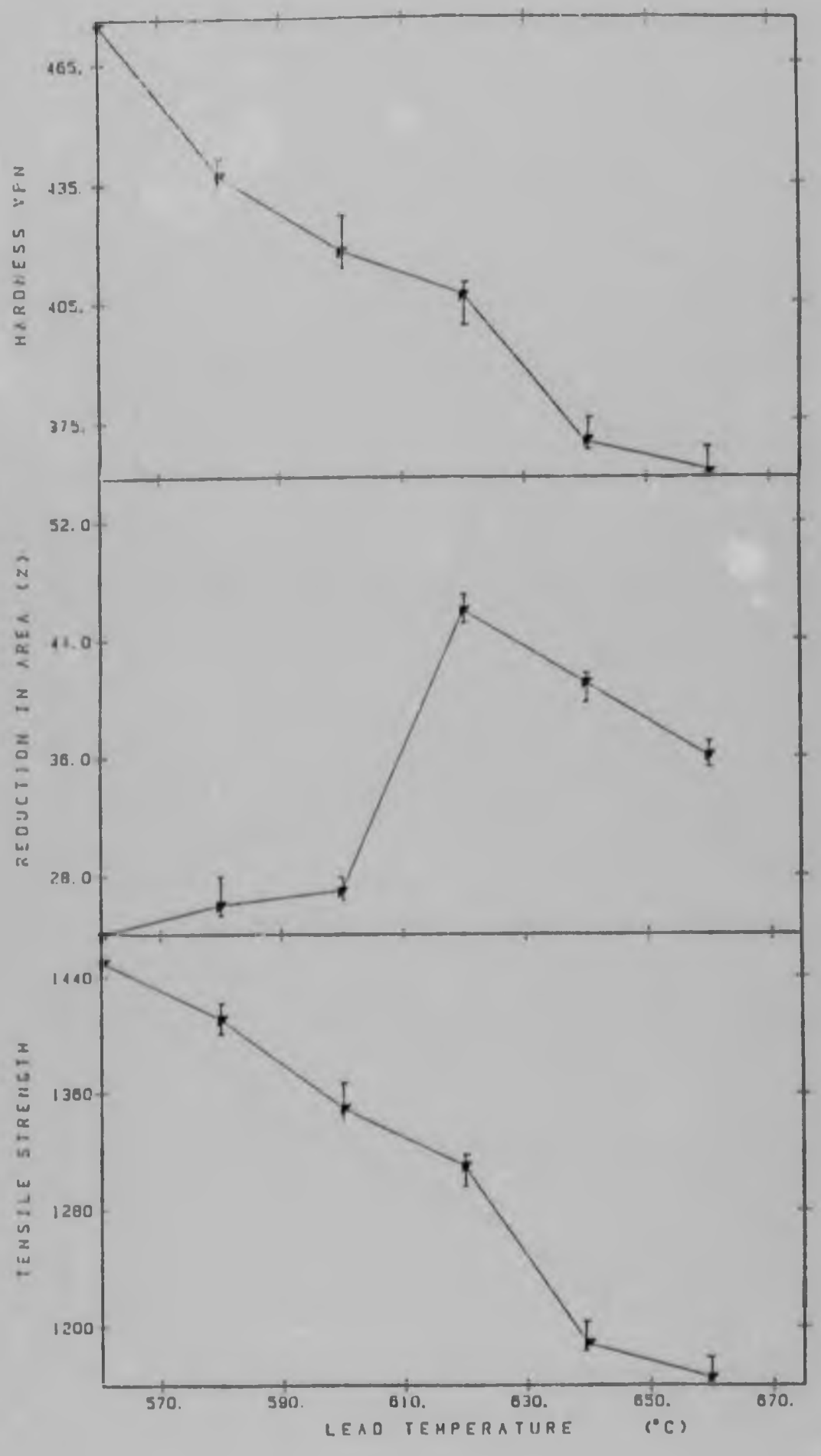

Figure 4.21 Mechanical properties of the 1Cr-1/4Mn alloy.

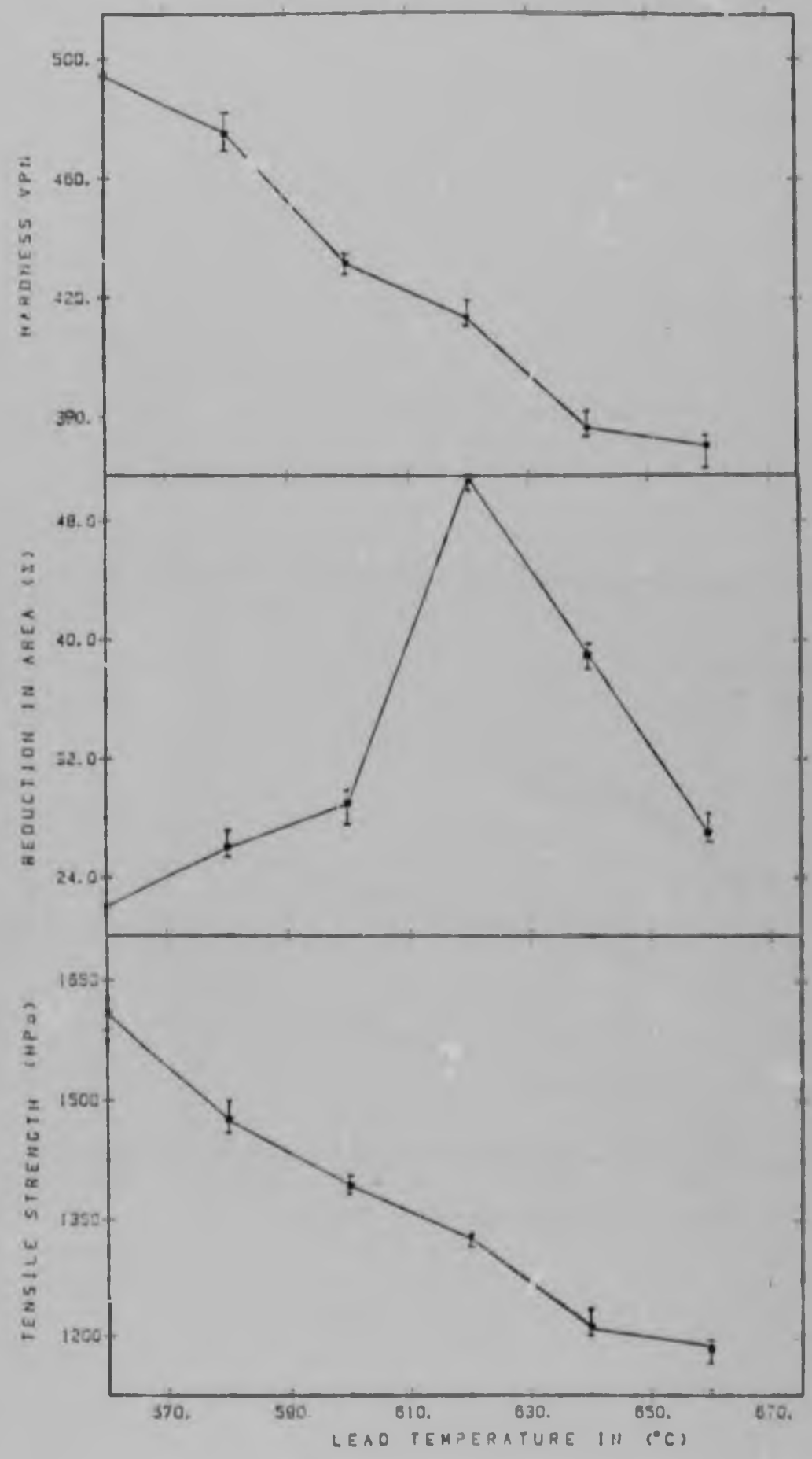

Figure 4.22 Mechanical properties of the 1Cr-1Mn alloy.

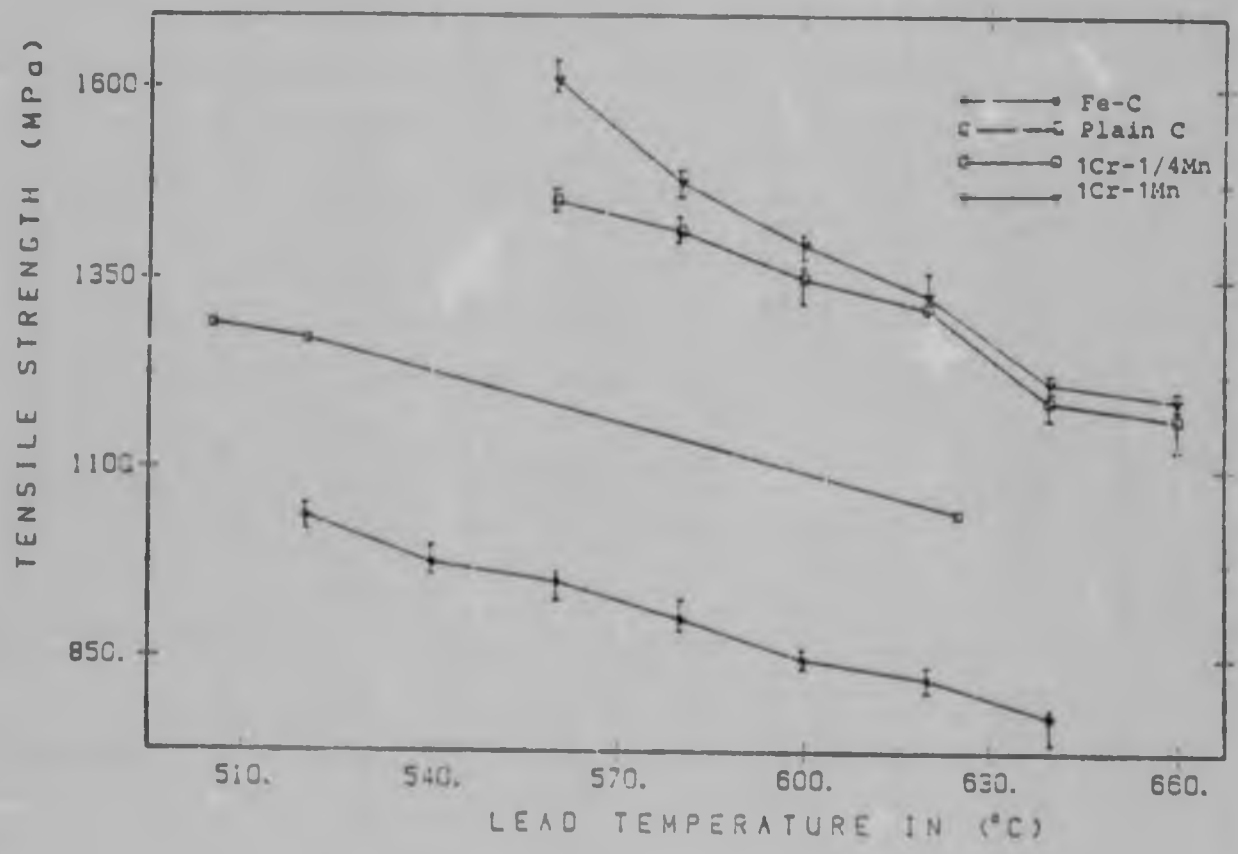

Figure 4.23 Tensile strength as a function of the lead bath temperature.

largest ductility was measured for a fully pearlitic structure, with a regular lamellar form. Very low strength values were measured for the high purity iron-carbon alloy.

Table 4.4 Mechanical properties of as-patented rods of the Fe-C and Cr-Mn alloys.

Steel	Lead temperature (°C)	Tensile strength (MPa)	R.A. (%)	Hardness (VPN)
Fe-C	520	1037	16.0	320
	540	975	18.6	303
	560	950	21.3	295
	580	901	22.3	280
	600	847	24.0	264
	620	821	26.1	255
	640	772	29.6	240
1Cr-1/4Mn	560	1450	24.6	475
	580	1411	26.0	437
	600	1349	27.0	418
	620	1310	45.8	407
	640	1188	40.6	370
	660	1165	36.1	362
1Cr-1Mn	560	1608	22.0	494
	580	1475	25.8	457
	600	1393	29.5	431
	620	1327	51.3	413
	640	1213	39.0	376
	660	1190	27.0	370
Plain - C commercial *	505	1290		400
	520	1270		4
	625	1070		323

* After Franklin et al (1980).

4.2.4 Drawing trials

4.2.4.1 Mechanical properties of the drawn wires

Drawing trials on the Cr-Mn alloys were carried out at Haggie Rand by Dockrat and Neff (1981).

Wires were drawn from 9.42mm diameter rods austenitised at 930°C for 8 minutes and transformed at 590°C for 4 minutes. The work hardening curves of the alloy steels and of a commercial plain carbon steel are plotted in Figure 4.24, and the values measured listed in Table 4.5.

A work hardening rate of 400MPa per unit strain was measured for the 1Cr-1/4Mn alloy. This is similar to the plain carbon steel. A slightly higher value, of 410MPa per unit strain was measured for the 1Cr-1Mn alloy.

The maximum as-drawn strength was achieved only with a total loss of residual ductility.

4.2.4.2 Conventional transmission electron microscopy of the drawn wires

Thin foils were prepared from transverse sections of the drawn wires. Transmission electron micrographs (Figure 4.25) showed a cellular substructure similar to that observed by Embury and Fisher (1966). In colonies in which the lamellae were not favourably orientated for slip,

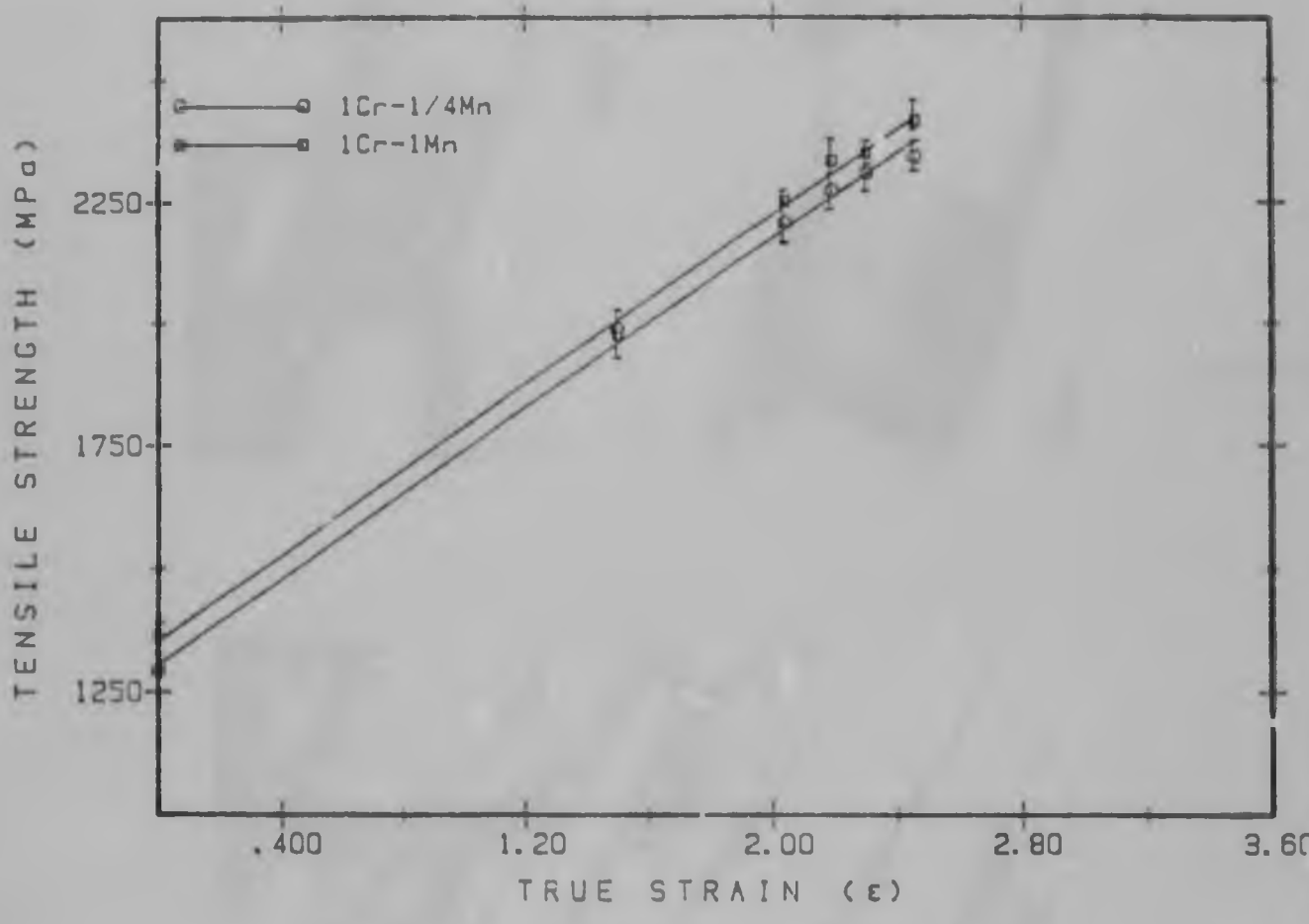

Figure 4.24 Work hardening curves of the alloys in the preliminary investigation.

(a)

(b)

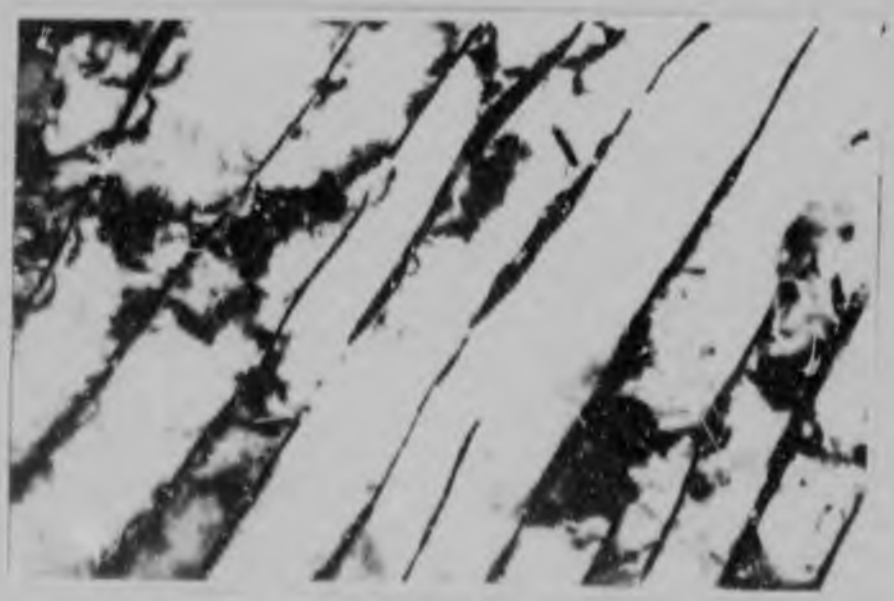

Figure 4.25 T E M micrographs of as-drawn wires showing cellular substructures. (a) Fe-C alloy, (b) 1Cr-1Mn alloy.

Table 4.5 As-drawn tensile strengths of the different alloys.

Alloy	True strain (ε)	Tensile strength (MPa)
Commercial Plain C *	0	1230
	1.0	1630
	1.5	1800
	2.0	2030
1Cr-1/4 Mn	0	1290
	1.5	1986
	2.04	2203
	2.19	2270
	2.3	2307
	2.46	2340
1Cr-1Mn	0	1360
	1.5	1973
	2.04	2250
	2.19	2333
	2.3	2350
	2.46	2416

* After Langford (1977).

considerable bending and fragmentation of the cementite lamellae were observed (Figure 4.26).

4.3 Further Discussion

4.3.1 TTT diagrams

The TTT diagrams were shifted to longer incubation and completion times due to the addition of alloying elements in agreement with the results reported by Jatczak (1973) and Franklin et al (1980). The 1Cr-1Mn alloy showed the longest reaction times, again supporting the evidence of Al-Salman et al (1979a) for the same alloy composition. The temperature of the nose of the pearlite curve appears to be very similar for both alloy steels. This may be explained by the balancing of the well documented effects of chromium additions raising the critical temperatures, and manganese lowering them.

Although the pearlite and bainite curves are clearly separated, they overlap in the temperature range 450 to 550 °C, as also reported by Kennon and Kaye (1982).

There is a reasonable agreement between the TTT diagrams obtained by dilatometry and optical microscopy. The only apparent discrepancy was a shorter incubation time in the 1Cr-1Mn diagram obtained metallographically. This is almost certainly due to the marked difference in grain size of the samples used in the two methods of determination.

(a)

0.1μm

(b)

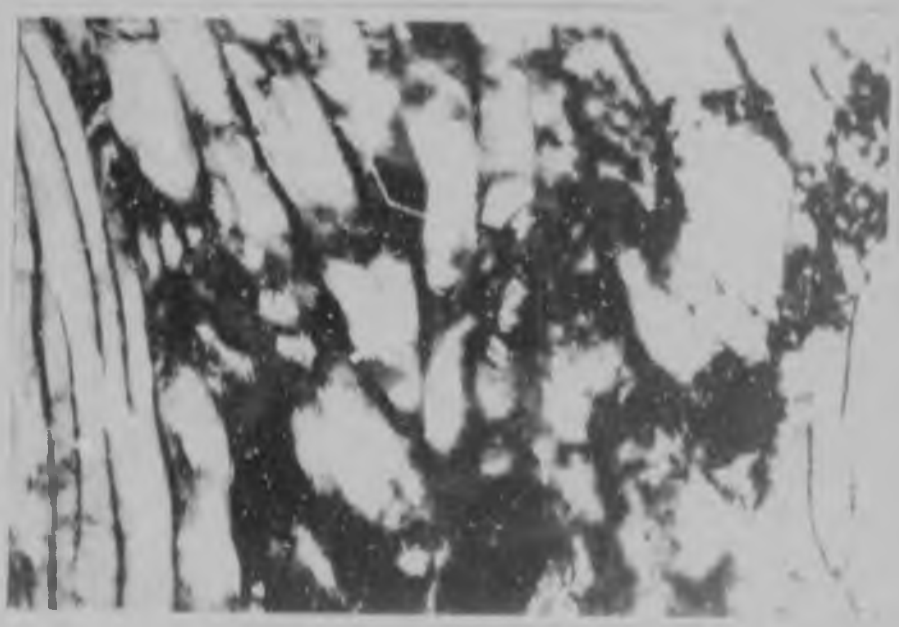

0.05μm

Figure 4.26 Bending and fragmentation of the pearlite lamellae as a result of the drawing process. (a) Fe-C alloy, (b) 1Cr-1Mn alloy.

(a)

0.1μm

(b)

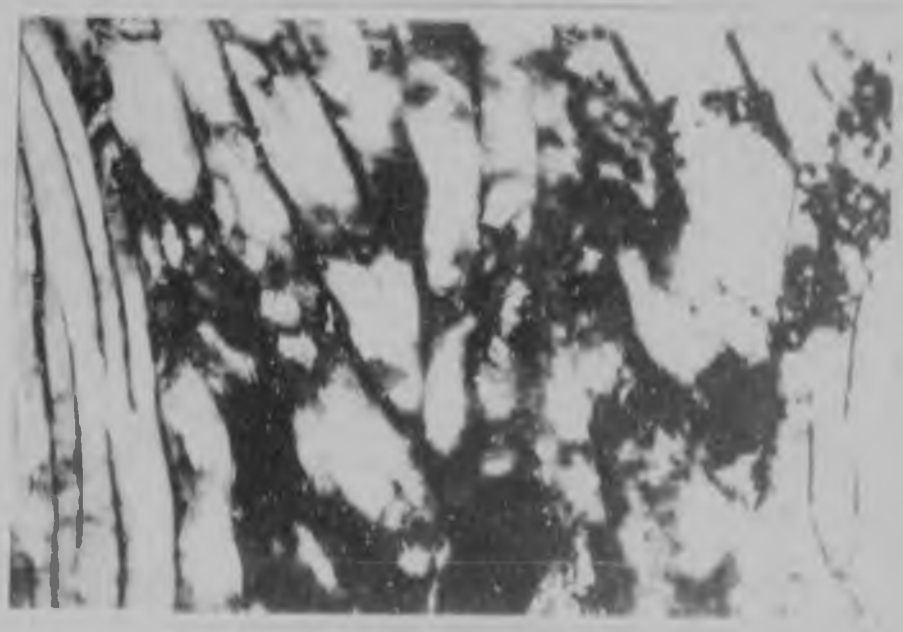

0.05μm

Figure 4.26 Bending and fragmentation of the pearlite lamellae as a result of the drawing process. (a) Fe-C alloy, (b) 1Cr-1Mn alloy.

In order to perform the experiments at temperatures of interest for wire drawing, relatively low transformation temperatures were chosen in the initial stage, and were subsequently increased in order to improve ductility.

4.3.2 Microstructural observations

At low transformation temperatures, the microstructure consisted of bainite and pearlite, the amount of bainite increasing with the undercooling. For a given transformation temperature, more bainite was observed in the 1Cr-1/4Mn steel. This is in agreement with Fletcher (1978), who has shown that by reducing manganese and chromium content the bainite kinetics are accelerated. The bainitic structure is detrimental for wire drawing purposes because of the coarseness and irregularity of this structure.

For the fully transformed samples, it was relatively easy to resolve the fine structures in the SEM and to measure the interlamellar spacings over many fields of view. The lamellar structure appeared to be finer and more uniform in the higher manganese steel. Davy and Glover (1968) also observed that in steels containing 1/4 and 1/2% manganese the pearlite tended to degenerate, while increasing the manganese content of a hypo-eutectoid steel to 1 - 2% diminished the tendency of the carbides to form as boundary films.

Refinement of the pearlite spacings due to chromium additions was reported by Mazzucato et al (1981), while conflicting results were reported by the Manchester group: Razik et al (1974; 1976) and Al Salman et al (1979a).

On the basis of the present results, the 1Cr-1Mn alloy represents a most promising composition for producing a uniform, fully pearlitic structure through isothermal transformation.

4.3.3 Mechanical properties

4.3.3.1 Effect of the austenitising treatment

The purpose of the austenitising treatment is to optimise homogeneity and grain size. In this preliminary study, austenitisation at 920 °C would not be expected to provide homogeneity. Austenitising at 1000 °C for short times will lead to grain growth and a decrease in hardness.

It appears that a holding time of 5 to 10 minutes at 950 °C is the most suitable austenitising treatment, this is reflected in the hardness values obtained after transformation. Similar trends were reported by Cahill and James (1968b) for a plain carbon eutectoid steel.

4.3.3.2 As-patented tensile strength

The tensile strength was found to increase with increasing undercooling. Although reduction in tensile strength which coincides with the formation of upper bainite was reported by Cahill and James (1968a) and Franklin et al (1980), high strength values were measured for the mixed microstructures. This may be due to the presence of very fine pearlite.

A significant difference was observed between the ductilities of the iron-carbon and the chromium-manganese alloys, as measured by the reduction in area. The relatively high as-patented tensile strength measured, showed the potential benefit of small manganese and chromium additions to a iron-carbon alloy.

While the high-purity plain carbon alloy studied is useful for providing theoretical baseline data, the results should not be compared in any way with commercial "plain-carbon" steels. The latter have manganese additions and impurities, both of which have a beneficial effect on strength.

4.4 Summary

These initial results derived for the effect of manganese and chromium alloying additions are in good agreement with the expected influence of these elements on the pearlite and bainite transformations. For the development of a fine, uniform pearlitic structure, the 1Cr-1Mn alloy appears the most promising by providing a reasonable incubation period without excessively increasing the completion time for the reaction. A further advantage is that the bainitic region is well separated from pearlite. But, while the rod tensile properties and as-drawn wire strength were better than in a plain carbon steel, the Cr-Mn alloys did not reach the project target.

In view of these results, it was decided to investigate another range of steels, containing silicon, as will be described in the next chapter.

CHAPTER FIVE - OTHER HIGH-PURITY ALLOYS

5.1 Introduction

Following the preliminary investigation, there was still a demand for higher strength levels. Silicon was selected as a promising further alloying addition since it is known to produce marked solid solution strengthening of the ferrite.

Silicon in large amounts in a steel is known to reduce the ductility, and because of this it is usual to keep the silicon content low. Even when used as a deoxidiser the limit is generally around 0.3%. However, some spring steels contain up to 2% silicon, and these are conventionally drawn prior to the final quenching and tempering treatment (Metals Handbook).

The aim of this investigation was to determine whether it is possible to develop fine pearlitic structures with improved mechanical properties and drawability in silicon-containing steels. It was decided to test alloys containing a maximum of 2% silicon; and since there is also some retarding influence on the pearlite reaction kinetics, systematic variations in the total alloy content were made by changing the manganese and chromium contents.

Two series of alloys were used in this study. The first was prepared at Sheffield University (these are referred to as Sheffield alloys) and the second using the facilities at the University of the Witwatersrand (Wits alloys). The chemical compositions in each alloy series are given in Tables 5.1 and 5.2 respectively.

Table 5.1 Chemical analyses of the Sheffield alloys (in weight %).

Alloy	C ± 0.01	Cr ± 0.02	Mn ± 0.02	Si ± 0.02	Others
2Si-1Mn	0.81	-	1.01	1.89	*
2Si-1Cr	0.82	0.98	-	1.88	*
1Si-1Cr-1Mn	0.83	1.00	0.97	0.98	*
2Si-1Cr-1Mn	0.86	0.97	0.96	1.95	*

* less than 0.02%

Table 5.2 Chemical analyses of the Wits alloys (in weight %).

Alloy	C +0.01	Cr +0.02	Si +0.02	S	P	N	Oth-ers
2Si-1Cr	0.80	0.99	1.88	0.0020	0.0012	0.0029	*
2Si-1Cr-0.5C	0.46	1.06	1.86	ND	ND	ND	*
2Si-1Cr-0.6C	0.61	1.03	1.87	ND	ND	ND	*
2Si-1Cr-0.7C	0.67	1.02	1.72	ND	ND	ND	*
2Si-1Cr-0.9C	0.92	1.02	1.85	ND	ND	0.0046	*
1.7Si-1Cr	0.80	1.00	1.65	0.0019	0.0010	0.0024	*

* Less than 0.02%
ND not determined

5.2 Results and Discussion

5.2.1 TTT diagram

Isothermal transformation diagrams were determined only for the high-purity alloys containing a nominal carbon content of 0.8%. These were determined again using high speed dilatometry, and the experimental curves are shown in Figures 5.1 to 5.4. The average grain size in all the alloys was approximately 120μm. It can be seen that in general the temperature ranges for the pearlite and bainite reactions are well defined. This facilitates the selection of transformation temperatures which should produce fully pearlitic fine microstructures.

The different combinations of alloying elements have different effects on the temperature, incubation time and completion time of the pearlite reaction. Comparing alloys containing 2Si-1Cr and 2Si-1Mn, it can be seen (Figure 5.5) that manganese produces a lower temperature for the nose of the pearlite C-curve and slightly increases the incubation time. The time taken for completion of the reaction is almost the same, with a minimum time of about 45 seconds.

The effect of adding chromium and manganese together to silicon-containing alloys is shown in Figure 5.6. Both the 2Si-1Cr-1Mn and 1Si-1Cr-1Mn alloys produce similar TTT diagrams. Both compositions shift the reaction C-curves to

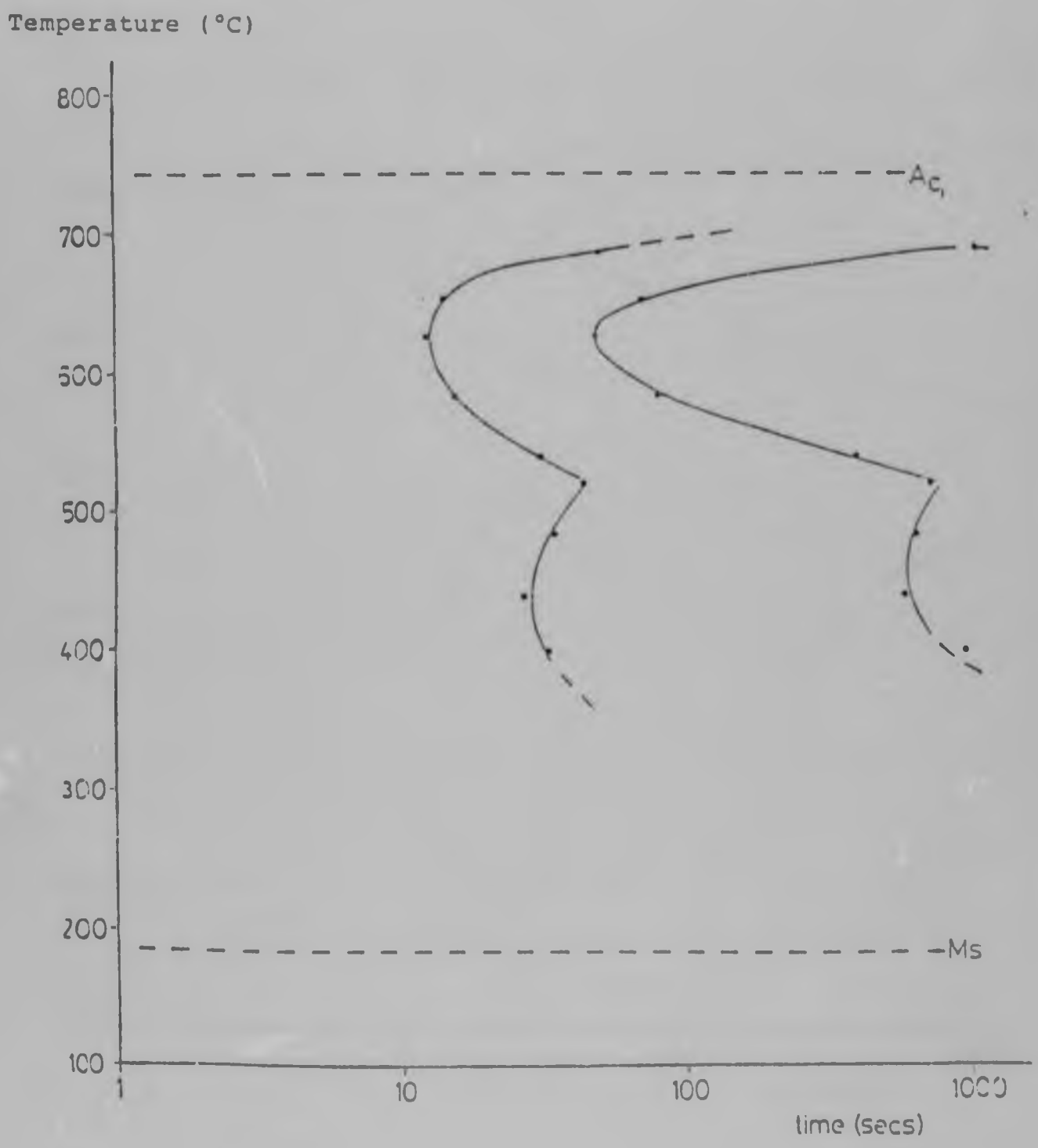

Figure 5.1 TTT diagram of the alloy 2Si-1Mn

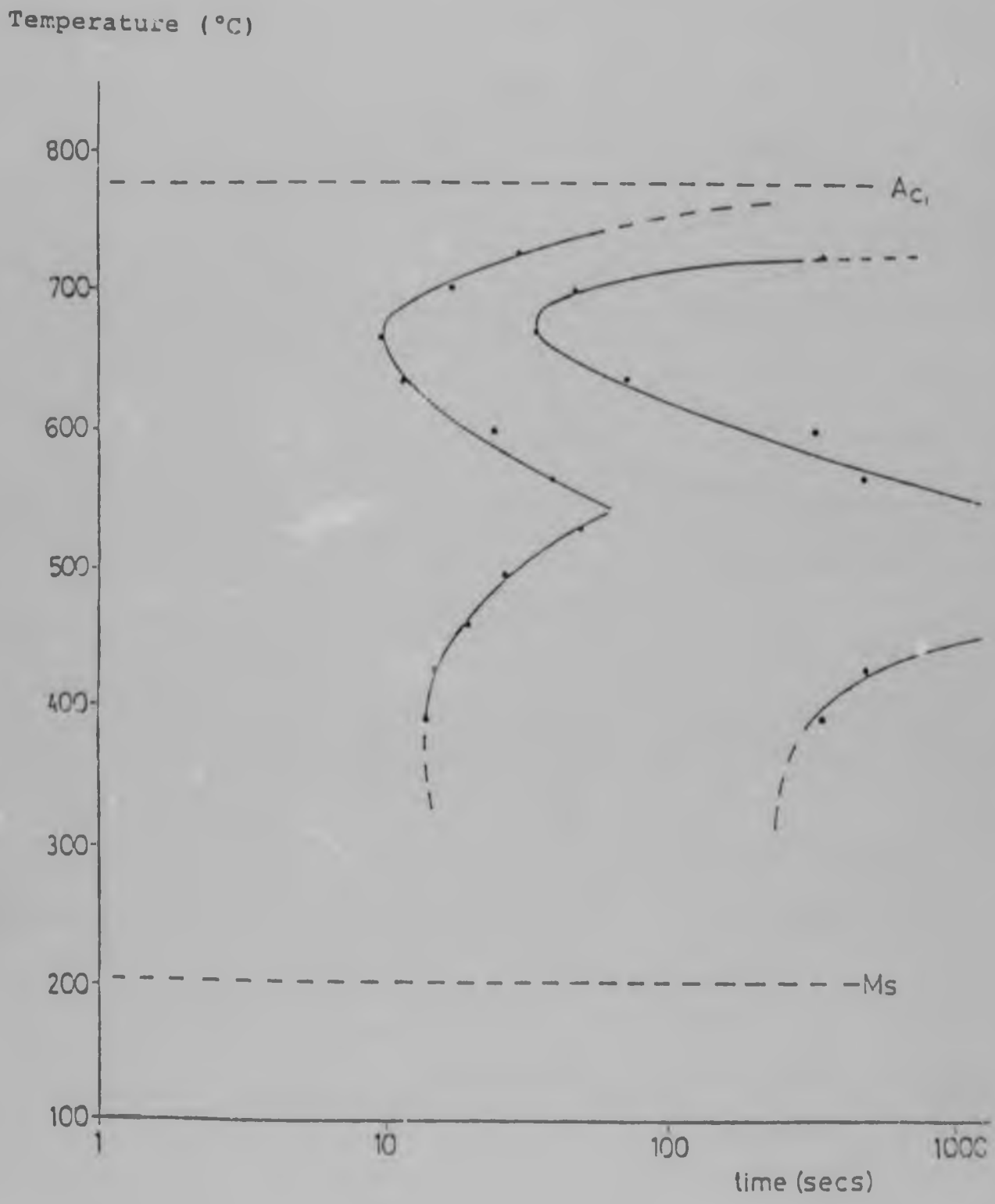

Figure 5.2 TTT diagram of the alloy 2Si-1Cr

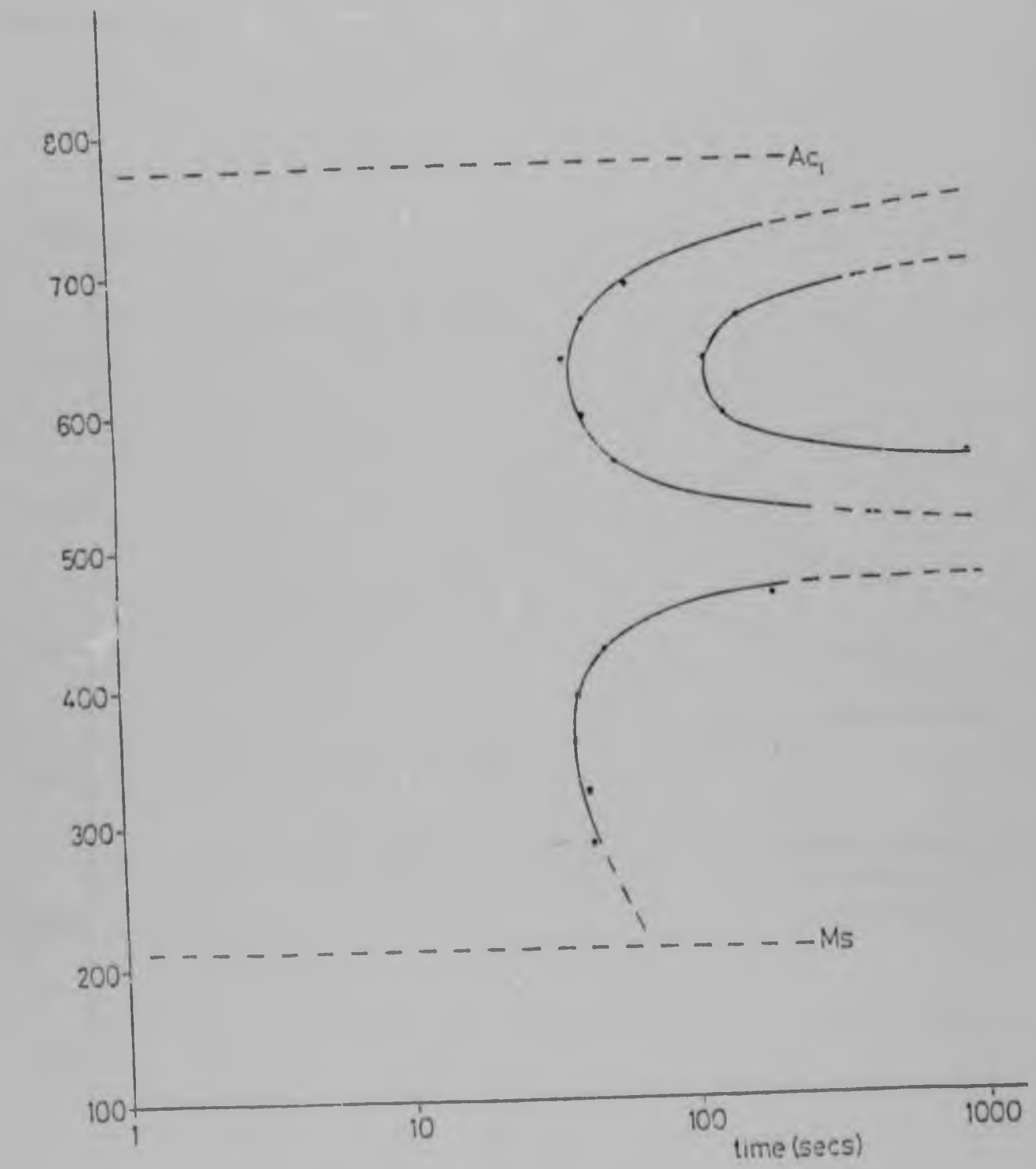

Figure 5.3 TTT diagram of the alloy 1Si-1Cr-1Mn

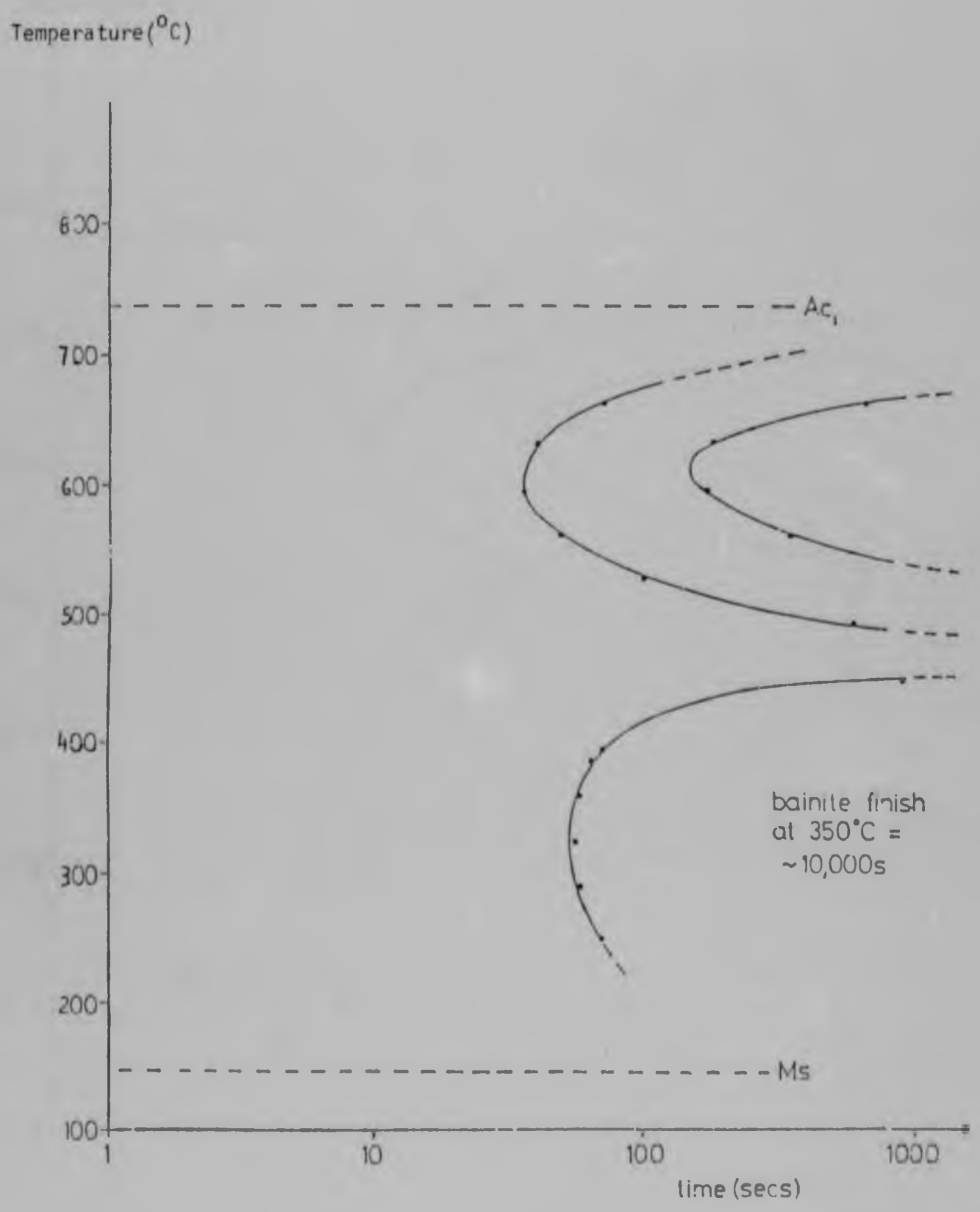

Figure 5.4 TTT diagram of the 2Si-1Cr-1Mn alloy

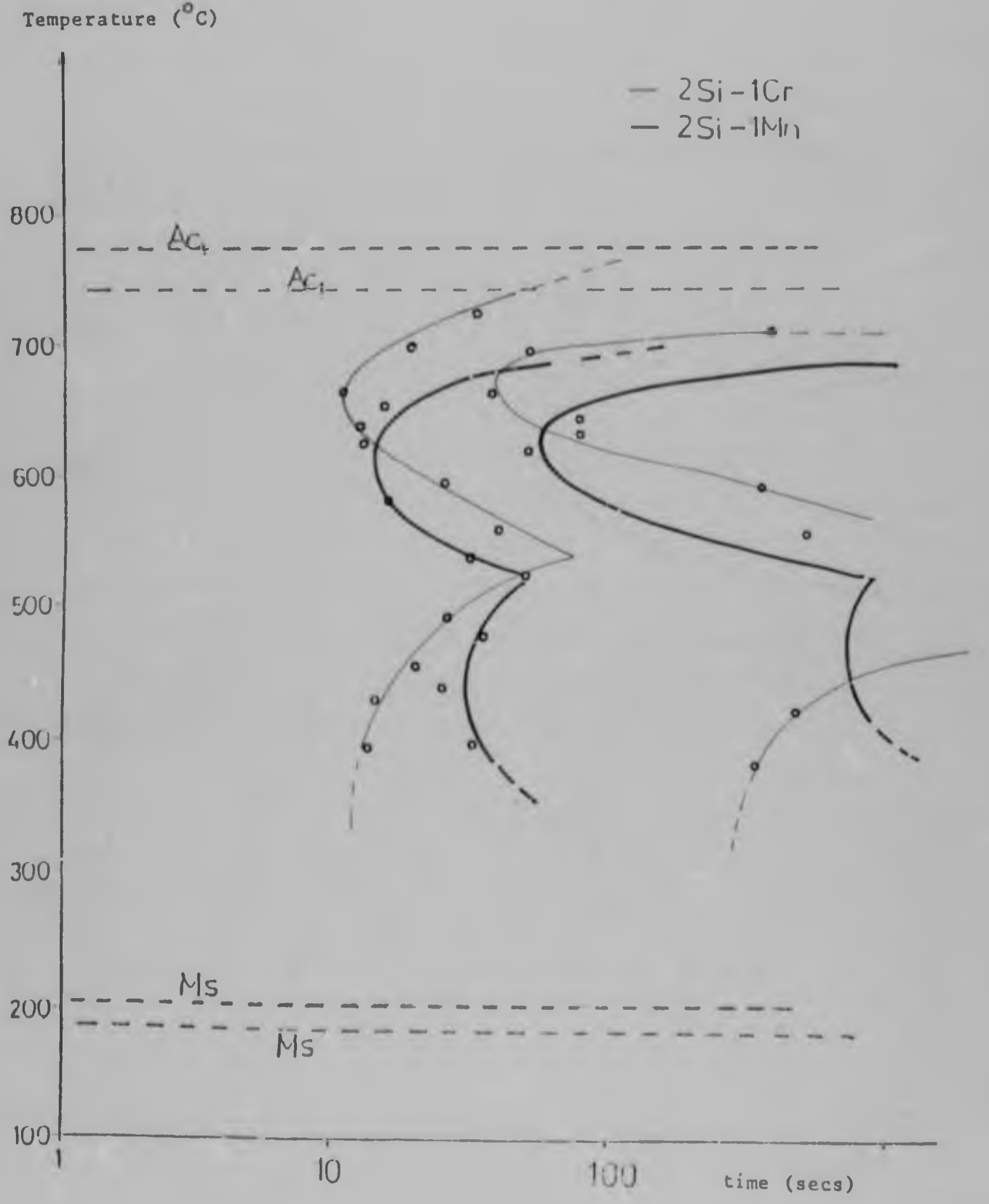

Figure 5.5 Combined TTT diagrams of the alloys 2Si-1Cr and 2Si-Mn

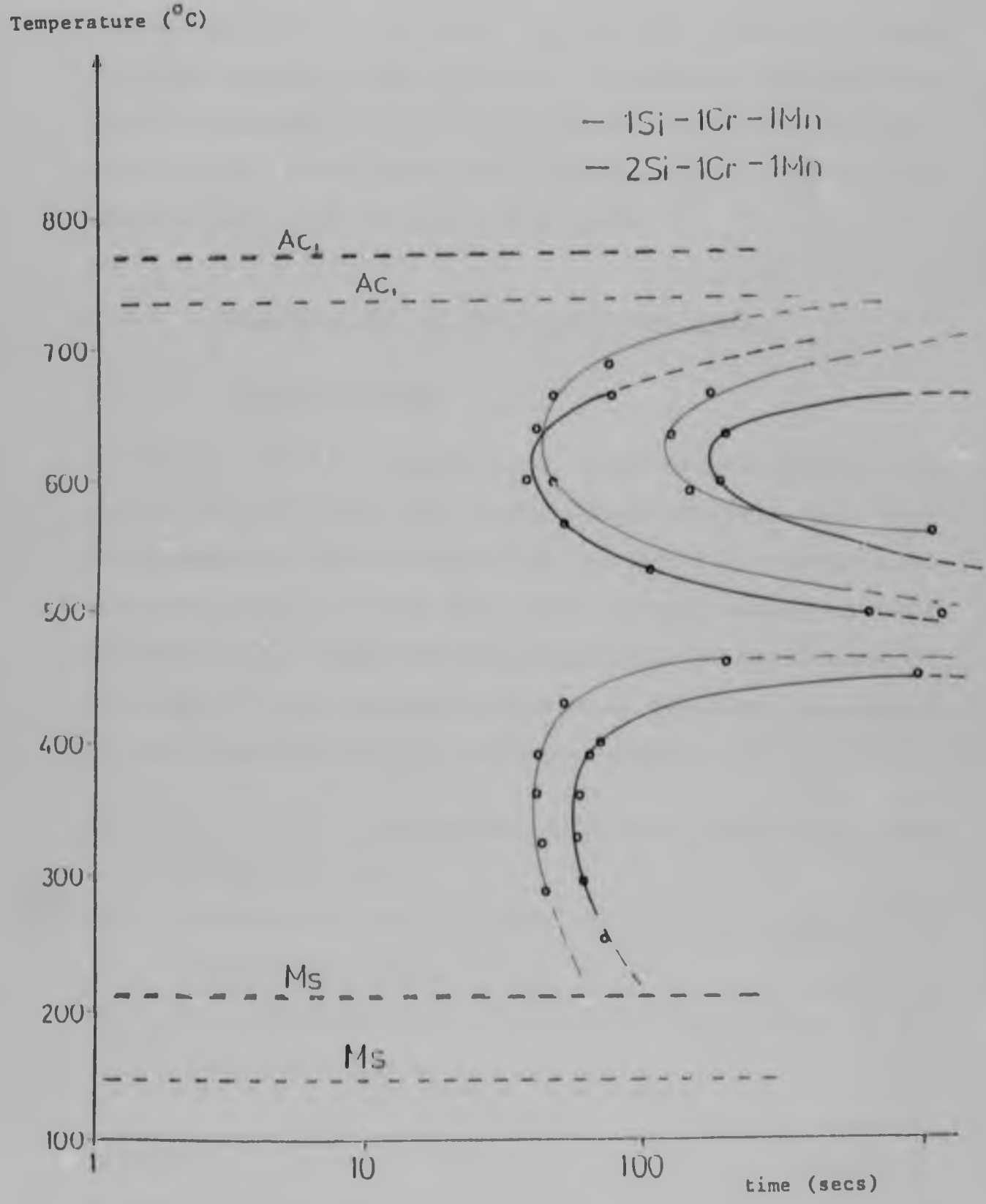

Figure 5.6 Combined TTT diagrams of the alloys 1Si-1Cr-1Mn and 2Si-Cr-1Mn

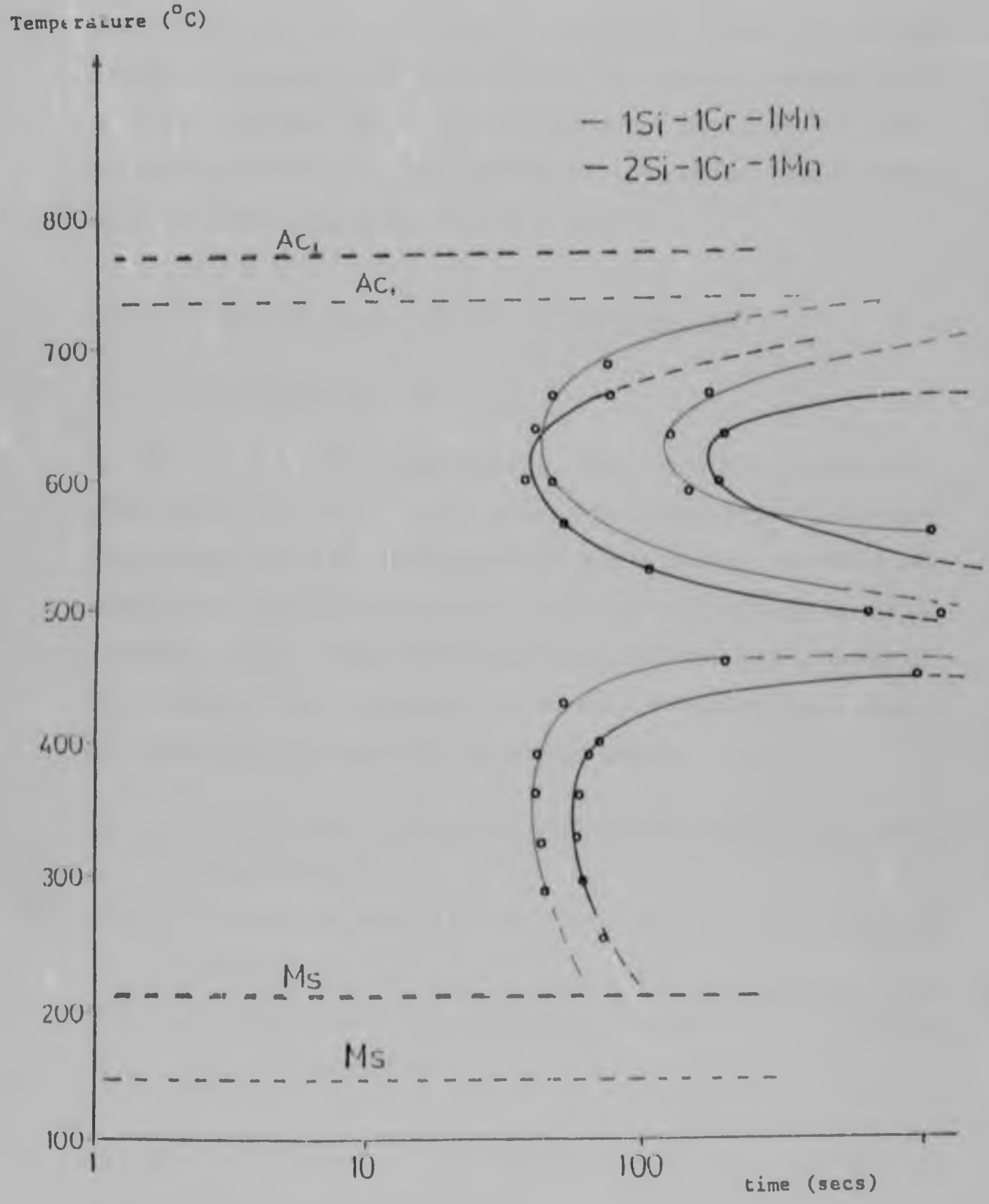

Figure 5.6 Combined TTT diagrams of the alloys 1Si-1Cr-1Mn and 2Si-Cr-1Mn

the right relative to the individual effects of chromium and manganese: the pearlite incubation time in these Si-Cr-Mn alloys is approximately 40 seconds compared with about 10 seconds for the Si-(Cr or Mn). The time for full transformation is also increased to 100 to 110 seconds compared with approximately 45 seconds.

5.2.2 Metallography of the as-patented rods

5.2.2.1 Light microscopy

In some of the early experiments, high strength levels were obtained, but with very poor ductilities. This was attributed to the presence of martensite, since even specimens heat treated for times corresponding to 100% transformation on the TTT diagrams exhibited small areas of this phase.It was considered necessary therefore to conduct an investigation with the following aims:

i) to estimate the prior austenite grain size (see Section 5.2.3.1);

ii) to confirm that the pearlite reaction had gone to completion; and

iii) to investigate the uniformity of the reaction in the rod cross-section.

In practical terms the martensite problem was overcome by extending transformation times.

The uniformity of the reaction was assessed by observing the distribution of the pearlite nodules in specimens partially transformed at 600°C, as shown in Figure 5.7. It can be seen clearly that the nodules are not uniformly distributed and that the size of the nodules varies across the diameter of the rod. Because of the relatively low transformation temperature, some upper bainite was also formed, and this may be one of the reasons for the non-uniformity of the pearlite nucleation. However, the prior austenite grain size is clearly delineated.

In fully transformed samples it was impossible to distinguish between the different phases (Figure 5.8).

5.2.2.2 Scanning electron microscopy (SEM)

All the silicon-containing alloys were studied in the SEM. For the 2Si-1Cr alloy, a systematic series of the microstructures for different heat treating times and temperatures is shown in Figure 5.9.

At 680 °C, the highest lead bath temperature tested, the cementite spheroidised during heat treatment (even after only 5 minutes). In the temperature range 660 to 600 °C the pearlite formed became progressively finer. Below 550 °C the structure began to degenerate and bainite formation was also observed. The amount of bainite in the

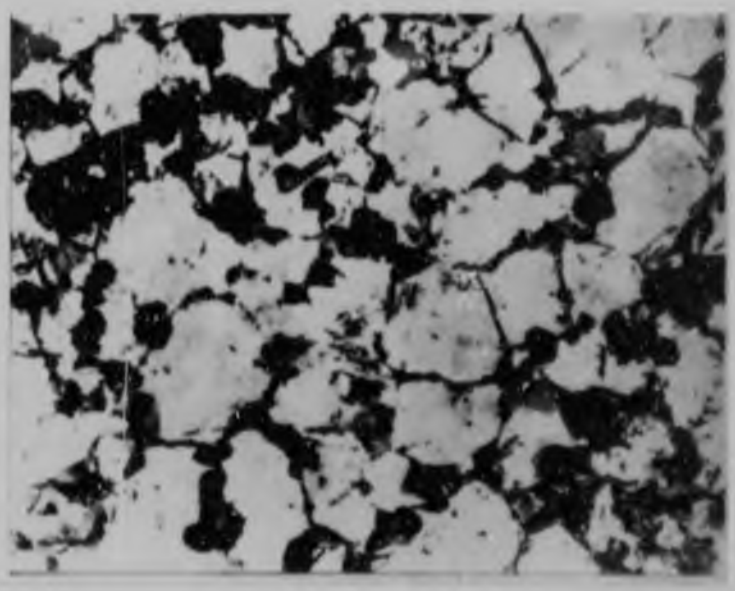

Figure 5.7 Light micrograph of the 2Si-1Cr alloy partially transformed at 600 °C following austenitisation at 1050 °C

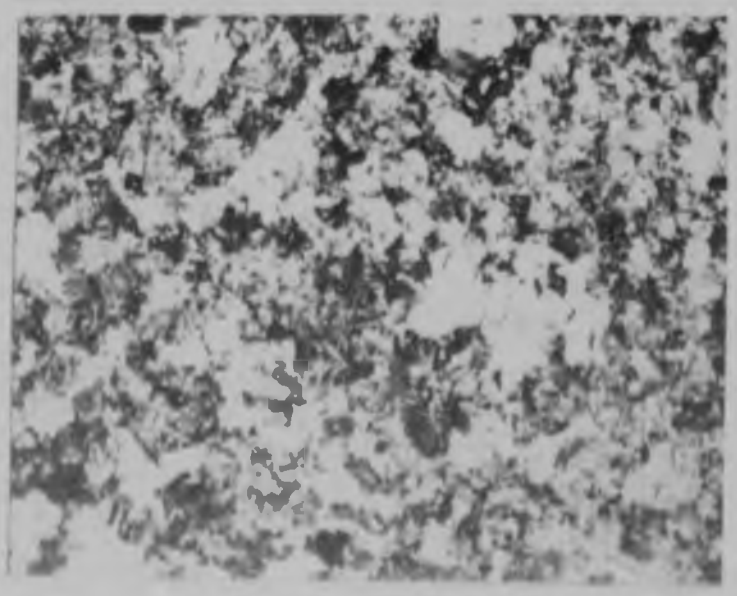

Figure 5.8 Light micrograph of a fully transformed structure

Fig
of
tr

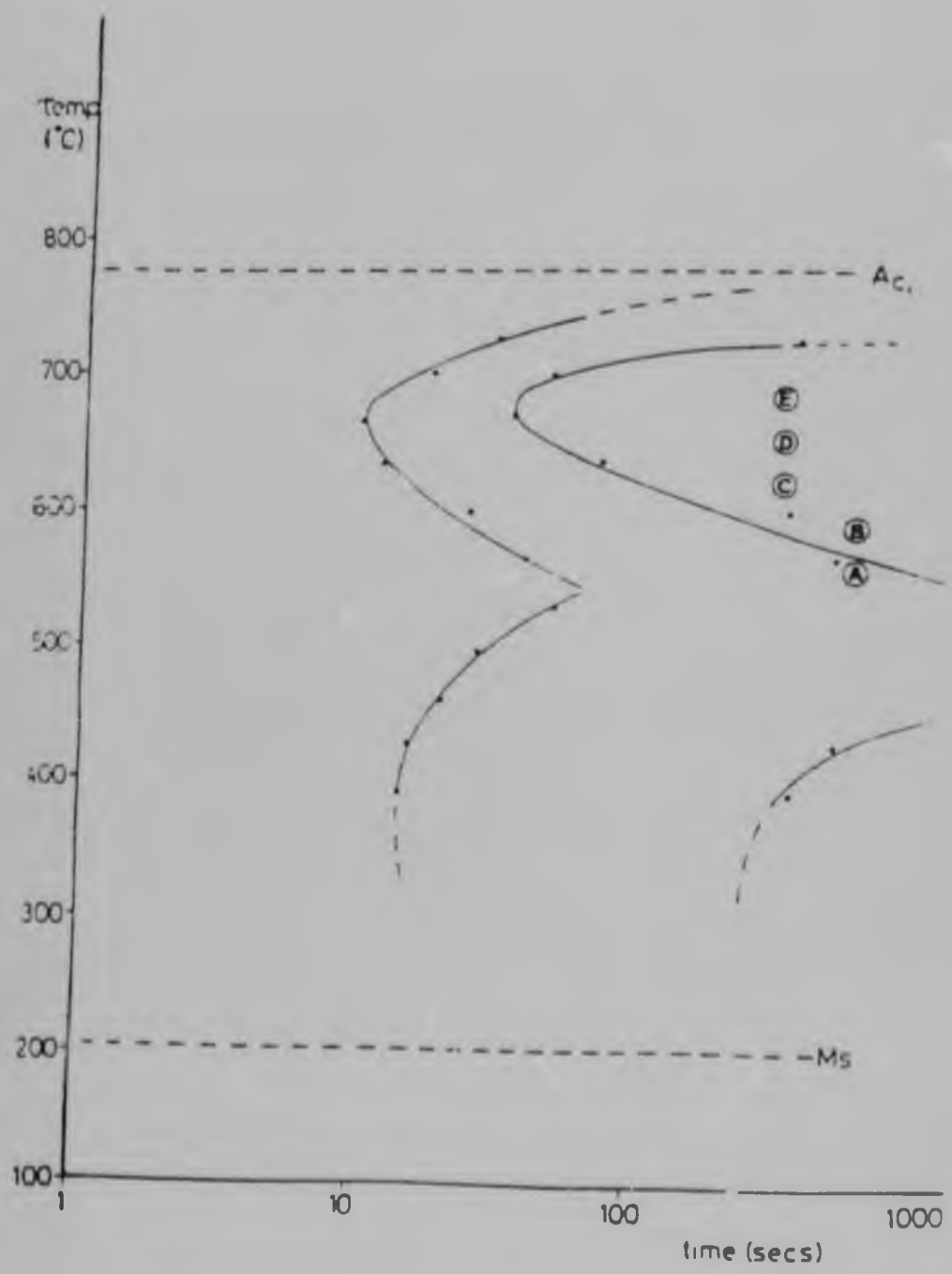

Figure 5.9 Systematic series of the microstructures of the 2Si-1Cr alloy submitted to different lead bath treatments (SEM micrographs)

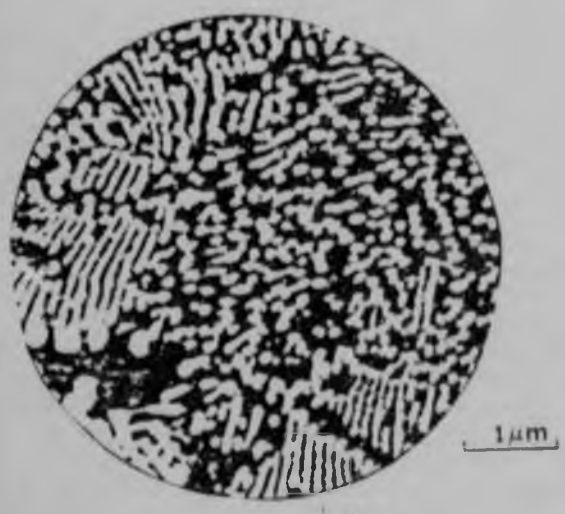

E. 680 °C, 5min.

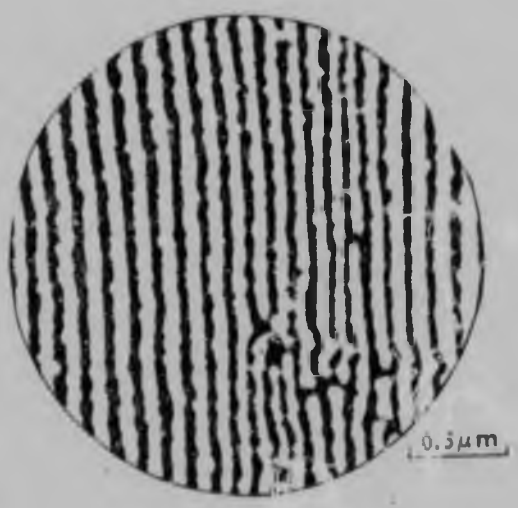

D. 660 °C, 5min.

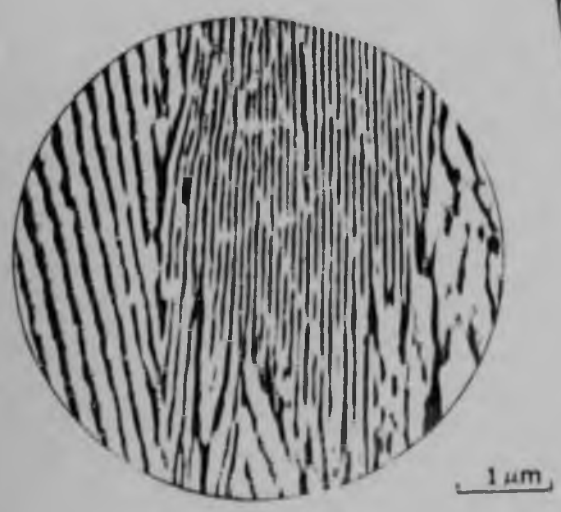

C. 630 °C, 15min.

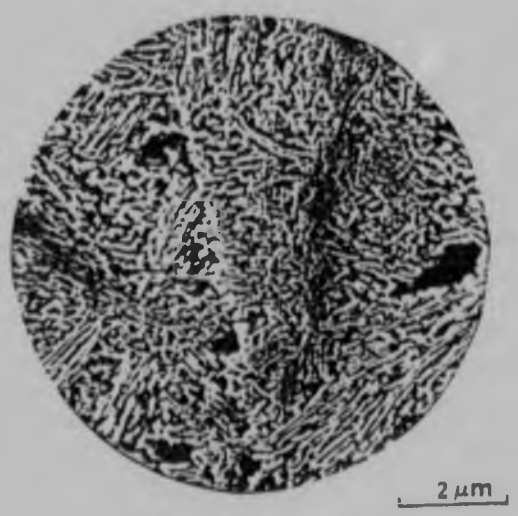

B. 600 °C, 15min.

A. 550 °C, 15min.

structure increased with decreasing transformation temperature.

The other alloys investigated revealed broadly similar structural changes over the transformation temperature ranges examined. The main differences can be considered by comparison with the results for the 2Si-1Cr alloy. The 1Si-1Cr-1Mn alloy produced a fairly regular, although coarser, pearlitic structure below 630°C (Figure 5.10).

The 2Si-1Mn and 2Si-1Cr-1Mn alloys produced a degenerate pearlite showing segmentation of the cementite lamellae for all the temperatures tested (Figure 5.11). These materials were therefore not considered to be suitable for further processing and evaluation.

The effect of holding time at the transformation temperatures on the microstructures was examined for the 2Si-1Cr and 1Si-Cr-1Mn alloys. The times at the transformation temperatures required before the onset of spheroidisation are summarised in Table 5.3. Some of the corresponding microstructures are shown in Figures 5.12 and 5.13.

(a)

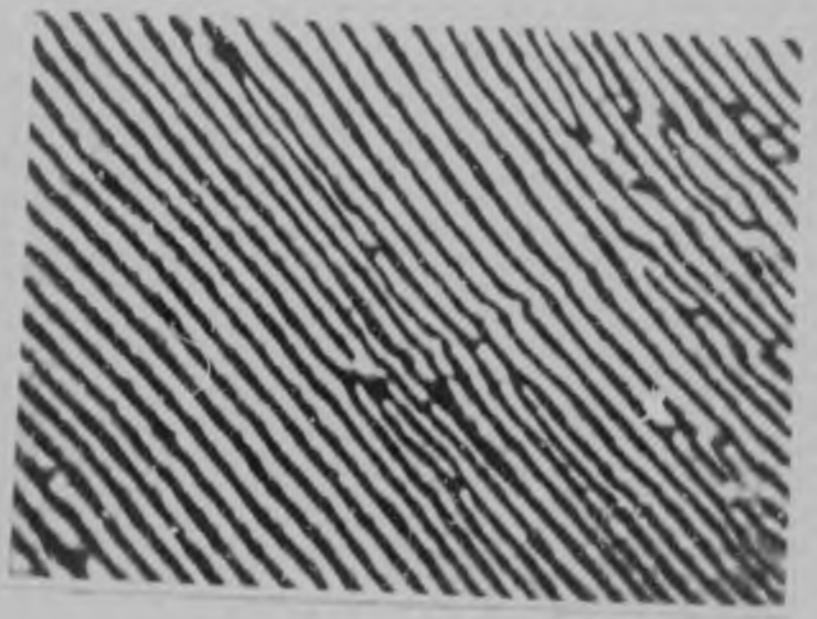

0.5μm

(b)

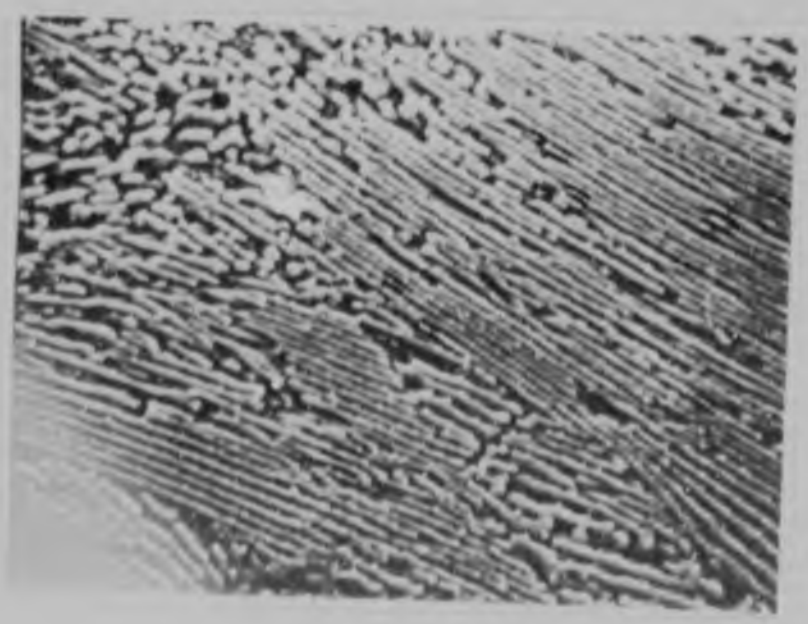

1μm

Figure 5.10 Fully transformed structures
(a) 2Si-1Cr at 660°C for 5 minutes
(b) 1Si-1Cr-1Mn at 630°C for 15 minutes
(SEM micrographs)

(a)

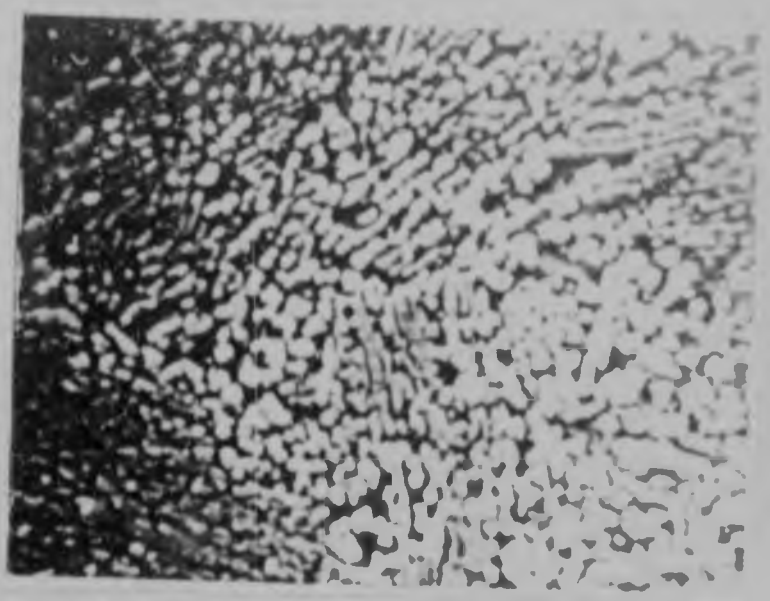

0.5um

(b)

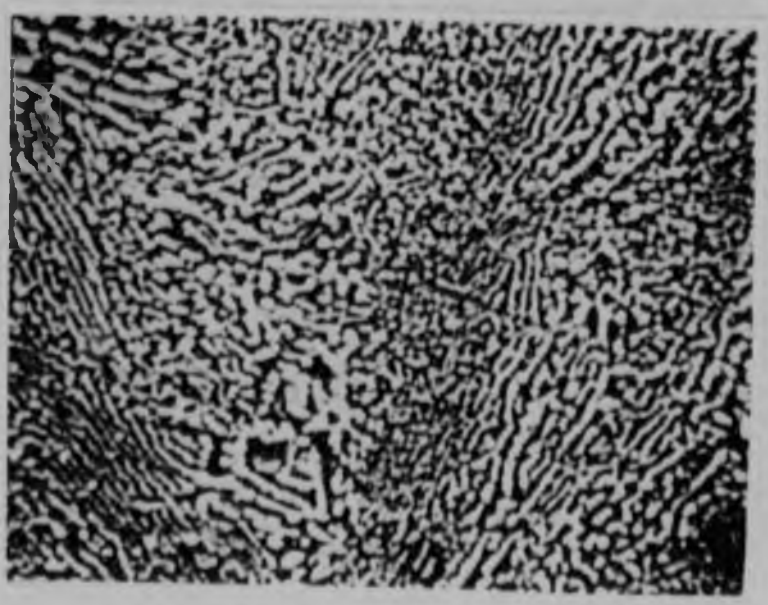

1 µm

Figure 5.11 SEM micrographs showing degenerate pearlite and fragmentation of the cementite lamellae
(a) 2Si-1Mn; and
(b) 2Si-1Cr-1Mn both transformed at 590 °C for 15 minutes

(a)

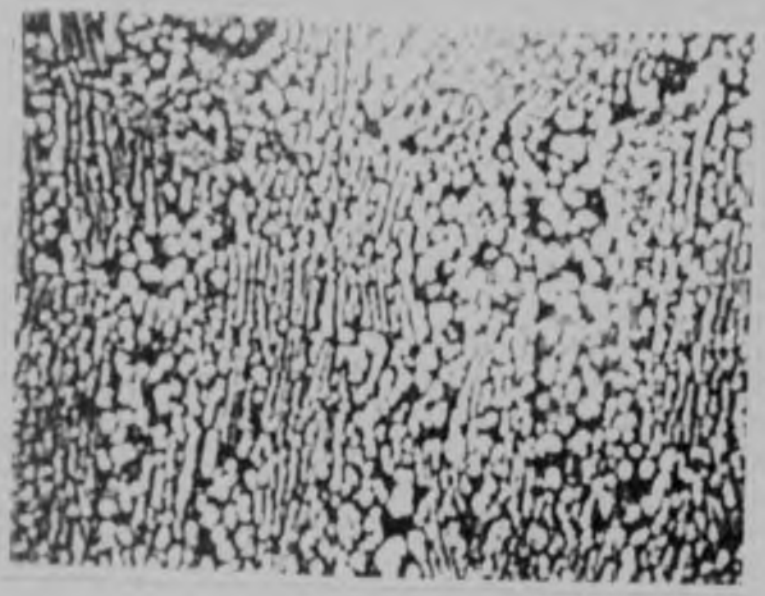

1 μm

(b)

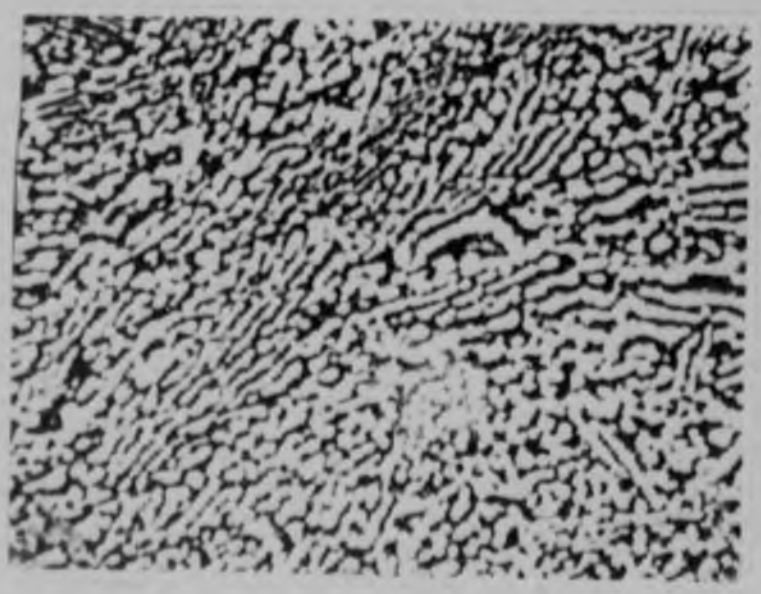

1 μm

Figure 5.12 Spheroidised microstructures obtained for relatively low transformation temperature (580 °C)
(a) 2Si-1Cr, 60 minutes
(b) 1Si-1Cr-1Mn, 45 minutes
(SEM micrographs)

(a)

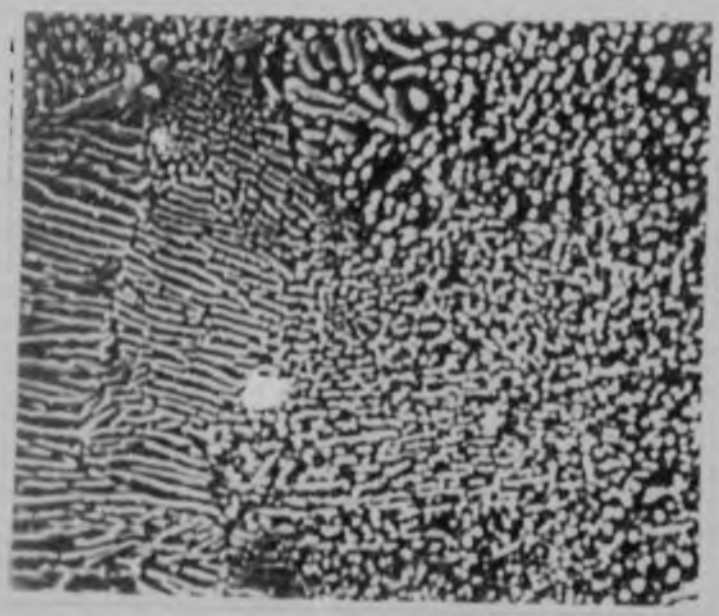

(b)

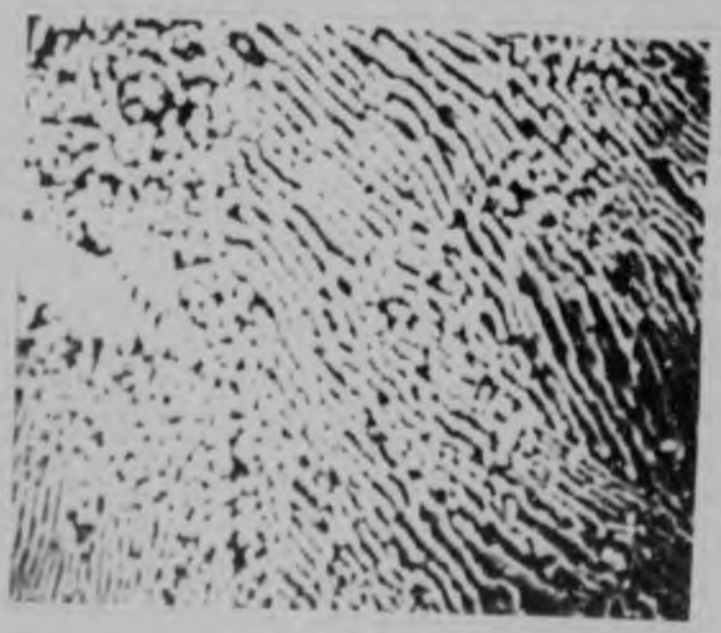

Figure 5.13 Spheroidised microstructures after transforming at relatively high temperatures
(a) 2Si-1Cr held at 680 °C for 10 minutes
(b) 1Si-1Cr-1Mn held at 650 °C for 15 minutes.
(SEM micrographs).

Table 5.3 Transformation times and temperatures required before the onset of spheroidisation in the 2Si-1Cr and 1Si-1Cr-1Mn alloys.

Temperature (°C)	Time (Minutes)	
	2Si-1Cr	1Si-1Cr-1Mn
580	60	45
590	45	30
650	20	15
660	10	-
680	5	-

5.2.2.3 Conventional transmission electron microscopy (CTEM)

Thin foils and replicas were prepared from those as-patented samples which showed the most uniform pearlitic structure (in the SEM); i.e. the 2Si-1Cr alloy.

The replicas produced were not generally suitable for detailed analysis of interlamellar spacings. However, they did reveal the fine, regular nature of the pearlite (Figure 5.14). Similar observations were made in thin foils (Figure 5.15a) although some segmented cementite was occassionally observed (Figure 5.15b). Although interlamellar spacings could be determined accurately in these foils, the practical problems involved in tilting experiments combined with the extremely small areas of observation precluded meaningful statistical analysis. Since most pearlites in this study could be resolved using SEM techniques it appears that this is adequate for studying the as-patented structures.

(a)

0.2μm

(b)

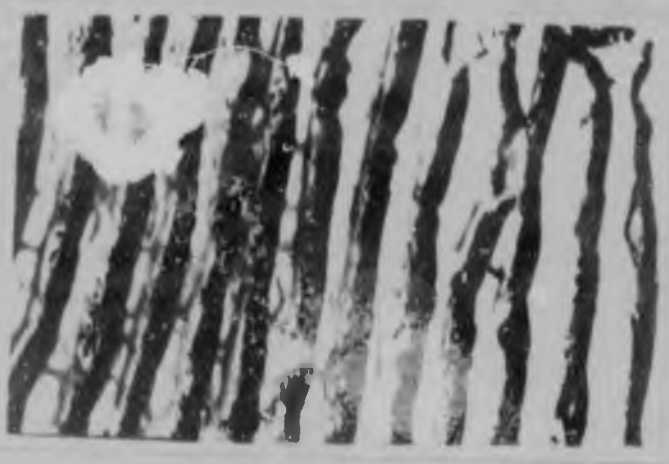

0.2μm

(c)

0.2μm

Figure 5.14 TEM replicas of as-patented structures in the 2Si-1Cr alloy, transformed at different times and temperatures
(a) 610 ℃, 5 minutes
(b) 640 ℃, 5 minutes
(c) 640 ℃, 10 minutes

(a)

0.1μm

(b)

0.1μm

Figure 5.15 As-patented structures of the 2Si-1Cr alloy transformed at 660°C for 5 minutes showing:
(a) a regular pearlitic structure
(b) fragmentation of the cementite lamellae
(Thin foils TEM micrographs)

5.2.3 Effect of the austenitising treatment on the pearlite properties

The effect of both austenitising time and temperature on the prior austenite grain size, microstructure and tensile properties were determined for the 2Si-1Cr alloy.

Hounsfield specimens were subjected to the nine different austenitising treatments listed in Table 5.4.

Table 5.4 Austenitising treatments of the 2Si-1Cr alloy.

Temperature (°C)	Time (Minutes)		
950	5	15	30
1000	5	15	30
1050	5	15	30

5.2.3.1 Prior austenite grain size and microstructure

The prior austenite grain size was measured for specimens austenitised at the temperatures listed in Table 5.4 for 30 minutes and partially transformed at 600 °C prior to water-quenching. The grain size was measured using the mean linear intercept method and the values obtained as a function of the austenitising temperature are plotted in

Figure 5.16. The finest grain size (75μm) was obtained, as expected, for the lower austenitising temperature.

SEM studies were carried out on all the samples subjected to different austenitising treatments and transformed at 600°C for 5 minutes. The resulting micrographs are given in Figure 5.17. Austenitising at 950 °C produced a structure along the prior austenite grain boundaries that appears bainitic. However, this structure could be free ferrite plus carbide caused by incomplete carbide dissolution.

In samples austenitised at 1000 °C a similar structure was observed after a holding time of 5 and 10 minutes. However, a longer soak of 30 minutes produced a very fine and uniform lamellar pearlite structure.

Austenitising at 1050°C appeared to lead to some degree of spheroidisation of the cementite lamellae on subsequent transformation.

5.2.3.2 As-patented tensile strength

Hounsfield specimens were tested which had been submitted to the different austenitising treatments and transformed at 600 °C for 5 minutes. The properties obtained are given in Table 5.5 and plotted in Figure 5.18.

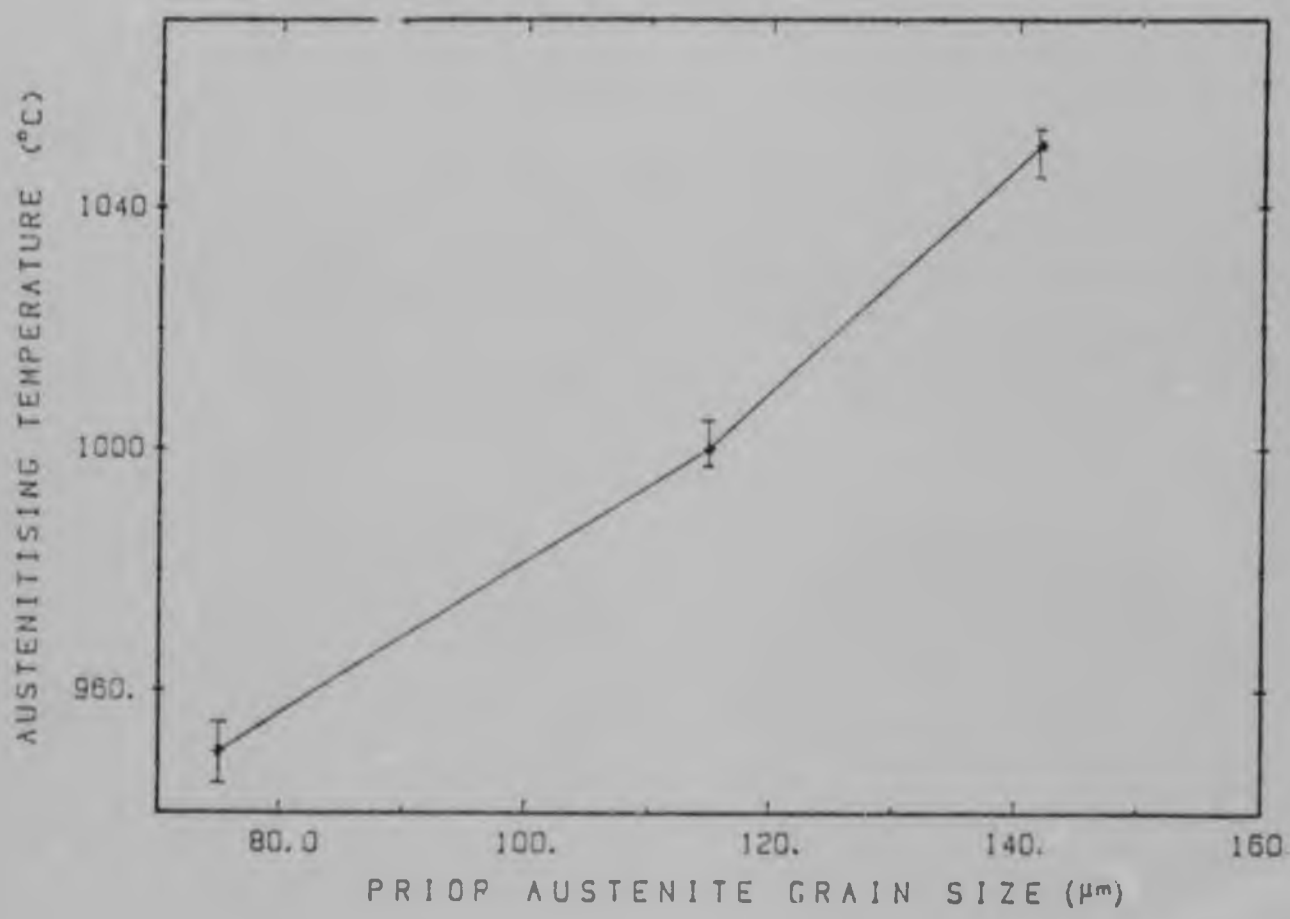

Figure 5.16 Prior austenite grain size of the 2Si-1Cr alloy as a function of the austenitising temperature (holding time 30 minutes)

105

100

95C

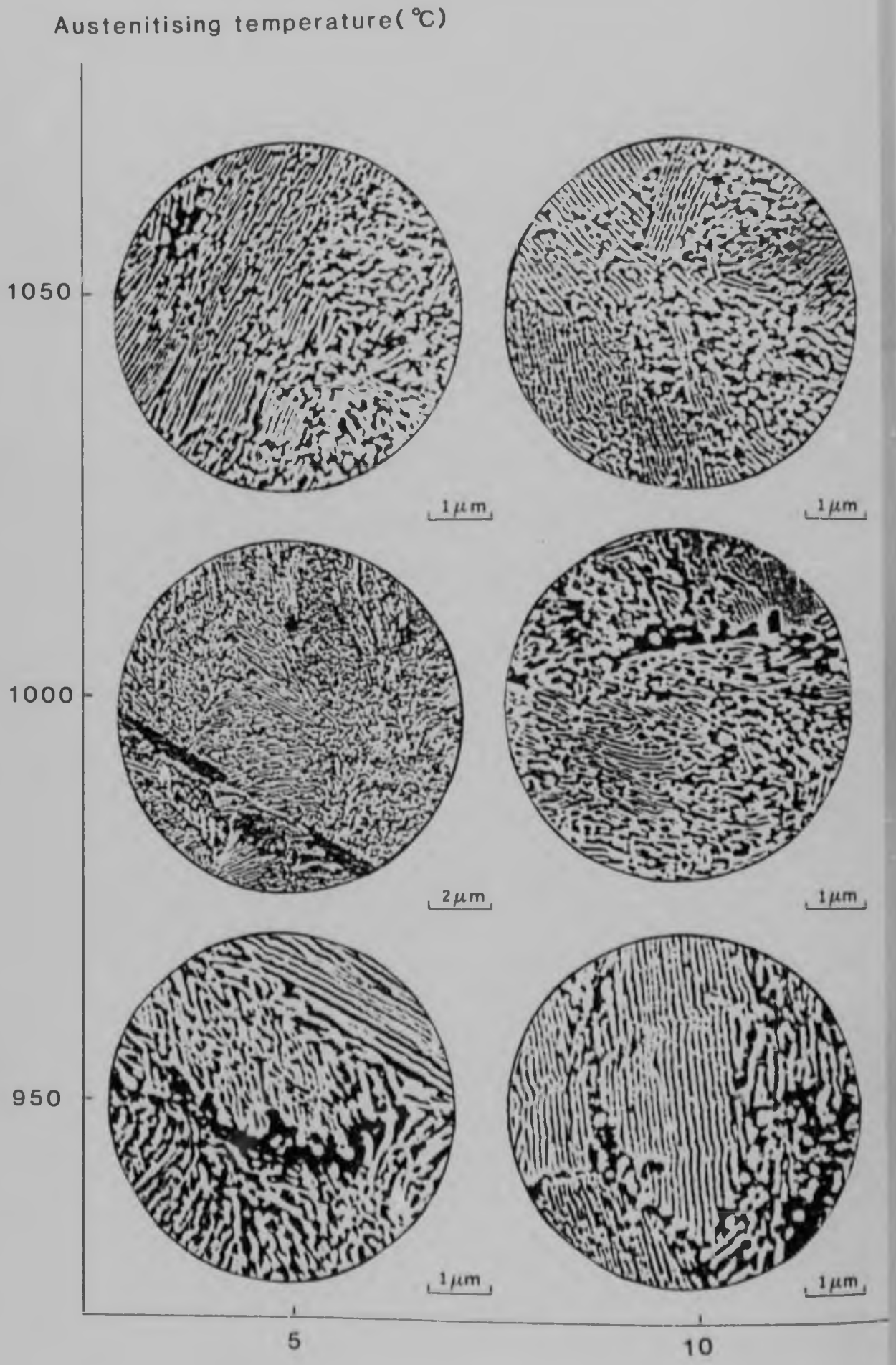

Figure 5.17 Effect of the austenitising treatment on the microstructure of the 2Si-1Cr alloy transformed at 660℃ for 5 minutes.

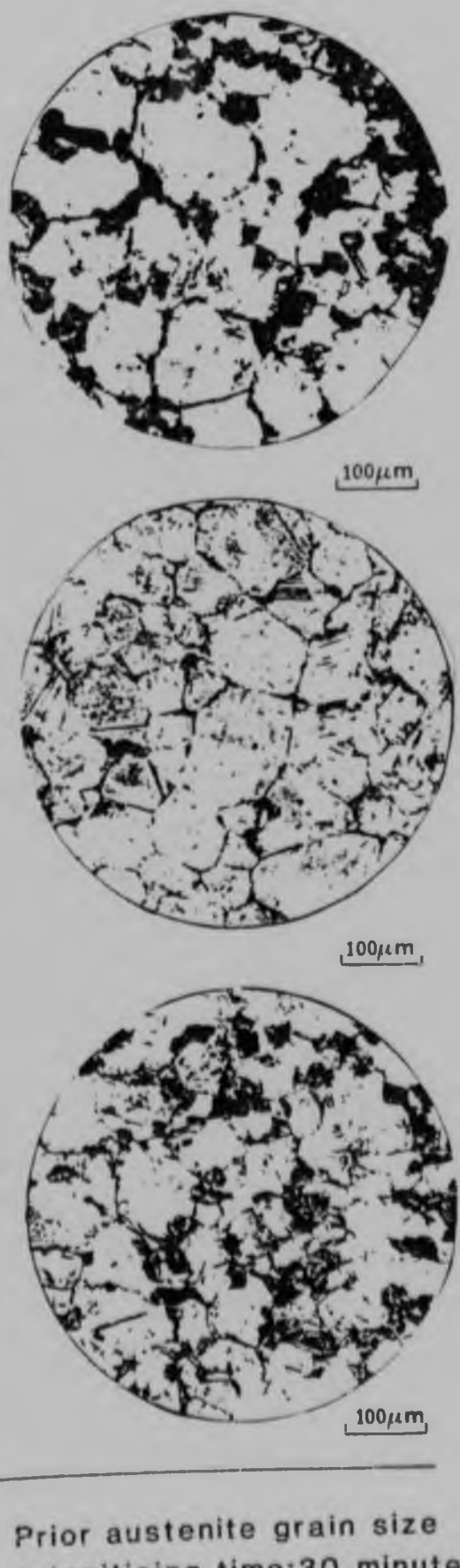

15

Austenitising time(minutes)

Prior austenite grain size
(austenitising time:30 minutes)

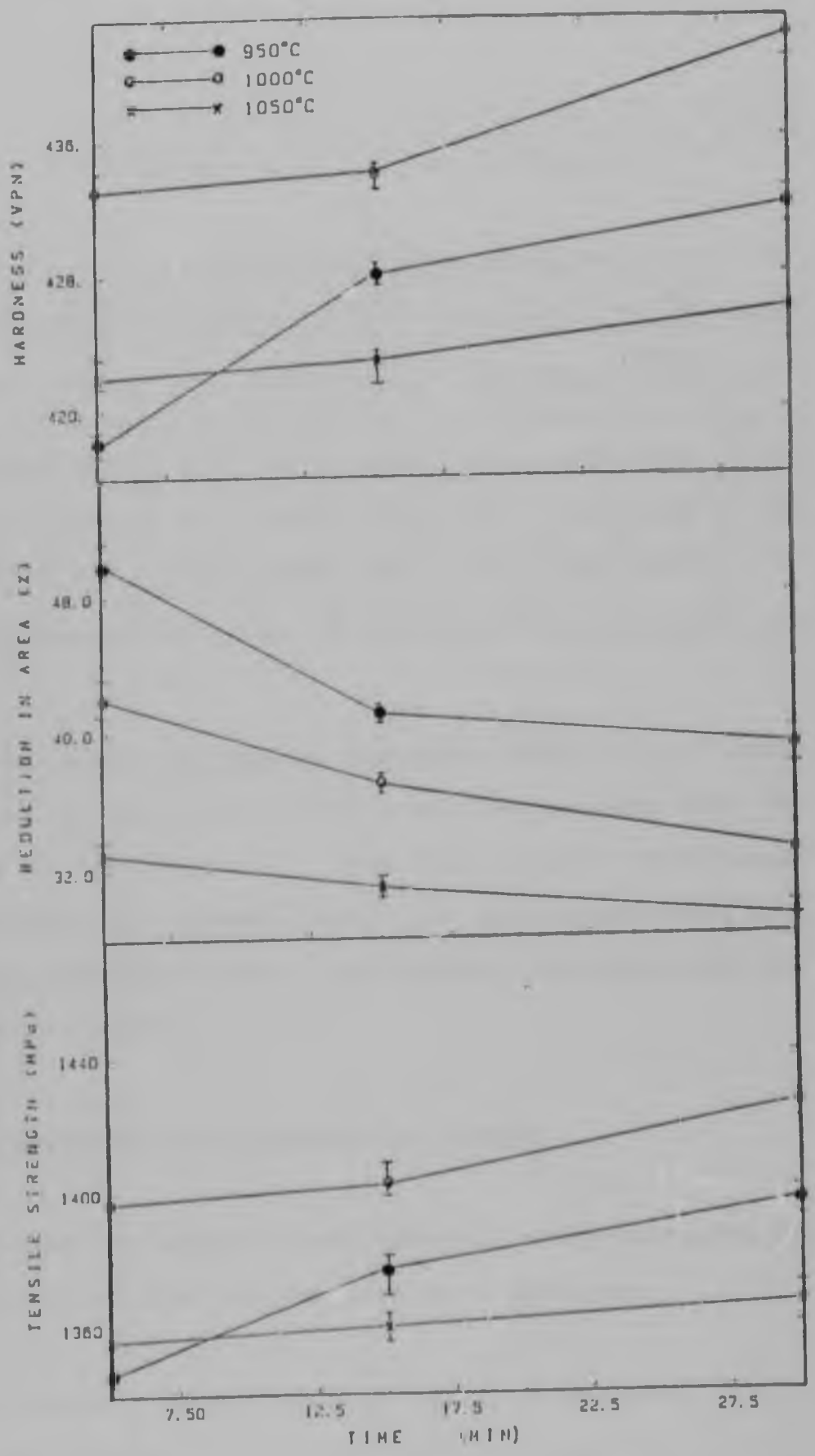

Figure 5.18 Effect of the austenitising treatment on the tensile properties of the 2Si-1Cr alloy

Table 5 5 Effect of the austenitising treatment on the as-patented properties of the 2Si-1Cr alloy (transformed at 600 °C for 5 minutes)

Time (minutes)	Austenitising Temperature (°C) 950			1000			1050		
	U.T.S (MPa)	Hardness (VPN)	R.A. (%)	U.T.S (MPa)	Hardness (VPN)	R.A. (%)	U.T.S (MPa)	Hardness (VPN)	R.A. (%)
5	1346	415	50	1397	433	42	1356	422	33
15	1377	427	41	1402	434	37	1360	423	31
30	1396	430	39	1420	442	33	1366	426	29

A small variation in tensile strength (50MPa) and a larger variation in ductility (20%) were observed for the different treatments. The ductility decreased systematically as austenitising time and temperature were increased, but the strength and hardness showed maxima for each time at 1000 °C.

5.2.4 Interlamellar spacing measurements

The interlamellar spacings were determined by measuring the average smallest spacing observed in a specimen.

A characteristic image analyser plot is shown in Figure 5.19. The chord length ("x" axis) gives the actual measurement of the spacings, the frequency of the specific

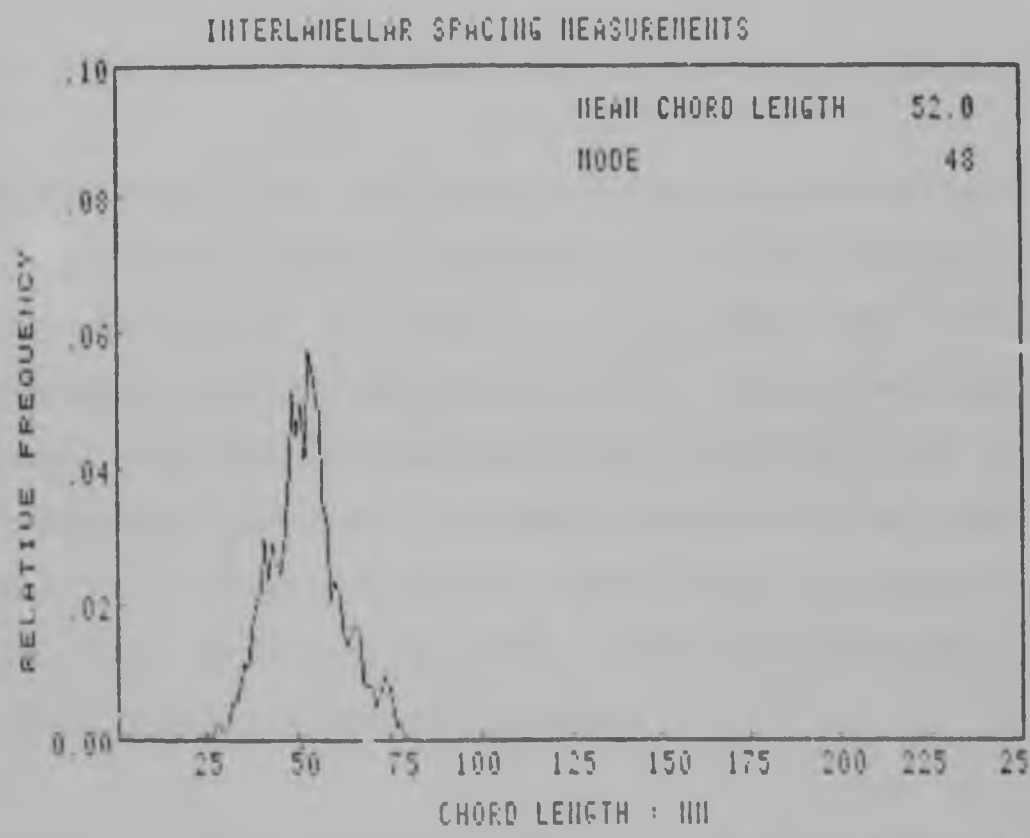

Figure 5.19 Image analyser plot of the interlamellar spacings measurements.

spacing is plotted in the "y" axis. For each specimen, twenty different graphs were plotted and the average smallest spacing was calculated.

Figure 5.20 shows the variation of the interlamellar spacing with transformation temperature for the different silicon-containing alloys. As expected the interlamellar spacing decreases with transformation temperature. The smallest spacing were associated with a bainite containing structure. Optimum combinations of high strength with adequate ductility were found at higher transformation temperatures, which produced the finest, regular fully pearlitic microstructures.

The effect of carbon content on the interlamellar spacing of the 2Si-1Cr alloy is plotted in Figure 5.21. It can be seen that an increase of 0.1% carbon led to a decrease of the interlamellar spacing by ±10nm.

The influence of the prior austenite grain size on the interlamellar spacing was also tested. However, this parameter appeared to have no influence.

The effect of silicon additions on the interlamellar spacing of the 1Cr-1Mn alloy is shown in Figure 5.22. A decrease in spacing was observed due to the addition of 1% silicon. However, increasing the silicon content by

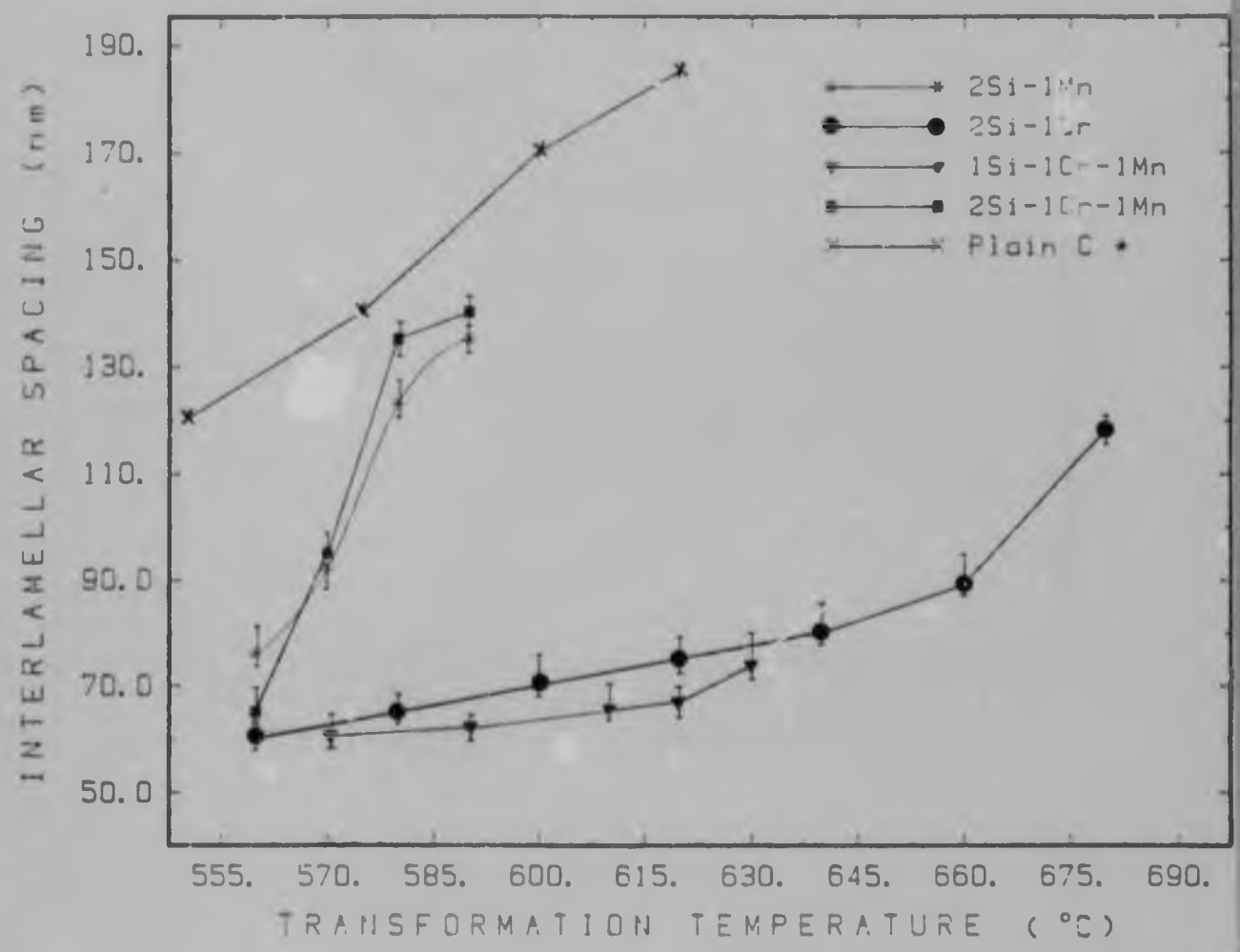

Figure 5.20 Variation of the interlamellar spacing with transformation temperature for different silicon containing alloys. The values are compared with a plain carbon steel.
* After Smith and Speirs.

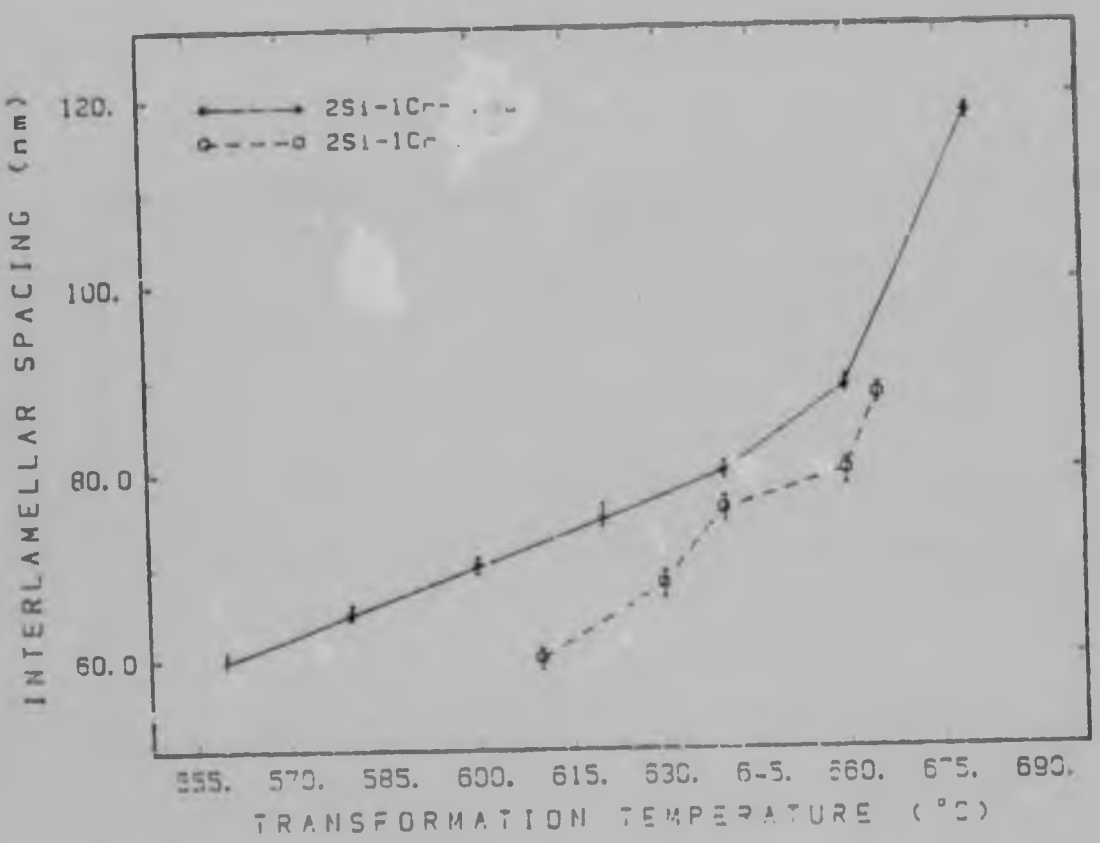

Figure 5.21 Effect of carbon content on the interlamellar spacing of the 2Si-1Cr base alloy.

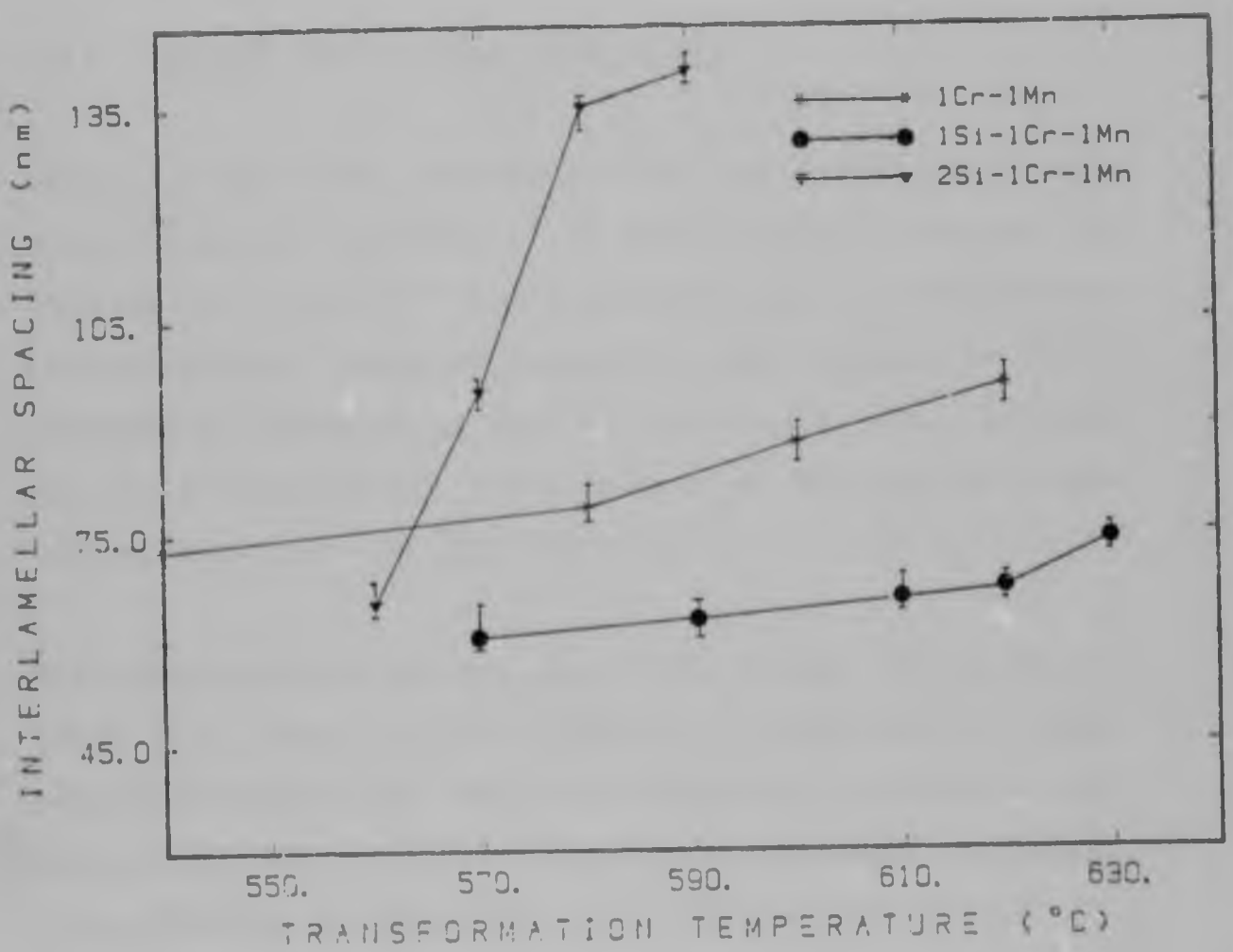

Figure 5.22 Effect of silicon content on the interlamellar spacing of the 1Cr-1Mn base alloy.

a further 1% to form 2Si-1Cr-1Mn had a marked effect. The apparent anomalous behaviour in the 2Si-1Cr-1Mn alloy (which increased the spacing) is due largely to the extremely degenerate structure produced which made interlamellar spacings measurements meaningless.

5.2.5 As-patented tensile properties

Tensile tests were carried out on the Sheffield alloys using Hounsfield specimens. An austenitising treatment of 30 minutes at 1000 °C was employed prior to isothermal transformation. Great difficulties were encountered while conducting these tests due to continuous axial defects derived from secondary pipes present in the original cast ingots, mainly in the 2Si-1Cr alloy.

The tensile strength and ductility values are given in Table 5.6. For low transformation temperatures, high tensile strengths and low ductilities were measured in all the alloys. The tensile strength decreased with increasing transformation temperatures, while ductility increased.

The effect of chromium or manganese additions on the 2Si alloy is shown in Figure 5.23. The strength levels of the 2Si-1Cr alloy were 250MPa higher than the 2Si-1Mn for all transformation temperatures.

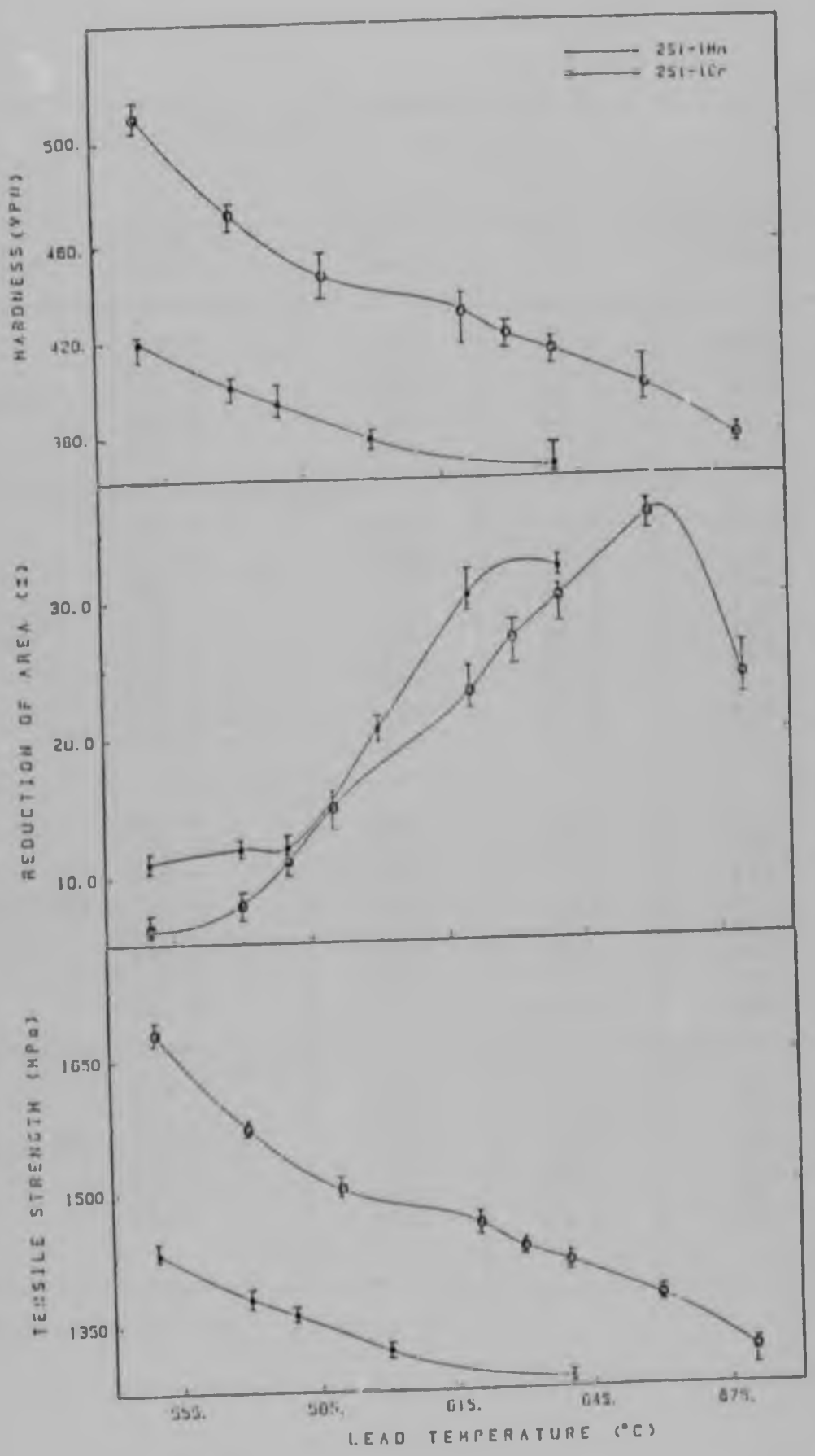

Figure 5.23 As-patented mechanical properties of the 2Si-1Cr and 2Si-1Mn alloys.

Table 5.6 As-patented properties of the Sheffield silicon-containing alloys.

Alloy	Lead Bath Temp. (°C)	U.T.S. (MPa)	R.A. (%)	Hardness (VPN)
2Si-1Mn	550 *	1430	11.2	443
	570 *	1380	12.1	429
	580 *	1360	12.7	423
	600 *	1320	20.5	410
	640 *	1286	32.2	399
2Si-1Cr	55[illegible] *	1690	6.0	517
	570 *	1680	8.0	514
	580 *	1570	11.1	484
	590 *	1550	15.3	479
	620 *	1460	23.4	452
	630,5 min.	1432	27.6	443
	640,5 min.	1415	30.0	439
	660,5 min.	1400	34.0	428
	680,5 min.	1316	24.1	410
1Si-1Cr-1Mn	550 *	1680	8.1	514
	570 *	1570	11.9	484
	590 *	1500	17.2	464
	600 *	1460	19.1	452
	610 *	1390	20.9	431
	620 *	1330	23.7	413
	630 *	1316	29.0	410
	650 *	1234	30.1	382
2Si-1Cr-1Mn	570 *	1690	8.0	517
	580 *	1654	12.0	508
	590 *	1620	13.2	497
	600 *	1560	14.1	480
	620 *	1470	17.5	463
	640 *	1414	19.8	437

* Transformation time - 15 minutes.

The effect of different silicon additions to the 1Cr-1Mn alloy is shown in Figure 5.24. A marked improvement in the strength of the 1Cr-1Mn alloy was achieved due to the silicon additions. Addition of 1% silicon showed an improvement of 100 MPa in the temperature region of interest. Further addition of 1% silicon (2Si-1Cr-1Mn) showed significant increase in strength.

Improved casting techniques were used to produce the Wits alloys, and no effects from secondary pipes were observed in the fabricated 2Si-1Cr rods. This allowed more accurate data to be obtained. The results of the rod tensile tests carried out on 12mm diameter rods of the 2Si-1Cr Wits alloy are listed in Table 5.7.

Table 5.7 Rod tensile properties of the 2Si-1Cr Wits alloy.

Transformation conditions	Tensile strength (MPa)	R.A. (%)
610 °C, 15 min.	1477	29
640 °C, 15 min.	1444	30
640 °C, 10 min.	1414	34
660 °C, 5 min.	1375	36

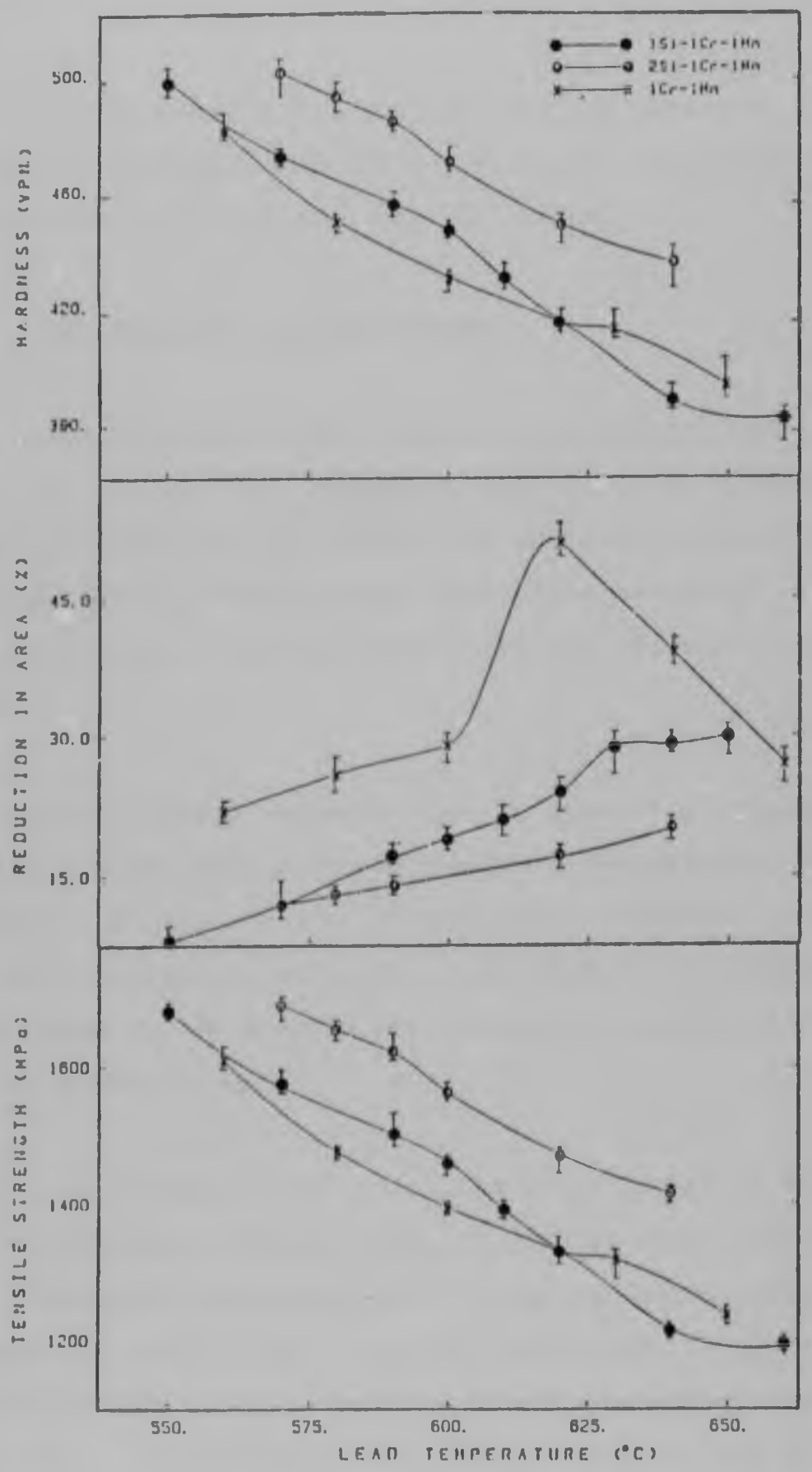

Figure 5.24 As-patented mechanical properties of the 1Si-1Cr-1Mn, 2Si-1Cr-1Mn and 1Cr-1Mn alloys.

From these determinations of the tensile strengths and corresponding ductilities it was possible to select the best combination for further drawing trials.

5.2.6 The effect of carbon contents

Since carbon is known to be a potent strengthening agent, a series of alloys was prepared with different carbon contents in order to investigate its influence on structure and properties. These alloys were based on the 2Si-1Cr composition with nominal carbon contents of 0.5 to 0.9% carbon.

The eutectoid carbon concentration is reduced by alloying with silicon and chromium and a value between 0.6 to 0.7% would be predicted for this 2Si-1Cr base. However, using the given patenting conditions no pro-eutectoid cementite was detected in the structures of the hyper-eutectoid 0.8 and 0.9% carbon alloys.

The tensile properties of these alloys are listed in Table 5.8 and plotted in Figure 5.25. It can be seen that the tensile strength increased with increasing carbon content, as expected, while the ductility decreased. Since the strength values of the 2Si-1Cr - 0.5, 0.6 and 0.7 C alloys were very low, compared with those of the 0.8 and 0.9 C steels, they were excluded from further investigations.

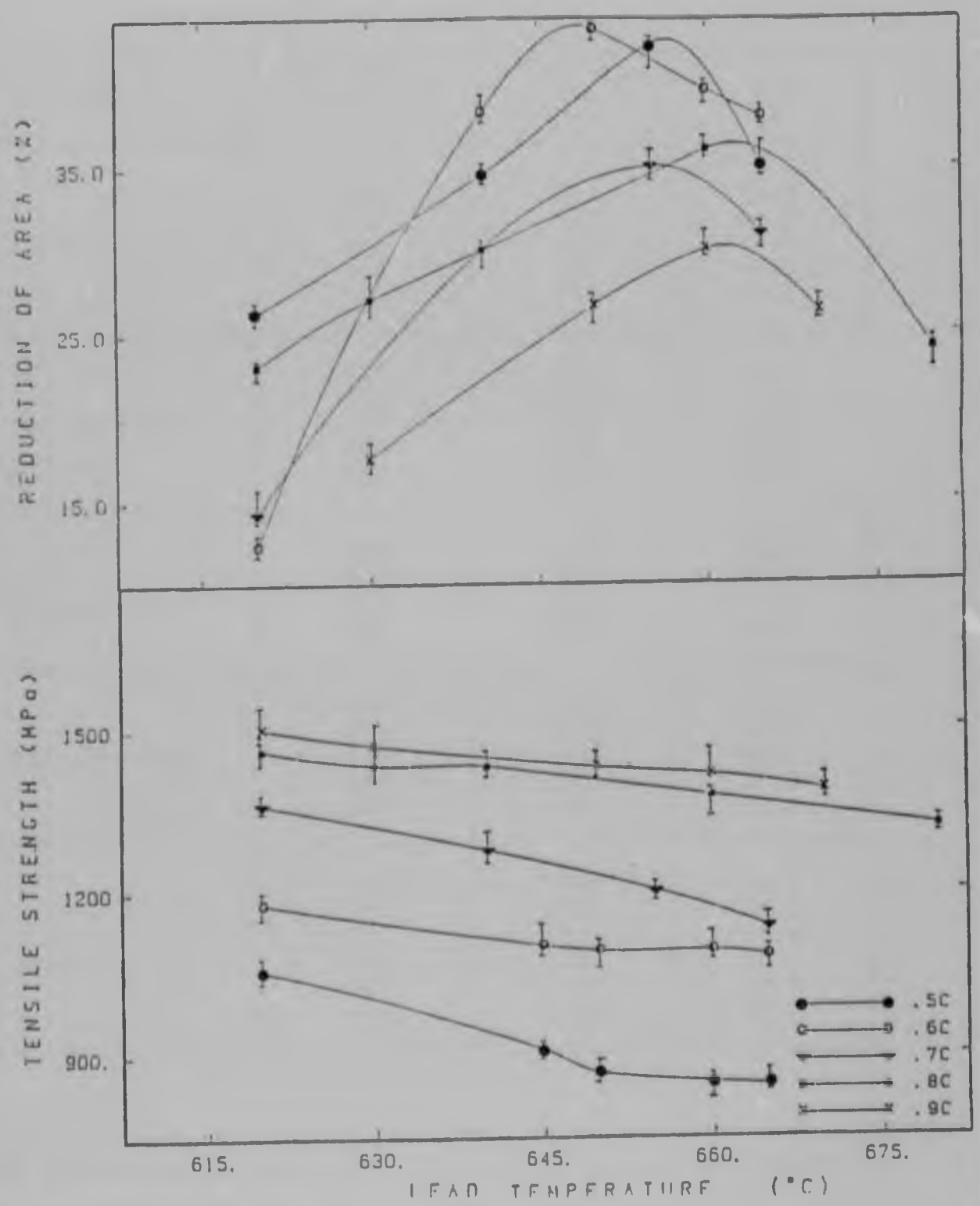

Figure 5.25 The effect of carbon content on the tensile properties of the 2Si-1Cr alloy.

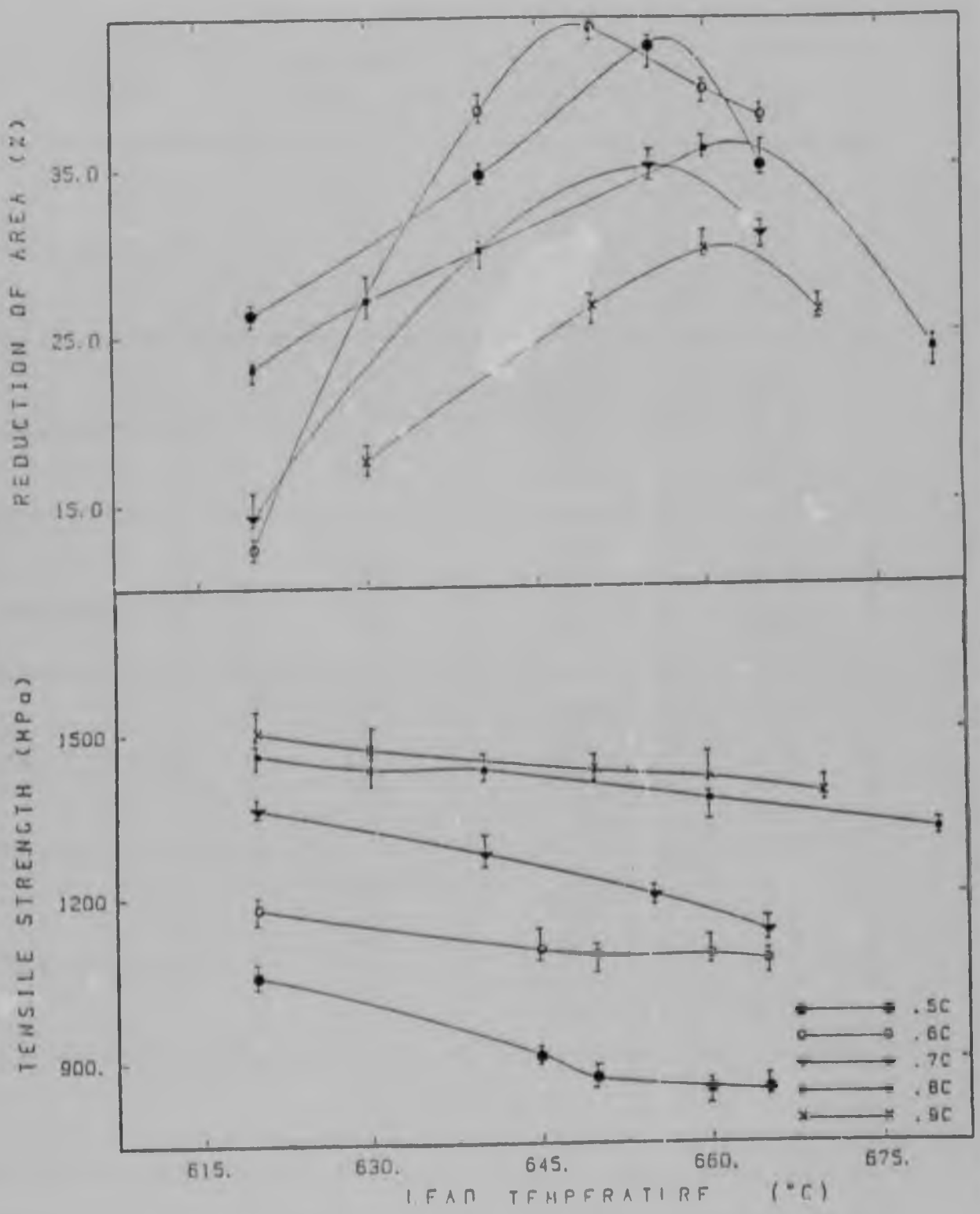

Figure 5.25 The effect of carbon content on the tensile properties of the 2Si-1Cr alloy.

Table 5.8 The effect of carbon-content on the tensile properties of the 2Si-1Cr alloy.

Alloy	Lead Bath Temperature (°C)	Tensile strength (MPa)	R.A. (%)
2Si-1Cr-0.5C	620	1054	10.4
	645	910	34.8
	650	866	48.5
	660	850	47.9
	665	844	35.1
2Si-1Cr-0.6C	620	1177	12.3
	645	1100	38.2
	655	1090	39.9
	660	1090	38.0
	665	1080	36.3
2Si-1Cr-0.7C	620	1360	14.2
	640	1275	30.0
	655	1200	35.1
	660	1133	28.6
2Si-1Cr-0.8C	620	1460	27.0
	630	1432	29.0
	640	1430	30.0
	660	1375	36.0
	680	1316	24.0
2Si-1Cr-0.9C	620	1500	13.8
	630	1468	24.0
	650	1427	26.6
	660	1413	30.0
	665	1387	33.0
	670	1384	26.2

The microstructures of the 2Si-1Cr alloy were described in detail in Section 5.2.2.2. The microstructures of the 2Si-1Cr-0.9C in the as-patented condition are shown in Figure 5.26. It can be seer that transformation for 5

(a)

(b)

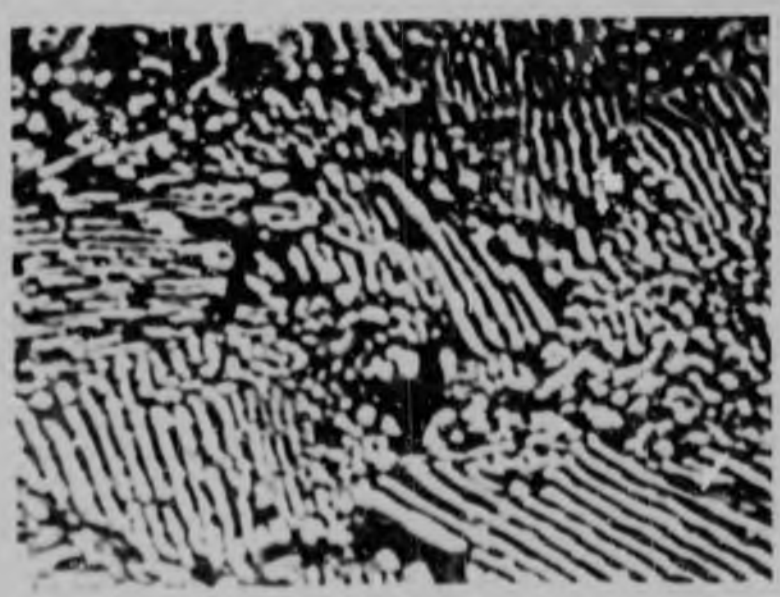

Figure 5.26 SEM micrographs of the 2Si-1Cr-0.9C alloy transformed at 665°C for
(a) 5 minutes;
(b) 10 minutes.

minutes of 663°C produced a very fine and uniform pearlitic structure (Figure 5.26a). A slightly longer soak (10 minutes) at this temperature initiated spheroidisation of the cementite lamellae (Figure 5.26b).

5.2.7 Drawing trials

Based on industrial experience, 25% ductility (R.A.) in the as-patented condition is required to provide adequate drawability. To achieve the goal of a drawn tensile strength of 2500MPa, given a realistic work hardening rate, an as-patented tensile strength of approximately 1400MPa is required.

These criteria were therefore used in the selection of alloys and heat treatments for subsequent drawing trials.

5.2.7.1 Initial drawing trials on the 2Si-1Cr-0.8C alloy

In the initial drawing trials the 2Si-1Cr alloy was austenitised at 1000°C for 30 minutes prior to transformation at the temperatures listed in Table 5.9. (No water cooling was used at this stage of the research).

Table 5.9 Transformation conditions of the 2Si-1Cr Sheffield alloy for the initial drawing trials.

Temperature (°C)	Time (minutes)
610	15
640	5
640	10
660	5

Samples were drawn from a nominal 10mm diameter rod to a final 3.15mm wire. The work hardening curves for the different samples are plotted in Figure 5.27 and the corresponding data is listed in Table 5.10.

It can be seen that the work hardening rate changes with transformation temperature. A minimum of 315MPa per unit strain was measured after transforming at 610°C, and a maximum of 375MPa per unit strain at 660°C.

The wire drawn from the rods transformed according to Table 5.9 exhibited high tensile strengths and very high remaining ductilities. It was decided therefore to use the same heat treatments in the subsequent tests carried out on the 2Si-1Cr Wits alloy. This material was drawn from 12mm diameter rod to 3.15mm wire. This permitted the study of the effect of greater drawing reductions (to a true strain of 2.68).

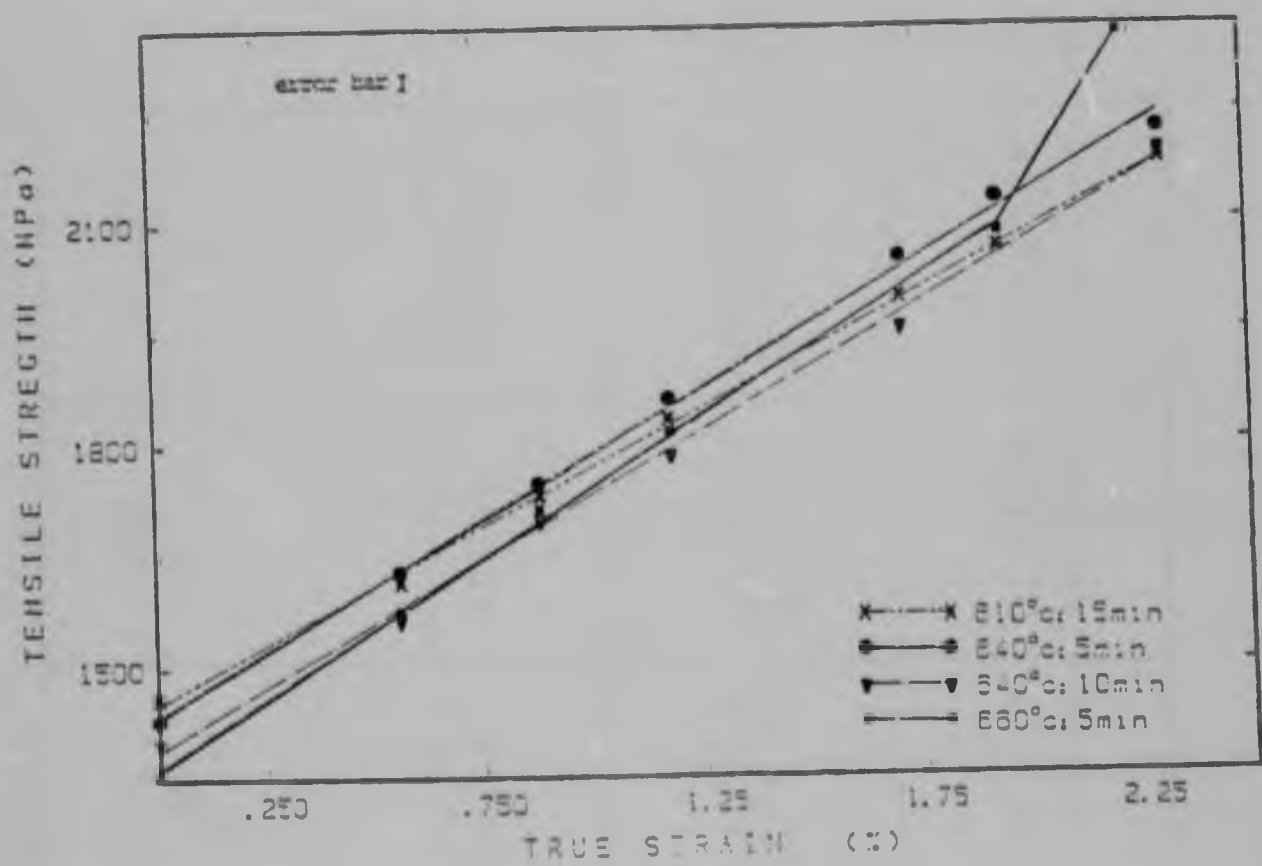

Figure 5.27 Work hardening curves of the 2Si-1Cr Sheffield alloy. (The error in each measurement is indicated by the error bar on the diagram).

Table 5.10 As-drawn properties of the 2Si-1Cr Sheffield alloy.

Lead bath temperature (°C)	True strain (ε)	Tensile strength (MPa)	R.A. (%)
610 15 min.	0	1510	28.0
	0.56	1615	26.4
	0.88	1726	37.0
	1.18	1832	44.0
	1.71	1995	49.5
	1.94	2061	47.5
	2.31	2181	50.3
640 5 min.	0	1415	30.0
	0.56	1626	40.0
	0.88	1747	45.6
	1.18	1857	50.0
	1.71	2048	51.0
	1.94	2127	51.0
	2.31	2219	53.8
640 10 min.	0	1400	34.0
	0.56	1570	40.4
	0.88	1699	41.0
	1.18	1796	48.5
	1.71	1956	52.0
	2.31	2194	50.8
660 5 min.	0	1374	34.0
	0.56	1575	47.0
	0.88	1711	40.9
	1.18	1815	46.0
	1.94	2083	43.4
	2.16	2533	33.6

The work hardening curves of the 2Si-1Cr Wits alloy are plotted in Figure 5.28 and the corresponding data given in Table 5.11. The work hardening rate was an average of 440MPa per unit strain, independent of the heat treatment, a more realistic result than that obtained for the 2Si-1Cr Sheffield alloy.

The rods transformed at 610 and 640°C reached the limit of drawability after drawing to a true strain of only 1,55, and achieved a corresponding strength of 2200MPa. The rod transformed at 660°C for 5 minutes, had an extremely high strength of 2700MPa and 36% ductility. Unfortunately the shear and torsion tests showed no remaining ductility: the shear elongation value was zero, and the torsion test gave a "C" type break after just 19 turns per 100 diameters.

5.2.7.2 Effect of water cooling

Wire ductility appears to be related to the heat generated during drawing, since if this is in excess of 100-150°C ageing can occur. In consequence, careful attention must be paid to water cooling ultra-high tensile wires during drawing.

Attempts to measure the temperature of the wire after each pass of the drawing using a contact thermocouple and a digital thermometer were not very successful, due to the temperature gradient along the wires.

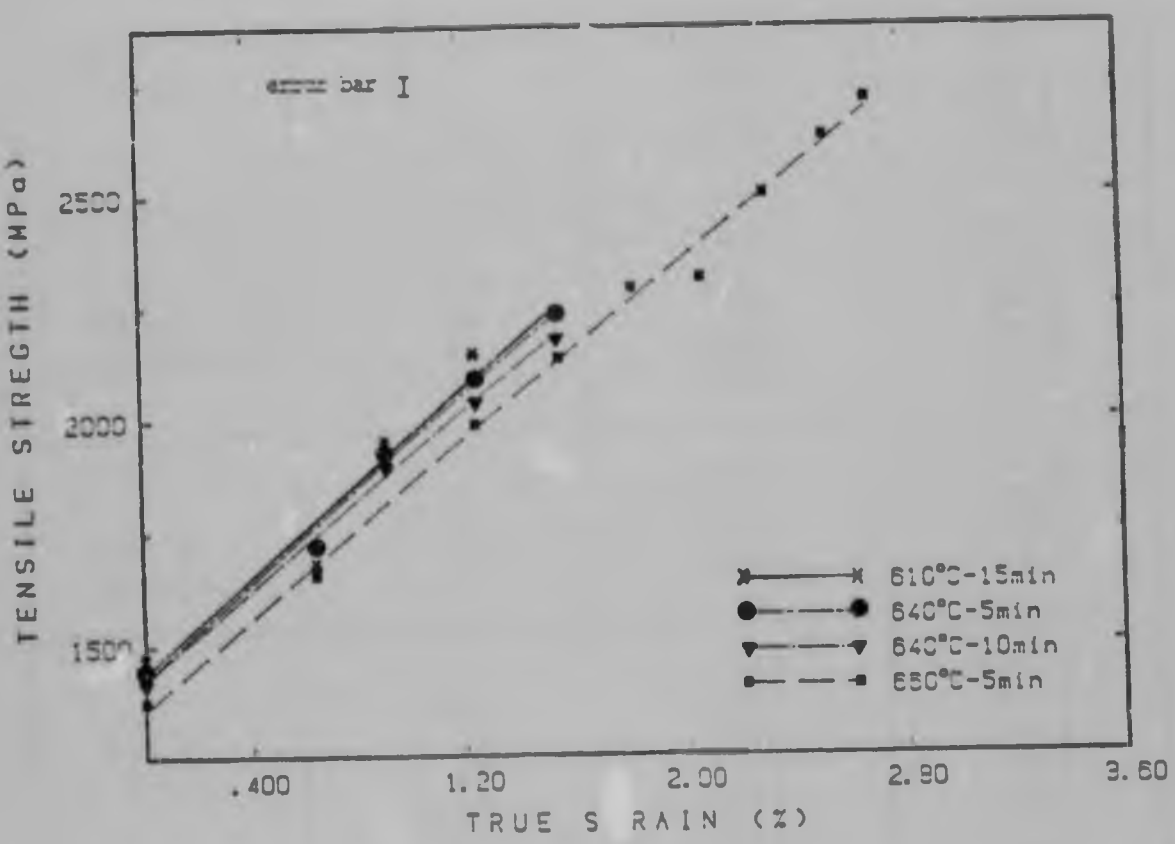

Figure 5.28 Work hardening curves of the 2Si-1Cr Wits alloy.

Table 5.11 As-drawn properties of the 2Si-1Cr Wits alloy.

Lead bath temperature (℃)	True strain (ε)	Tensile strength (MPa)	R.A. (%)
610 C 15 min.	0	1477	29.0
	0.65	1678	29.2
	0.92	1953	25.1
	1.25	2114	23.2
	1.55	2232	17.0
640 C 5 min.	0	1444	30.1
	0.65	1721	33.0
	0.92	1928	40.0
	1.25	2086	50.1
	1.55	2286	50.3
640 C 10 min.	0	1414	34.0
	0.92	1899	24.3
	1.25	2042	48.1
	1.55	2042	48.0
660 C 5 min.	0	1375	36.2
	0.65	1657	41.0
	1.25	1989	51.4
	1.55	2135	49.1
	1.82	2289	52.3
	2.30	2499	47.4
	2.52	2628	44.0
	2.68	2712	36.0

In an attempt to determine the influence of water cooling on the final properties of drawn wire, two different drawing trials were carried out. In one test, water cooling was used after the 6.42mm diameter (ε = 1.25) and all successive dies, and drawing was continued to a true strain of 2.81. The mechanical properties after each pass and the wire test results are given in Table 5.12. In the

other trial, water cooling was applied only after the 3.79mm diameter die (ε = 2.30). The results of this test are given in Table 5.13.

From these results it is clear that water cooling does improve the ductility of the wires, while the decrease in strength is rather small. As a result of the water cooling, wires of 3.7mm and less were found to be almost at room temperature immediately after drawing. In all the subsequent drawing trials water cooling was used from the 6.42mm diameter die.

Table 5.12 As-drawn properties of the 2Si-1Cr Wits alloy, using water cooling after the 6.42mm and successive dies.

True strain (ε)	Tensile strength (MPa)	R.A. (%)	Shear elongation (%)	Torsion test Turns/ 100ϕ	Break Type
0	1375	36.0			
*1.25	1860	45.9			
1.55	1950	48.0			
1.82	2075	48.2			
2.01	2200	52.1			
2.30	2300	52.0			
2.52	2415	47.6	1.4		$29A_2$
2.68	2580	37.1	1.6		$30A_1$
2.81	2640	34.0	0.9		Split

* water cooling applied from this die onwards.

Table 5.13 As-drawn properties of the 2Si-1Cr Wits alloy, using water cooling after the 3.79mm and successive dies.

True strain (ε)	Tensile strength (MPa)	R.A. (%)	Shear elongation (%)	Torsion test Turns/ 100ϕ	Break Type
0	1375	36.0			
1.25	1850	43.1			
1.55	1970	47.1			
1.82	2140	48.8			
2.08	2215	49.0			
*2.30	2360	48.0			
2.52	2460	43.7	1.3		$15A_2$
2.68	2540	42.0	0.8		33B
2.81	2684	33.0	1.0		23C

* Water cooling applied from this die onwards.

5.2.7.3 Drawing trials of other silicon-containing alloys

The as-drawn properties of the 2Si-1Mn, 1Si-1Cr-1Mn and 2Si-1Cr-0.9C alloys were evaluated. The 0.9C wire was drawn from 12mm rod, and the other two alloys from nominal 10mm diameter rods.

The data obtained from the different drawing trials is listed in Table 5.14. The work hardening curves of the 2Si-1Mn and 1Si-1Cr-1Mn alloys are compared with the

Table 5.14 As-drawn properties of other silicon-containing alloys.

Alloy	Lead bath temperature (°C)	True Strain (ε)	Tensile strength (MPa)	R.A. (%)
2Si-1Mn Sheffield	620 C 10 min.	0	1275	30.0
		0.29	1498	28.1
		0.62	1602	31.4
		0.92	1688	32.0
		1.19	1778	36.2
		1.44	1822	43.5
		1.8.	1958	49.0
		2.03	1989	47.0
1Si-1Cr-1Mn Sheffield	630 C 5 min.	0	1316	
		0.92	1665	
		1.72	1986	
		1.87	1993	
		2.03	2000	
		2.28	2225	31.8
		2.58	2294	35.7
		2.71	2411	28.6
		2.94	2702	
2Si-1Cr-0.9C Wits	665 C 5 min.	0	1387	33.0
		1.25	1977	38.1
		1.55	2040	39.5
		1.82	2192	46.3
		2.07	2273	28.0
		2.30	2437	28.1
		2.52	2588	26.2
		2.68	2650	25.0

2Si-1Cr alloy in Figure 5.29. The measured work hardening rates for these three alloys were 324MPa, 384MPa and 439MPa per unit strain, respectively.

The effect of carbon content on the work hardening rate can be seen by comparing the work hardening curves of the 2Si-1Cr-0.8C and 2Si-1Cr-0.9C alloys (Figure 5.30). The work hardening rate of the 0.9C alloy was found to be 458MPa per unit strain, an improvement of 20MPa per unit strain on the 0.8C alloy. After drawing the 0.9C steel to a true strain of 2.67, a sharp increase in strength and decrease in ductility were noticed. This may be due to ageing during the drawing process.

For ease of reference and rapid comparison, the major properties determined for patented rods and drawn wires in alloys containing silicon are summarised in Table 5.15.

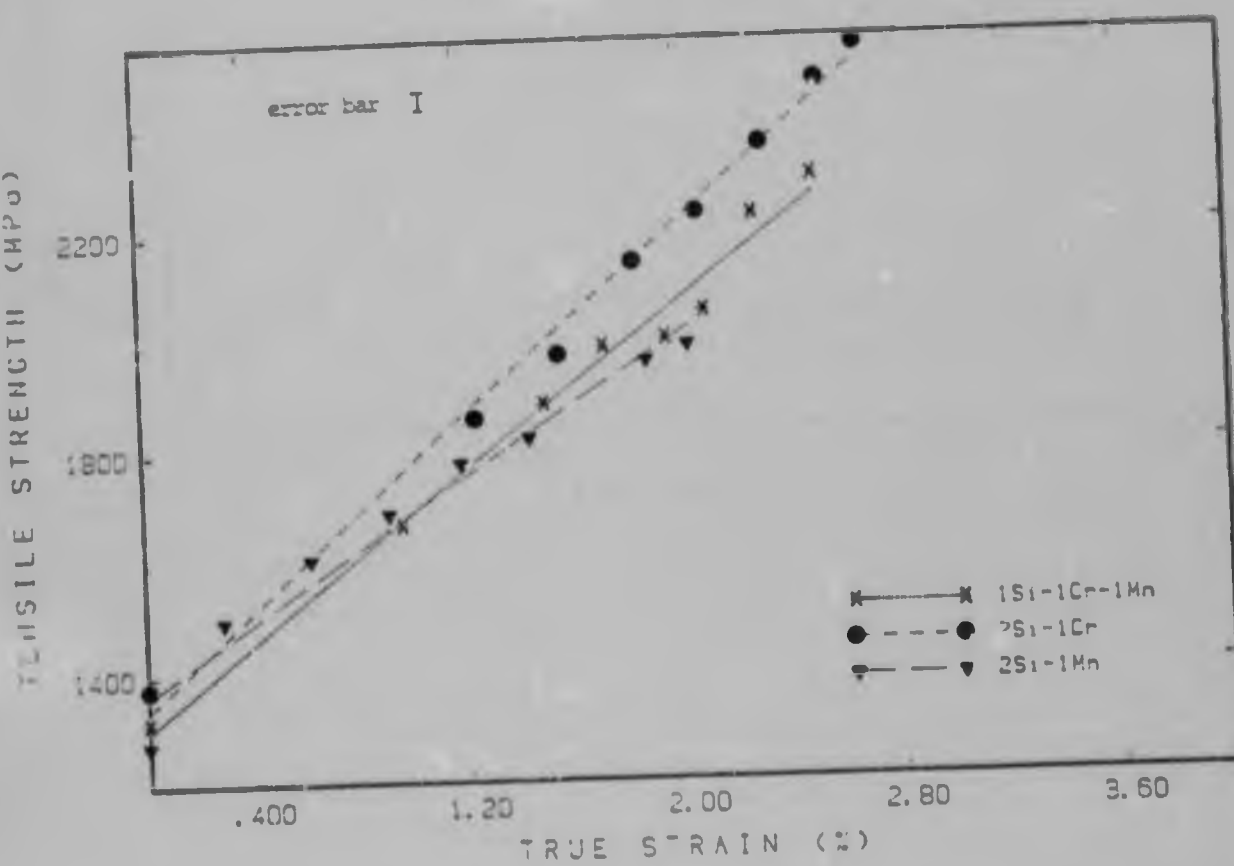

Figure 5.2) Work hardening curves of the 2Si-1Mn and 1Si-1Cr-1Mn alloys, compared with the 2Si-1Cr alloy.

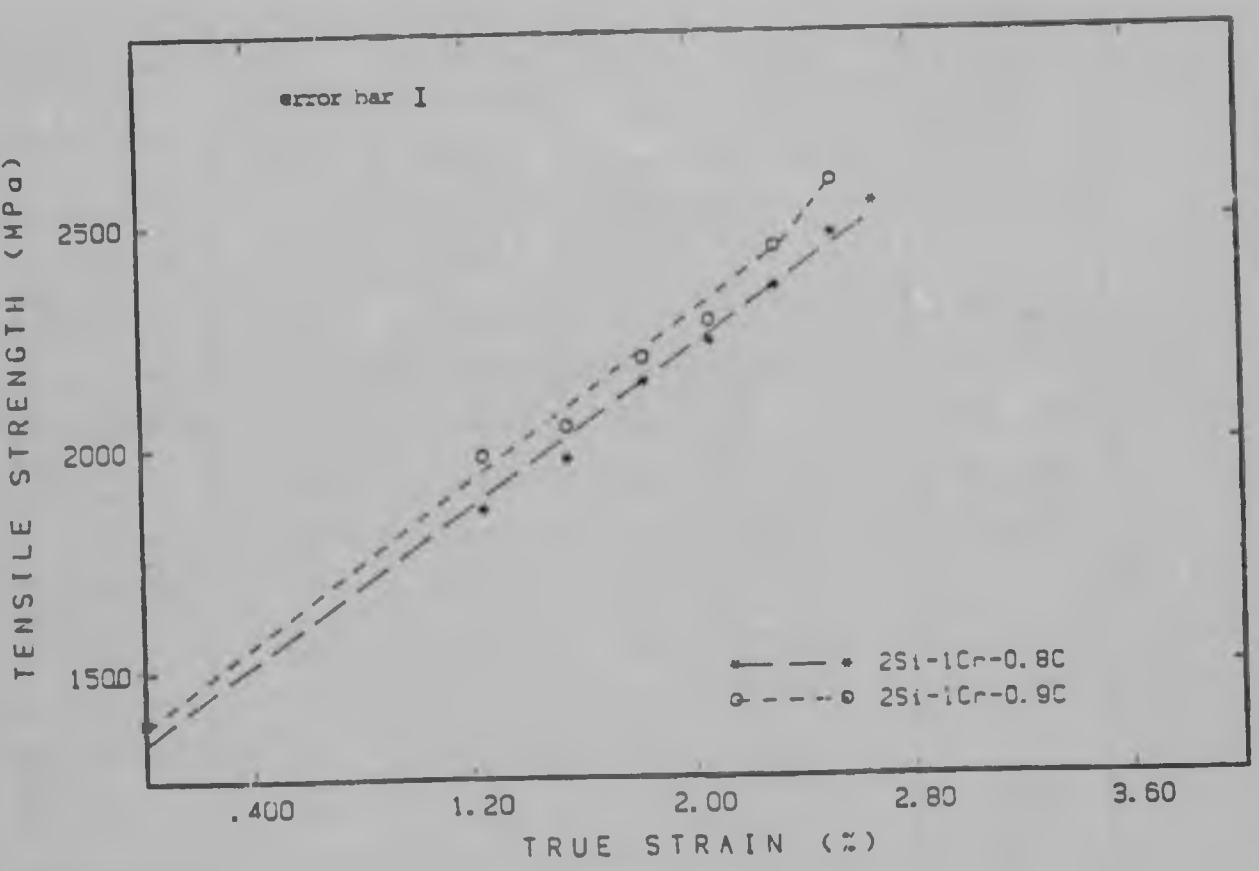

Figure 5.30 The effect of carbon content on the work-hardening rate of the 2Si-1Cr alloy.

Table 5.15 As-drawn properties of the high purity silicon-containing alloys.

Alloy/ transformation conditions	Total Reduction (%)	Tensile Strength (MPa)	R.A. (%)	Shear elongation (%)	Torsion turns/ 100ϕ Break type
2Si-1Cr * 660 °C, 5 min.	0	1375	36.0		
	93	2580	37.0	1.65	30 A_1
2Si-1Cr-0.9C 665 °C, 5 min.	0	1387	33.0		
	93	2650	25.0	0.9	20.5B
1Si-1Cr-1Mn* 630 °C, 5 min.	0	1316	29.0		
	94	2411	18.0	0.6	
2Si-1Mn * 620 °C, 10 min.	0	1275	30.0		
	88	1989	47.0	1.4	31 A_2
1.7Si-1Cr* 660 °C, 5 min.	0	1317	37.5		
	93	2500	35.5	1.2	25.5B

* all 0.8C.

5.2.8 Transmission electron microscopy of drawn wires

Transverse sections of wires subjected to different drawing reductions were studied using CTEM. Many thin foils of all the alloys were studied and the same observations were made in each. Representative micrographs illustrating the main features of the drawn structure are described below.

The refinement of the pearlite structure with increasing drawing reductions can be seen in Figure 5.31. Well-defined cellular substructures are also clearly evident. In the final drawing stages, a progressive decrease in the interlamellar spacing and in the width of the lamellae was observed, as well as some fragmentation of the lamellae (Figure 5.32).

The alignment of the lamellae in the longitudinal (drawing) direction can be seen in Figure 5.33. The gradual development of the rings in the diffraction patterns due to texture formation is shown in Figure 5.34.

5.2.9 Reproducibility of results

The results obtained indicated that the most promising alloy was that containing 2Si-1Cr. It was decided therefore to confirm that consistently good mechanical properties could be achieved in this alloy by comparing the results obtained from different melts of similar composition. The analyses of the major elements are given in Table 5.16.

As-patented tensile strengths were measured in Hounsfield and rod specimens from the different batches and the fluctuations in the results were of the order of 5%.

(a)

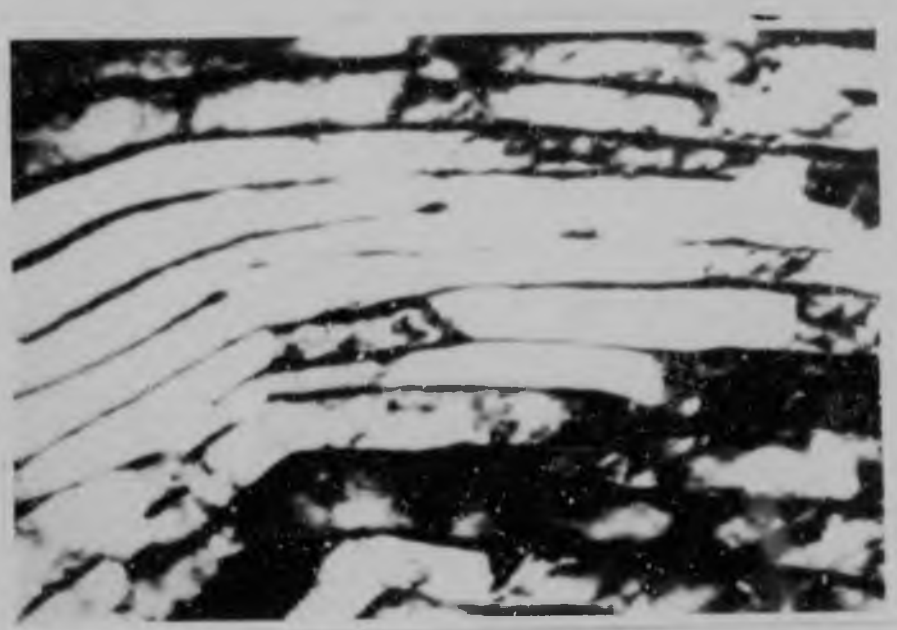

0.1μm

(b)

0.05μm

Figure 5.31 As-drawn structures of the 2Si-1Cr alloy subjected to different drawing reductions.
(a) 79%;
(b) 87.5%
(TEM micrographs)

(a)

0.05μm

(b)

0.1μm

Figure 5.32 As-drawn microstructures of wires drawn to 93% reduction.
(a) Refinement of the lamellar structure;
(b) Fragmentation of the cementite lamellae.
(TEM micrographs)

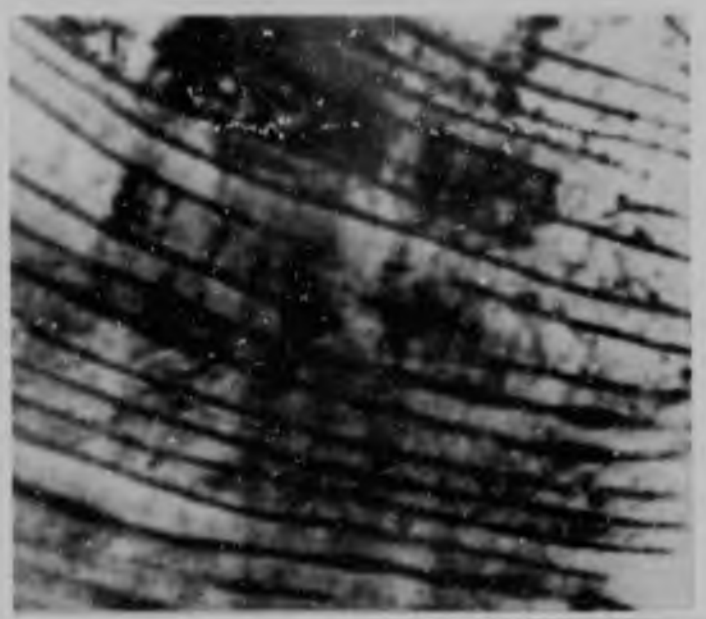

0.1μm

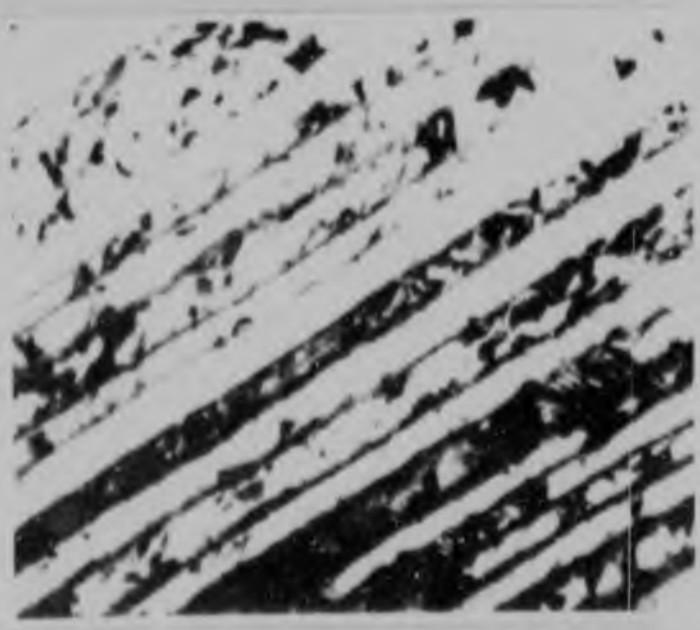

0.1μm

Figure 5.33 Alignment of the cementite lamellae in the drawing direction (TEM micrographs).

(a)

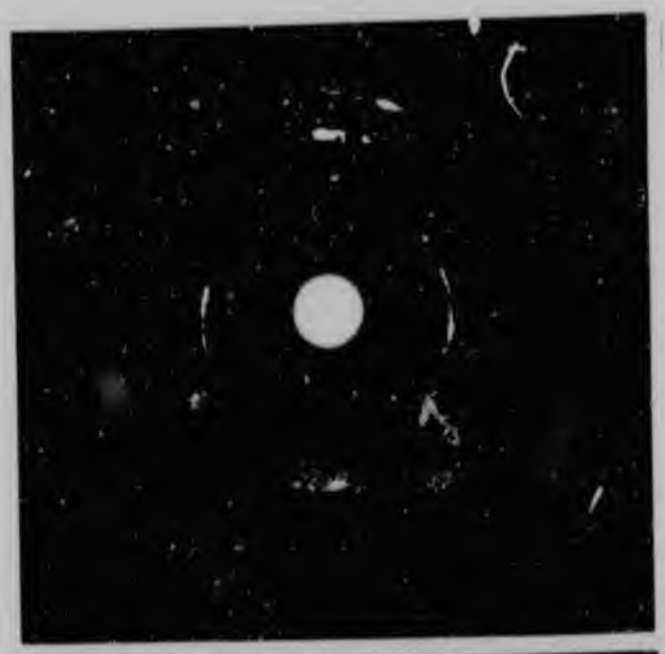

(b)

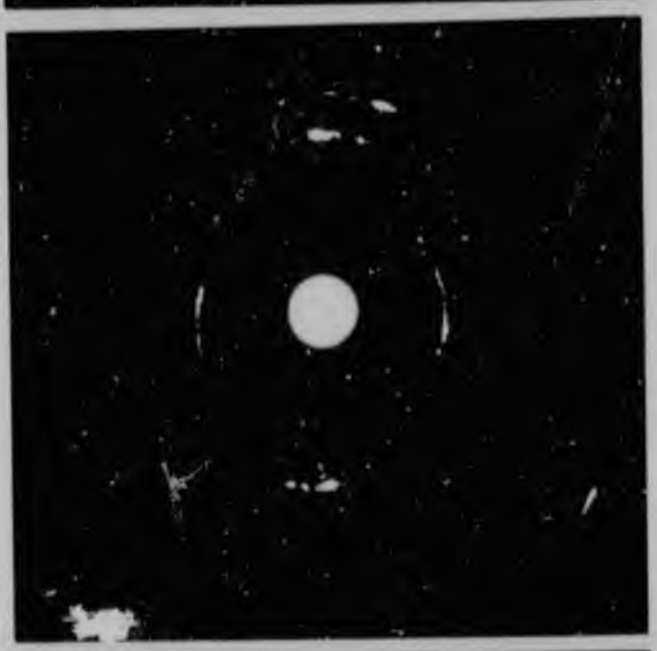

(c)

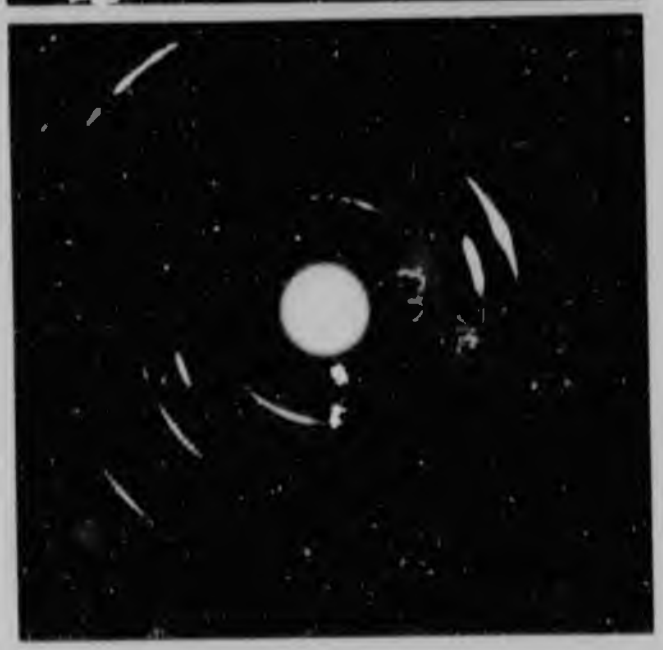

Figure 5.34 Electron difraction patterns obtained from material with different drawing reductions.
(a) 79%
(b) 87.5%
(c) 93%

Table 5.16 Compositions cf the different melts of the 2Si-1Cr Wits alloy.

Batch number	Composition (Wt%) C	Si	Cr
V - 50	0.83	1.85	1.04
V - 52	0.8	1.64	0.98
V - 85	0.8	1.83	0.99
V - 86	0.8	1.91	1.00

The results obtained during the drawing trials on the different steels are given in Table 5.17. The relatively high as-drawn tensile strength obtained for batches V-50 and V-52 were probably due to ageing, since appropriate water cooling was not introduced in the initial stages of the research. Nevertheless, it is clear that consistently high strength with adequate residual ductility can be achieved.

The results obtained therefore are reliable and can be used as a basis for further research.

Table 5.17 As-drawn properties of different melts of the 2Si-1Cr Wits alloy.

UTS (MPa) / True strain (ε)	Batch Number V-50	V-52	V-85	V-86
0	1356	1366	1375	1389
1.25	1989	1906	1860	1893
1.55	2135	2012	1970	2019
1.82	2289	2143	2140	2137
2.07	2312	2245	2230	2245
2.30	2499	2339	2350	2330
2.51	2628	2464	2470	2445
2.67	2712	2629	2580	2593
As-drawn	No Water Cooling		Water Cooling	
R.A. (%)	20	23	37	40
Shear elongation	0.15	0.65	1.65	1.2
turns/100ϕ	13	21	30	28
Break type	C	C	A1	B

5.3 Further Discussion

5.3.1 TTT diagrams

Examination of the TTT diagrams of the different alloys showed that the Si-Mn and Si-Cr alloys had shorter incubation periods than the Si-Cr-Mn alloys. A similar effect was observed for the completion time of the reaction.

Some idea of the effects of individual elements can be deduced by comparing the transformation characteristics of the alloys studied in this part of the investigation with those of the earlier 1Cr-1Mn composition.

The 2Si-1Mn alloy then represents the substitution of 1% chromium by 2% silicon. This decreased the incubation time from 25 to 12 seconds, while the temperature of the pearlite "nose" remained unchanged at 620 °C.

The substitution of 1% manganese by 2% silicon can be assessed by comparison of the 1Cr-1Mn with the 2Si-1Cr alloy. The incubation period was reduced further (to 10 seconds) and the temperature of the nose of the C curve was increased (to 670 °C).

The cumulative effect of silicon additions to the 1Cr-1Mn alloy can be seen in the alloys 1Si-1Cr-1Mn and

2Si-1Cr-1Mn. The addition of 1% silicon increased the incubation time (from 25 to 40 seconds) but had little effect on the temperature of the pearlite nose. Further silicon additions (2%), also increased the incubation period (to 40 seconds) and lowered the temperature of the nose of the pearlite C-curve (to 600°C).

The findings for the 2Si-1Cr and 2Si-1Mn steels are in agreement with Cockett and Davis (1963), Franklin et al (1980) and Al-Salman et al (1979b) who observed that the addition of silicon to a eutectoid steel caused the displacement of the nose of the TTT curve to higher temperatures, and to slightly longer times.

Although the incubation time in the steels is significantly greater than a plain carbon eutectoid steel, the transformation to pearlite is still quite rapid. Thus, such compositions appear suitable for the development of uniform fine pearlite microstructures using existing commercial facilities.

5.3.2 Microstructural observations

In the light microscopy investigation of partially transformed samples it was observed that the pearlite nodule size and distribution was not uniform. This suggested that the use of starting material in the as-cast

and rolled condition was not satisfactory in terms of achieving complete homogeneity during austenitisation. Further consideration should be given therefore to the application of a homogenisation heat treatment.

In the scanning electron microscope, traces of upper bainite were found for low transformation temperatures in all the alloys. These would be deleterious to mechanical properties and higher transformation temperatures were chosen in materials used for drawing trials.

The most regular and uniform lamellar structure was observed in the 2Si-1Cr alloy. This is in agreement with Mehl and Hagel (1956). In a study of the pearlite curvature in different steels they mentioned that silicon steels exhibit a "straighter" pearlite.

Transforming the 2Si-1Cr alloy at 660°C for 5 minutes led to the formation of very fine pearlite. In this alloy the cementite tends to spheroidise very rapidly if the soaking time is increased to only ten minutes, or if the transformation temperature is slightly increased to 680°C.

It is known that heterogeneous austenite promotes the transformation of austenite to spheroidised microstructures (Krauss (1980), Parusov et al (1978)). It has been suggested that the coarser the pearlite structure the more

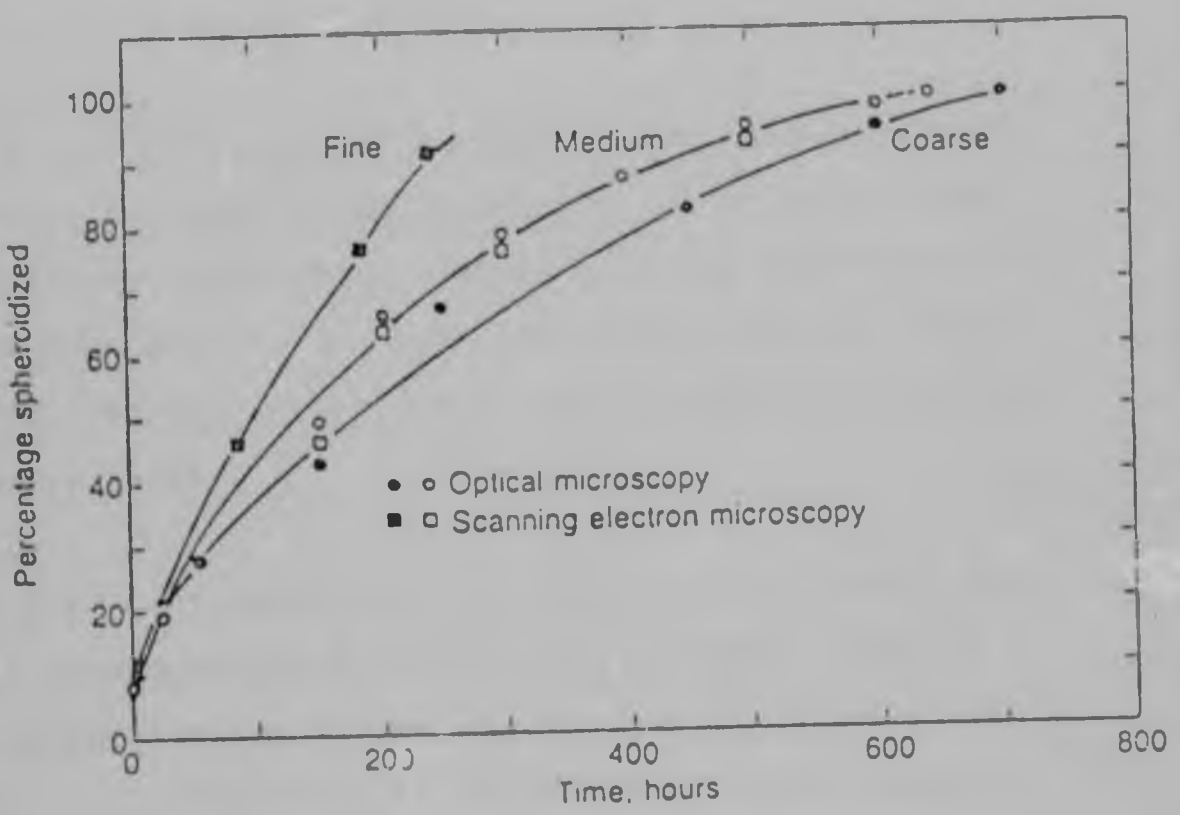

Figure 5.35 Progress of spheroidisation at 700°C of fine, medium and coarse pearlites in a steel containing 0.74%C and 0.71%Si. After Chattopadhyay and Sellars(1977)

difficult it is to spheroidise it, and that more regular finer pearlite structures spheroidise easily and rapidly (Reed Hill (1964) and Chattopadhyay and Sellars (1977), (Figure 5.35)). Spheroidised microstructures are stable because the cementite particles then have minimum interfacial area per unit volume.

Guiva et al (1978) proposed a model for the spheroidisation of pearlite in terms of the nucleation and growth of areas of granular ferrite-carbide mixtures. It was found that in high carbon steels, silicon additions enabled these granular aggregates to form over a relatively wide temperature range.

It has also been suggested that silicon must affect the surface energy of Fe_3C (G.D.W. Smith, 1983). Thus the rapid spheroidisation of cementite in the 2Si-1Cr alloy may be due to a combination of all these factors: granular mixture formation, surface energy effects and austenite heterogeneity.

5.3.3 The effect of the austenitising treatment

Different austenitising conditions were tested for the 2Si-1Cr alloy. The highest as-patented strength was obtained for an austenitising temperature of 1000 °C. Although this resulted in the lowest ductility observed, it

was still sufficient for further drawing trials. An austenitising temperature above 1000 °C produced only slightly lower strength, despite a considerable increase in grain size.

Austenitising temperatures below 1000 °C were found to be insufficient to produce optimum properties. Similar results were obtained by Cahill and James (1968a) for an austenitising temperature of 960 °C.

Low austenitising temperatures produce a finer grained austenite. This reduces the incubation time for pearlite formation and transformation may occur at progressively higher temperatures. Pearlite is therefore formed in the region of the nose of the TTT curve, well above the temperature required to produce the optimum fine interlamellar spacings.

Longer austenitising times at all temperatures produced an increase in strength. This may be attributed to the more effective and complete dissolution of alloy or mixed carbides, as proposed by Franklin and Allen (1980).

The austenitising heat treatment is of considerable importance in the production of high quality steel for cold-working. In particular, Billington et al (1981) suggested that control of the austenite grain size prior to

transformation is crucial, since this determines the optimum cooling rate through transformation in any given steel.

5.3.4 Interlamellar spacing measurements

No meaningful differences were observed for the interlamellar spacing of the different alloys, however, there was a marked decrease in spacing when compared with a commercial plain carbon steel.

A decrease in the interlamellar spacing due to an increase in carbon content was observed, as reported by Pellisier et al (1942) and Payne and Smith (1968), however no influence was observed due to a change in the prior austenite grain size, this is also in agreement with Pellisier et al (1942), Marder and Bramfitt (1976), Roósz and Gaczí (1981).

5.3.5 The as-patented tensile strength

The mechanical properties can also be compared by reference to the addition or substitution by silicon in the 1Cr-1Mn alloy. The addition of silicon to the 1Cr-1Mn alloy led to a substantial increase in strength. The maximum strength was measured for the 2Si-1Cr-Mn alloy, but with low ductility.

Substitution of chromium or manganese in the 1Cr-1Mn alloy by 2% silicon led to improved tensile properties in the 2Si-1Cr alloy, while the 2Si-1Mn alloy had inferior properties. Low tensile strength values in a manganese-containing steel have also been reported by Franklin et al (1980). The high tensile values obtained at low transformation temperatures are related to a mixed bainite and fine pearlite structure, as discussed in Section 4.3.3.2.

High strength (1375MPa) and good ductility (36%) were measured for the alloy 2Si-1Cr-0.8C transformed at 660°C for 5 minutes. This is also in agreement with Franklin et al (1980) who observed that the transformation temperatures corresponding to the maximum tensile strength increased as the level of silicon increased.

For all transformation temperatures, the chromium-containing alloys showed an increase in strength in the region of 250MPa, in relation to the 2Si-1Mn steel. This is in agreement with Gladman et al (1972) who found that manganese in solid solution appears to have no significant effect on the tensile strength.

5.3.6 The effect of carbon content

Although hyper-eutectoid phases (particularly cementite) are deleterious to the properties of pearlitic steels, no traces of this phase were found in the 0.9C steel. The drawing trials also suggest that no pro-eutectoid phase had formed, since precipitation of cementite along the grain boundaries lowers drawability and toughness, even in high quality steels (Franklin et al (1980), and Guerrieri et al (1983)).

Silicon is known to be one of the best possible additions in order to retard the kinetics of pro-eutectoid cementite formation. Heckel and Paxton (1960) studied the thickening of cementite films in hyper-eutectoid steels. A very slow growth rate was observed in a silicon-containing, compared with a plain, carbon steel. This effect was attributed to a silicon (ferrite stabiliser) build up at the interface. The role of silicon is further substantiated by the fact that it has only negligible solubility in cementite. Silicon rejection at the advancing interface would cause a continually increasing build up because of its low diffusivity. This leads to a retardation in growth by a combination of the necessity of silicon removal before cementite can form and its effect on increasing the activity of carbon in austenite, thus reducing locally the carbon activity gradient.

The tensile strength was found to increase with increasing carbon content, as expected, while the ductility showed the opposite trend. At transformation temperatures of 665°C the structure consisted of a very fine, uniform pearlite. However, the pearlite morphology at 680 °C was unsatisfactory, with significant islands containing no carbides and partially spheroidised pearlite. At a transformation temperature of 620 °C, the structure appeared to become degenerate. Degenerate pearlite was also observed in the low (0.5 to 0.7%) carbon 2Si-1Cr steels. This is in agreement with Cheetham and Ridley (1975) who observed that pearlite degeneracy increased as the carbon content of a steel decreased.

5.3.7 As-drawn properties

A considerable in ease in the tensile properties was achieved as a result of the drawing. However, the strengths obtained in the 2Si-1Mn (1989MPa) and 1Si-1Cr-1Mn (2411MPa) alloys were low relative to the 2Si-1Cr steel (2580MPa).

The 2Si-1Cr Sheffield alloy was anomalous. Transformation at different temperatures gave different work hardening rates during drawing. This is difficult to explain, but is probably due to lack of experience and poor technique in the initial drawing trials.

The abrupt increase in strength observed in many cases after the last pass of drawing may be due to ageing of the wires. This will arise if inadequate wire cooling is applied.

The high carbon alloy (2Si-1Cr-0.9C) was drawn to achieve a strength of 2650MPa and 25% ductility after a 93% drawing reduction. These are excellent values considering the work of Chandhok et al (1966), who found a total loss of ductility after drawing a 0.9% carbon commercial steel to 86% reduction.

The work hardening rates also varied. The 2Si-1Mn alloy exhibited a very low value (324MPa per unit strain) the 1Si-1Cr-1Mn gave 348MPa, which is slightly lowe a plain carbon steel (Langford, 1977). The work h. ..ing rates for the 2Si-1Cr-0.8 and 0.9C steels were 439 and 458MPa per unit strain respectively. This supports a previous suggestion that the work hardening rate increases with carbon content (Shipley, 1962).

A great deal of consideration has been given to drawing conditions. The cooling of wire during drawing was recommended by Smith and Speirs, and by Sturgeon and Guy (1963). The latter have shown that by protecting the internal surfaces of the capstan wall from corrosion, improvements in cooling can be obtained.

Another factor which must be emphasised is die design and the amount of reduction at each stage. Willemse et al (1982) have shown that the residual state of stress of cold-drawn wires is influenced by these parameters. Brandal and Valberg (1982) took the view that a drawing practice characterised by small reductions should be avoided because central bursts, reported also by Avitzur (1983), and cup and cone wire breaks may occur due to the instability of flow pattern.

In the present research the reduction per pass of drawing was in the range 19 to 25%; and the use of direct cooling of the wire in later experiments considerably improved the ductility of the final product. An as-drawn strength in the region of 2600MPa was obtained in this work by using a combination of silicon and chromium additions together with high carbon levels and optimum patenting conditions. The alloy 2Si-1Cr-0.8C achieved an as-drawn strength of 2580MPa with a residual ductility of 37% and the torsion and shear tests results were in excess of the minimum requirements of commercial specifications. This showed the advantage of lead patenting over the continuous cooling "Stelmor" process reported by Pesche et al (1982).

Improved as-drawn properties as a result of chromium and silicon additions have also been reported by Takahashi et al (1980) and Ochiani et al (1983).

5.4 Summary

In this part of the investigation, the effects of silicon on the transformation characteristics and the as-patented and drawn mechanical properties of chromium-manganese steels were studied. It was found that the 2Si-1Cr-0.8C composition gave the highest as-drawn strength, combined with adequate ductility.

The influence of carbon content was also studied. Alloys containing less than 0.8% exhibited very poor as-patented properties and were not drawn. Increasing the carbon concentration by 0.1% (to 0.9%) improved the as-patented properties, but ductility decreased rapidly during drawing. This may be due to ageing of the wire through insufficient cooling.

Based on these results, it was decided to assess the effects of alloying on commercial purity plain carbon steels.

CHAPTER SIX - COMMERCIAL PURITY ALLOYS

6.1 Introduction

The previous work was carried out on alloys prepared from high-purity base materials. However, industrial steels contain significant amounts of manganese, sulphur, phosphorus and other impurities. Since the 2Si-1Cr alloy gave the best combination of properties in the earlier studies, it was decided to prepare two similar compositions using commercial Fe-Mn-0.8C as the starting stock. The analyses of these alloys are listed in Table 6.1.

Table 6.1 Chemical compositions of commercial grade Wits alloys (in weight %)

Alloy	C	Cr	Mn	Si	S	P	N	Others
2Si-1Cr	0.8	1.01	0.70	1.85	0.035	0.011	0.008	*
1.7Si-1Cr	0.79	1.02	0.72	1.70	0.033	0.010	0.008	*

* less than 0.02%.

6.2 Results and Discussion

6.2.1 TTT diagrams

Although the commercial alloys appear to have very similar compositions to the high purity 2Si-1Cr-1Mn alloy, it should be noted that in the former alloys the manganese was added to cou[illegible]he deleterious effects of sulphur on mechanical [illegible]rties. Thus, most manganese may be combined in the form of sulphides with little in solid solution. Nevertheless, the TTT diagram determined for the high purity alloy was used to select appropriate transformation temperatures (see Figure 5.4).

6.2.2 Mechanical properties and microstructures

Hounsfield specimens were austenitised for 30 minutes at 1000°C then transformed in the temperature range 580 to 630°C (with 10°C intervals of undercooling) for 5 and 10 minutes. The as-patented tensile properties as a function of the different transformation treatments are given in Tables 6.2 and 6.3, and plotted in Figures 6.1 and 6.2. For both commercial alloys very high tensile values were obtained at low transformation temperatures. Again, this may be due to a bainite-containing structure as discussed in Section 4.3.3.2.

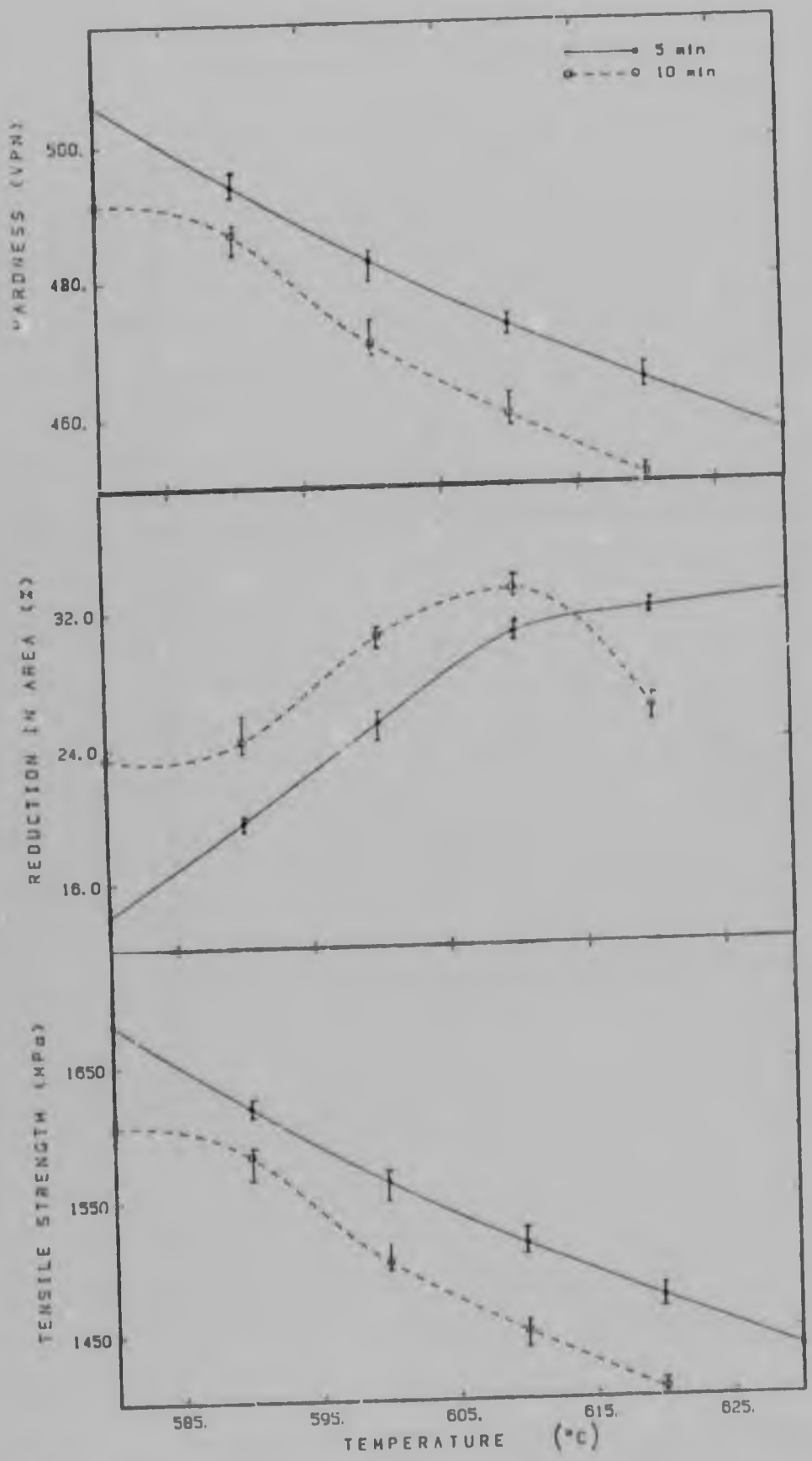

Figure 6.1 As-patented mechanical properties of the 1.7Si-1Cr commercial grade alloy.

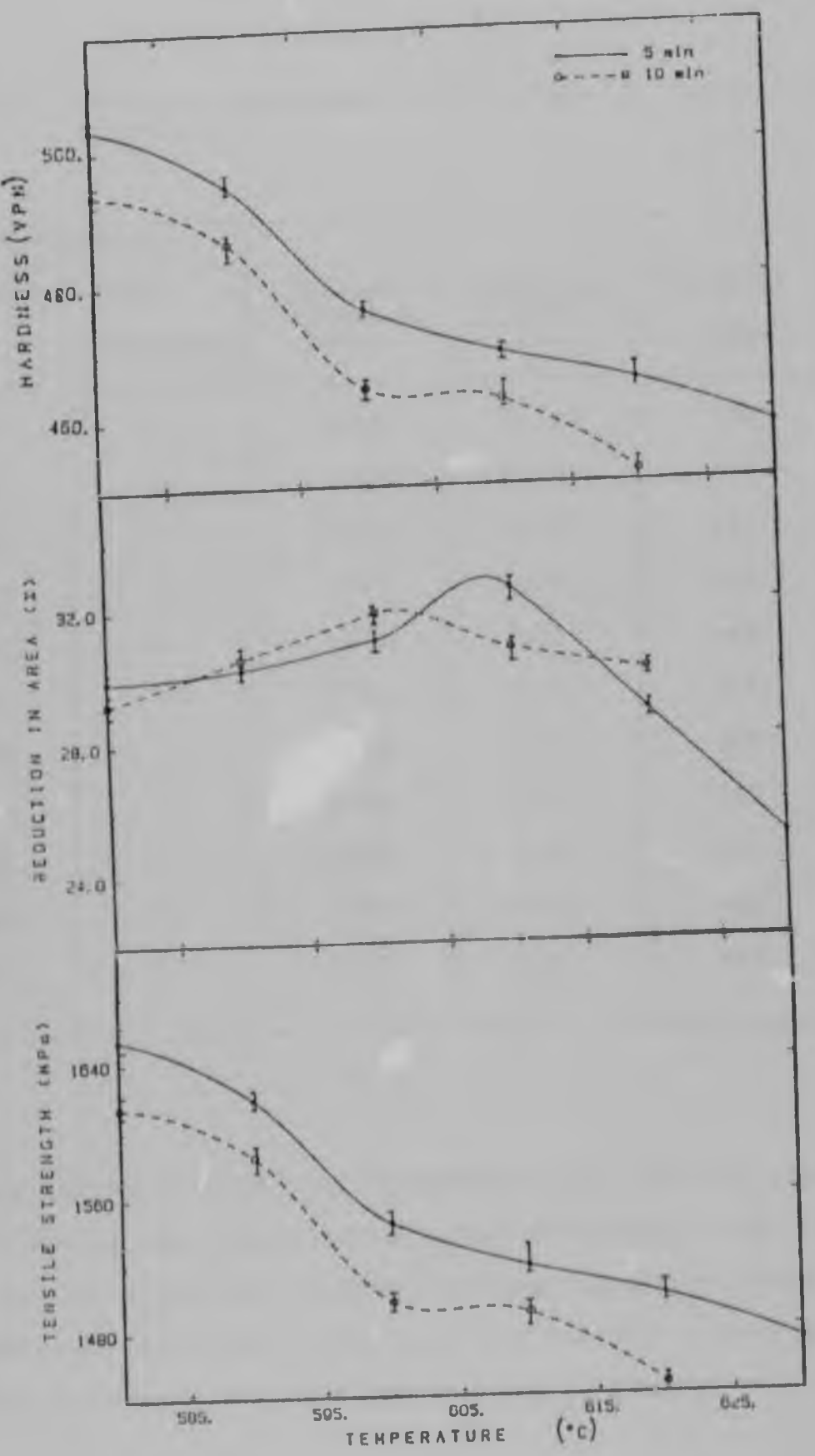

Figure 6.2 As-patented mechanical properties of the 2Si-1Cr commercial grade alloy.

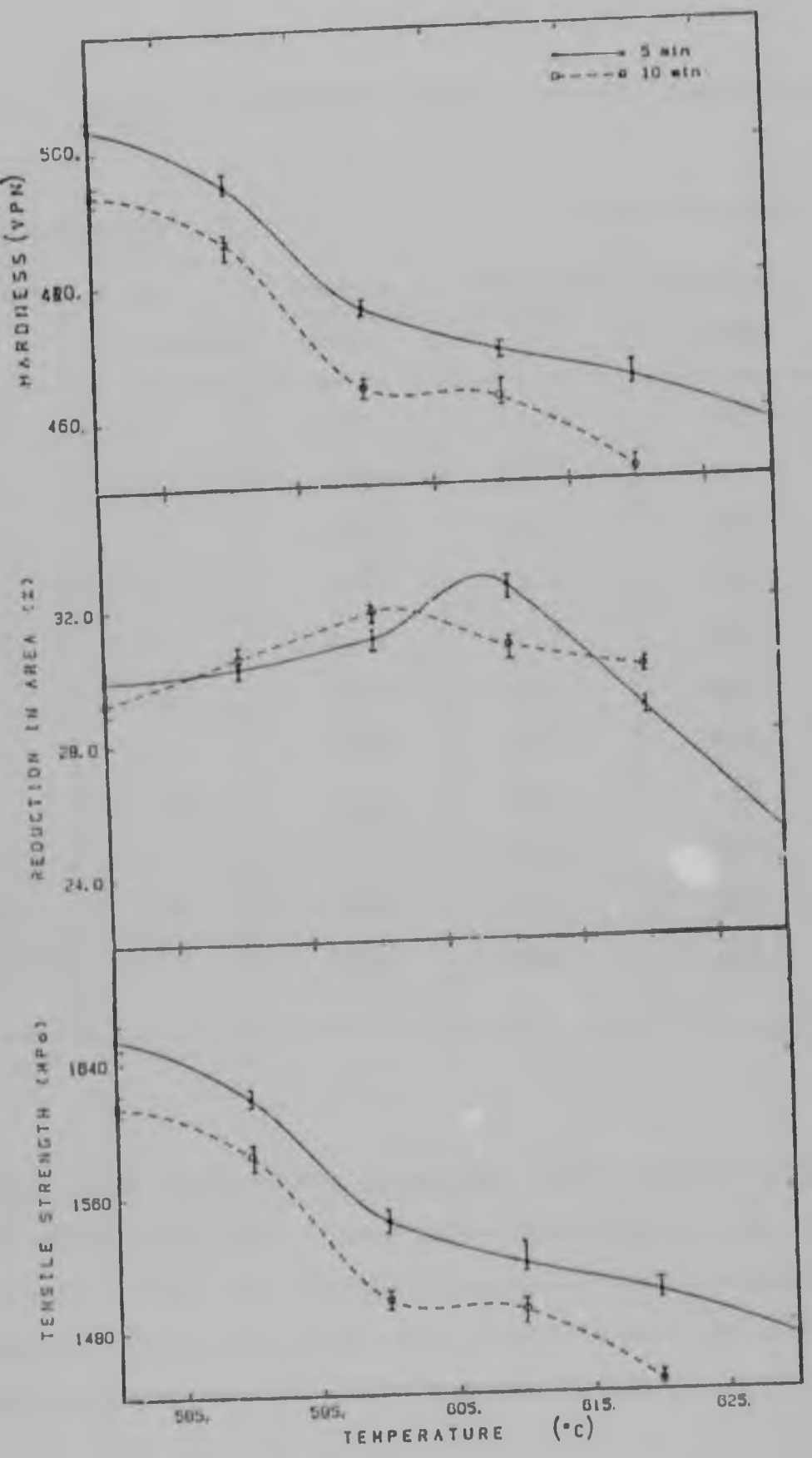

Figure 6.2 As-patented mechanical properties of the 2Si-1Cr commercial grade alloy.

Table 6.2 Tensile properties of the 1.7Si-1Cr commercial alloy.

Heat Treatment		Tensile strength (MPa)	Reduction in area (%)	Hardness (VPN)
Temperature (°C)	Time (Minutes)			
580	5	1681	14.03	530
580	10	1606	23.4	491
590	5	1619	19.5	497
590	10	1583	24.3	486
600	5	1563	25.3	481
600	10	1503	30.4	464
610	5	1516	30.5	468
610	10	1450	33.0	449
620	5	1475	31.8	456
620	10	1406	26.0	436
630	5	1436	32.6	445

The ductilities measured for specimens of the 2Si-1Cr alloy transformed at low temperatures appear abnormally high. In the 1.7Si-1Cr alloy the highest tensile strength combined with adequate ductility (>30% R.A.) was 1516MPa. This was provided by transformation for 5 minutes at 610°C.

Table 6.3 Tensile properties of the 2Si-1Cr commercial alloy.

Heat Treatment		Tensile strength (MPa)	Reduction in area (%)	Hardness (VPN)
Temperature (°C)	Time (minutes)			
580	5	1654	29.9	506
580	10	1614	29.2	494
590	5	1619	30.2	497
590	10	1584	30.5	486
600	5	1544	31.0	478
600	10	1497	31.8	484
610	5	1518	33.3	470
610	10	1490	30.7	461
620	5	1500	28.8	464
620	10	1446	30.5	448
630	5	1472	25.0	456

6.2.3 Scanning electron microscopy

Samples transformed at 610°C for 5 minutes were examined in the SEM in order to characterise the as-patented structure. The pearlite appeared to be very fine and regular (Figure 6.3). Interlamellar spacings (measured from SEM micrographs) were found to be of the order of 80 to 100nm.

(a)

0.5μm

(b)

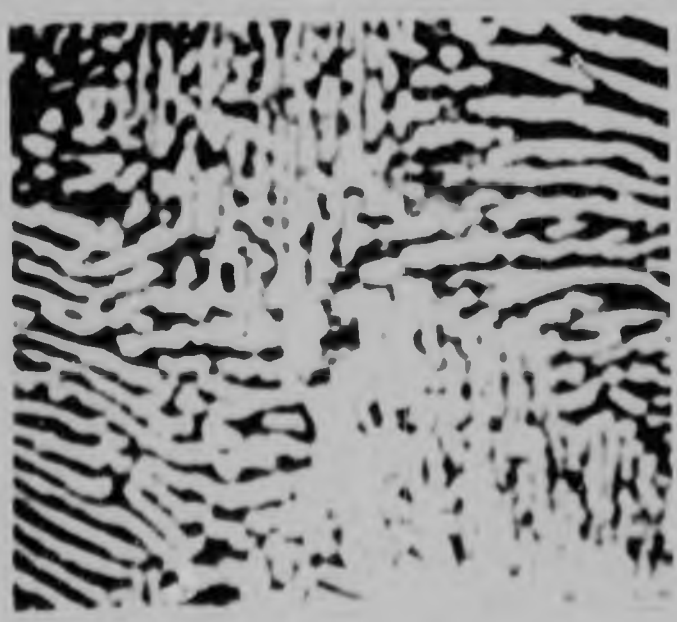

0.5μm

Figure 6.3 SEM micrographs of alloys of commercial grade transformed at 610°C for 5 minutes
(a) 1.7Si-1Cr
(b) 2Si-1Cr

Such a fine pearlitic structure should be very suitable for wire drawing. This combined with the good mechanical properties suggested that 5 minutes at 610°C was the most appropriate transformation heat treatment and this was selected as standard for the drawing trials.

6.2.4 Drawing trials

For the drawing trials, 500mm long rods were transformed using the standard conditions (5 minutes at 610 °C). Despite its apparent superior ductility, the 2Si-1Cr alloy could not be pointed. Attempts to do so resulted in continual fracturing of the rods. No drawing trials were possible using this alloy. Although difficult to point, the 1.7Si-1Cr alloy was successfully drawn to a true strain of 2.07 (87.5% total reduction). This produced an as-drawn strength of 2432MPa. However, poor drawability was noticed during all the drawing trials.

Further drawing to 93% reduction increased the strength to 2650MPa. Unfortunately, at this strength level all ductility appeared to be lost, although no absolute measure could be obtained due to splitting of the wires.

The work hardening curve of the 1.7Si-1Cr alloy is plotted in Figure 6.4 and compared with that of a plain carbon commercial steel. A work hardening rate of 432MPa per unit

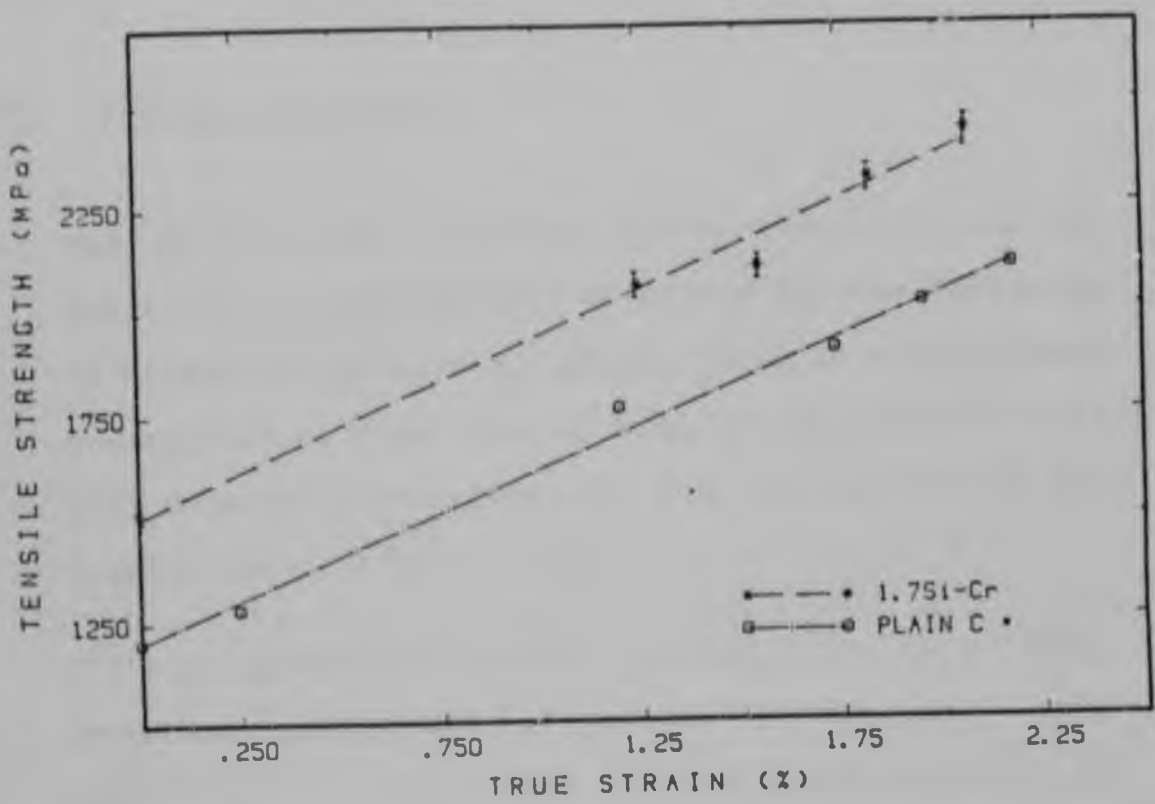

Figure 6.4 Work hardening curves of the alloy 1.7Si-1Cr of c mmercial grade and a plain carbon steel.
* After Haggie Rand (1979).

strain was measured for the alloy steel which is an improvement on the work hardening rate of the plain carbon steel.

6.3 Further Discussion

a. One of the main problems encountered during the fabrication of the commercial alloys was the formation of central pipes during casting. This is a well-known phenomenon in high carbon, high silicon steels when both elements contribute to the contraction of the liquid steel (Strauss, 1970).

Although primary pipes were removed prior to rolling, secondary pipes could have existed in the rods. This could have been one reason for the low drawability of these alloys, which caused difficulties in pointing the rods prior to drawing and continuous splitting of the wires during drawing. Despite all the obstacles a tensile strength of 2650MPa was achieved, after drawing the rods to a total reduction of 93%.

b. The work hardening rate measured for the 2Si-1Cr commercial alloy was very similar to the value obtained for the high purity alloy of the same nominal composition. However, the as-patented tensile strengths measured for the commercial steel were higher and the ductilities lower. This may be

accounted for, in part, by the presence of manganese in excess of that required to fix the sulphur, providing solid solution strengthening.

c. A fully pearlitic structure with the finest pearlite spacings was obtained at a lower transformation temperature (610°C) compared with the high-purity 2Si-1Cr (660°C). This could be explained in terms of the hypothesis presented by Picklesimer et al (1960). In steels of high purity, nucleation occurs mainly on free surfaces at higher transformation temperatures. This suggests that in alloys of lower purity and in commercial alloys there is impurity catalysis of nucleation.

d. The study of commercial purity alloys was intended to determine whether the good results obtained in high purity material could be reproduced. If successful, then attempts could be made to produce the alloys on an industrial scale, using relatively unsophisticated production methods.

In the literature the benefits of high purity to the properties of high carbon, high tensile steel wires has been widely reported. One of the major factors considered has been the effect on the ductility of wires. Reduction in the ductility of wires is apparently associated with

macrosegregation of sulphur and carbon, and the latter may also cause the formation of free cementite at prior austenite grain boundaries. These facts have been reported by many authors, for example Cottrell (1963), Gladman et al (1970), Edwards et al (1979), Stacey (1980) and Guerrieri et al (1983).

Even in high tensile strength steels for purposes other than wire rods, the benefit of high-purity steels compositions compared with steels of normal purity has been demonstrated (Cottrell and Turner, 1962).

An increasing tendency to use ultra-pure materials and vacuum melting techniques was reported by Capus and Mayer as early as 1960 and by Cottrell et al in 1963.

The importance of steel purity in the achievement of high strength together with good ductility and toughness was also emphasised by Franklin and Allen (1980). They suggested that non-metallic inclusions are detrimental. This view was supported by Demeyer (1981). Theis and Klemm (1982) also suggested that good microscopic cleanliness was required in high carbon rods used for the production of fine wires.

6.4 Summary

The attempt to test the properties of a 2Si-1Cr commercial grade alloy was disappointing.

Many problems were encountered during the fabrication of the alloys, due to pipe formation, which was found to be detrimental for drawing purposes.

The lead bath temperatures chosen for isothermally transf[illegible]ng the rods prior to drawing were apparently too low. A slight increase in the temperature may have provided higher ductility but with a lower tensile strength.

6.4 Summary

The attempt to test the properties of a 2Si-1Cr commercial grade alloy was disappointing.

Many problems were encountered during the fabrication of the alloys, due to pipe formation, which was found to be detrimental for drawing purposes.

The lead bath temperatures chosen for isothermally transforming the rods prior to drawing were apparently too low. A slight increase in the temperature may have provided higher ductility but with a lower tensile strength.

CHAPTER SEVEN - AGEING TRIALS

7.1 Introduction

Practical experience has shown that drawn plain carbon eutectoid steels are subject to ageing at temperatures of 50 °C (Shipley, 1982). It was decided therefore to carry out ageing trials on the experimental UHT (ultra high tensile) material.

Tests were performed on the high purity 2Si-1Cr alloys drawn from 12mm diameter to 3.79mm (90% reduction) using full water cooling. Specimens were also prepared from material drawn to 3.40mm (92%) and 3.15mm (93%). For each drawing reduction, shear test specimens were heat treated at 50 °C for between one and 96 hours. Wires submitted to ageing trials were placed in a refrigerator immediately after drawing in order to prevent further ageing at room temperature.

7.2 Results and Discussion

7.2.1 Shear tests

Shear tests were conducted in order to evaluate the ductility of the wires as a result of different ageing treatments (Stephenson et al, 1983). A minimum of three samples was tested for each heat treatment. The shear

elongation values measured are listed in Table 7.1 and plotted in Figure 7.1. Shear values below 1.0 were considered as poor ductility of the wires.

Table 7.1 Shear ductility values obtained during ageing trials at 50 °C.

Wire \ Time (Hours)	1	10	50	96
1.7Si-1Cr-0.8C 660 °C, 5 min. (92% reduction)	1.4 1.5 1.5	1.5 1.5	1.3	
1.7Si-1Cr-0.8C 660 °C, 5 min. (93% reduction)	1.2 1.6	1.2 1.6	1.6 1.4 1.6	
2Si-1Cr-0.8C 660 °C, 5 min. (90% reduction)	2.2 2.3 0.3	0.8 1.5 1.6	1.8 0.9 1.7	0
2Si-1Cr-0.8C 660 °C, 5 min. (92% reduction)	1.6 0	1.1 1.2	0 0.2 1.4	
2Si-1Cr-0.8C 660 °C, 5 min. (93% reduction)	1.2 1.0 1.5	1.4 1.4 1.2	1.4 1.4	1.4
2Si-1Cr-0.9C 665 °C, 5 min. (93% reduction)	0 1.1 1.0 0.8		1.1 0 0.2	

7.2.2 Transmis ion electron microscopy

Thin foils were prepared from different samples subjected to ageing trials. There were no apparent differences between the microstructures observed in the "aged" samples

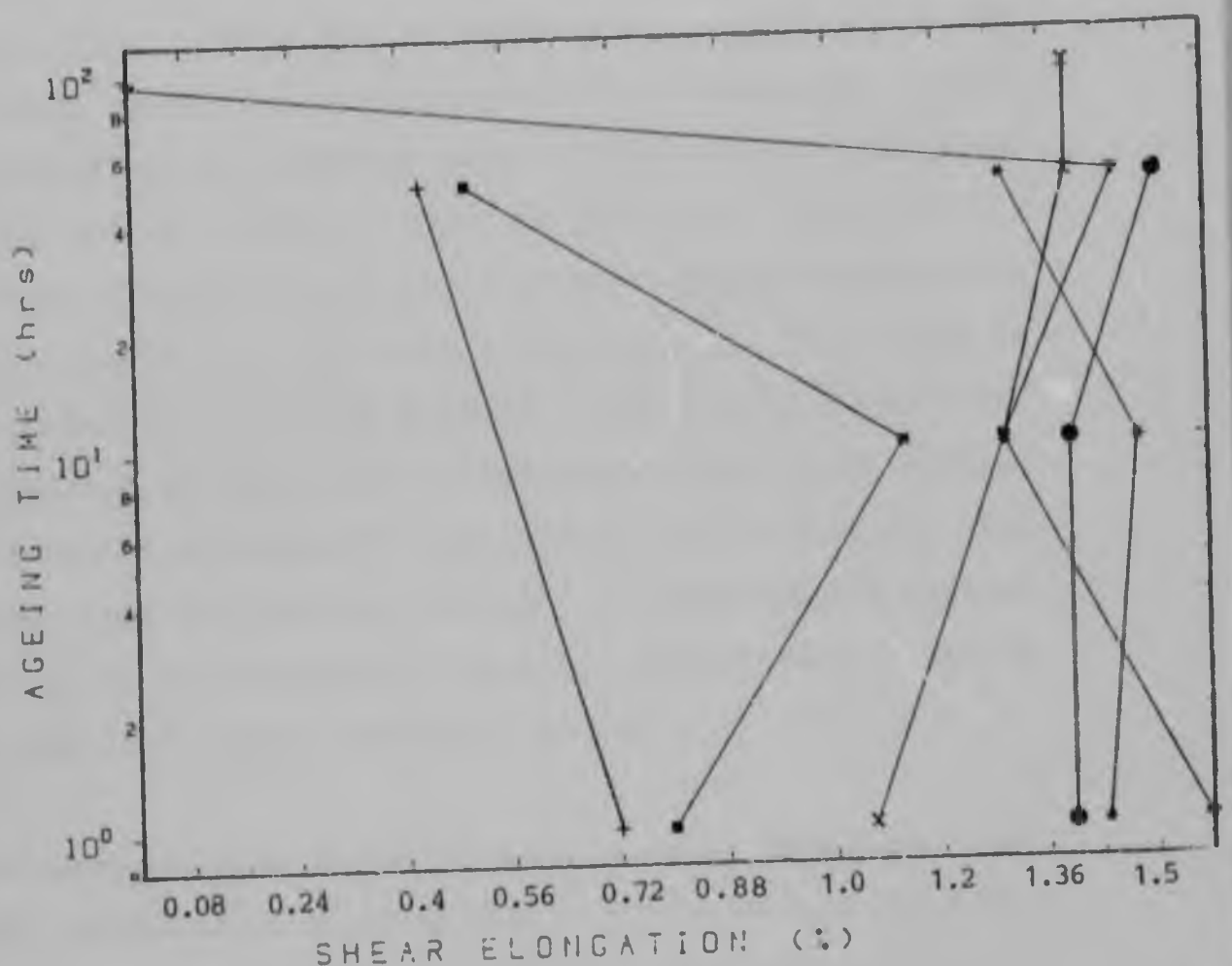

1.7Si-1Cr	/ 92% *
1.7Si-1Cr	/ 93% *
2Si-1Cr	/ 90% *
2Si-1Cr	/ 92% *
2Si-1Cr	/ 93% *
2Si-1Cr-.9C/	93%

*all 0.8%C

Figure 7.1 Shear elongation as a function of the ageing time at 50 °C and the total reduction

(Figure 7.2) and those seen in the as-drawn material (Figure 5.31). There was no evidence of precipitation even at high magnifications (X160,000). However, some structural changes were apparent in plain-carbon wire after ageing for one week at 50°C (Figure 7.3). The ferrite exhibits a distinct equiaxed cellular substructure which was not observed in the as-drawn material. This could be indicative of a recovery process. Although this would not be expected at such a low temperature, sufficient driving force could possibly be supplied by the extremely high deformations employed in drawing. It does suggest however that in the early stages of ageing, the dislocations are in fact mobile in order to achieve recovery.

An attempt was made to precipitate carbides in a commercial plain carbon steel wire by heat treating samples at 200°C for 15 minutes. 2Si-1Cr samples were also given a similar treatment. Although the shear values measured for the plain carbon steel after ageing were zero, no unusual features were identified.

7.3 Further Discussion

The shear values measured after the ageing trials appear generally to be acceptable in terms of the ductility of the wires. It seems that the shear ductility of the wires with larger diameter is low compared with finer wires. The reason for this could be that the ductility of the wires

(a)

0.05μm

(b)

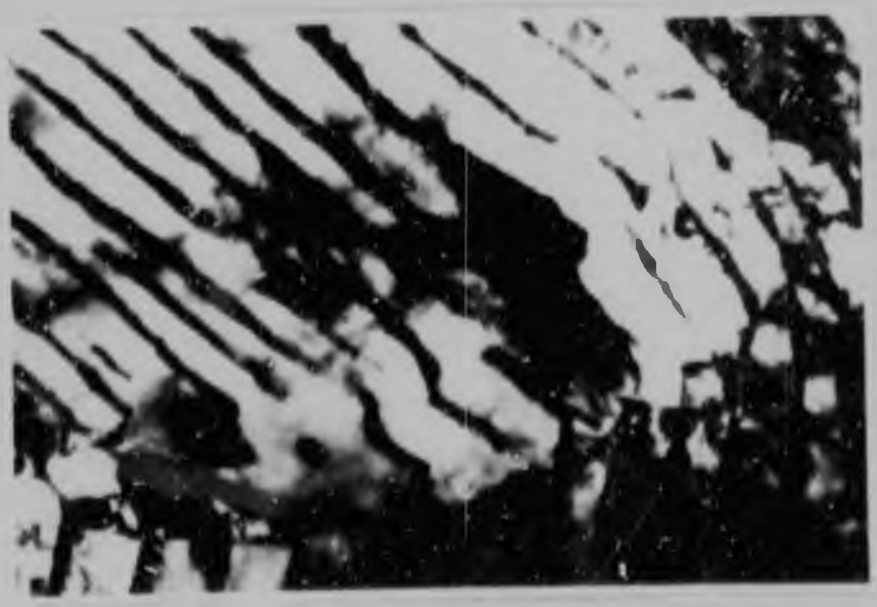

0.05μm

Figure 7.2 TEM micrographs of samples submitted to ageing trials
(a) 2Si-1Cr
(b) Plain carbon steel

0.1μm

0.1μm

Figure 7.3 Equiaxed structure in a plain carbon steel after ageing for one week at 50 °C (TEM micrographs)

increases with drawing reduction, as suggested by White (1983).

Transmission electron microscopy observations on the wires did not show any precipitation of carbides as a result of the ageing heat treatment. This may be due to a number of reasons, some of which are listed below:

i) The time (96 hours) at 50°C, may be insufficient to produce observable microscopic changes.

ii) Similarly, the time (15 minutes) at 200°C may not be enough.

iii) The alloy steel may "not age", possibly due to the presence of silicon (Leslie (1961), Ochiani et al (1983)).

iv) The loss of ductility on ageing may be caused by features too small to be detected using electron microscopy. (For example, dislocations could be pinned by Cottrell atmospheres of carbon atoms).

In relation to item iv), other investigative techniques should be considered. Another method of studying the ageing of heavily drawn wires is field ion microscopy. Although this has been used by Waugh et al (1981), G.D.W. Smith (1983) dismisses this approach by explaining that dislocation configurations will relax during the process of

preparing field ion specimens. Further changes in configuration will take place when the electric field is applied to produce the image, since there is a mechanical stress associated with the field, leading to slip deformation during the imaging process, and pinning of all the mobile dislocations.

G.D.W. Smith (1983) suggested that the high level of deformation present in a heavily drawn wire presumably aids the migration of carbon atoms. The presence of both point and line defects in both the ferrite and cementite phases will enhance carbon migration, and the refinement of the interlamellar spacing will cut down the distance over which carbon atoms have to move in order to effectively pin all the mobile dislocations. According to G.D.W. Smith the only effective way to reduce the seriousness of this effect is to attempt to inhibit the mobility of carbon.

A remedial action that may be taken during wire manufacture is restricting the reduction of area and applying additional wire cooling on the wire drawing machines.

CHAPTER EIGHT - CONCLUSIONS

The findings of this investigation may be summarised as follows:

1. The addition of chromium, manganese and silicon to eutectoid carbon steels shifted the TTT diagrams to longer incubation times and to higher transformation temperatures. Additions of silicon appear potentially useful in inhibiting pro-eutectoid cementite formation, as well as in direct strengthening.

2. Alloying also increased strength. In the Cr-Mn alloy series, the 1Cr-1Mn produced the highest as-patented and drawn strengths: 1360MPa and 2461MPa respectively.

   In the Si-containing alloys, the addition of 1% chromium to the 2Si-1Mn composition resulted in a remarkable increase in as-patented strength (to ≈1600 MPa) but with very poor ductility. The 2Si-1Cr-0.8C alloy gave the highest as-patented strength, 1375MPa (with sufficient ductility) and produced wire with strength in excess of the 2500MPa goal: 2580MPa. This was achieved with the retention of adequate

remaining ductility, indicated by good shear and torsion test results.

The major strengthening mechanism was the refinement of the pearlite interlamellar spacing. Increasing silicon levels had the general effect of increasing the optimum isothermal transformation temperature at which fine pearlite was formed. However, ncreased strengths through increases in work hardening rate were observed in some alloys: 410MPa/unit strain in the 1Cr-1Mn alloy and 440MPa/unit strain in the 2Si-1Cr-0.8 alloy.

3. Strength was also influenced strongly by carbon content. A 2Si-1Cr-0.9C alloy developed a drawn strength of 2650MPa, with a work hardening rate of 458MPa/unit strain.

   Reducing the carbon content below 0.8% resulted in inferior strengths, partially due to increased degeneracy of the pearlitic structure.

4. Increased degeneracy of the pearlite was found in the alloys 2Si-1Mn and 2Si-1Cr-1Mn.

5. Silicon-containing steels were found to exhibit spheroidisation of the pearlitic cementite after

relatively short times at high temperatures, close to the transformation temperatures employed.

6. Heat treatment also influenced the microstructures and properties obtained.

Austenitising time and temperature were found to have a large effect on as-patented strength and structure.

Continuously stirred molten lead has proved to be the best available quenching medium. However, initial agitation of the samples is recommended to minimise recalescence. Since small temperature changes markedly affect resultant properties, close temperature control is mandatory.

7. The conditions during wire drawing also have a profound effect on mechanical properties. Heating of the wire can result in an ageing phenomenon, resulting in high strength but poor ductility. Additions of 2% silicon reduced the susceptibility to ageing, except with the high (0.9%) carbon content.

8. The most promising high purity composition (2Si-1Cr) was also prepared using a commercial eutectoid steel base. High strengths were obtained but with poor ductility. This may be explained in terms of the

manganese content and the increased impurity level. The rapid ageing effect during drawing may be due to the high nitrogen and phosphorus contents.

9. The 2Si-1Cr-0.8C steel appears to offer the best current composition for commercial exploitation. However, several factors must be considered.

In the laboratory, there were considerable yield losses due to primary pipe formation in the ingots. Commercial production would therefore require special casting techniques, such as the use of exothermic hot tops on ingot moulds.

Purity also markedly affects properties. It would be beneficial therefore to produce "cleaner" steel commercially. This could be accomplished using techniques such as vacuum degassing or electroslag refining to reduce phosphorus, sulphur and nitrogen contents and minimise non-metallic inclusions. This will improve drawability.

CHAPTER NINE - SUGGESTIONS FOR FURTHER WORK

The results obtained from this study of Si-Cr-Mn steels appear most encouraging. However, further work is required in order to optimise alloy composition and properties. Some suggestions are presented below.

1. In future work, attention must be given to the application of a homogenisation heat treatment. Austenite inhomogeneity (in terms of both alloying elements and carbon) will markedly affect pearlite nucleation, distribution and in particular interlamellar spacing. This must be eliminated in order to obtain the ideal fine uniform pearlite for subsequent drawing.

   A soak of one hour or more at 1200-1250°C should be sufficient to achieve at least uniformity of carbon concentration. A suitable grain size can be restored through proper selection of a re-austenitising heat treatment.

2. Compared with the 2Si-1Cr alloy, the 2Si-1Cr-1Mn composition exhibited high strength but lower ductility (with an inferior microstructure). The commercial 2Si-1Cr alloy, containing 0.7%Mn, also had high strength, an improved structure and intermediate ductility.

CHAPTER NINE - SUGGESTIONS FOR FURTHER WORK

The results obtained from this study of Si-Cr-Mn steels appear most encouraging. However, further work is required in order to optimise alloy composition and properties. Some suggestions are presented below.

1. In future work, attention must be given to the application of a homogenisation heat treatment. Austenite inhomogeneity (in terms of both alloying elements and carbon) will markedly affect pearlite nucleation, distribution and in particular interlamellar spacing. This must be eliminated in order to obtain the ideal fine uniform pearlite for subsequent drawing.

   A soak of one hour or more at 1200-1250°C should be sufficient to achieve at least uniformity of carbon concentration. A suitable grain size can be restored through proper selection of a re-austenitising heat treatment.

2. Compared with the 2Si-1Cr alloy, the 2Si-1Cr-1Mn composition exhibited high strength but lower ductility (with an inferior microstructure). The commercial 2Si-1Cr alloy, containing 0.7%Mn, also had high strength, an improved structure and intermediate ductility.

Further work is required therefore to determine an optimum manganese content or silicon:manganese ratio. In the first instance, alloys based on 2(Si+Mn)-Cr should be studied. This investigation could include a re-assessment of the 1Si-1Cr-1Mn alloy which, due to defect problems, gave unreliable results in the present study.

3. Drawability and susceptibility to ageing appear to be strongly dependent on the cleanliness, purity and freedom of defects of the steel. It is suggested therefore that all future studies, both laboratory and industrial, should employ the highest purity material possible.

4. Wire drawing conditions must also be optimised and carefully controlled. Factors to be considered are wire drawing lubrication, speed of drawing, die design and reduction per die. A separate study should be made regarding the detailed influence of interpass cooling on drawn properties and susceptibility to ageing.

5. In order to increase our understanding of the fundamental effects of alloying additions on the strength of pearlite, further detailed studies are required on, for example, partitioning of solutes

between ferrite and cementite and segregation to the growth interface. This may require advanced experimental techniques, such as STEM/EDS and FIM/atom probe.

6. A detailed study must also be made of ageing in UHT wires. The mechanism of loss of ductility must be identified, so that the problem can be overcome through alloying or modification of production conditions.

7. It is still not clear whether bainite is always deleterious to the properties of drawn wires. It would be useful therefore to investigate the drawability of a fully bainitic microstructure in one of the existing experimental alloys (possibly the 2Si-1Cr-0.8C).

8. Future alloy development studies should be extended to include the evaluation of properties other than tensile strength and ductility. These should include weldability and fatigue properties, and possibly stress corrosion cracking and fracture toughness.

REFERENCES

Aaronson, H.I. (1954) Ph.D. Thesis. Carnegie Institute of Technology, Pittsburgh, Pennsylvania, U.S.A.

Aaronson, H.I., Domian H.A. and Pound, G.M. (1966). Transactions Metallurgical Society AIME, vol. 236, p. 781.

Aernoudt, E. and Sevillano J.G. (1973). Influence of the mode of deformation on the hardening of ferrite and pearlitic carbon steels at large strains. Journal of Iron and Steel Institute (Oct), p. 718.

Agarwal, P.K. and Brimacombe, J.K. (1981). Mathematical model of heat flow and austenite-pearlite transformation in eutectoid carbon steel rods for wire. Metallurgical Transactions, vol. 12B, p. 121.

Alekseyev, L.A., Levi, R.B., Kogan, L.I., Matroknina, E.F. and Entin R.I. (1979). Concerning the incubation period of the pearlite transformation. Physics of Metals & Metallography, vol. 47, no. 5, p. 1005.

Allan, N.P., Rees, W.P., Hopkins, B.E. and Tipler, H.R. (1953). Journal of Iron and Steel Institute, vol. 174, p. 108.

Al-Salman, S.A., Lorimer, G.W. and Ridley, N. (1979a). Pearlite growth kinetics and partitioning in a Cr-Mn eutectoid steel. Metallurgical Transactions A, vol. 10A, p. 1703.

Al-Salman, S.A. Lorimer, G.W. and Ridley, N. (1979b). Partitioning of silicon during pearlite growth in a eutectoid steel, Acta Metallurgica, vol. 27, p. 1391.

Al-Salman, S.A., Cliff, G., Lorimer, G.W. and Ridley, N. (1979c). Solute partitioning in pearlite. Proc. Conf. Microanalysis in the transmission electron microscope. Manchester, August 1979, U.K.

Armstrong, R. and Sturgeon G.M. (1965). Wire Industry, vol. 32, p. 73.

Asundi, M.K. and West, D.R.F. (1966a). The kinetics of pearlite growth in ternary aluminium bronzes containing zinc or tin. Journal of Iron and Steel Institute, vol. 94, p. 327.

Asundi, M.K. and West, D.R.F (1966b). The kinetics of pearlite growth in binary aluminium bronzes. Journal of Iron and Steel Institute, vol. 94, p. 19.

Avitzur, B. (1983) Handbook of metal forming processes. John Wiley & Sons N.Y., p. 99.

Baan, M., Roosz, A. and Gacsi, Z. (1977). Determination of the true interlamellar spacing in pearlite. Kohaszat at, Vol 110, p. 391. (in Hungarian).

Barnby, J.T. and Johnson, M.R. (1969). Fracture in pearlitic steels. Metals Science Journal, vol. 3, p. 155.

Belaiew, N.T. (1922). The inner structure of the pearlite grain. Journal of Iron and Steel Institute, vol. 1, p. 201.

Bernstein, I.M., Park, Y.J., Bouse, G.K. and Hyzak, J.M. (1976). Microstructural control of cleavage fracture in pearlitic steels. 4th Int. Conf. in Strength of metals and alloys, vol. 2, p. 587.

Billington, J.C., Foden, J., Slater, I.G. and Russell, R.B. (1981). Preparation of hot rolled carbon rod for cold working. Wire Industry (Oct), p. 729.

Bolling, G.F. and Richman, R.H. (1970). Forced velocity pearlite. Metallurgical Transactions, vol. 1, p. 2095.

Bolze, G., Puls, M.P. and Kirkaldy, J.S. (1972). Contribution to the theory of eutectoid and eutectic transformations. Acta Metallurgica, vol. 20, p. 73.

Bouse, G.K., Bernstein, I.H. and Stone, D.H. (1978). Role of alloying and microstructure on the strength and toughness of experimental rail steels. ASTM STP 644. Rail steels development processing and use, p. 145.

Bramfitt, B.L. and Marder, A.R. (1973). Effect of cooling rate and alloying on the transformation of austenite. Metallurgical Transactions, vol. 4, p. 2291.

Brandal, S. and Valberg, H. (1982). Analysis of the deformation process during wiredrawing by means of the finite element method. Wire Journal International, March, p. 64.

Brandt, W.H. (1945). Journal of Applied Physics, vol. 16, p. 139.

Brown, D. and Ridley, N. (1966). Rates of nucleation and growth and interlamellar spacing of pearlite in a low alloy eutectoid steel, Journal of Iron and Steel Irstitute, Aug., p. 811.

Brown, D. and Ridley, N. (1969). Kinetics of the pearlite reaction in high-purity nickel eutectoid steels, Journal of Iron and Steel Institute, Sept. p. 1232.

Butcher, B.R. and Pettit, H.R. (1966). Tensile deformation and cracking of plain high carbon steels containing pearlite, Journal of Iron and Steel Institute, May, p. 469.

Cahill, T. and James, B.A. (1968a). Effect of patenting variables on the structure and properties of patented rods. Continuous Heat Treatment of Wire. Iron and Steel Institute publication 113, p. 3.

Cahill, T. and James, B.A. (1968b). The effect of patenting variables on the structure and properties of patented rod. Wire and Wire Products, Feb , p. 64.

Cahn, J.W. (1959). Acta Metallurgica, vol. 7, p. 18.

Cahn, J.W. (1962). Acta Metallurgica, vol. 10, p. 789.

Cahn, J.W. and Fullman, R.L. (1956). On the use of lineal analysis for obtaining particle size distribution functions in opaque samples. Transactions AIME Journal of Metals, May, p. 610.

Cahn, J.W. and Hagel, W.C. (1962). Theory of the pearlite reaction. The decomposition of austenite by diffusional processes. (eds Zackay and Aaronson). Intersience, John Wiley, N.Y., p. 131.

Cahn, J.W. and Hagel, W.C. (1963). Divergent pearlite in a manganese eutectoid steel. Acta Metallurgica, vol. 11, p. 561.

Capus, J.M. and Mayer, G. (1960). Journal of Iron and Steel Institute, vol. 196, p. 149.

Chadwick, G.A. and Edmonds, D.V. (1973). Unidirectional growth of pearlite in steels. Proc. Int. Symp. on Chemical Metallurgy of Iron and Steel, p. 264.

Chance, J. and Ridley, N. (1978). Pearlite formation in a eutectoid steel containing 0.3%Mo. Modern Metallog. Conf. & Exhibition. Birmingham, U.K., p. 36.

Chance, J. and Ridley, N. (1981). Chromium partitioning during isothermal transformation of a eutectoid steel. Metallurgical Transactions A, Vol 12A, p. 1905.

Chandhok, U.K., Kasak, A. and Hirth, J.P. (1966). Structures and Strengthening mechanism in carbon steel wire. Transactions ASM, vol. 59, p. 288.

Chattopadhyay, S. and Sellars, C.M. (1977). Quantitative measure of pearlite spheroidisation. Metallography, vol. 10, p. 89.

Cheetham, D. and Ridley, N. (1973). Isovelocity and isothermal pearlite growth in a eutectoid steel. Journal of Iron and Steel Institute, vol. 211, p. 648.

Cheetham, D. and Ridley, N. (1975). Pearlite interlamellar spacing and morphologies in hypo-eutectoid steels. Metal Science, vol. 9, p. 411.

Coates, D.E. (1973). Diffusional growth limitations and hardenability, Metallurgical Transactions, vol. 4, p. 2313.

Cockett, G.H. and Davis, C.D. (1963). The lattice expansion of Fe-Si alloys and the volume change at the A_3 point, Journal of Iron and Steel Institute, vol. 201, p. 110.

Cordon, B.W., Timiney, P., Mottishaw, T.D. and Smith, G.D.W. (1983). Development of microalloyed pearlitic steels for wire drawing applications. Develop. in the drawing of metals. The Metal Society, London, May.

Cottrell, A.H. (1953). Dislocations and plastic flow in crystals. Int. Series of monographs in physics. Claredon Press, Oxford, p. 147.

Cottrell, C.L.M. and Turner, M.J. (1962). Journal of Iron and Steel Institute, vol. 200, p. 380.

Cottrell, C.L.M. (1963). Hydrogen in steel. Iron and Steel Institute, special report 73, p. 33.

Cottrell, C.L.M., Langstone, P.F. and Rendall, J.H. (1963). Improved properties of extra high purity steel at tensile strengths up to 150 tons per square inch. Journal of Iron and Steel Institute, vol. 201, p. 1032.

Davy, L.G.T. and Glover, S.G. (1968). Ferrite-Pearlite structures : The role of interfacial energy. The Journal of the Australian Institute of Metals, vol. 13, no. 2, p. 71.

De Hoff, R.T. and Rhines, F.N. (1968). Quantitative Microscopy. Materials Science and Engineering Series. McGraw Hill N.Y., pp. 99-167.

Demeyere, E.G. (1981). Influence of non-metallic inclusions in high and low carbon wire rod on workability during wire drawing and on mechanical properties of products. Wire Journal, vol. 14, no. 1, p. 72.

Dewey, M.A.P. and Bries G.W. (1966). Structure of heavily cold drawn eutectoid steel. Journal of Iron and Steel Institute, Feb. p. 102.

Digges, T.G. (1938). Transactions ASM, vol. 26, p. 408.

Dippenaar, R.J. and Honeycombe, R.W.K. (1973). The crystallography and nucleation of pearlite. Proceedings Royal Society of London A, vol. 333, p. 455.

Edwards, L., Miller, M.K., Williams, P.R. and Smith, G.D.W. (1979). Investigation of the relationship between carbon and sulphur segregation on the drawability of high carbon steel rod. Wire Journal, Dec, p 68.

Embury, J.D. and Fisher, R.M. (1966). The structure and properties of drawn pearlite. Acta Metallurgica, vol. 14, p. 147.

Embury, J.D., Keh, A.S. and Fisher, R.M. (1966). Substructural strengthening in materials subject to large plastic strains. Transactions AIME, vol. 236, p. 1252.

Embury, J.D. (1971). Strengthening methods in crystals. Applied Science Publ. (ed. A. Kelly and R.B. Nicholson), p. 331.

Evsyukov, M.F. and Pritomanova, M.I. (1975). Effect of dendrite segregation of manganese on growth rate of pearlite. Metal Science and Heat Treat., vol. 17, p. 381.

Fletcher, F.B. (1978). Development of high strength chromium-molybdenum rail steel with improved weldability. Climax Molybdenum Co. of Michigan, U.S.A.

Franklin, J.R. and Allen, C. (1980). The patenting of steel rod and wire. Wire Industry, p. 958.

Franklin, J.R., Preston, R.R. and Allen, C. (1980) Heat treatment and alloying of drawn wires. Wire Industry, p. 967.

Garratt-Reed, J. and Mottishaw, T.D. (1983). First observations of solute redistribution at the pearlite growth front in alloy steels. Electron Microscopy and Analysis. Institute of Physics, London.

Gensamer, M., Persall, E.B. and Smith, G.V. (1940). The mechanical properties of the isothermal decomposition products of austenite. Transactions ASM, vol. 28, p. 340.

Gensamer, M., Persall, E.B., Pellini, W.S. and Low, J.R. jr. (1942). The tensile properties of pearlite, bainite and spheroidite. Transactions ASM, vol. 30, p. 983.

Gladman, T., Holmes, B. and Pickering, F.B. (1970). Work hardening of low carbon steels. Journal of Iron and Steel Institute, vol. 208, p. 172.

Gladman, T., McIvor, I.D. and Pickering, F.B. (1972). Some aspects of the structure-properties relationship in high carbon ferrite-pearlite steels, Journal of Iron and Steel Institute, Dec, p. 916.

Grange, R.A. (1947). Transactions ASM, vol. 35, p. 879.

Gregory, B., Hall, H.T. and Bullock, G. (1961). Transactions ASM, vol. 54, p. 106.

Guerrieri, A., Mascanzoni, A. and Mazzucato, F. (1983). Properties of controlled cooled high carbon steels for prestressed concrete wire. Wire Industry, June, p. 313.

Guiva, R.T., Leuchenko, A.A. and Tanako, I.I. (1978). Structure formation in high carbon steels. Steel in the USSR, vol. 8, no. 9, p. 529.

Hahn, G.T. et al (1962). Journal of Iron and Steel Institute, vol. 200, p. 234.

Hahn, J.H. and Okumuva, H.Y. (1983). Austenitising temperature effect on the isothermal transformation of A-6150 steel. Wire Journal International, Feb, p. 58.

Garratt-Reed, J. and Mottishaw, T.D. (1983). First observations of solute redistribution at the pearlite growth front in alloy steels. Electron Microscopy and Analysis. Institute of Physics, London.

Gensamer, M., Persall, E.B. and Smith, G.V. (1940). The mechanical properties of the isothermal decomposition products of austenite. Transactions ASM, vol. 28, p. 340.

Gensamer, M., Persall, E.B., Pellini, W.S. and Low, J.R. jr. (1942). The tensile properties of pearlite, bainite and spheroidite. Transactions ASM, vol. 30, p. 983.

Gladman, T., Holmes, B. and Pickering, F.B. (1970). Work hardening of low carbon steels. Journal of Iron and Steel Institute, vol. 208, p. 172.

Gladman, T., McIvor, I.D. and Pickering, F.B. (1972). Some aspects of the structure-properties relationship in high carbon ferrite-pearlite steels, Journal of Iron and Steel Institute, Dec, p. 916.

Grange, R.A. (1947). Transactions ASM, vol. 35, p. 879.

Gregory, B., Hall, H.T. and Bullock, G. (1961). Transactions ASM, vol. 54, p. 106.

Guerrieri, A., Mascanzoni, A. and Mazzucato, F. (1983). Properties of controlled cooled high carbon steels for prestressed concrete wire. Wire Industry, June, p. 313.

Guiva, R.T., Leuchenko, A.A. and Tanako, I.I. (1978). Structure formation in high carbon steels. Steel in the USSR, vol. 8, no. 9, p. 529.

Hahn, G.T. et al (1962). Journal of Iron and Steel Institute, vol. 200, p. 234.

Hahn, J.H. and Okumuva, H.Y. (1983). Austenitising temperature effect on the isothermal transformation of A-6150 steel. Wire Journal International, Feb, p. 56.

Harris, R. and McCann, J. (1968). High temperature decomposition of austenite. Conference Report. Journal of Iron and Steel Institute, May, p. 502.

Hawbolt, E.B., Chaw, B. and Brimacombe, J.K., (1983). Kinetics of the austenite-pearlite transformation in eutectoid carbon steel. Metallurgical Transactions A, vol. 14A, p. 1803.

Heckel, R.W. and Paxton, H.W. (1960). Rates of growth of cementite in hypereutectoid steels. Transactions AIME, vol. 218, p. 77.

Henry, R.J. (1970). The effect of strain rate on pearlite morphology and microcracking. Metallurgical Transactions, vol. 1, p. 1073.

Hillert, M. (1957). Jernkont Ann, vol. 141, p. 757.

Hillert, M. (1962). The formation of pearlite. The Decomposition of Austenite by Diffusional Processes. Interscience (ed. Zackay & Aaronson), p. 197.

Hillert, M. (1968). The role of interfaces in phase transformations. Proc. of an Int. Symp. on the Mechanism of Phase Transformations in Crystalline Solids. Monograph and Report Series, vol. 33, p. 231.

Hillert, M. and Sundman, B. (1976). A treatment of the solute drag on moving grain boundaries and phase interfaces in binary alloys, Acta metallurgica, vol. 24, p. 731.

Hillnhagen, E. and Schauf, E. (1980). Two surface analyses of polished sections on the scanning Electron Microscope. Practical Metallography, vol. 17, p. 29.

Honeycombe, R.W.K. (1981). Steels, Microstructure and Properties. Edward Arnold (publishers) Ltd. London.

Hugo, J.P. and Woodhead, J.H. (1957). Correlation of tensile properties with microstructure for some 3% Ni steels. Journal of Iron and Steel Institute, June, p. 174.

Hull, F.C., Colton, R.A. and Mehl, R.F. (1942). Rate of formation and rate of growth of pearlite. Transactions A.I.M.E., vol. 150, p. 185.

Hultgren, A. (1951). Jernkon. Ann., vol. 153, p. 403.

Hyzak, J.M. and Bernstein, I.M. (1976). The role of microstructure on the strength and toughness of a fully pearlitic steel, Metallurgical Transaction A, vol. 7A, p. 1217.

Jatczak, C.F. (1973). Hadenability in high carbon steels. Metallurgical Transactions, vol. 4, p. 2267.

Karlsson, B. and Linden, G. (1975). Plastic deformation of eutectoid steel with different cementite morphology. Materials Science and Engineering, vol. 17, p. 153.

Kennon, N.F. and Kaye, N.A. (1982). Isothermal transformation of austenite to pearlite and upper-bainite in eutectoid steels. Metallurgical Transactions A, vol. 13A, p. 975.

Korzekwa, D.A., Matlock, D.K. and Krauss, G. (1982). Ageing susceptibility of retained and epitaxial ferrite in dual-phase steels. Metallurgical Transactions A, vol. 13A, p. 2061.

Krauss, G. (1980). Principles of Heat Treatment of Steel. ASM.

Kristhal, M.A. (1970). Diffusion Processes in Iron Alloys. Translated from Russian by A. Wald and J.J. Becker. Israel Program for Scientific Translations, Jerusalem.

Langford, G. (1977). A study of the deformation of patented steel wire. Metallurgical Transactions, vol. 1, p. 465.

Langford, G. (1970). Deformation of pearlite. Metallurgical Transactions, vol. 8A, p. 861.

Lenasson, C.G. and Bergtröm, Y. (1976). On the plastic deformation of pearlite in uniaxial straining and wire drawing. 4th Int. Conf. on Strength of Metals and Alloys, vol. 1, p. 141.

Leslie, W.C. (1961). The quench ageing of low carbon iron and iron manganese alloys. An electron microscopy study. Acta Metallurgica, vol. 9, p. 1004.

Lewis, M. and Ward, C. (1978). The effect of small additions of vanadium on pearlitic steels. Modern Metallography Conference and Exhibition. Birmingham U.K. (Sept), p. 37.

Lindborg, V. (1968). Morphology of fracture in pearlite. Transactions ASM, vol. 61, p. 500.

Liska, L.A. (1980). Contribution towards solving the problems of high speed drawings. Wire Journal, Feb. p. 81.

Lücke, K. and Stüwe, H. (1971). On the theory of impurity controlled grain boundary motion, vol. 19, p. 1087.

Malik, H.I. (1979). Effect of alloy addition on the interlamellar spacing of pearlite. Arch Eisenhüttenwes, vol. 50, no. 10, p. 449.

Marder, A.R. and Branfitt, B.L. (1975). Effect of continuous cooling on the morphology and kinetics of pearlite. Metallurgical Transactions A. Vol. 6A, p. 2009.

Marder, A.R. and Bramfitt, B.L. (1976). The effect of morphology on the strength of pearlite. Metallurgical Transactions, vol. 7A, p. 365.

Marich, S. and Curcio, P. (1978). Development of high strength alloyed rail steel suitable for heavy duty applications. ASTM STP 664, Rail steel development and use, p. 167.

Mazzucato, F., Mascanzoni, A. and Guerrieri, A. (1981). Prestressing drawn products from control cooled wire rods manufactured from continuously cast steel. Wire Association, 4th European Regional Meeting, Lake Como, Italy.

Mehl, R.F. and Hagel, W.C. (1956). The austenite-pearlite reaction. Progress in Metal Physics, vol. 6, p. 74.

Mellor, B.G. and Chadwick, G.A. (1974). The unidirectional growth of copper-iridium eutectoid alloy. Metals Science, vol. 8, p. 65.

Mellor, B.G. and Edmonds, D.V. (1977). Unidirectional transformation of Fe-0.8C-Co alloys. Part I. Process per structure relationship and the significance of pearlite interlamellar spacing measurements. Metallurgical Transactions A, vol. 8A, p. 763.

Metals Handbook (1978). A.S.M., vol. 1, 9th edition, p. 115.

Miller, L.E. and Smith, G.C. (1970). Tensile fracture in carbon steels, Journal of Iron and Steel Institute, vol. 208. p. 998.

Miller, M.K. and Smith, G.D.W. (1977). Atom probe microanalysis of a pearlite steel. Metal Science, July, p. 249.

Miller, M.K., Beaven, P.A., Lewis, R.J. and Smith, G.D.W. (1978). Atom probe microanalysis studies of some commercially important steels. Surface Science, vol. 70, p. 470.

Morgan, R. and Ralph, B. (1968). A field ion microscopy study of pearlite. Journal of Iron and Steel Institute, vol. 206, p. 1138.

Mottishaw, T.D. (1984). Effects of alloying additions on the properties of pearlitic steels. D. Phil. Thesis, Oxford University.

Mottishaw, T.D. and Smith, G.D.W. (1983). Microalloyed pearlitic steels for the wire industry. Mechanisms of alloy element redistribution and strengthening in chromium-vanadium eutectoid steels. Proc. of Int. Conf. on Technology and Applications of High Strength Low Alloy Steels. Philadelphia.

McIvor, I.D. (1973). Effect of high manganese content on interlamellar spacing of isothermally transformed pearlite. Proc. Int. Symp. on Chemical Metallurgy of Iron and Steel, p. 272.

Nakamura, Y. and Fujii, S. (1974). Wire Journal, p. 73.

Nicholson, M.E. (1954). Journal of Metals (AIMM) Eng., p. 1071.

Nishimura, T., Fujiwara, T. and Tamaka, Y. (1980). Some aspects of drawing high carbon steel wire for prestressed concrete strand. Wire Journal, p. 64.

Ochiani, I., Nagumo, M., Amakawa, T. and Takahashi, T. (1983). Direct patented high strength steel wire rod strengthened by silicon. Wire Journal International, p. 72.

Ohmori, Y., Davenport, A.T. and Honeycombe, R.W.K. (1972). Transactions Iron and Steel Institute of Japan, vol. 12, p. 128.

Parcel, R.W. and Mehl, R.F. (1952). Transactions AIME, vol. 194, p. 771.

Park, Y.J. and Bernstein, I.M. (1977). Effective grain size for cleavege fracture in pearlite eutectoid steel. Fracture 1977, 2, ICF4, Waterloo, Canada, June 19-24, p. 33.

Park, Y.J. and Bernstein, I.M. (1979). The process of crack initiation and effective grain size for cleavege fracture in pearlitic eutectoid steel. Metallurgical Transactions A, Vol. 10A, p. 1653.

Parsons, D.E., Malis, T.F. and Boyd, J.D. (1983). Microalloying and precipitation in Cr-V rail steels. Proc. Int. Conf. on Technology and Applications of High Strength Low Alloy Steel. Philadelphia.

Parusov, V.V., Dolzhenkov, I.I. and Evsyukov, M.F. (1978). An investigation of the transformation kinetics of supercooled austenite into globular pearlite. Russian Metallurgy, vol. 3, p. 102.

Patent No. 1404796. Nippon Steel Coorporation.

Pawelski, O. and Keuper, R. (1984). Investigation of direct cooling in drawing steel wire. Wire Journal International, Jan., p. 86.

Payne, D. and Smith, B.F. Fundamentals of the patenting process. Unpublished report. British Ropes Ltd.

Payne, D. and Smith, B.F. (1968). Transformation of steel during patenting. Continuous Heat Treatment of Wire. ISI publication, vol. 113, p. 28.

Pellisier, G.E., Hawkes, M.F., Johnson, W.A. and Mehl, R.F. (1942). The interlamellar spacing of pearlite. Transactions ASM, vol. 30, p. 1049.

Pepe, J.J. (1973). Deformation structure and the tensile fracture characteristic of a cold worked 1080 pearlitic steel. Metallurgical Transactions, vol. 4, p. 2455.

Pesche, F., Hollande, M., Le Quere, J.L. and Tassin, S. (1982). Improving the characteristics and performance of high carbon wire rod. Wire Journal International, p. 87.

Pickering, F.B. (1965). Iron and Steel, March-April.

Pickering, F.B. (1978). Physical Metallurgy and the Design of Steels. Applied Science Publishers, London, p. 148.

Pickle:imer, M.L., McElroy, D.L., Kegley, T.M. jr., Stansburg, E.E. and Frye, J.H. jr. (1960). Effect of manganese on the austenite-pearlite transformation. Transactions of the Metallurgical Society of AIME, vol. 218, p. 473.

Pitsch, W. (1962). Acta Metallurgica, vol. 10, p. 79.

Porter, D.A. and Easterling, K.E. (1978). Dynamic studies of the tensile deformation and fracture of pearlite using high resolution 200kv SEM. Scandinavian Journal of metallurgy, p. 55.

Porter, D.A., Easterling, K.E. and Smith, G.D.W. (1978a). Dynamic studies of the tensile deformation and fracture of pearlite. Acta Metallurgica, vol. 126, p. 1405.

Porter, D.E., Easterling, K.E. and Smith, G.D.W. (1979). The mechanism of deformation of pearlite. Interdisciplinary Symp. on the Mechanism of Deformation on Fracture. University of Lulea, Sept. 1978, Pergamon Press.

Puls, M.P. and Kirkaldy, J.S. (1972). The pearlite reaction. Metallurgical Transactions, vol. 8, Nov., p. 2777.

Purdy, G.R., Weichert, D.H. and Kirkaldy, J.S. (1964). Transactions TMS - AIME, vol. 230, p. 1025.

Puttick, K.E. (1957). Journal of Iron and Steel Institute, vol. 185, p. 161.

Querales, A. and Byrne, J.G. (1980). Effect of thermomechanical treatment on the mechanical behaviour of eutectoid steel. Metallurgical transactions A, vol. 11A, p. 255.

Razik, N.A., Lorimer, G.W. and Ridley, N. (1974). An investigation of manganese partitioning during the austenite-pearlite transformation using analytical electron microscopy. Acta Metallurgica, vol. 22, p. 1249.

Razik, N.A., Lorimer, G.W. and Ridley, N. (1976). Chromium partitioning during the austenite-pearlite transformation. Metallurgical Transactions A, vol. 7A, p. 209.

Reed-Hill, R.E. (1964). Physical Metallurgy Principles. University Series in Physical Metallurgy. D. van Nostrand, N.Y., p. 739.

Ridley, N. (1976). Effect of alloy additions on pearlite growth kinetics. Heat Treatment 76. Proc. of the 16th Int. Heat Treat. Conf. Stratford upon Avon, 6-7 May p. 14.

Ridley, N. (1984). A Review of the data on the interlamellar spacing of pearlite. Metallurgical Transactions, vol. 15A, p. 1019.

Ridley, N., Brown, D. and Malik, H.I. (1973). Effect of some alloying additions on the kinetics of pearlite growth. Proc. Int. Symp. in Chemical Metallurgy of Iron and Steel, p. 268.

Ridley, N. and Burgers, D. (1984). Partitioning of Co during pearlite growth in a eutectoid steel. Metal Science, vol. 18, Jan., p. 7.

Ridley, N., Lewis, M.T. and Morrison, W.B. (1981). Effect of small additions of vanadium on the strength of pearlitic steels. Advances in the Phys. Met. and Appl. of Steels. Proc. of an Int. Conf. University of Liverpool 21-24 Sept 1981, p. 129.

Roberts, G.A. and Mehl, R.F. (1943). Transactions ASM, vol. 31, p. 613.

Roősz, A., Gáczi, Z. and Baán, M.K. (1980). A simple method for determining the true interlamellar spacing. Metallography, vol. 13, p. 299.

Roősz, A. and Gáczi, Z. (1981). The correlation of the average true interlamellar spacing of pearlite on the transformation temperature in DIN 39 Cr4 steel. Metallography, vol. 14, p. 129.

Rosenfield, A.R., Hahn, G.T. and Embury, J.D. (1972). Fracture of steels containing pearlite. Metallurgical Transactions, vol. 3, p. 2797.

Russev, K., Budurov, S., Danailov, D. and Lazarova, T. (1974). On the kinetics of pearlite transformation of a eutectoid steel by continuous cooling. Z. Metallkunde, p. 687.

Schmidt, C.G. and Miller, A.K. (1982). The effect of solutes on the strength and strain hardening behaviour of alloys. Acta Metallurgica, vol. 30, p. 615.

Shapiro, J.M. and Kirkaldy, J.S. (1968). Theory of decomposition of eutectoids assuming local equilibrium and phase boundary diffusion. Acta Metalurgica, vol. 16, p. 579.

Sharma, R.C, Purdy, G.R. and Kinkaldy, J.S. (1979). Kinetics of the pearlite reaction in Fe-C-Cr. Metallurgical Transactions, vol 10A, p. 1129.

Shipley, E.A. (1962). High strength steel wire. Special report 76. High Strength Steels. The Iron and Steel Institute, p. 93.

Shipley, E.A. (1982). Private communication.

Smith, B.F. (1977). Wire Journal, October, p. 56, November, p. 68.

Smith, B.F. and Speirs, D.L. Factors affecting the strength of high carbon steel wire. Unpublished report. British Ropes Limited.

Smith, D.W. and Mehl, R.F. (1935). Transactions AIME, vol. 116, p. 330.

Smith, G.D.W., Smith, D.A. and Easterling, K.E. (1973). The structure and strength of heavily drawn pearlitic steel wire. Proc. Conf. on Microstructure of Alloys. Institute of Metals and I.S.I. London, p. 75.

Smith, G.D.W., Garratt-Reed, A.J. and Van der Sande, J.D. (1981). Comparison between quantitative microanalysis with high spatial resolution. Proc. of the Conf held at UMIST/Manchester 25-27 March 1981.

Smith, G.D.W. (1983). Private communication.

Smith, G.V. and Mehl, R.F. (1942). Transactions AIME, vol. 150, p. 211.

Smith, Y.E. and Fletcher, F.B. (1978). Alloy steels for high strength as rolled rails. ASTM STP 644. Rail Steels Development Processing and Use, p. 212.

Stacey, A.C. (1980). The influence of segregation on the drawability of high carbon steel rod. Wire Journal, March, p. 92.

Stephenson, A., Timiny, P. and Walton, J.M. (1983). Strain ageing in high tensile carbon steel wire for roping purposes. Int. Conf. on Develop. on the Drawing of Metals, London, p. 219.

Strauss, K. (1970). Applied Science in the Casting of Metals. Pergamon Press, Oxford, p. 68.

Sturgeon, G.M. and Guy, V.H. (1963). The cooling of wire during drawing. Journal of the Iron and Steel Institute, vol. 201, p. 437.

Sundquist, B.E. (1969). The effect of alloying elements and pressure on the growth of pearlite. Acta Metallurgica, vol. 17, Aug., p. 967.

Takahashi, T., Nagumo, M. and Asano, Y. (1980). Strengthening of hard drawn steel wire with improved ductility. Wire Journal, nov., p. 78.

Theis, K. and Klemm, M. (1982). Production of high carbon wire rod from continuous cast billets. Wire Journal, January, p. 67.

Waugh, A.R., Paetke, S. and Edmonds, D.V. (1981). A study of segregation to the dislocation substructure in patented steel wire using atom probe techniques. Metallography, vol. 14, p. 237.

Wert, (1952). Transactions American Institute of Mining (Metall) Engrs. Vol. 194, p. 602.

White, P. (1983). Private communication.

Williams, P.R. (1980). The effect of microalloying additions on pearlitic steels. Ph.D. Thesis University of Oxford.

Willimse, P.F., Naughton, B.P. and Verbraak, C.A., X-ray residual stress measurements on cold drawn steel wire. Material Science and Engineering, vol. 56, p. 25.

Yamada, Y., Kawakami, H., Nakamuna, Y. and Tsuji, K. (1983). Strain ageing of high carbon steel wires. Wire Journal, vol. 33, p. 122.

Zener, C. (1946) Kinetics of the decomposition of austenite. Transactions AIME, vol. 167, p. 550.

Zikeev, N.N. and Gusienov, R.K. (1979) Effect of chromium on the properties of high strength steels 30N 9k4 M7. Trans. Metalledenie Termicheskaye Obrabotka Metallov. vol. 5, p. 383.

Zubov, V. Ya. (1972). Patenting of steel wire. Metall. Termich. Obrab. Metallov, vol. 9, p. 383.

APPENDIX A

IBAS PROGRAM LIST PRGM # 830

COMMAND	PARAMS		SWITCHES	CONSTANTS
1 TVON			ONLINE	
2 TVINP	INP	1		
3 FILTER	INP	2		
	OUT	4	ENHCON	
4 EDIT	INP	4		
	OUT	4		
	AUX	3		
5 DISC2L	INP	4	BINARY	
	OUT	4		
	LEV1	147		
	LEV2	255		
6 MEDIAN	INP	4		
	OUT	4		
	SIZE	5		
	RANK	13		
7 BTHINN	INP	4		
	OUT	4	LNENDS	
	AGE	3	MARGIN	
	TSTP	10		
8 DISC1L	INP	4	BINARY	
	OUT	4	INVERT	
	LEVL	1		
9 INVERT	INP	4		
10 CLROVL	INP	4		
11 AUTOCH	INP	4		
	FHST	100	SQUARE	
	FHN	220		
	SPAC	20		
	FILE	10		
12 PAUSE				